Spring 1-1-2010

3D Seismic Interpretation of a Meteorite Impact, Red Wing Creek Field, Williston Basin, Western North Dakota

Benjamin David Herber
bherber@gmail.com

3D Seismic Interpretation of a Meteorite Impact, Red Wing Creek Field, Williston Basin, western North Dakota

By

BENJAMIN DAVID HERBER

B.S., Geological Sciences, University of Texas at Austin, 2005

A thesis submitted to the

Faculty of the Graduate School of the

University of Colorado in partial fulfillment

of the requirements for the degree of

Master of Science

Department of Geological Sciences

2010

This thesis entitled:

3D Seismic Interpretation of a Meteorite Impact, Red Wing Creek Field, Williston Basin, western North Dakota

By: Benjamin Herber

has been approved for the Department of Geological Sciences

_____

Paul Weimer

_____

Renaud Bouroullec

Date:_____

The final copy of this thesis has been examined by the signatories, and we have found that both the content and the form meet the acceptable presentation standard of scholarly work in the above mentioned discipline

Herber, Benjamin David (M.S. Geological Sciences)

3D Seismic Interpretation of a Meteorite Impact, Red Wing Creek Field, Williston Basin, western North Dakota

Thesis directed by Professor Paul Weimer

Abstract

The Red Wing Creek Field in the Williston Basin was discovered in 1972, and is one of a few well-known petroleum fields in the world to produce from a structure associated with a meteorite impact. Interpretation of a 3-D seismic dataset, covering 145 km^2 over Red Wing Creek Field, shows that the crater has a diameter of 9.1 km and can be divided into three unique structural zones. First, the central uplift complex has a maximum diameter of 5.1 km, and consists of an uplifted central core, composed entirely of strata of the Mississippian Madison Group, and a flanking inner rim. The seismic reflectivity within the central core is poor, but well log data indicates extensive stratigraphic repetition. The central core is surrounded by an annular rim (1.7 km wide), which is structurally thickened by imbricate thrusts that dip towards the central core. This rim comprises eight distinct radial sectors, segmented by nine high-angle, reverse faults.

The second portion of the crater is a depressed annular trough with a maximum diameter of 1.5 km; its inner limit is bounded by antithetic normal faults and its outer limit by concentrically linked normal faults that dip toward the central part of the crater. This group of faults marks the edge of the third zone, the outer rim. The outer rim is

slightly uplifted, relatively undisturbed, and its strata dip at a maximum angle of 8° away from the central crater.

Through detailed mapping of the stratigraphy and structural features within the Red Wing Creek seismic dataset, a multistep kinematic model of crater formation has been developed. The first step is the contact/compression stage that produced a shockwave, which propagated as deep as the Middle Devonian strata. The next stage was the excavation stage that removed the Upper Mississippian through Triassic/Jurassic section in the central crater. The final stage of formation is the modification stage, which produced most of the structural features, present in the crater's final morphology (folding, outward directed thrusting, and radial faulting), due to the interaction of the inward collapsing crater walls and the outward collapsing central uplift complex.

Acknowledgements

First, I would like to thank my advisor Dr. Paul Weimer for giving me the opportunity to attend graduate school at the University of Colorado and for allowing me to work on such a unique project as Red Wing Creek. Completion of this project would not have been possible without his guidance and support. I would also like to thank Dr. Renaud Bouroullec for his input, editing, and participation on my committee. Finally, I would like to thank Dr. Joe Smyth for participating in my thesis defense.

This project would not have been possible without the financial support of True Oil Company. I would like to thank Hank and Dave True for their generosity and for allowing me the use of their data. I would especially like to thank Roger Barton for his constant patience. His input was integral to the completion of this thesis. Also, I would like to thank Dan Behringer, Dan Ruland, and Tom Walker for their input along the way. A big thanks goes to Dr. Geoff Dorn at TerraSpark Geosciences for allowing me to use their seismic attribute software. Such a detailed structural interpretation would not have been possible without it. I'm also very grateful to Dr. Stan Hammon and Mick Coady for their generosity of time and for helping me out of a variety of technical jams.

Many people along the way supplied valuable input that guided my work. Ken Fredricks and Kent Campell from Fusion were very helpful in deciphering what the seismic attributes were telling me about such a complex structure as Red Wing Creek. Duff Kerr's input, based on his early work at Red Wing Creek, completely opened my eyes to what was really happening in the structure. The amazing work he did in the late 60's and early 70's heavily influenced my final interpretation. I would also like to thank

Dr. John Warme and Dr. Roy Kligfield for their input to the project. Thanks to Dr. Chunju Huang and Dr. Shu Jiang for the early work they did on the project. Jay Austin and Nathan Rogers were my technical saviors during this project. Their help allowed me to avoid getting bogged down in the time eating software messes that come along too often. I'd also like to thank Jay for always reminding me of the futility of being a Dallas Cowboys fan.

I would like to thank my parents and sister for their love, example, and constant support (also for never buying the thermometer under the hot water trick). Finally, I would like to thank my grandfather, Dr. Jim L. Kidd, for showing me that no obstacle is big enough to keep you from achieving your educational goals.

CONTENTS

Tables

Table

Figures

INTRODUCTION

The Red Wing Creek field is located in McKenzie County, western North Dakota, in the Williston Basin (**Figure 1**). Discovered in 1972, the origin of the Red Wing Creek structure was considered anomalous until exploration drilling experienced an unusually thick oil column in its central portion. The Red Wing Creek structure was interpreted (Brenan, et al. 1975) and later confirmed (Koeberl, et al. 1996) to be a product of a meteor impact. Its origin places it in a unique category of oil and gas fields producing from impact related structures (**Table 1).**

In 1968, Shell Oil Company drilled the first well in township T148N-R101W (**Figures 2-4**), which would later be the location of the 1972 True Oil discovery well. Despite the fact that the No. 22X-28 Government well was a dry hole, the unusually thick and structurally shallow Mississippian and Pennsylvanian section made the results of the well the most significant well drilled in the Williston Basin since the Nesson Anticline was drilled in April 1951 (Brenan et al., 1975). After acquiring a 2-D seismic survey in 1965 (**Figure 5)**, workers were able to map an annular trough paired with a structural high at the Mississippian level. The central portion of the line was treated as a data washout zone, and was, therefore, avoided as an exploration target (**Figure 2)**. Initially, twelve interpretations of the circular feature that included compressional tectonics, salt diapirism, igneous intrusion, reef growth, salt dissolution, and combinations of these features (Brenan et al., 1975). The meteorite impact theory was included in the list of possible explanations but was considered to be less probable (Stone, 2005). There has also been speculation that Red Wing Creek is a popup

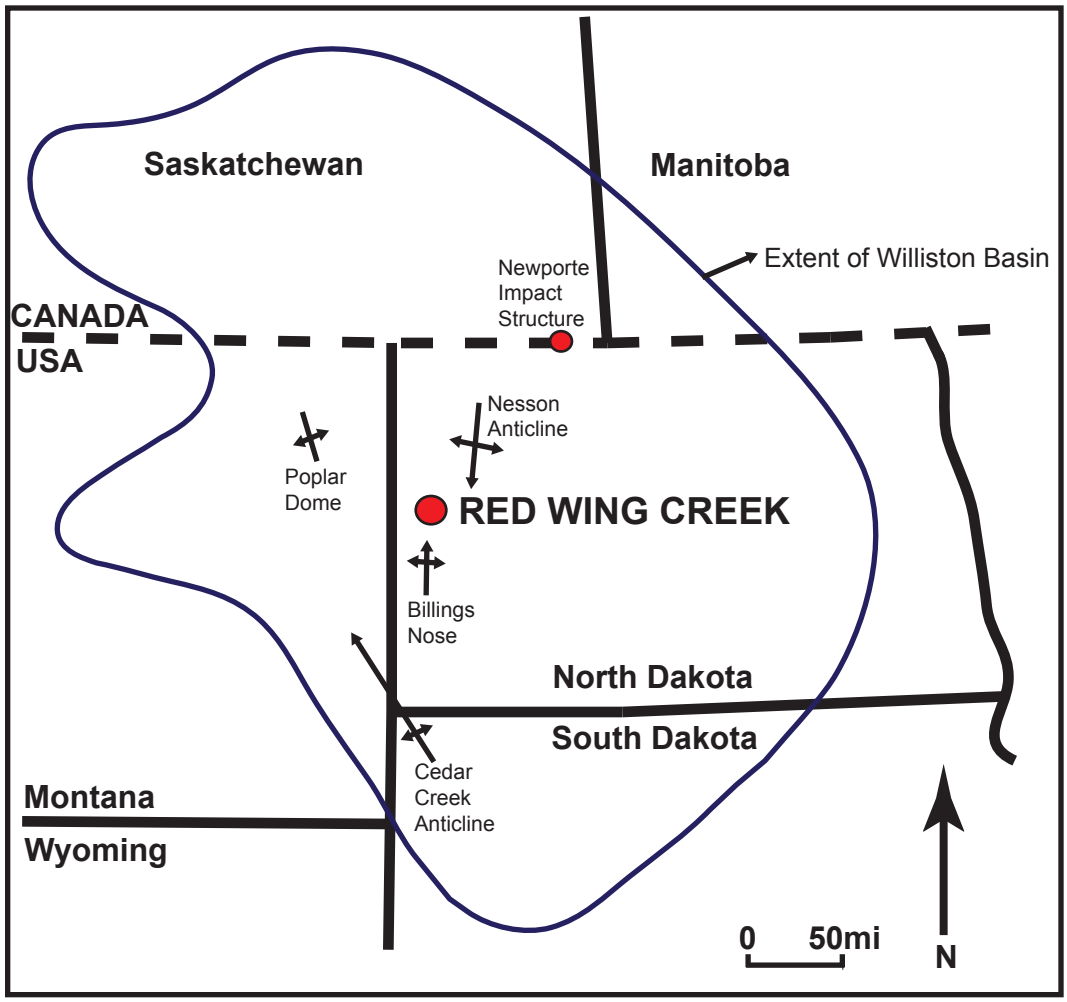

Figure 1. Location map of the Red Wing Creek in Western North Dakota, Williston Basin. Major anticlines and the location of the Newporte impact crater are annotated. (modified from Koeberl et al., 1996 and Sonnenberg and Pramudito, 2009).

Name	Location	Diameter	Age	Discovery Year	Reservoir Rock Type	Primary Reserves
Ames	Major County, Oklahoma	13 km, 8 mi	Early Ordovician	1991	Carbonates, Granite	25 MMBO 15 BCFG
Avak	Point Barrow, Alaska	12 km, 7.5 mi	Cretaceous-Tertiary	1949	Sandstones	39 BFCG
Calvin	Cass County, Michigan	4.8km, 3 mi	Lower Ordovician	1978	Carbonates	3 MMBO
Chicxulub	Yucatan Peninsula, Mexico	300 km, 180 mi	Cretaceous-Tertiary	1974	Carbonates	30,000 MMBO 15,000 BCFG
Marquez	Leon County, Texas	12.7 km, 7.9 mi	Early Tertiary	1977	Sandstones	.10 - .15 MMBO 5-7 BCFG
Newporte	Renville County, North Dakota	3.2 km, 2 mi	Cambrian Ordovician	1977	Carbonates	15 MMBO
Red Wing Creek	McKenzie County, North Dakota	9 km, 5.6 mi	Early Jurassic	1972	Carbonates	60 MMBO
Sierra Madera	Pecos County, Texas	13 km, 8 mi	Late Cretaceous	1977	Carbonates	270 BCFG
Steen River	N.W. Alberta, Canada	25 km, 15.5 mi	Middle Cretaceous	1968	Carbonates	3-5 MMBO+

Table 1. List of confrimed petroleum producing impact structures in North America (modified from Donofrio, 1997)

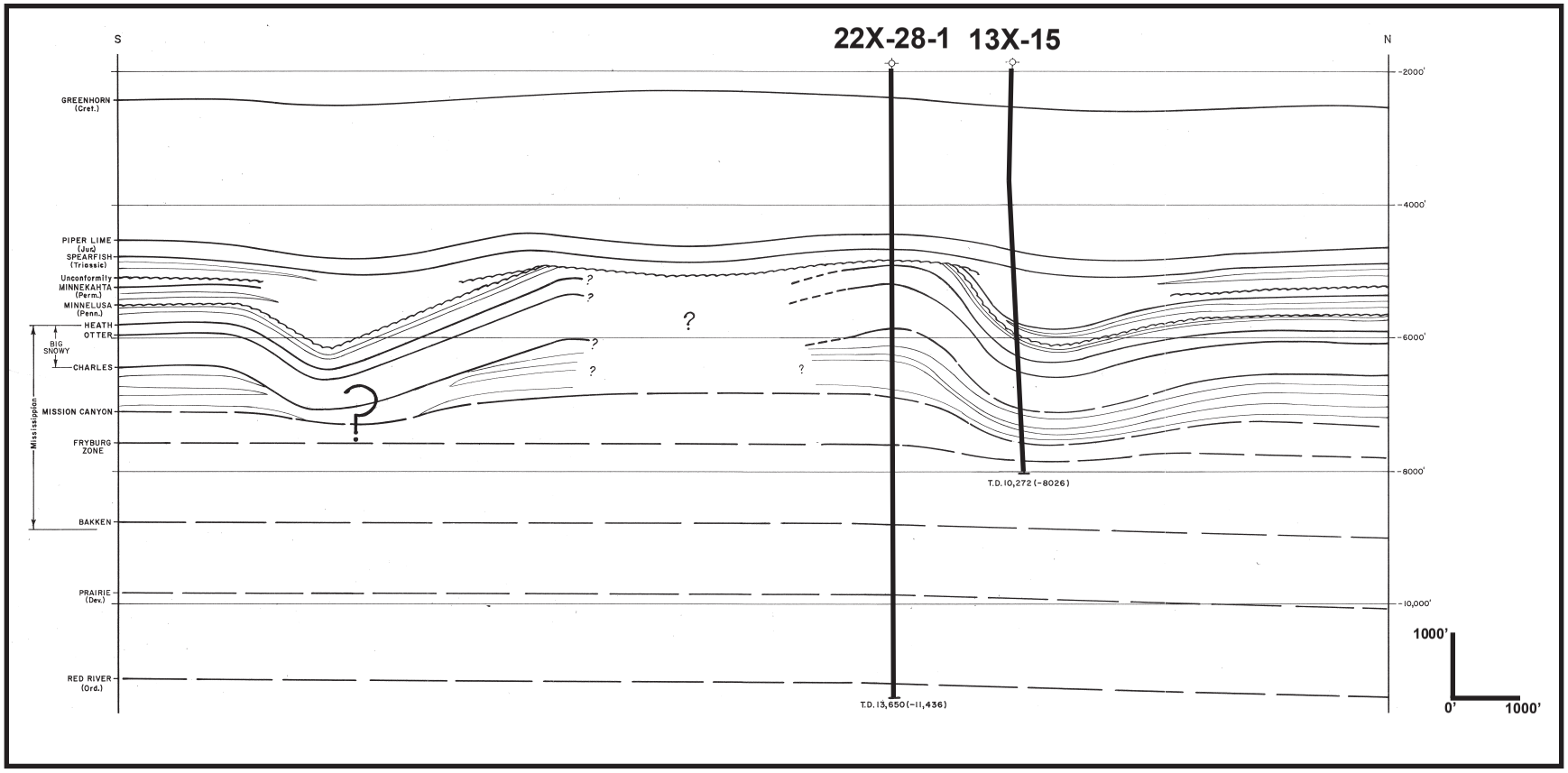

Figure 2. Original 1972 cross section of the Red Wing Creek structure based on 2D seismic data. The well paths for the 22X-28 and the 13X-15 are highlighted. Originally, the central portion was considered a data washout zone(courtesy of D. Kerr).

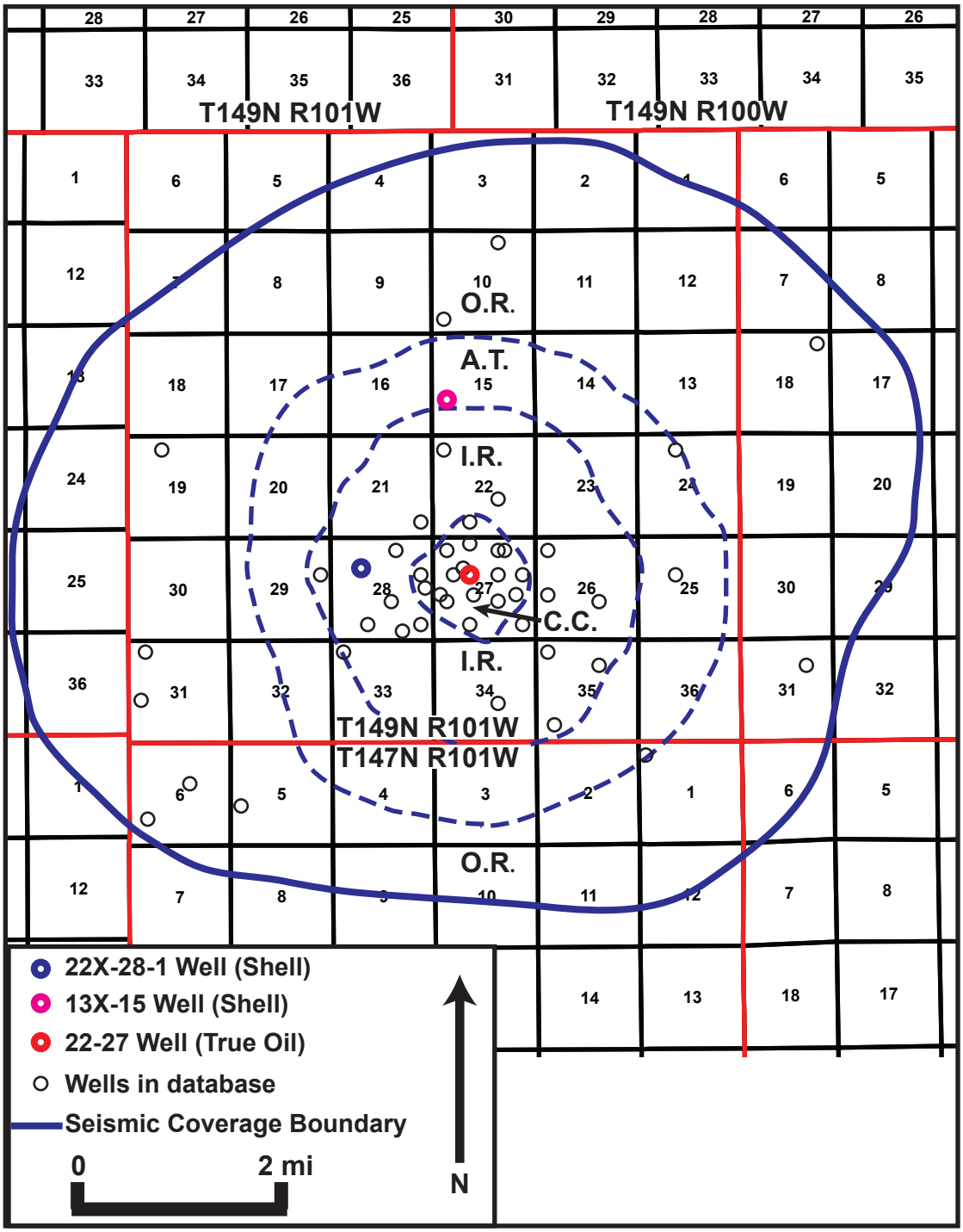

Figure 3. Landgrid map showing all wells in the Red Wing Creek field. The two original Shell wells and the True Oil discovery well are highlighted by heavy circles. The coverage area of the 3D seismic dataset is represented by the dashed line. The blue dashed lines represent major structural zones: outer rim (O.R.), annular trough (A.T.), inner rim (I.R.), and the central core (C.C.)

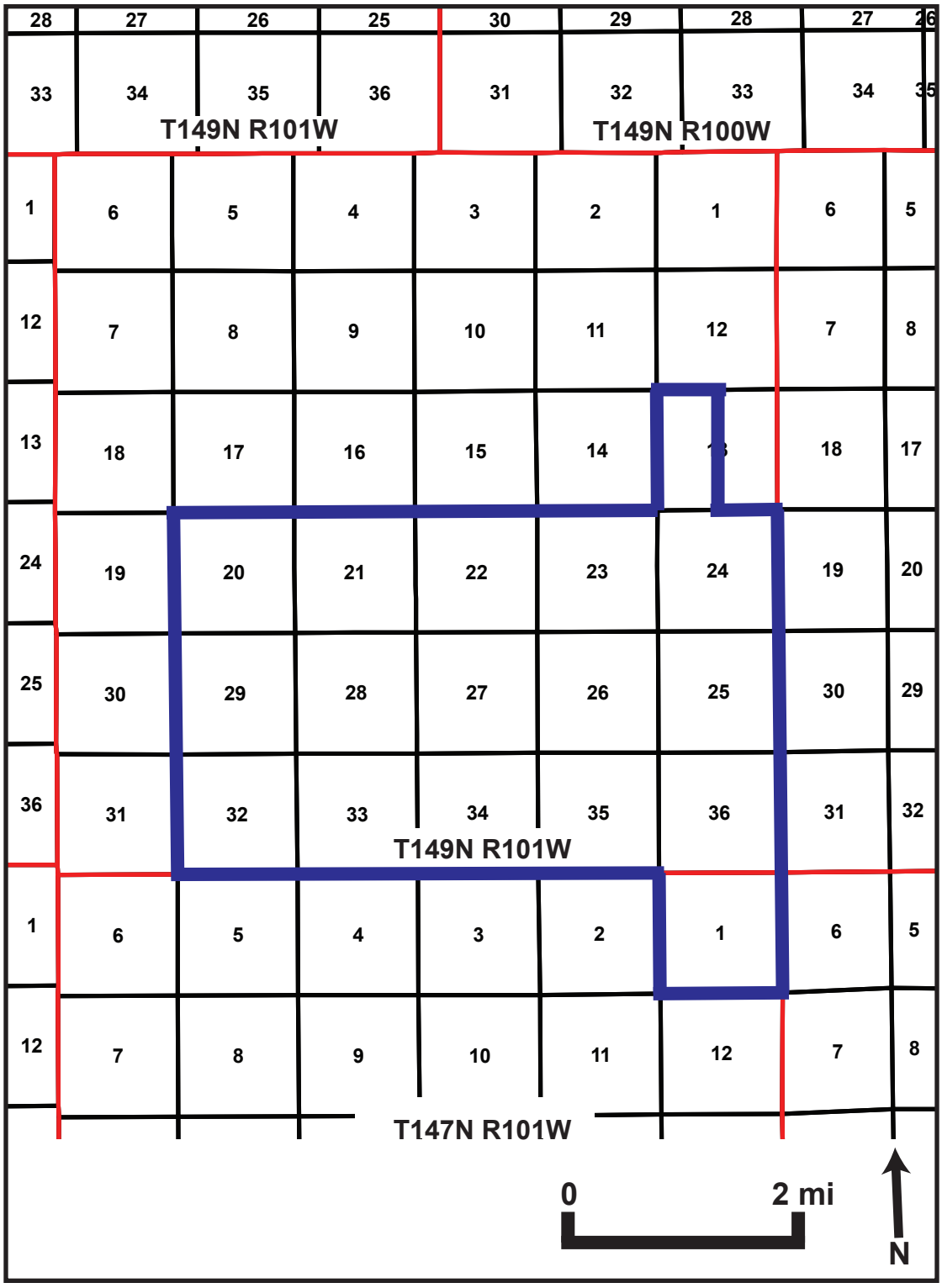

Figure 4. Landgrid map of Red Wing Creek Field in McKenzie County, North Dakota. The blue outline represents the boundary of the Madison Pool, as defined by the state of North Dakota.

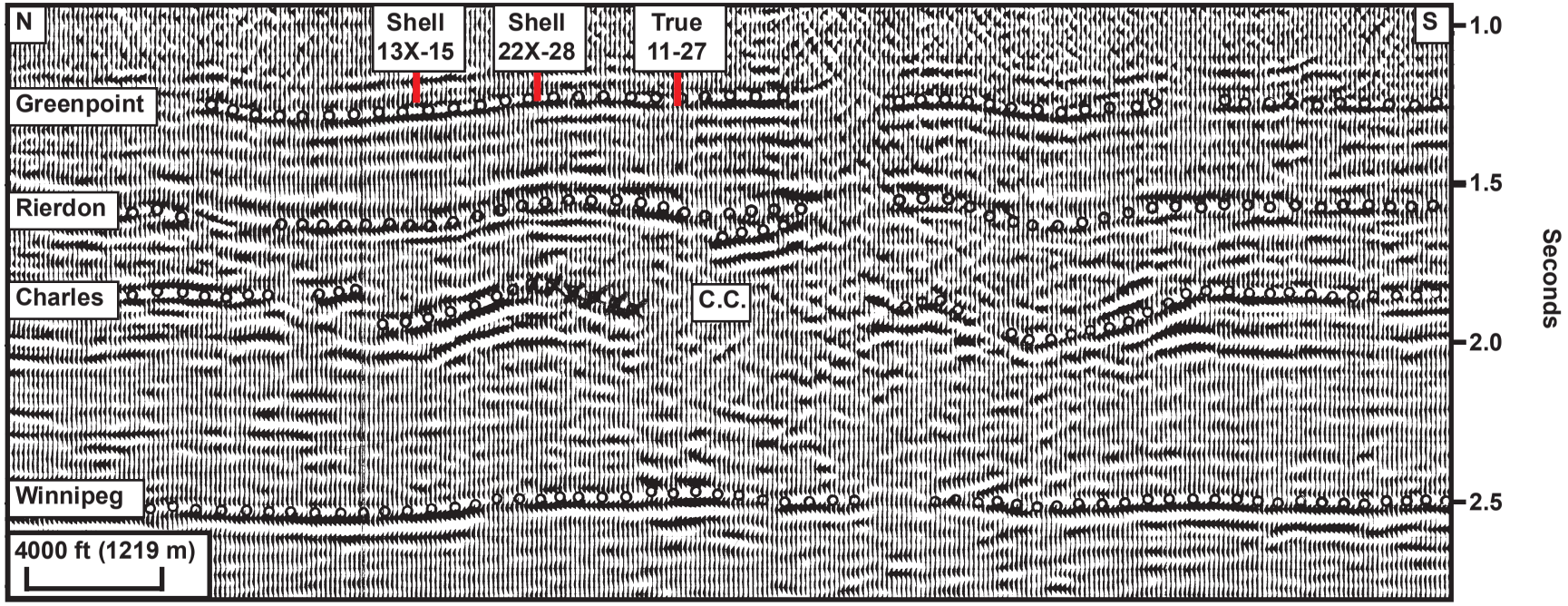

Figure 5. North-south seismic profile from the original 2-D seismic data set (acquired in 1965) and original horizon interpretation of Red Wing Creek. The locations of the first three wells drilled in the field are annotated. The central core (C.C) was a complete data wash-out zone and was avoided by the first two Shell wells. The True Oil discovery well was the first to drill the central core and encountered a 2,850 foot 869 m) thick oil column (Modified from Stone, 2005).

structure related to the intersection of two strike slip faults (Bridges, 1978, 1987; Stone, 2005).

The site of the 22X-28 well was chosen as the first drilling location due to the presence of a structural high at the edge of the data washout zone (**Figure 5)**. Although the 22X-28 well was a dry hole, oil shows and the unusual thickness of the Mississipian Mission Canyon section led Shell to drill the Turnquist 13X-15 in the adjacent structural low (D. Kerr, personal communication, 2009). This well was also dry and the Red Wing Creek acreage, held by Shell, was relinquished and left inactive until it was drilled by True Oil Company in August 1972. Rainbow Resources initially sold the acreage to True based upon a structural high mapped on the Ordovician Red River Formation (D. Kerr, personal communication, 2009), but the initial well was drilled centrally in the data washout zone that had been previously avoided. The #22-27 Burlington Northern well encountered 2,850 feet (869 m) of Mississippian oil column where regionally there was normally 100 foot (30 m) thick oil columns with 15 net feet (4.57 m) of pay (Brenan et al., 1975). Upon discovery, there was renewed enthusiasm and the success at Red Wing Creek that led to extensive drilling as well as many discoveries and new play concepts in the deepest part of the Williston Basin (J. Rogers, personal communication, 2009) (**Figure 6**).

Production at Red Wing Creek began in October 1972 and in the following seven years, 23 wells were drilled in addition to the #22-27 discovery well. Activity slowed from 1980 to 1994 with only four wells being drilled in the field. With the acquisition of 3D seismic data in 2001, ten additional wells were drilled at Red Wing Creek. Of the 39 wells drilled in the field, 24 of those have been drilled within the central core or in the

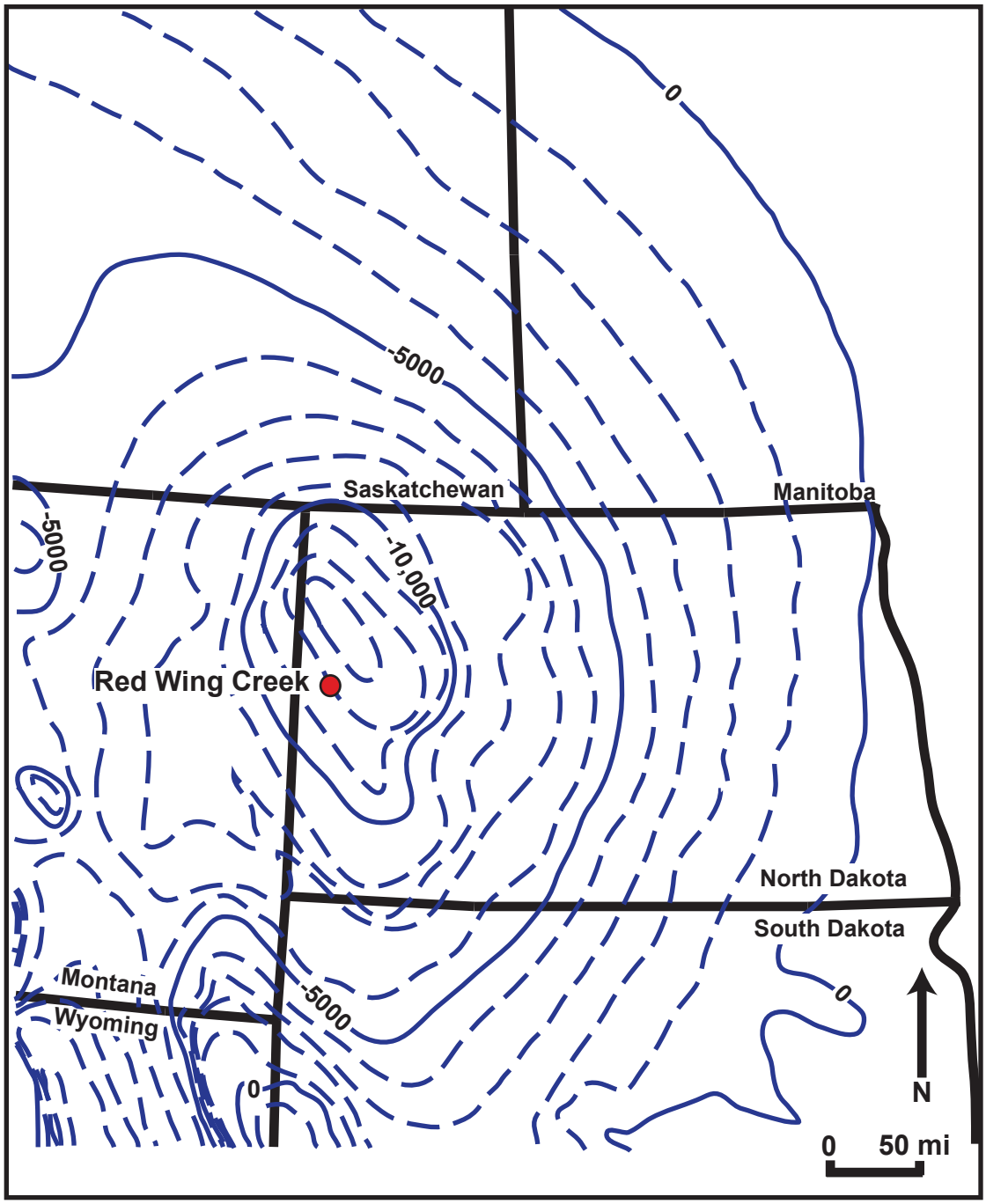

Figure 6. Regional structural contour map of the top basement of the Williston Basin. Red Wing Creek Field is located near the structurally deepest portion of the basin. Depth is subsea and the contour interval is 1000 feet (305 m) (modified from Brenan et al., 1975).

immediately adjacent inner rim (**Figure 3)**, which was avoided by early exploration wells (**Figure 2)**. To date, 97% of the 17MMBO produced has come from the central core, and 22 of the 24 wells in this zone are still producing. Current estimates place the total reserves at Red Wing Creek to be more than 60MMBO (**Table 2)** (R. Barton, personal communication, 2009).

This thesis aims to provide the most thorough structural interpretation of the Red Wing Creek meteorite impact feature to date. The main objectives are to:

(1) integrate 3D seismic data with available well data in order to provide an accurate picture of the three dimensional nature of the Red Wing Creek structure at multiple levels;

(2) interpret and describe distinct structural styles and their distribution across the Red Wing Creek structure;

(3) provide an explanation for the source of the sediment that fills the crater space between the crater floor and the overlying, draping sediments; and

(4) develop a kinematic model for the formation of the Red Wing Creek structure that follows the progression from compression to the post-modification stage.

DATA SET

The data set for this study consists of a 3D depth migrated seismic data cube, 3D seismic attribute volumes, and wireline logs, all of which were provided by True Oil Company. The original pre-stack time migrated 3D seismic volume was acquired by Quantam Geophysics in 2001, and the pre-stack depth migrated volume was generated

Red Wing Creek Field
McKenzie County, North Dakota, T148N-R101W

Operator	True Oil Company
Discovery Date	1972
First Production	October 1972
Maximum Oil Column Thickness	3090 feet (942 m)
Net Reservoir Pay Thickness	1605 feet (489 m)
Reservoir lithology	Fractured carbonates
Number of wells	39 Wells
Total Production	17 MMBO
Total Reserves Estimate	60 MMBO
Reservoir Age	Mississippian
Drive Mechanism	Gas Solution
Fracture Permeability	30-50 mD
Matrix Permeability	>1 mD
API Gravity	42.4°
Viscosity	.25 cp
Reservoir Temperature	241°F (116°C)
Original Gas-Oil Ratio	947CF/bbl:1
Current Gas-Oil Ratio	2500SCF/bbl:1
Seals	Evaporites
Status	Producing
Source of Information	Roger Barton, personal communication, 2009

Table 2. Field summary of Red Wing Creek in McKenzie county North Dakota.

in 2004, by Tricon Geophysics. The PSDM dataset covers approximately 56 square miles (145 square km) (**Figure 3**) and has a total of 547 lines and 472 traces with a bin spacing of 88 feet by 88 feet (26m x 26m). The data have a record length of 18,015 feet (5490 m) with a sampling interval of 15 feet (4.57 m). All depth annotations with seismic lines are in measured depth. There is a 2200 foot (670.6 m) datum that corresponds with average sea level in the area.

In 2007, Geo-Texture Technologies reprocessed the PSDM data for True Oil to generate a Principal Component Filtered (PC-Filt) volume that specifically preserves discontinuities within the seismic data set. The PC-Filt process reduces noise in the seismic data and preserves discontinuities, which allows for a better structural interpretation of the data as well as input for the generation of additional seismic attributes. All structural and stratigraphic interpretation was done using the PC-Filt depth volume, and all attributes used in the study were generated from the PC-Filt volume by Geo-Texture Technologies or within Schlumberger Petrel and TerraSpark Geosciences Insight Earth. Seismic interpretation was done using SMT Kingdom Suite, Schlumberger Petrel, and TerraSpark Geosciences Insight Earth.

True Oil Company provided all well data used in the project. There are 52 wells in the project with varying log suites, which include gamma ray and resistivity. Log interpretation was done within IHS Petra and SMT Kingdom Suite; wells were originally tied to the seismic volume to aid in the pre stack depth migration.

REGIONAL SETTING AND PETROLEUM PRODUCTION IN THE WILLISTON BASIN

The Williston Basin is primarily an intacratonic basin that covers a large area (133,000 mi^2/345,000 km^2) of the northern Great Plains in the western parts of North and South Dakota, eastern Montana, and southern Saskatchewan and Manitoba (**Figure 1)** (Gerhard, et al., 1991)**.** Initital sedimentation began in North Dakota during the Late Cambrian and continued through the Tertiary; more than 15,000 ft (4575 m) of strata were deposited; the Paleozoic strata are 10,000 ft (3048 m) thick and the Mesozoic strata are 5,000 (1524 m) thick (**Figures 7, 8)**. During the Early to Middle Paleozoic, the basin was filled with shallow marine carbonates with some siliciclastic deposits. There was also considerable evaporite deposition of supratidal or shallow marine origin. From the Late Paleozoic to Tertiary, the depositional conditions changed to primarily siliciclastic deposition (Peterson and MacCary, 1987).

Basin subsidence began during the Middle Ordovician and continued through the Mesozoic with minor periods of deformation. The uniform rates of subsidence and the lack of major tectonic events allows for the Paleozoic and Mesozoic stratigraphy to be correlated regionally for hundreds of miles without major interruptions or stratigraphic changes. This stratigraphic continuity was the primary condition that made the Red Wing Creek structure so anomalous when first recognized during the late 1960's to early 1970's (**Figure 9**).

Several erosional events in the Williston Basin occurred during the Siluro-Devonian, Late Mississippian, and Early Triassic. These erosional events were associated with minor deformation and resulted in the shifting of the basin axis, folding and faulting along Precambrian lines of weakness in a northwest and northeast strike direction, and truncation along the basin margins (Brenan et al., 1975). During the latest

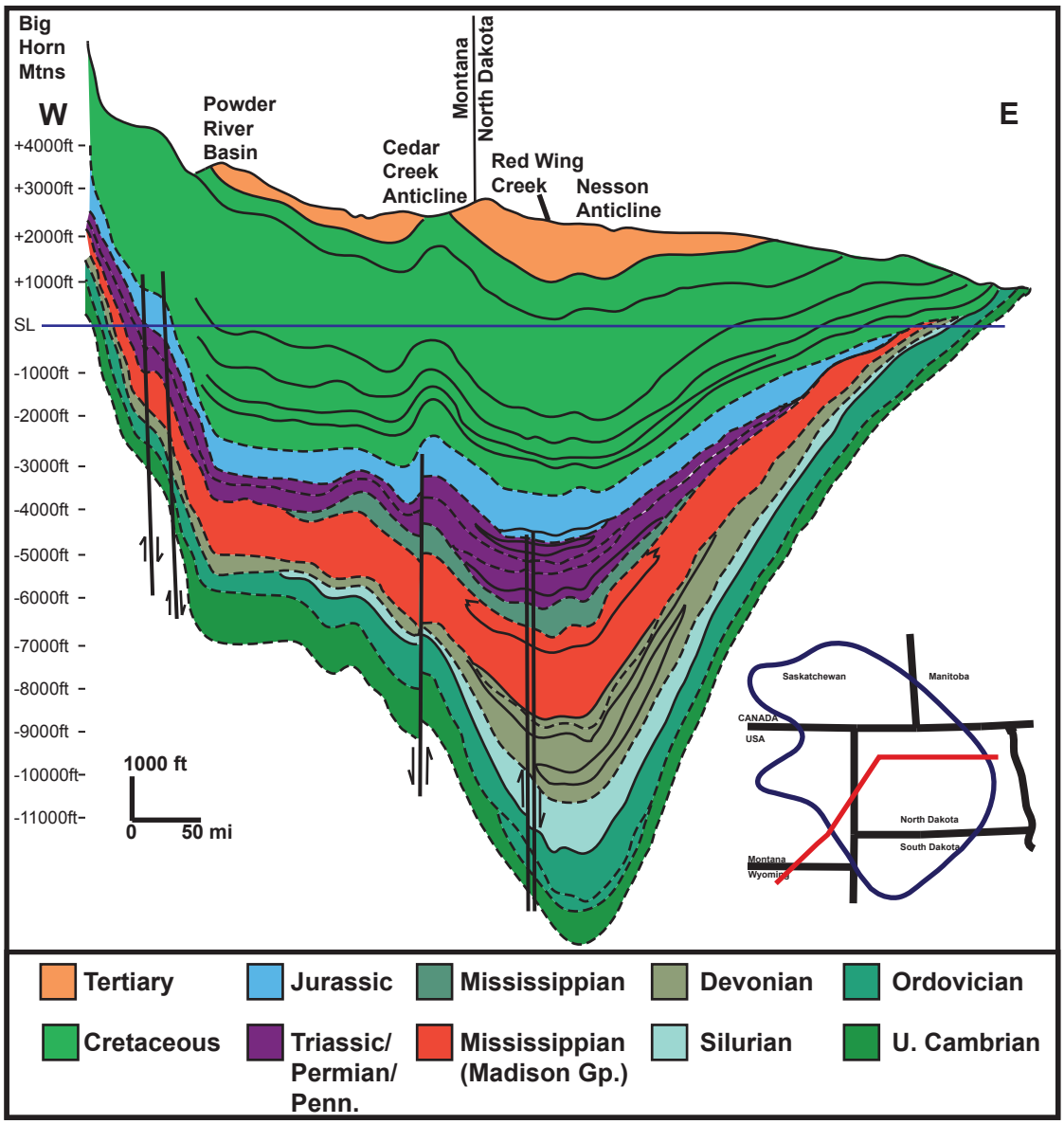

Figure 7. Regional west to east structural cross section through the Williston Basin. The projected location of Red Wing Creek is plotted at the surface. (Modified from Peterson et al., 1987).

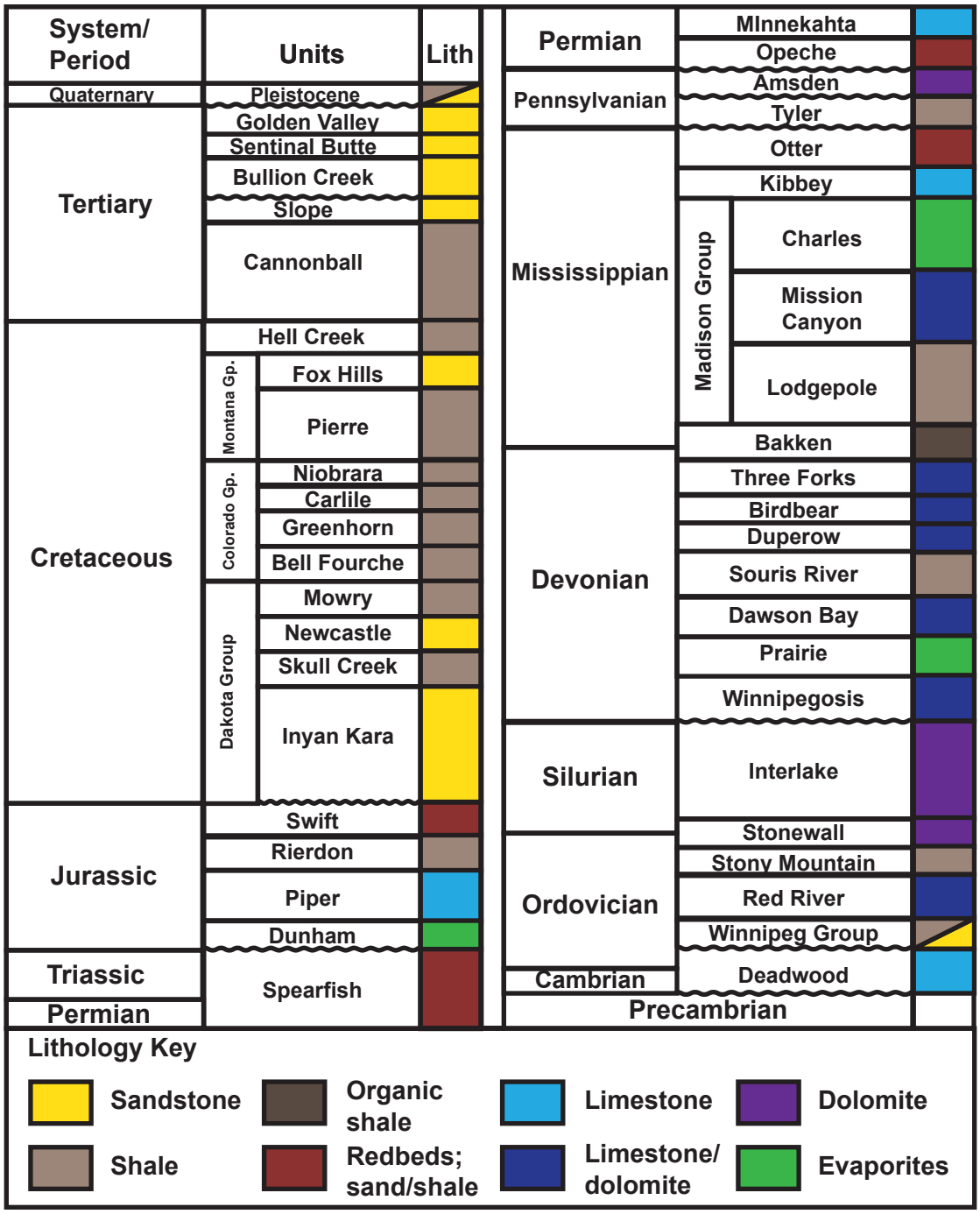

Figure 8. Generalized Williston Basin stratigraphic chart for Williams County, North Dakota. The Red Wing Creek structure is approximately 30 miles (48 km) south of the Williams county line. The lithology of each formation is color coded according to their regional expression (modified from Bluemle et al., 1981).

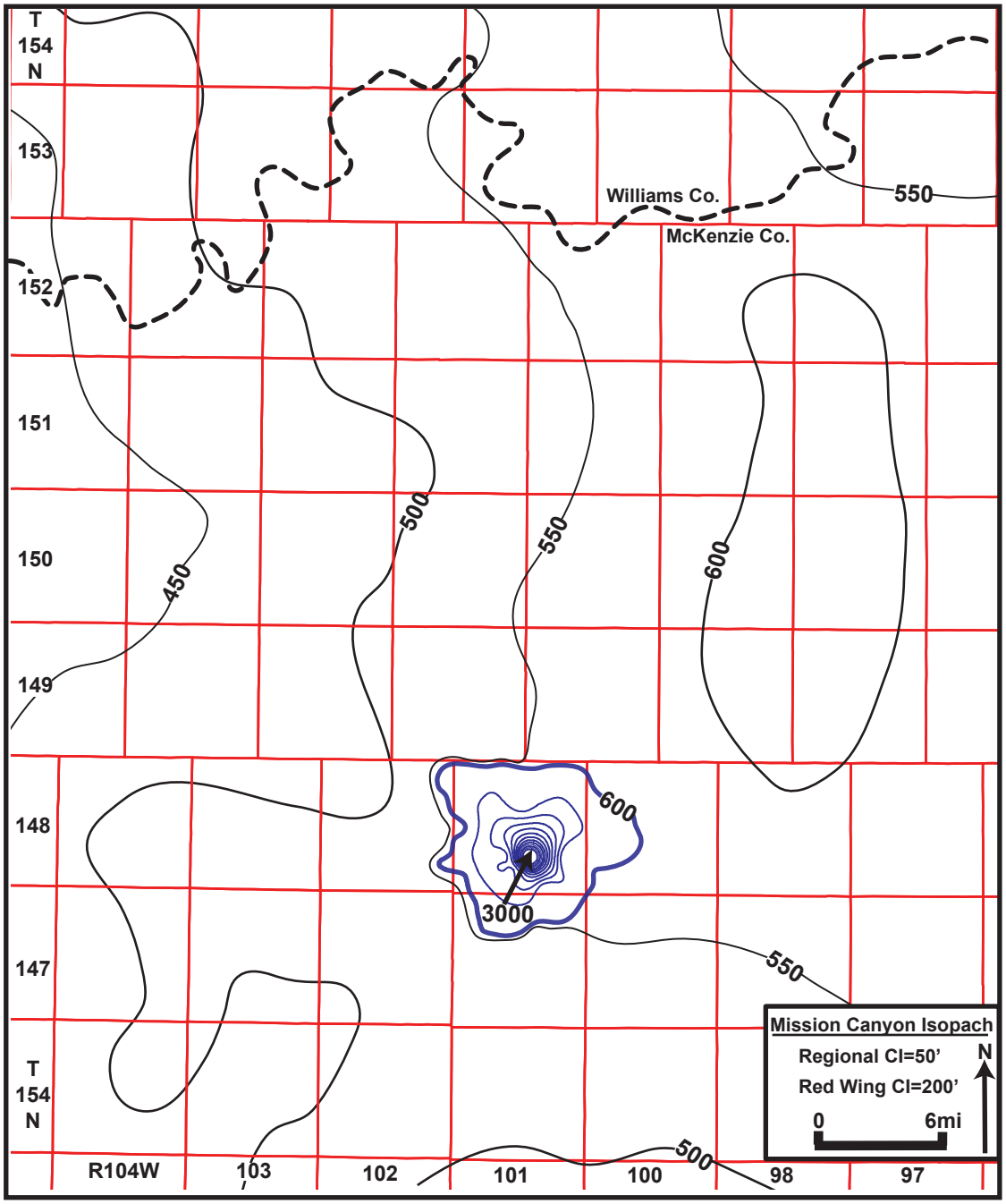

Figure 9. Regional isopach map of the Mississippian Mission Canyon Formation. Regionally in the Williston Basin, thicknesses and structure are relatively undisturbed. The Mississippian formation thicknesses make the Red Wing Creek structure highly anomalous (modified from Brenan et al., 1975).

Cretaceous to early Tertiary, the Laramide orogeny caused a period of significant deformation in the Rocky Mountain region. The effects of the Laramide orogeny causes the development of the Cedar Creek Anticline and Poplar Dome in the western Williston Basin (**Figure 1)**; The central Williston Basin had only minor effects along reactivated Precambrian joints and fractures.

Petroleum reservoirs are present at many stratigraphic levels ranging from the Upper Cambrian to Cretaceous in the Williston Basin (**Figure 10)**. However, primary petroleum production has come from Paleozoic strata. Since production began in the North Dakota portion of the Williston Basin in 1951, there have been several exploration cycles that focused on different play types. Current exploration activity focuses heavily on horizontal drilling for oil in the Upper Devonian to Lower Mississippian Bakken Formation. Estimated undiscovered resources in the North Dakota, Montana, and South Dakota portions of the Williston as of 2008 are approximately 3,800 MMBO and 3,700 BCFG (Anna et al., 2008); most of the remaining oil and gas resources are thought to reside in the Bakken Formation.

DETAILS OF RED WING CREEK PETROLEUM SYSTEM

Reservoir

The Mississippian Madison Group consists of the Mission Canyon, Charles, and Lodgepole Formations (**Figure 8**), which is the most productive interval in the North Dakota portion of the Williston (**Table 3**). The Madison Group is interpreted to be a marine shelf/ramp series (Gutschick and Sandberg, 1983) that extended from New

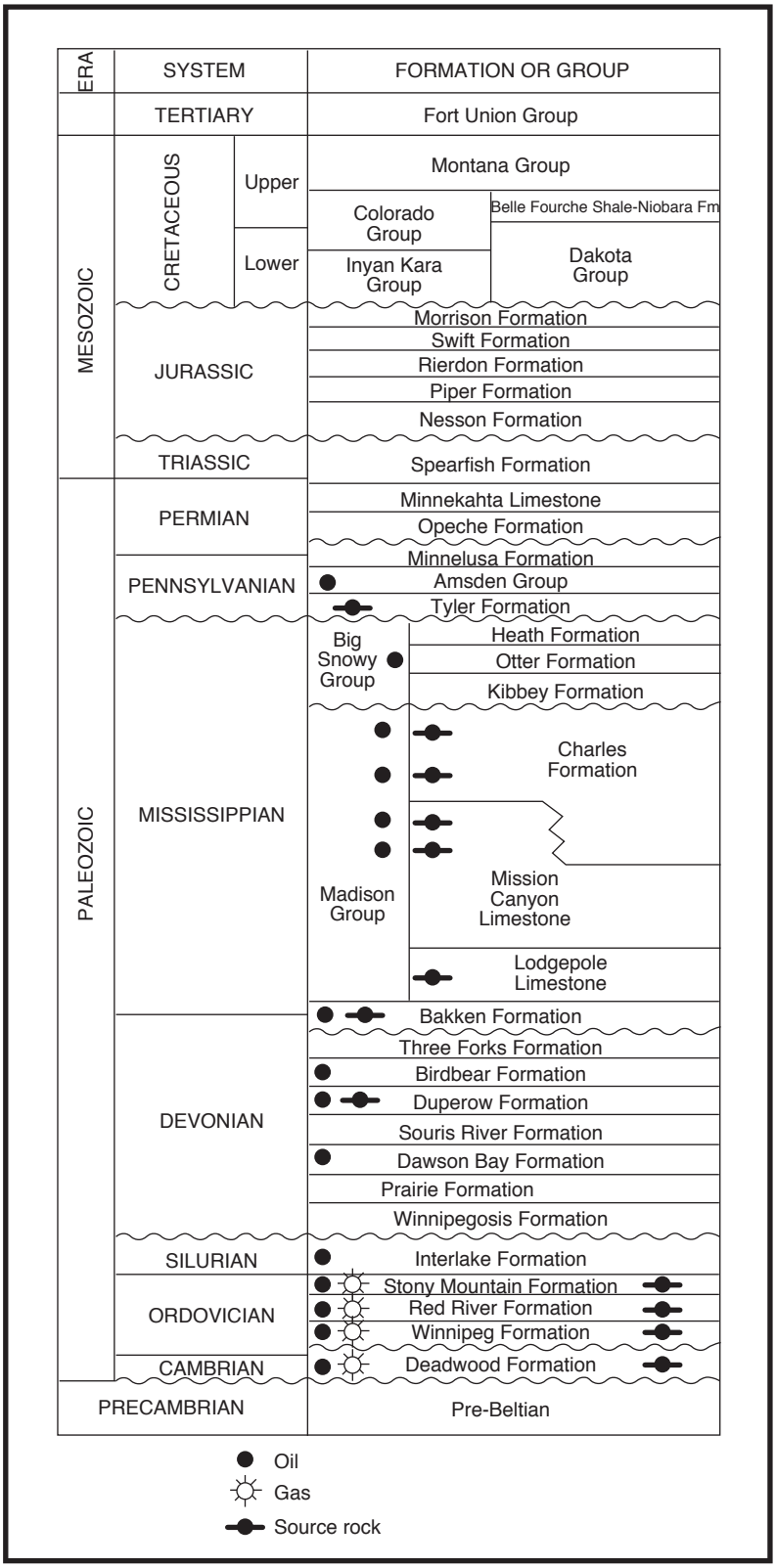

Figure 10. Stratigraphic section of Paleozoic and Mesozoic intervals highlighting the formations that are reservoirs and source rocks (from Peterson, 1995).

Formation/Group	Barrels Produced	Percentage	Total Wells
BAKKEN	119635155	6.8603	1563
BAKKEN/THREE FORKS	188597	0.0108	7
BIRDBEAR	18136909	1.0400	171
CAMBRO/ORDOVICIAN	387176	0.0222	5
DAKOTA	315	0.0000	4
DAWSON BAY	4032007	0.2312	14
DEADWOOD	953	0.0001	1
DEVONIAN	98911118	5.6719	137
DUPEROW	49727047	2.8515	337
GUNTON	236806	0.0136	10
HEATH	65917437	3.7799	197
INTERLAKE	8568	0.0005	1
LODGEPOLE	55848939	3.2026	48
LODGEPOLE/BAKKEN	5883	0.0003	1
MADISON	**905377939**	**51.9176**	**5469**
MIDALE/NESSON	1818475	0.1043	40
MISSION CANYON	17553	0.0010	1
ORDOVICIAN	31810060	1.8241	121
RATCLIFFE	185398	0.0106	4
RED RIVER	104102671	5.9696	689
RED RIVER B	113449677	6.5056	531
RED RIVER C	11829	0.0007	1
RIVAL	452757	0.0260	4
SANISH	13224939	0.7584	58
SILURIAN	63483762	3.6404	220
SOURIS RIVER	58090	0.0033	2
SPEARFISH	632947	0.0363	26
SPEARFISH/CHARLES	49200313	2.8213	210
SPEARFISH/MADISON	4466889	0.2561	95
STONEWALL	15197571	0.8715	124
STONY MOUNTAIN	5668	0.0003	1
THREE FORKS	2037	0.0001	2
TYLER	14908944	0.8549	80
TYLER A	2937874	0.1685	7
WINNIPEG	138542	0.0079	3
WINNIPEG/DEADWOOD	32220	0.0018	6
WINNIPEGOSIS	9320480	0.5345	55
TOTALS	**1,743,873,545**	100.0000	10,245

Table 3. Cumulative oil production chart through 2009 from the North Dakota portion of the Williston Basin. The majority of historical oil production has come from the Mississippian Madison Group, particularly the Mission Canyon formation (modified from North Dakota Industrial Commission, Oil and Gas Division, 2009).

Mexico to Canada, and is thought to represent a second order sequence that lasted approximately 12 million years (Sloss, 1963). This sequence is capped by a major karsted disconformity that represents a hiatus of 5 to 34 million years (Sonnenfeld, 1996). This unconformity also corresponds to the top of the Kaskaskia Sequence (Sloss, 1963).

Through December 2009, the Madison Group had produced 905 MMBO, which comprises slightly more than one-half of the cumulative oil production in North Dakota. Total cumulative oil production from the North Dakota portion of the Williston is 1,743 MMBO (**Table 3**).

The Mississippian stratigraphic section, undisturbed in the Williston Basin, has an average thickness of 1000 ft (304 m) (**Figure 11)**. In the central core of the Red Wing Creek structure, the Mississippian stratigraphic section has a maximum thickness of 4000 ft (1219 m) due to structural repetition of the Madison Group. Three reservoir intervals are present at Red Wing Creek Field: the Mission Canyon, Charles, and Kibbey Formations (**Figure 10**). All three are Mississippian in age, but only the Mission Canyon and Charles Formations are present in the central core of the structure, which comprises 97% of the 17 MMBO produced to date.

The Mission Canyon Formation is primarily thick-bedded, fossiliferous, or oolitic limestone (**Figure 8**) interbedded with dolomites and anhydrites (Peterson, 1987). Toward the central part of the Williston Basin, the Mission Canyon Formation is primarily composed of crystalline limestone but the dolomite percentages increase toward the edges of the basin (Peterson, 1987). The depositional environment is

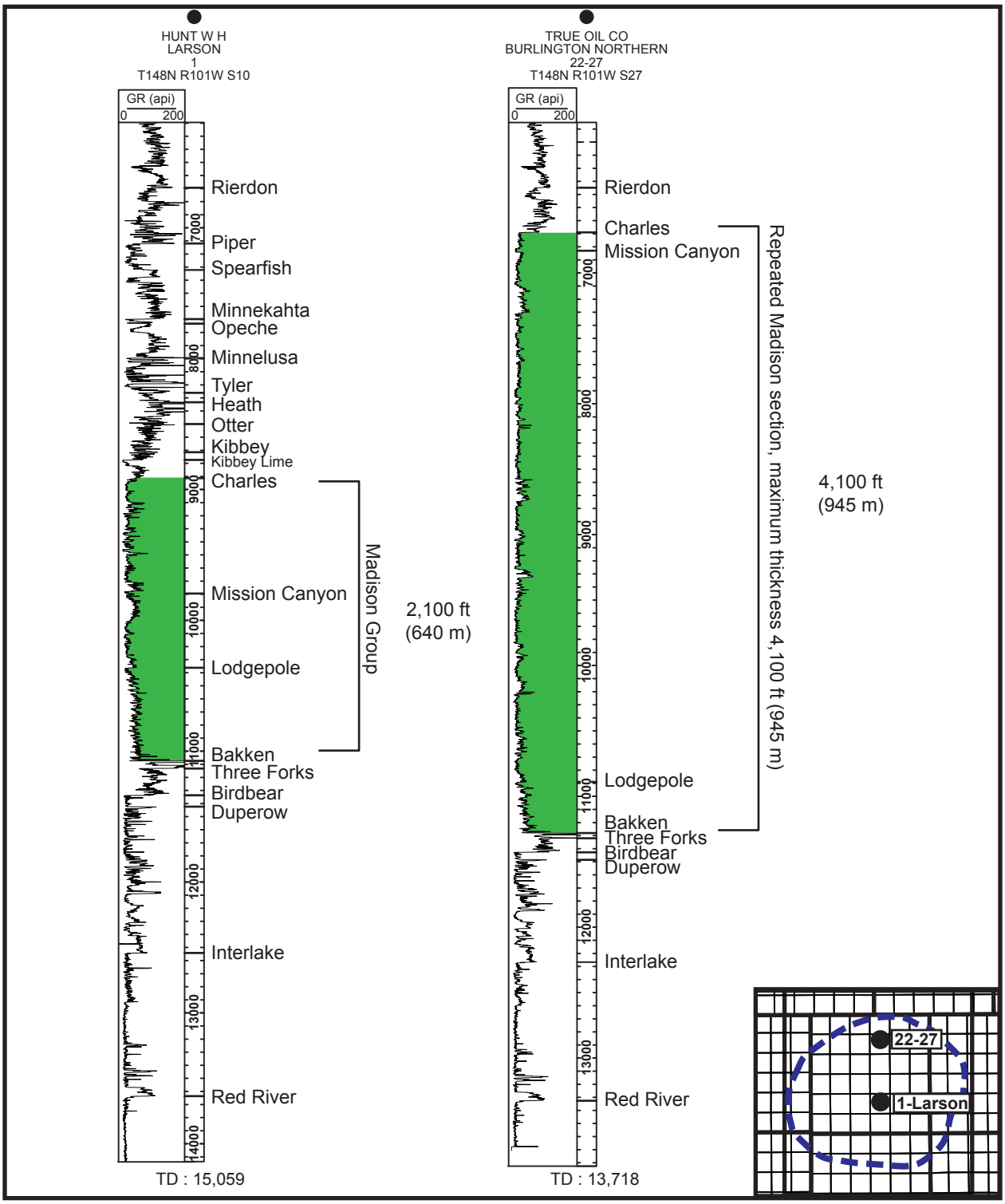

Figure 11. Comparison of GR log from the Larson 1 well (undeformed Paleozoic strata) with the BN-22-27 well (deformed Paleozoic strata) in the central core of the Red Wing Creek structure. Abnormal GR stratigraphic thicknesses are due to major repetition of the Mississsippian Madison Group. The Bakken to Interlake interval is thin due to the impact shockwave compression.The wells are approximately 3.2 miles (5.2 km) apart. Depths are measured depth. The logs are hung on the Jurassic Rierdon Formation.

interpreted to have been an open marine to coastal sabkha setting (Lindsay, 1988). The overlying Charles Formation is primarily interbedded limestones, shales, and evaporites (halite and anhydrite) that were deposited in a restricted marine environment. Importantly, the seismic velocities of the Charles Formation's evaporites are considerably slower than the Mission Canyon Formation.

The shallowest reservoir interval at Red Wing Creek is the Mississippian Kibbey Formation. The Kibbey primarily consists of shale, siltsone and sandstone deposited in a shallow marine setting (Peterson, 1987). In the middle of the Kibbey Formation, a regionally extensive carbonate unit is present that is referred to as the "Kibbey Lime." Production from the Kibbey Formation is rare in the Williston Basin, and the Red Wing Creek Field is one of the few locations that has a well producing from this interval.

Production at Red Wing Creek comes entirely from a fractured reservoir that has a permbeability of 30 to 50 mD. Matrix permeability of the reservoir is less than 1 mD of permeability (R. Barton, personal communication, 2009). The reservoir's drive mechanism is gas solution. The Mission Canyon reservoirs at Red Wing Creek produce through secondary porosity, which contrasts with this formation's production in most of the Williston Basin. Surrounding fields with an undisturbed Mississippian stratigraphic section commonly have oil columns that are less than 100 ft (30 m) thick. The anomalously thick Mississippian section in the brecciated central core, at Red Wing Creek, has an oil column up to 3,090 ft (942 m) thick with a net reservoir pay of 1,605 ft (489 m) (**Table 2)**. The original oil-water contact in the discovery well was at -7,600 ft (2316 m) subsea depth; as the field has been produced, the oil-water contact has risen to -7,400 ft (-2256 m) subsea depth and shallower.

Source Rocks and Oil Characteristics

Within the Williston basin, Paleozoic source rocks are present in the Cambrian, Ordovician, Devonian, Mississippian, and Pennsylvanian strata (**Figure 10)** (Peterson, 1995). Currently, no source rock studies have been done in Red Wing Creek Field, but the source has been interpreted as the Bakken shale due to regional source studies and oil occurrences within the field (R. Barton, personal communication, 2010).

Within the field, the oil has a 42.4° API gravity, a viscosity of 0.25 cp, and a reservoir temperature of 241° F (116° C). The original gas/oil ratio was 947CF/bbl:1 and the current GOR is approximately 2500SCF/bbl:1 (R. Barton, personal communication, 2009). Gas that is produced at Red Wing Creek is reinjected to maintain reservoir pressure. One unique aspect of the oil is the presence of dissolved salt (up to 2% by weight).

Seal

Because there has been no production from strata overlying the Upper Mississippian Kibbey Formation, the seal at Red Wing Creek has been interpreted as the evaporite facies within the Charles Formation (**Figure 8)**. Fracturing is interpreted to extend upward through the most brittle formations (i.e. limestones and dolomites) and does not extend into the more ductile formations in the field (evaporites). Importantly, a Triassic through the Middle Jurassic unconformity erodes the upper part of the deformed strata. The oldest formation that completely covers the entire crater is the Jurassic Rierdon and Piper Formations (**Figure 8)**.

ECONOMIC POTENTIAL OF IMPACT CRATERS AND CRATER TYPES

Economic Potential of Impact Craters

Lunar craters have been recognized for centuries. The cause of these features was debated until the mid 20th century. A meteor impact as a cause for terrestrial craters was first suggested in 1903 for Barringer Crater (Meteor Crater), Arizona (Barringer, 1905). The general consensus in 1903 and for decades to follow was that large craters were formed by explosive events that were attributable to volcanic activity (Hodge, 1994). The meteorite impact theory was still debatable until the late 1950's to early 1960's until scientists began to publish studies that illustrated the geologic process of cratering as a result of meteorite impact (Melosh, 1989).

Since the discovery of Barringer Crater, there have been 176 confirmed impact craters identified in the world (**Figure 12)** (Earth Impact Database, 2009), with an average of five new craters discovered per year (Grieve, 2005). The original interest in Barringer crater was for its economic potential, and as more terrestrial impact craters were discovered, the economic potential of these structures was recognized. Of the 176 confirmed craters, 35 are known to have some economic potential (petroleum and minerals), and 20 have actually produced some sort of economic resource (Grieve and Masaitis, 1994; Grieve, 1997). The latest estimate of the total value produced from impact-related structures in North America is estimated at $15 billion dollars per year from petroleum and mineral production (Grieve, 2005). Red Wing Creek Field is included in this list of petroleum producing impact structures with fields like the Newporte structure (**Figure 1)** in North Dakota (total reserves of 15 MMBO) and the Ames structure in Oklahoma. The Ames Structure's primary reserves are estimated to be up to 50 MMBO and 20 BCFG (Donofrio, 1997).

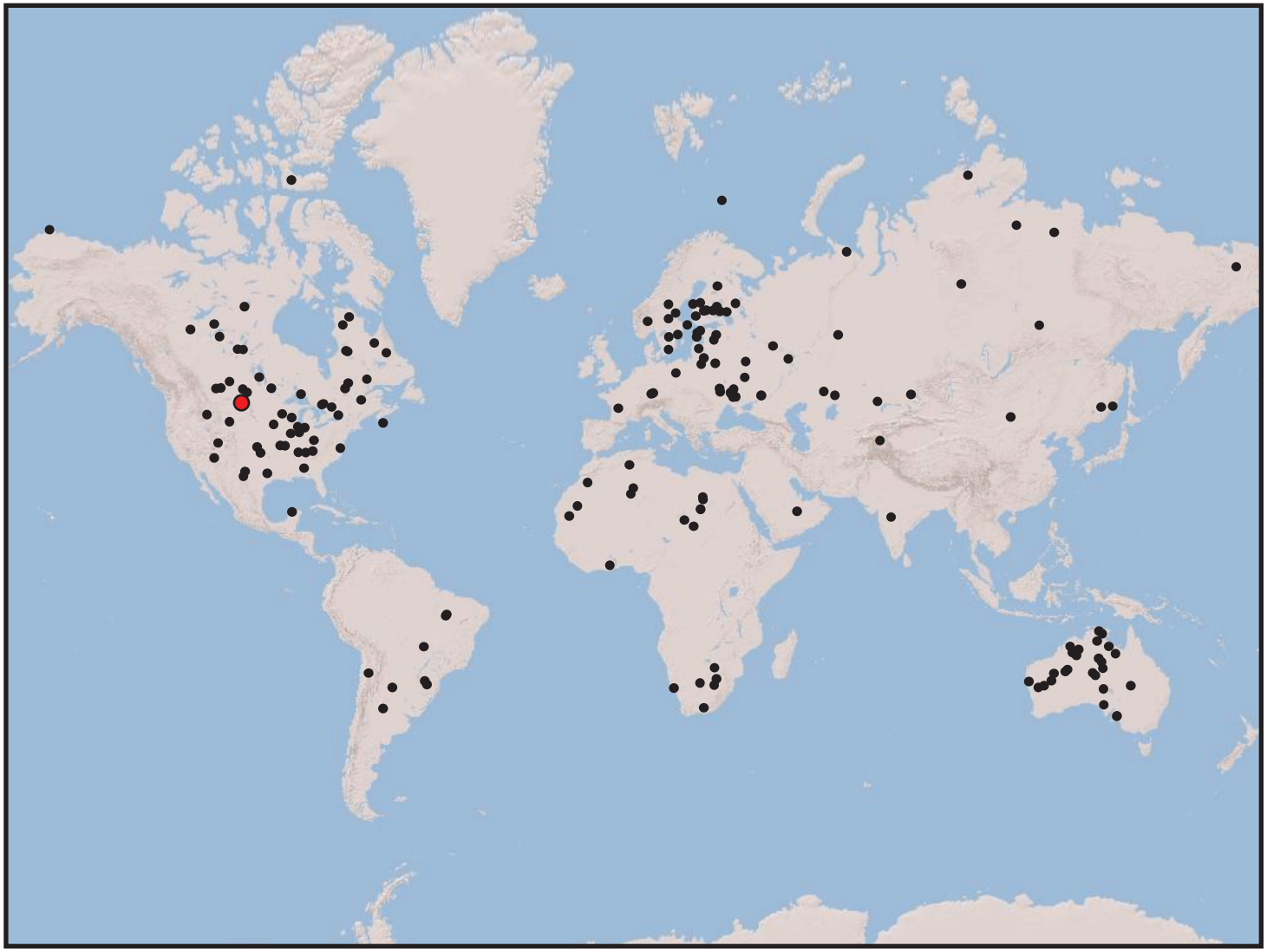

Figure 12. Locations of all confirmed impacts from the Earth Impact Database on a world topographic map (Earth Impact Database, 2009). Location of Red Wing Creek is highlighted in red.

The Cantarell Field of southern Mexico is the largest petroleum field associated with a meteorite impact. The reservoir formed by carbonate bank collapse that resulted from the seismic energy produced by the Chicxulub impact, which is approximately 220 miles (350 km) to the east (Grajales-Nishimura et al., 2000). The field is located in the Campeche Bank, offshore of southern Mexico, and produces from faulted Cretaceous-Tertiary carbonate breccias. Total primary reserves from this area are estimated to be as large as 30 billion barrels and 15 trillion cubic feet of gas (Donofrio, 1997). More than 60% of Mexico's daily production comes from Cantarell field. Grieve (2005) estimates that meteorite impacts and related structures in North America produce a total value of 15 billion dollars per year. The majority of this amount is derived from Cantarell Field.

CRATER CLASSIFICATION

Impact craters are classified according to their size and morphologies. The two main classifications are simple and complex meteor craters (Melosh, 1989). The final crater morphology is dependent upon the target lithology (sedimentary or crystalline), the diameter of the crater, and the surface gravity at the site of the impact. Simple craters, on earth, have a smaller diameter in comparison to lunar craters. Simple, lunar craters can have a much larger diameter than terrestrial craters before their morphology changes to a complex crater (Melosh, 1989).

Simple Craters

The smaller of the two major crater classifications is referred to as simple impact craters. On Earth, these often have a diameter that is smaller than 3-4 km (1.9-2.4 miles) depending upon the target rock lithology, and a symmetrical bowl shaped morphology with a raised outer rim **(Figure 13)**. Those simple impact craters, which have a purely sedimentary target lithology (non-crystalline target lithology), tend to have a smaller diameter. Where the diameter is larger, the crater's morphology changes to a complex impact feature (Osinski, 2006). In contrast, lunar craters with this morphology can be as large as 15 km (9.3 miles) before their morphology changes to a complex crater. Lunar crater's final depth: diameter ratio is usually about 1:5 (Melosh and Ivanov, 1999). Within the crater, there are few topographical features that disrupt the parabolic shape of the crater floor (**Figure 13)**. Coring of simple craters (e.g. Brent Crater in Ontario, Canada) has revealed that the crater fill is usually composed of broken rock debris and shock melted rock that is left over from the excavation of the crater cavity (Grieve, et al. 1977, Melosh and Ivanov, 1999). Volumetrically, the initial crater fill takes up one-half of the volume of space above the crater floor (Melosh and Ivanov, 1999). Because the brecciated crater fill is derived primarily from the crater walls, simple impact craters form by a collapsing event of the crater rim directly immediately after the initial excavation stage. The final crater rim edge is left at the angle of repose, which is approximately 30° (Melosh, 1989).

Complex Craters

Once craters reach a specific diameter, they begin to form a series of diagnostic morphological features that differentiate them from simple, parabolic-shaped craters (Melosh, 1989). The most diagnostic feature of these complex craters is the central

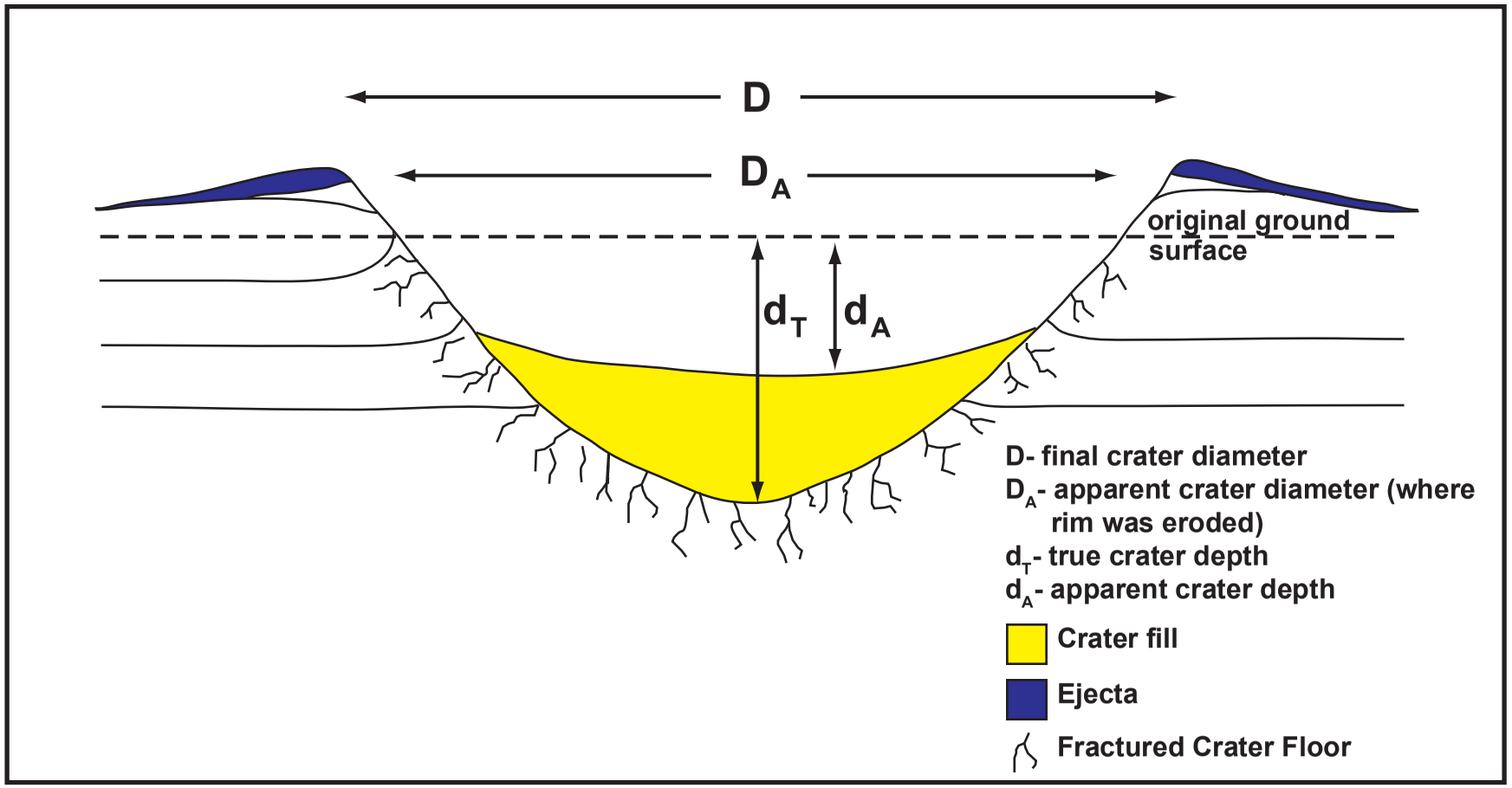

Figure 13. Schematic cross section of a simple impact crater. The crater fill is composed primarily of collapse breccia from the crater rim and melt rocks from the crater floor. Final simple crater depth to diameter ratio is usually close to 1:5 and the volume of the crater fill is approximately half of the crater volume (Modified from Osinski, 2006).

uplift or peak (**Figure 14)**. On Earth, the transition from simple to complex crater morphology occurs at diameter length of 2-4 km (1.2-2.4 miles) and is dependant on the lithology of the target rock (Grieve, 2006). The larger crater diameter results in a significant increase in the amount of collapse from the crater rim, and the largest confirmed terrestrial crater is the Vredfort impact in South Africa with a diameter that is estimated to be 250 to 300 km (155-186 miles) in length (Grieve et al., 2008). A complex crater on asteroid 4 Vespa is estimated to have a diameter as large as 460 km (285 miles) across (Melosh and Ivanov, 1999).

Unlike the diagnostic parabolic shape of simple craters (**Figure 13)**, complex impact craters develop several characteristic features within the crater and along the crater's rim (**Figure 14)**. The most notable features that form during complex crater collapse are a raised central uplift (**CU, Figure 14)** or peak, flat floors or troughs (**AT, Figure 14)**, and terraced, inwardly slumped outer rims (**OR, Figure14)**. The terraced outer rim forms by collapse after impact and consists of a series of concentric, linked normal faults (Melosh and Ivanov, 1999). The central peak is not composed of debris that has collapsed from the outer rim, rather is composed of rocks that sat at or below the crater floor and were uplifted to a height that is equal to approximately 8 percent of the crater's diameter (Melosh, 1989). The crater floor, or rim syncline, is filled by melted rock or an allochthonous breccia from the collapsing crater walls, which is similar to the crater fill that is observed at simple craters. According to these criteria, Red Wing Creek is a small, complex crater with a preserved central uplift, annular trough, and a raised outer rim (**Figures 15, 16)**.

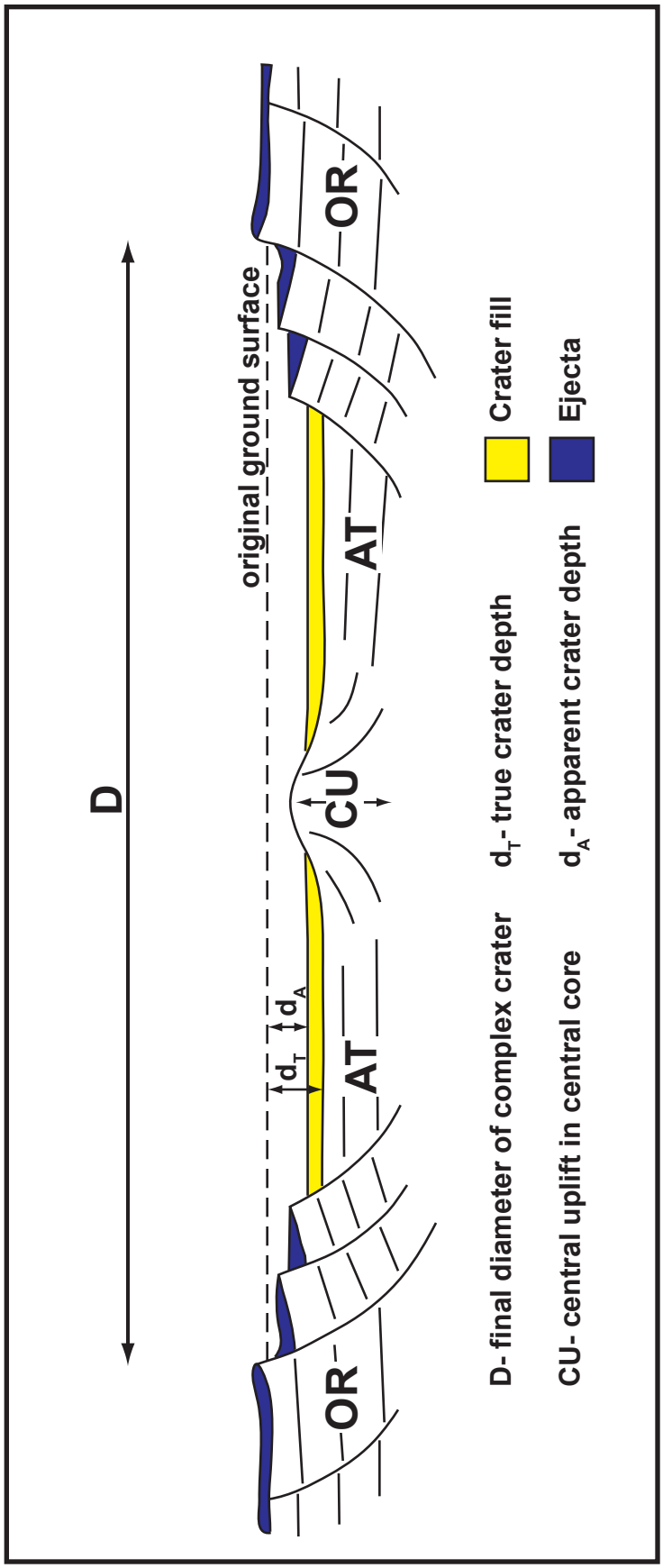

Figure 14. Cross section of a complex impact crater. Complex craters have three distinctive morphological features. The first is a raised, terraced outer rim (OR), a depressed annular syncline or trough (AT), and the central crater, which is usually expressed by a central uplift (CU) or peak (Modified from Osinksi, 2006).

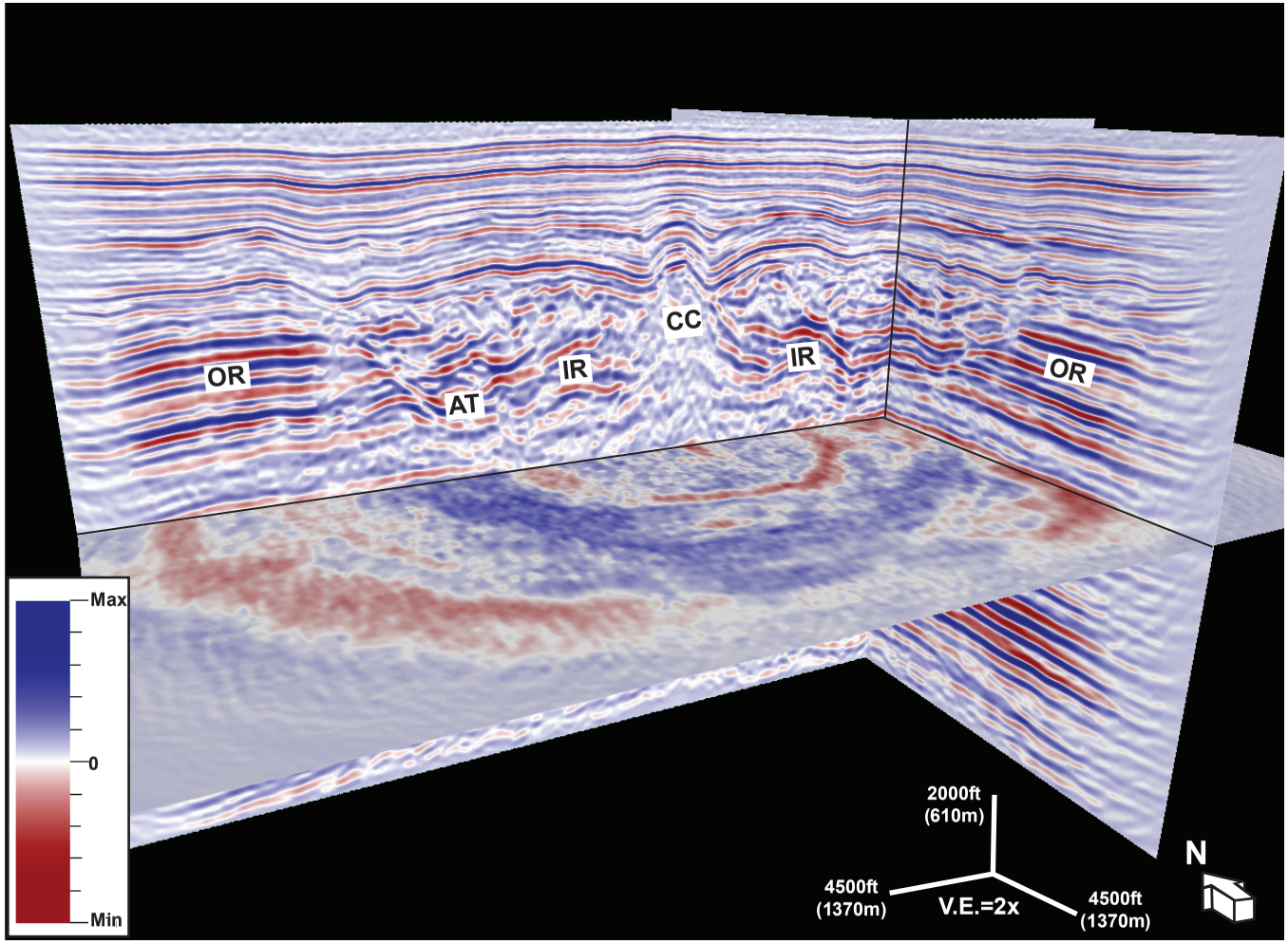

Figure 15. 3-D seismic chair display of the Red Wing Creek crater. The depth slice is at the Bakken Formation level below the crater. The vertical slice shows the transition from the undeformed, normal section outside of the crater to the highly deformed section within the crater. Key structural and geomorphic zones are annotated: outer rim (OR), annular trough (AT), and the central uplift complex consisting of the inner rim (IR) and central core (CC). Refer to Figure 17 for location of vertical seismic profiles.

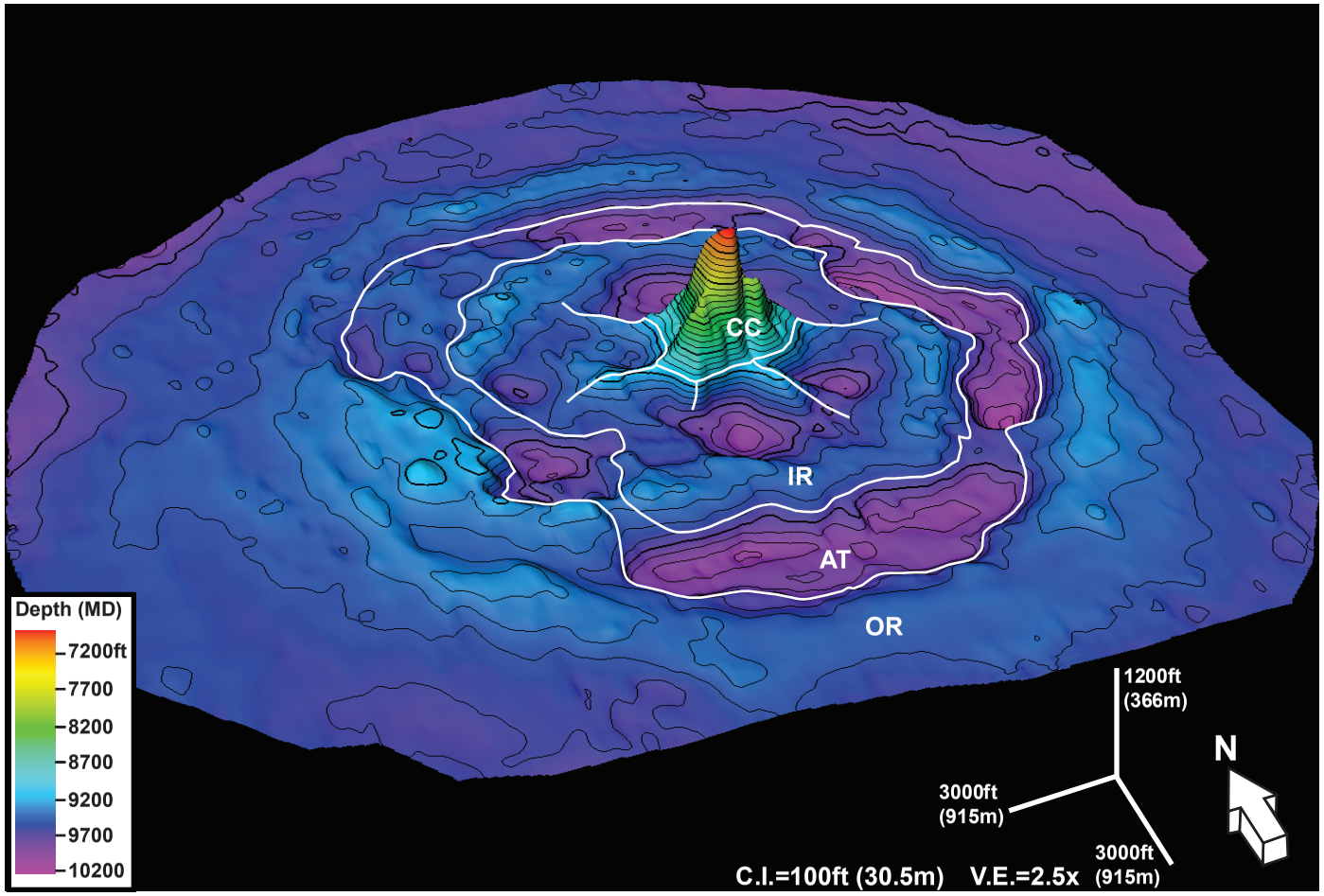

Figure 16. Three dimensional depth map of the top Mission Canyon Formation. In the central uplift, the surface represents the shallowest depth where the Mission Canyon is intersected by penetrating wells. Wells that penetrate the central uplift indicate significant repetition of the Mission Canyon interval resulting in an abnormally thick Madison Group section. At its shallowest depth, the Mission Canyon is uplifted 3000 feet (914.4) higher than the adjacent annular trough and more than 2000 feet (609.6) higher than the outer rim. Major structural zones and radial faults (represented by white radial lines) are annotated and outlined: outer rim (OR), annular trough (AT), and the central uplift complex composed of the inner rim (IR) and the central core (CC). At the Mission Canyon formation level, the radial faults don't reach the edge of the inner rim but transition to a radial fold as illustrated in Figure 47.

As the crater diameter increases due to continued crater wall collapse, the central uplift will also begin to collapse and form an uplifted inner ring, which occurs at approximately one-half of the rim diameter (**Figure 14)**. These complex crater morphologies are referred to as “peak ring craters” and have been observed on Earth, Mercury, Mars, Venus, and on the Moon (Melosh, 1989).

In addition to the two primary categories, some large craters can have additional rings than the amount of rings present in typical peak ring craters. For example, the Chicxulub crater in Mexico is one of a few terrestrial multi-ring craters (Morgan et al., 1997). In general, the formation of these features is due to a low-viscosity layer that exists below the crater floor (Melosh and Ivanov, 1999).

METHODOLOGY

Several methods were utilized to adequately describe and interpret the Red Wing Creek data set. The first method was a seismic attribute analysis used to detect high-angle faults in a depth-oriented view of the seismic attribute data. The remaining low-angle faults were interpreted in a vertical profile view of the seismic data. The next method was to integrate the well log and seismic data sets to make an accurate stratrigraphic interpretation, which honors the faults interpreted in previous methods. The final method was a series of seismic amplitude extractions, of the crater fill, to delineate discrete collapse blocks.

Seismic attribute analysis for structural interpretation

Due to the structurally complex nature of the Red Wing Creek structure, several different methods were used to adequately interpret the feature. Traditional

interpretation of vertical seismic profiles proved to be difficult because the distribution and length of the faults vary abruptly in three dimensions, due to the circular fault pattern. By interpreting seismic attributes in plan view, individual faults can be mapped and fault orientations can be better recognized and interpreted.

Two workflows utilizing seismic attributes were used to map high-angle faults around the Red Wing Creek structure. The initial input for these workflows was a 3-D PSDM data set that had undergone principal component processing (PC-Filt). The PC-Filt volume was used for seismic interpretation because this processing method reduces noise in the seismic data set while preserving amplitude discontinuities. The final product is a 3D seismic volume where amplitude edges have been preserved (**Figure 15)**. Amplitude edge preservation is particularly important in this data set due to the highly faulted nature of the Red Wing Creek structure.

From the PC-Filt PSDM volume, a coherency-like volume was generated. This attribute, referred to as the Edge Stacked attribute (**Figure 17)**, is similar to coherency, which is a measurement of seismic waveform similarity through cross-correlation and semblance (Chopra and Marfurt, 2007). The Edge Stacked attribute is effective in delineating breaks in continuity in plan view; however, these breaks are often discontinuous vertically and interpreting continuous fault surfaces using the coherency attribute accurately is difficult. For faults to be picked from the coherency-like data, the coherency breaks must be aligned in depth to represent a fault surface. For this first workflow, the linear discontinuities are traced in vertically and laterally to form a relative probability fault-enhanced volume (**Figures 18, 19)**. The continuity along probable fault planes is enhanced and discontinuities unrelated to faulting are removed (Dorn et al.

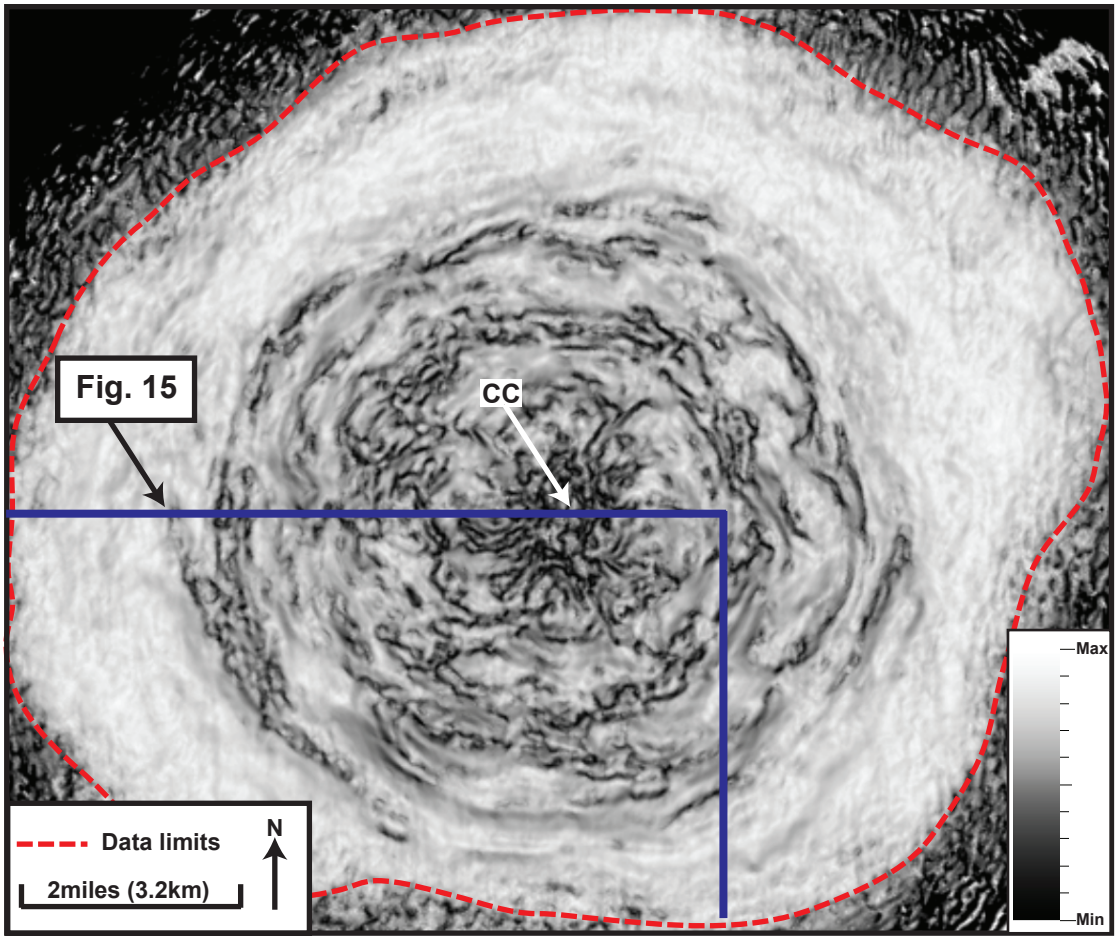

Figure 17. Plan view of the Edge Stacked seismic attribute at the Mississippian Mission Canyon Formation level. This attribute is similar to the coherency attribute because it measures seismic waveform similiarities. The dark lineations mark breaks in similarities or faults and are assigned low values. The lighter zones represent higher similarity values or no faulting. The red dashed lines indicates the limits of the 3-D seismic survey. The dark blue lines indicate the locations of the vertical seismic profiles illustrated in Figure 15. Note the chaotic nature of the edge stacked attribute within the central core (CC). This is indicative of the poor seismic quality present in this structural zone. Therefore, an accurate structural interpetation within the central core wasn't possible.

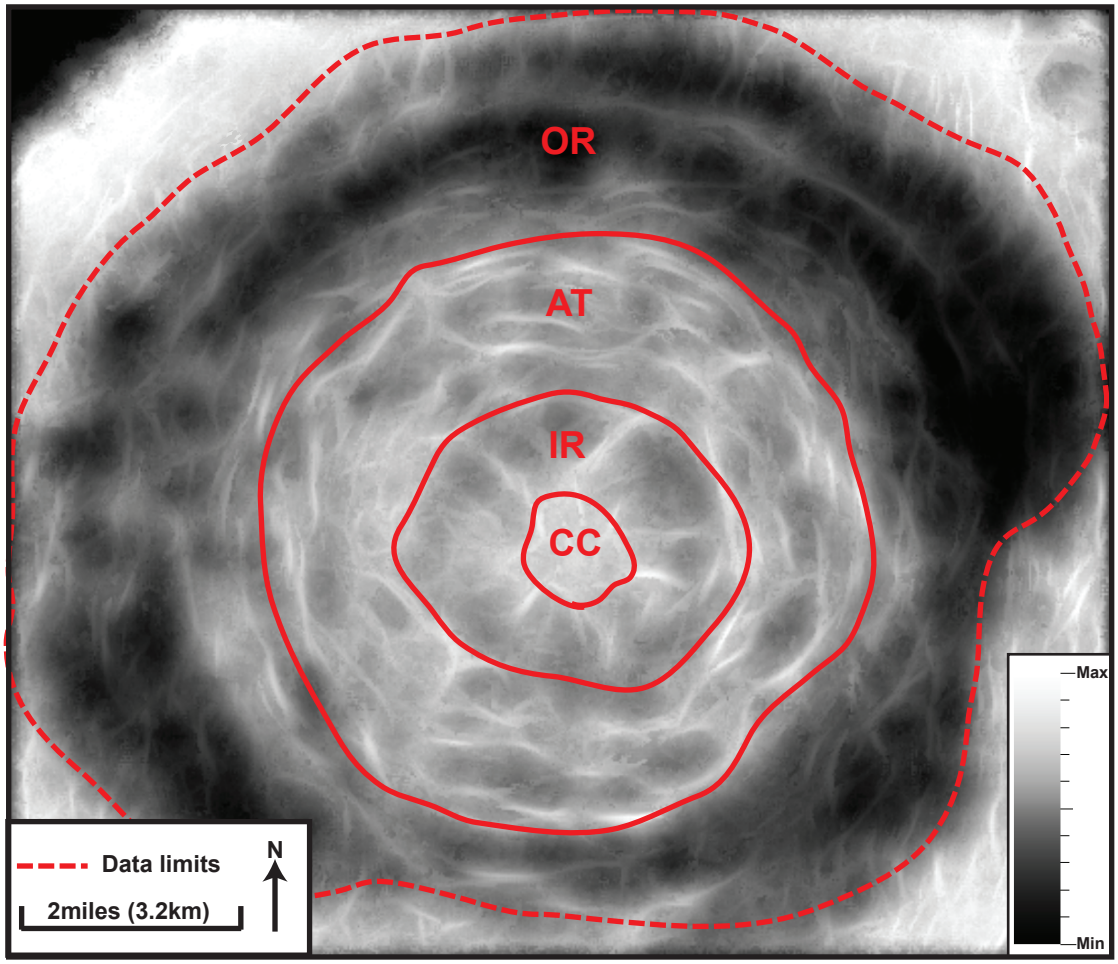

Figure 18. Fault enhanced seismic attribute in plan view at the Mississippian Mission Canyon Formation level. The fault enhanced attribute is a relative probability volume that aligns breaks in coherency into continuous fault surfaces. Lighter values represent those zones where breaks in coherency have been traced in depth and in azimuth and align to form a fault surface. The red dashed line indicates the limit of the 3-D seimic volume. Major structural zones are annotated: OR (outer rim), AT (annular trough), IR (inner rim), and CC (central core).

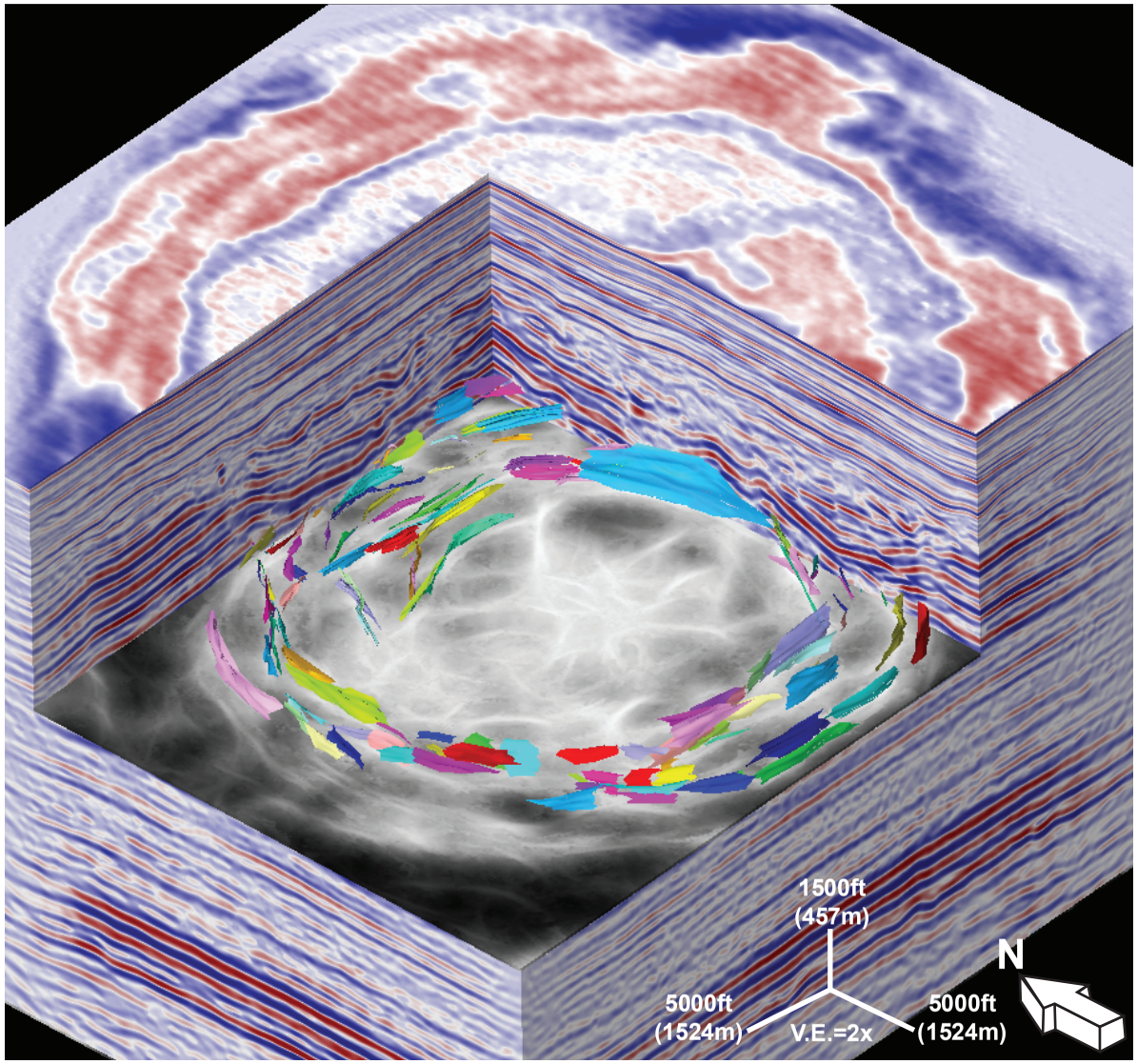

Figure 19. Seismic chair display of the fault enhanced seismic attribute at the Mississippian Mission Canyon Formation level with intersecting faults present at the crater rim boundary. This attribute was used to interpret high angle faults within the crater.

2005). High-angle faults were then interpreted from the fault enhanced attribute from the crater rim to the central uplift of the crater.

The second workflow used for structural interpretation of high-angle faults was the Ant Tracking algorithm (**Figures 20, 21)**. As with the fault enhanced attribute, the basic input was a coherency-like attribute that detects breaks in continuity within the PSDM data set. This algorithm searches for the shortest path in three dimensions to the next coherency break. The final product is a volume where adjacent breaks in coherency have been connected to form continuous fault surfaces and to eliminate features associated with stratigraphic heterogeneities (Chopra and Marfurt, 2007). Overall, these two structural attribute methods generated similar results, but still were complementary; cumulatively, the methods provided a more complete and detailed structural picture along the Mississippian reservoir level.

Although the described structural attribute methods are effective in detection and interpretation of high-angle faults, their usefulness is limited in detection of low-angle structural features. Within the Red Wing Creek structure, there is a mixture of high-angle normal faults, high-angle thrust faults, and low-angle thrust faults. The low-angle thrust faults are not detected with the Fault Enhanced or Ant Tracking attributes because they are most likely seen as discontinuities related to stratigraphy and are filtered out. Traditional interpretation on vertical seismic profiles is the only method that was utilized to accurately interpret these low-angle, structural features.

Well-to-Seismic Ties

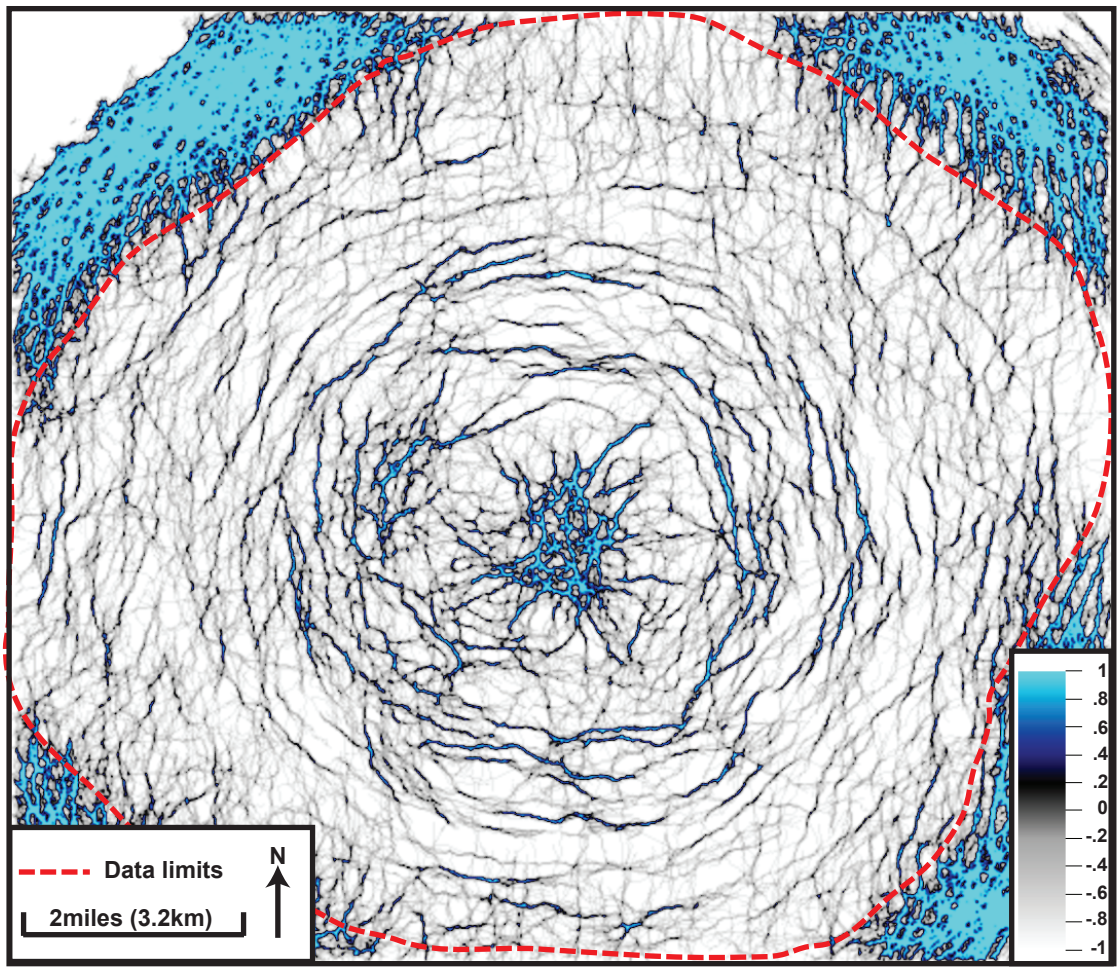

Figure 20. Plan view of aggressive Ant Tracking seismic attribute at the Mississippian Mission Canyon Formation level. The Ant Tracking algorithm takes a coherency-like attribute as the input and connects the zones of low coherency in depth. The blue zones on the attribute slice are indicative of a connected zone of low coherency or a fault. Along with the fault enhanced attribute, the Ant Tracking seismic attribute was utilized to interpret high angle faults within the crater. This attribute also illustrates the chaotic nature of the seismic data within the central uplift.The red dashed line indicates the limits of the 3-D seismic volume.

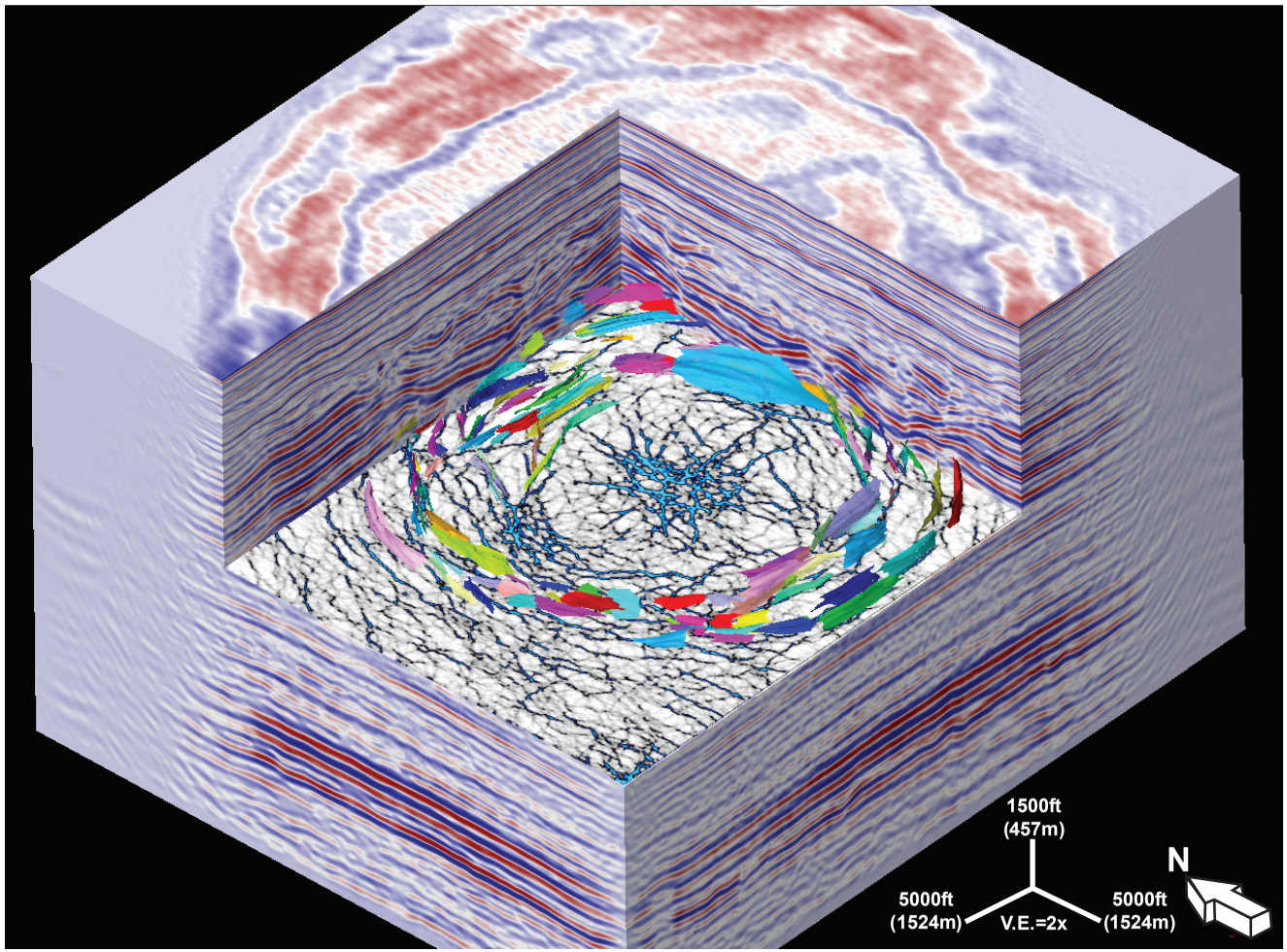

Figure 21. Aggressive Ant Tracking attribute chair display at the Mississippian level with a sampling of interpreted, high angle faults within the crater.

Accurate well-to-seismic ties are crucial for an accurate structural interpretation in highly deformed areas. Wells were initially correlated to the seismic, and the corresponding formation tops were then correlated throughout the seismic data set. No synthetic seismograms needed to be generated to tie the wells to the seismic data set. In general, there were few inconsistencies between the formation tops and the regionally correlated horizons, and where inconsistencies were present, the mis-tie was within one seismic reflection (**Figure 22**). If a well-to-seismic correlation was questionable, the well tops in the remainder of the field were used as a reference as to where the stratigraphic top should correlate with the seismic survey.

There is one zone where the discrepancy between the seismic and well ties is so great that the seismic data are ignored altogether. Specifically, the #22-27 well is located in the center of the central core (**Figure 3)** and penetrates as deep as the Ordovician Red River Formation. Inconsistencies between the well and seismic data that are as great as 500 feet (152m), and the well data indicate that there is a significant depression instead of an uplift beneath the central core (**Figure 23)**. This mistie occurs directly beneath the central core where there is an apparent seismic “pullup”, i.e. a decrease in the depth of the seismic reflection. This “pullup” was first noticed in the original 2D, time based seismic data in the early 1970’s and was attributed to the lack of Mississippian evaporites within the central core. Because the central core consists primarily of Mississippian carbonate strata, the seismic velocities are considerably faster than in the rest of the field where evaporites are present. The localized area of higher velocities is responsible for the data pullup seen in time based seismic surveys over Red Wing Creek. When the pre-stack depth migration processing was done, this pullup

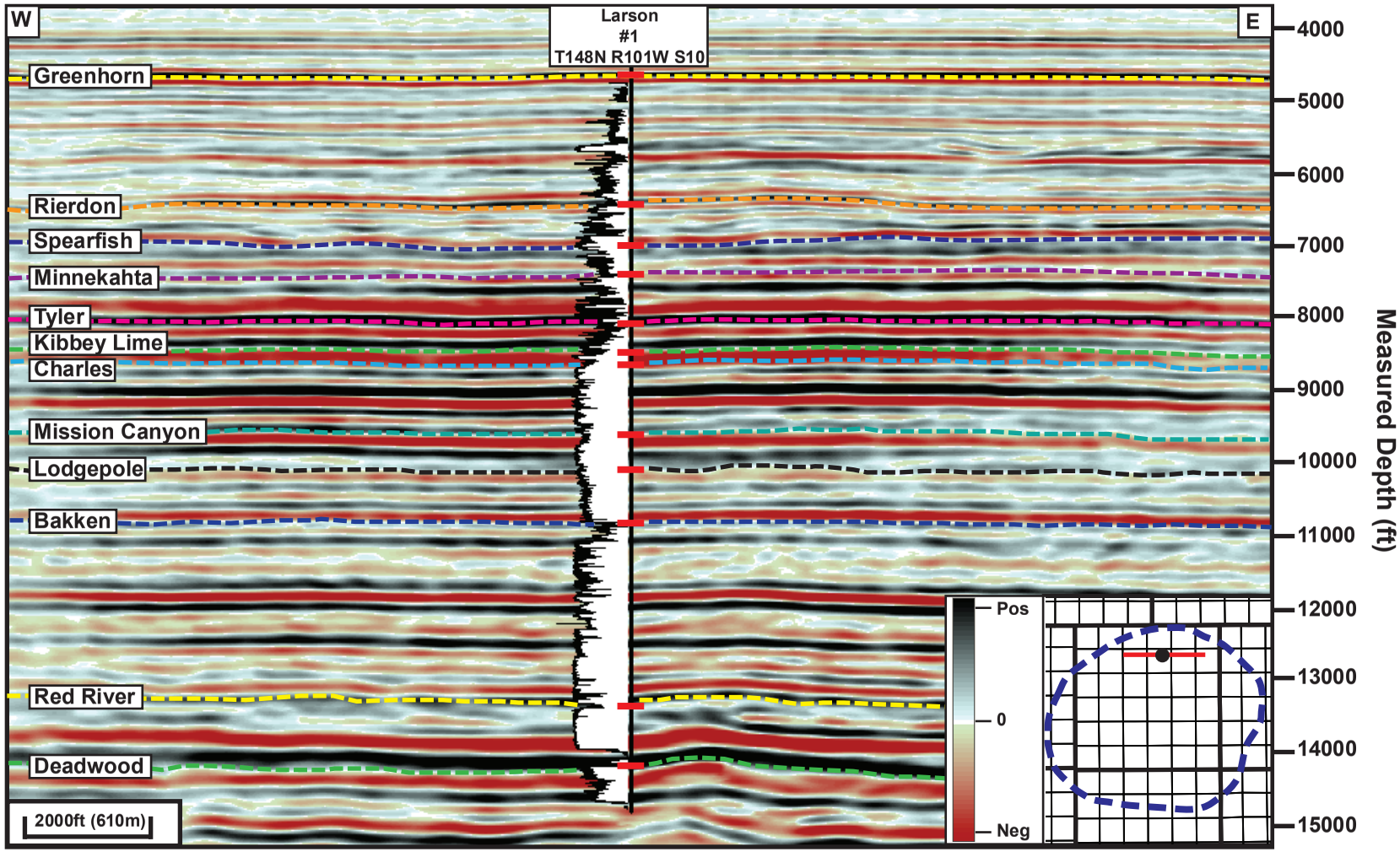

Figure 22. Seismic profile showing key stratigraphic horizons and how they tie the GR log from the Larson #1 well. Most well to seismic ties, across the field, were consistent within one seismic reflection. The index map shows the location of the vertical seismic profile. The blue dashed line on this and following maps represents the limit of the seismic data set.

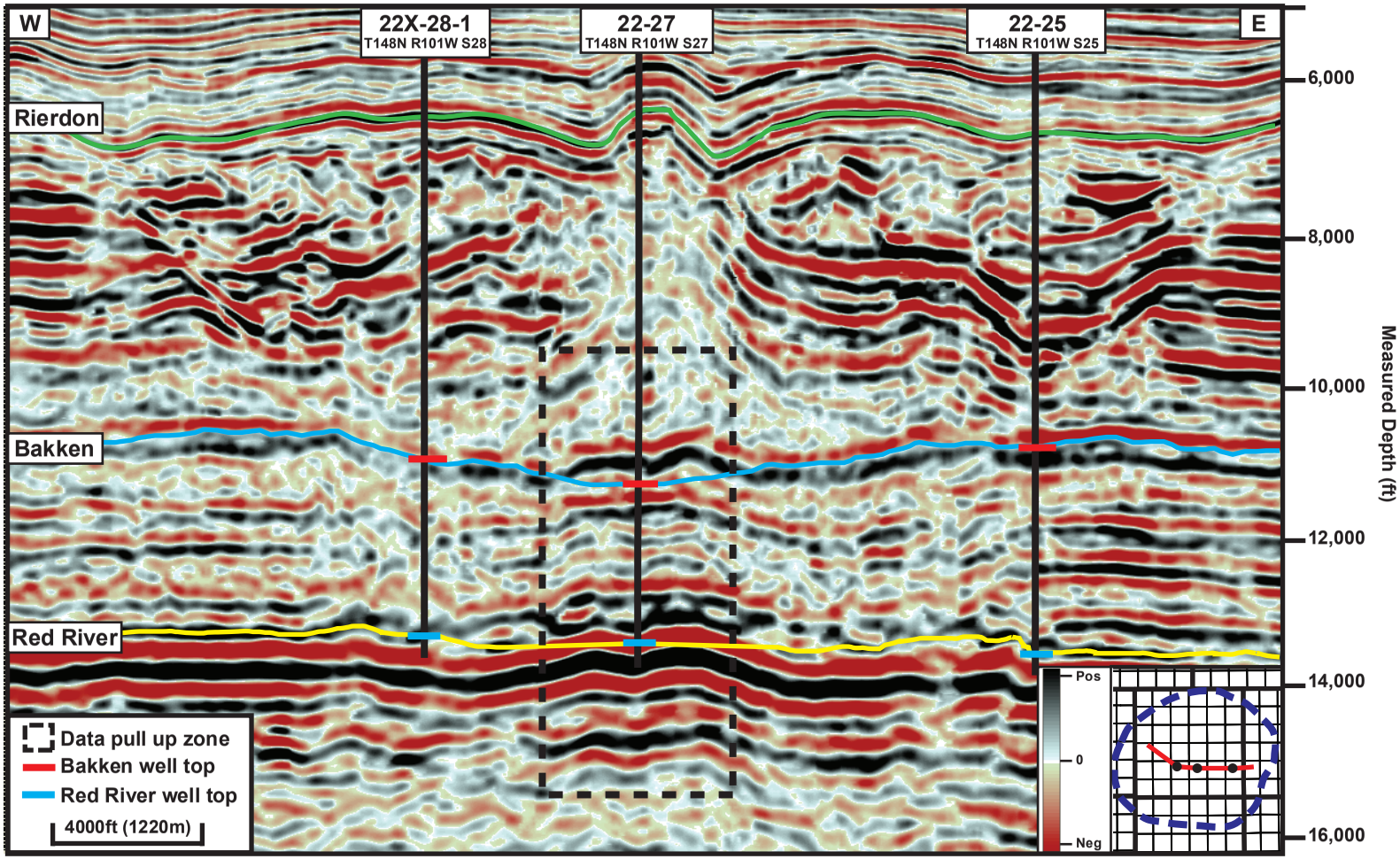

Figure 23. Seismic profile across the crater shows a seismic data pull-up beneath the central core. Stratigraphic tops from the 22-27 well show that the top of the Bakken Formation is actually depressed beneath the central core. The PSDM data shows a major uplift of these stratigraphic levels beneath the central core and should be ignored. The location of the seismic profile is shown in the landgrid map.

below the central core was not resolved and remains in the current depth volume. Thus, this pullup should be ignored as a migration artifact in following images throughout this thesis.

Crater-fill interpretation

The shallowest interval that is studied in detail is the crater-fill strata that lie on the crater floor. The crater-fill strata consist primarily of collapse blocks derived from the uplifted crater walls that formed during modification. To accurately delineate the extent and geometries of the collapse blocks, a volumetric attribute method was needed. Because there were multiple stages of collapse from the crater wall, collapse blocks are dipping at different angles. The blocks that directly overlie the crater floor are primarily dip concordant with the underlying strata. For these blocks, the seismic data set was flattened on the crater floor and dip magnitude and dip similarity attribute volumes were generated to image the extent of the collapse blocks. The overlying blocks, in contrast, are not dip concordant with the crater floor, and therefore the attribute volume crosscuts the amplitude data.

To compensate for the varying dip angles of the collapse blocks (**Figure 24)**, a volumetric amplitude extraction was generated from the flattened crater floor (at the base) to the overlying, draping Jurassic strata (at the top). By measuring the maximum amplitude from the crater floor to 400 feet above (122m), the extent and geometries of all of the collapse blocks that fill the crater were imaged. The amplitude extraction was verified by manually picking each collapse block separately in the seismic volume.

DESCRIPTION

Figure 24a. Uninterpreted seismic profile of the eastern crater floor that corresponds with Figure 24b. Location of seismic profile is show in index map.

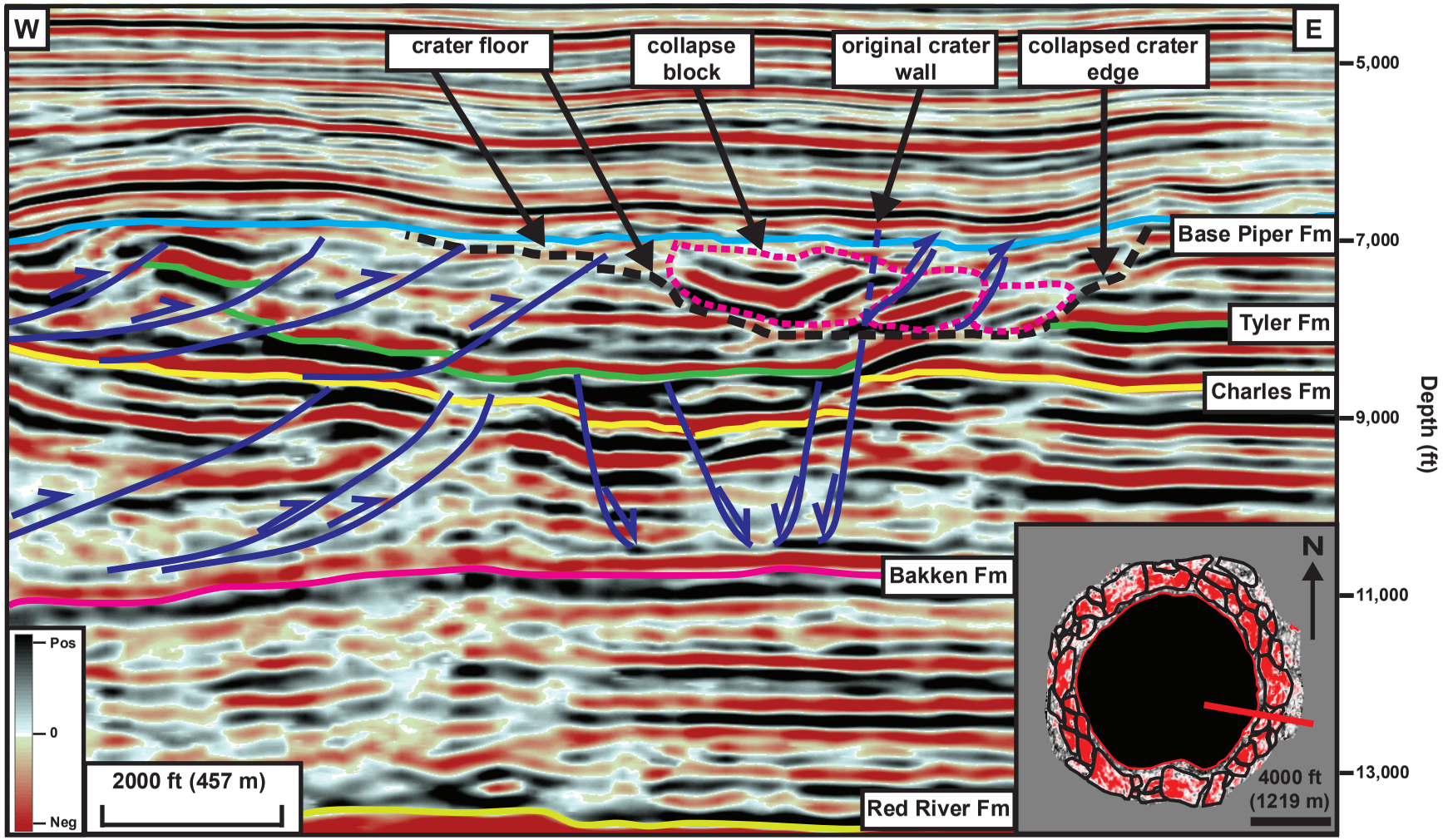

Figure 24b. Seismic profile of the eastern crater floor. The crater floor is deformed by outward directed, imbricate thrusts that detached at the Charles Formation level. The high amplitude collapse blocks were derived from the oversteepened crater wall and their inner limit is controlled by the topography of the crater floor that rises toward the central uplift. The dashed pink polygons indicate the edges of individual collapse blocks. Location of seismic profile is show in index map.

The complexity of the Red Wing Creek structure affects three discrete stratigraphic levels with associated abrupt changes in structural styles. Thus, the deformed area will be described in discrete stratigraphic levels, and then further subdivided according to structurally or morphologically significant features. The section underlying the primary impact structure, which shows some deformation, is described first. Stratigraphically, this section ranges from the Ordovician Red River Formation to the Devonian Bakken Formation (**Figure 23)**. The middle zone contains the primary structure of the Red Wing Creek impact; this zone extends from the top of the Bakken Formation to the Permian-Triassic Spearfish Formation (**Figure 25)**. The upper zone represents the crater fill and includes the Middle to Upper Permian section to the overlying Jurassic strata.

Lower Zone-Red River to Bakken Formation

The isopach map of the Red River to Bakken interval in the study area reveals several regionally extensive trends (**Figure 26)**. First, the interval thins from the northeast to the southwest of the study area. Second, a localized thin in the southwestern portion of the field that is due to a structural high at the Ordovician level whose expression decreases shallower in the section. The last and most significant trend is the central portion of the interval that is approximately 400 feet (122m) thinner than surrounding areas (**Figures 26-30)**.

The Middle Ordovician to Upper Devonian section shows some evidence of deformation due to the impact, but the majority of this section is unaltered and resembles the regional stratigraphic patterns seen elsewhere in the basin. Ten wells

Figure 25a. Uninterpreted seismic profile through northern crater floor. Location of profile is show in the index map.

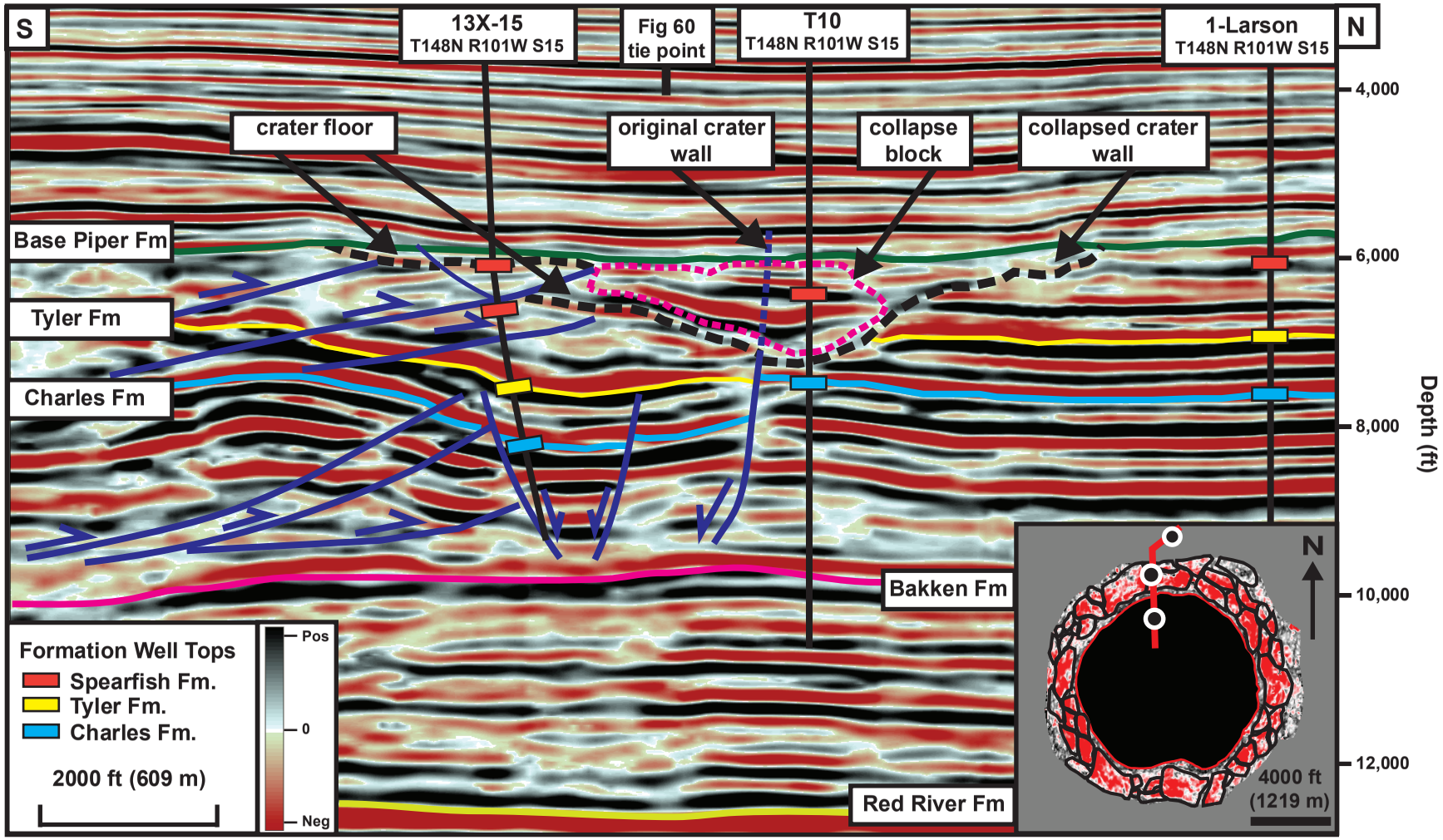

Figure 25b. Seismic profile through northern crater floor. Well data shows that the anomalously thick Permian Spearfish Formation in well 13X-15 is due to the imbricate thrust faults that detach within the Charles Formation. The well data from the T10 well shows that the collapse blocks are derived from the Permian stratigraphic section that was present in the oversteepened crater wall before it collapsed. The normal stratigraphic section is shown in the 1-Larson well that intersects the outer rim. Location of profile and wells is show in the index map. Also, location of tie point with with the seismic profile shown in Figure 60b is annotated.

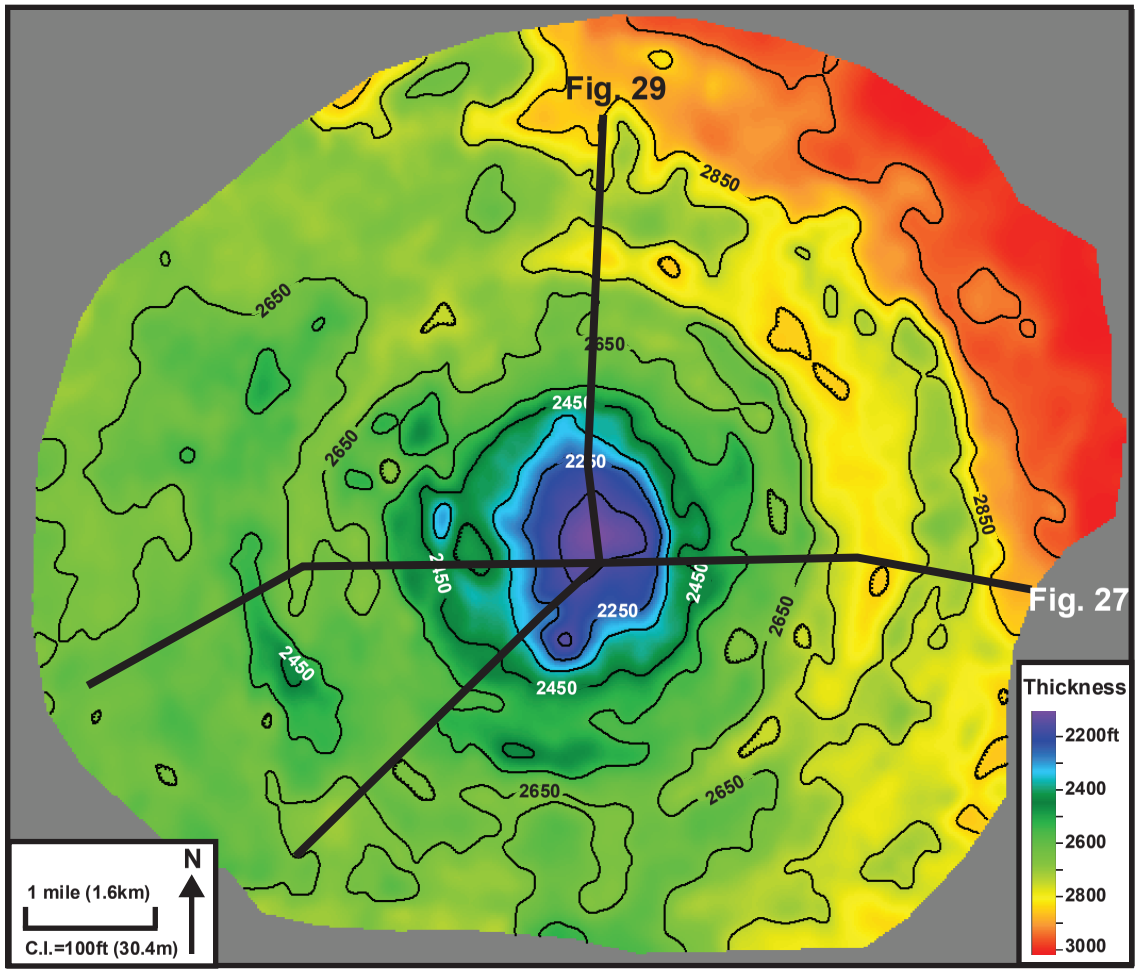

Figure 26. Isopach map of the top Red River to top Bakken Formation.This isopach illustrates the compression that has occured within the Upper Devonian stratigraphic section below the crater. The section below the Souris River formation, which includes the Red River Formation, appears to be relatively undisturbed by the shock-wave that compressed the overying strata. Black lines represent the locations of well log sections in Figures 27, 29.

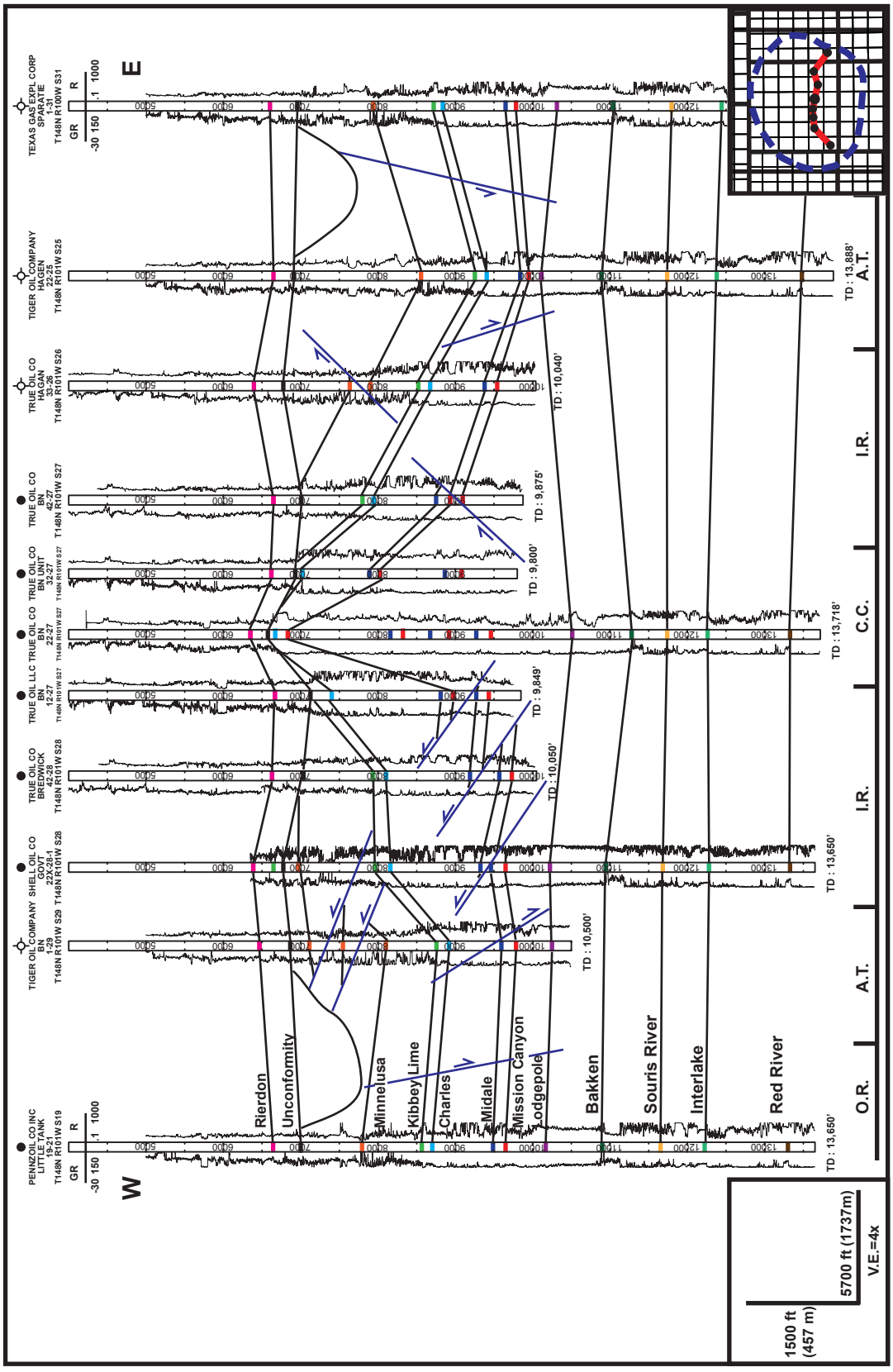

Figure 27. Well log cross section across Red Wing Creek crater. The wells show evidence of stratigraphic repetition, which correlate to mapped thrust faults in the 3-D seismic data. Within the central uplift, well data indicates that there are multiple levels of repetition of the Madison Group. Location of cross section and wells is shown in the index map. Major structural zones are annotated: outer rim (O.R.), annular trough (A.T.), inner rim (I.R.), and central core (C.C.).

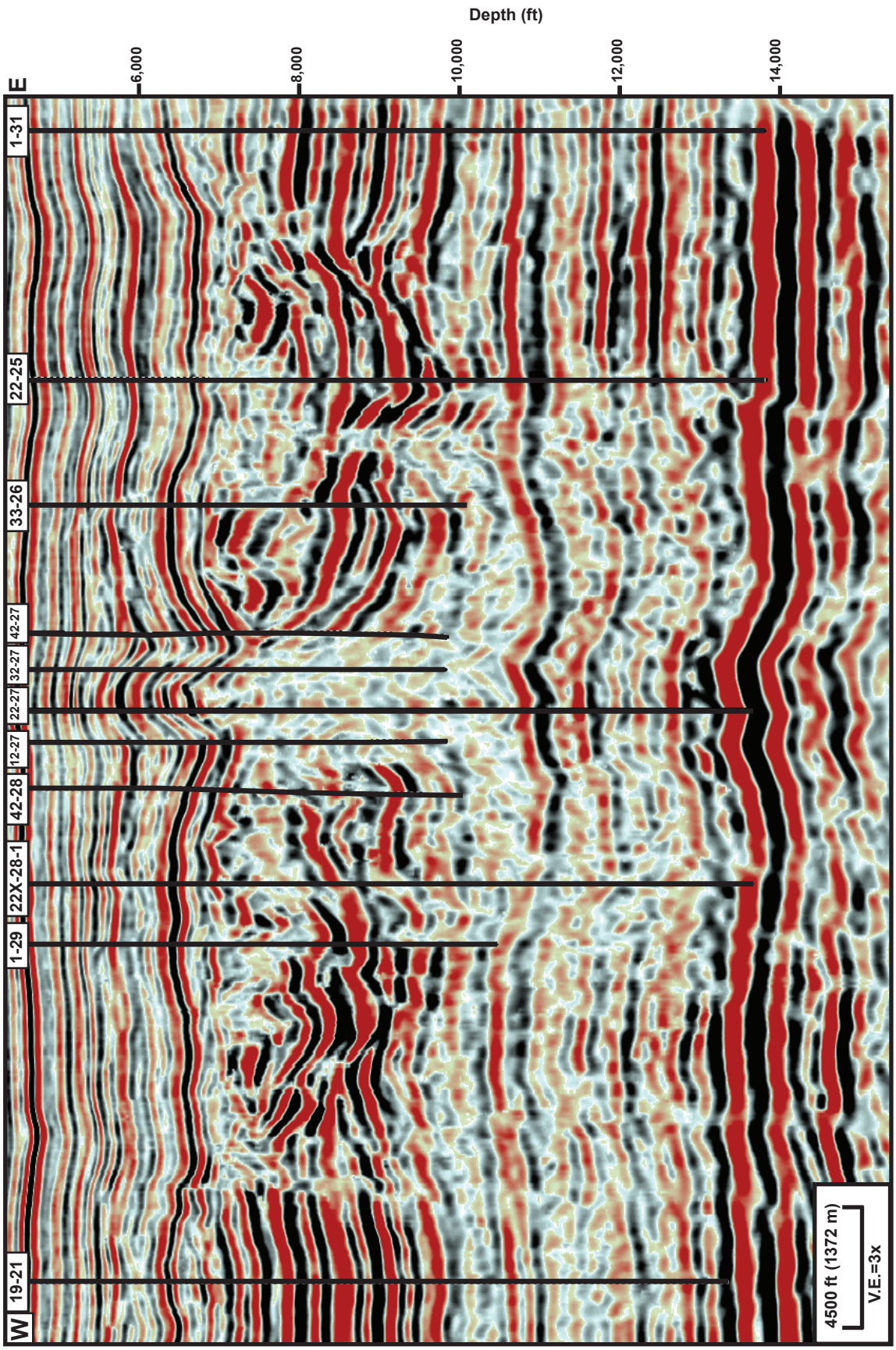

Figure 28a. Uninterpreted seismic profile that corresponds with seismic profile in Figure 28b. Refer to Figure 27 for profile location and orientation.

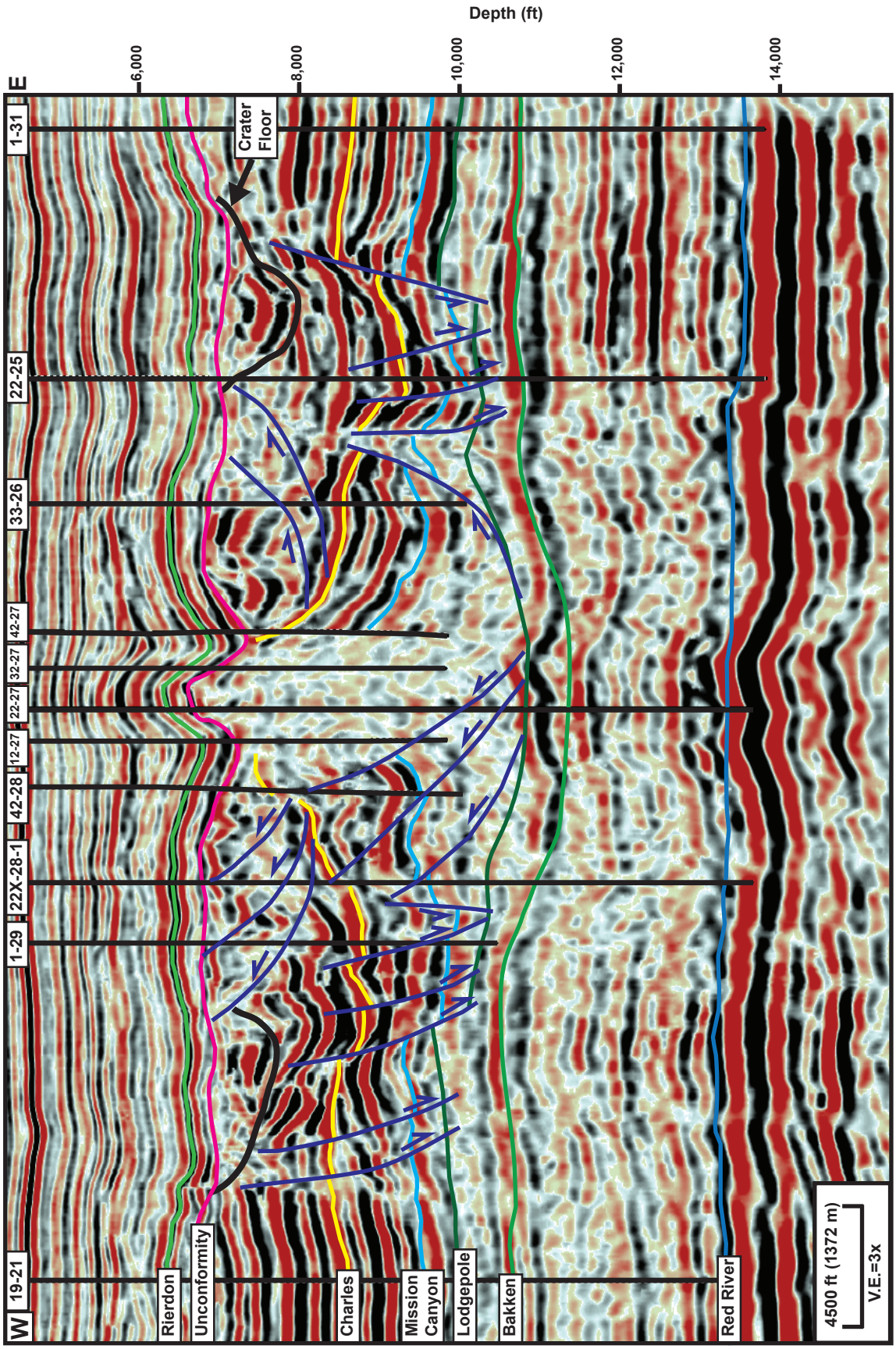

Figure 28b. Interpreted seismic profile that corresponds with the log cross section in figure 27. Refer to Figure 27 for profile location and orientation.

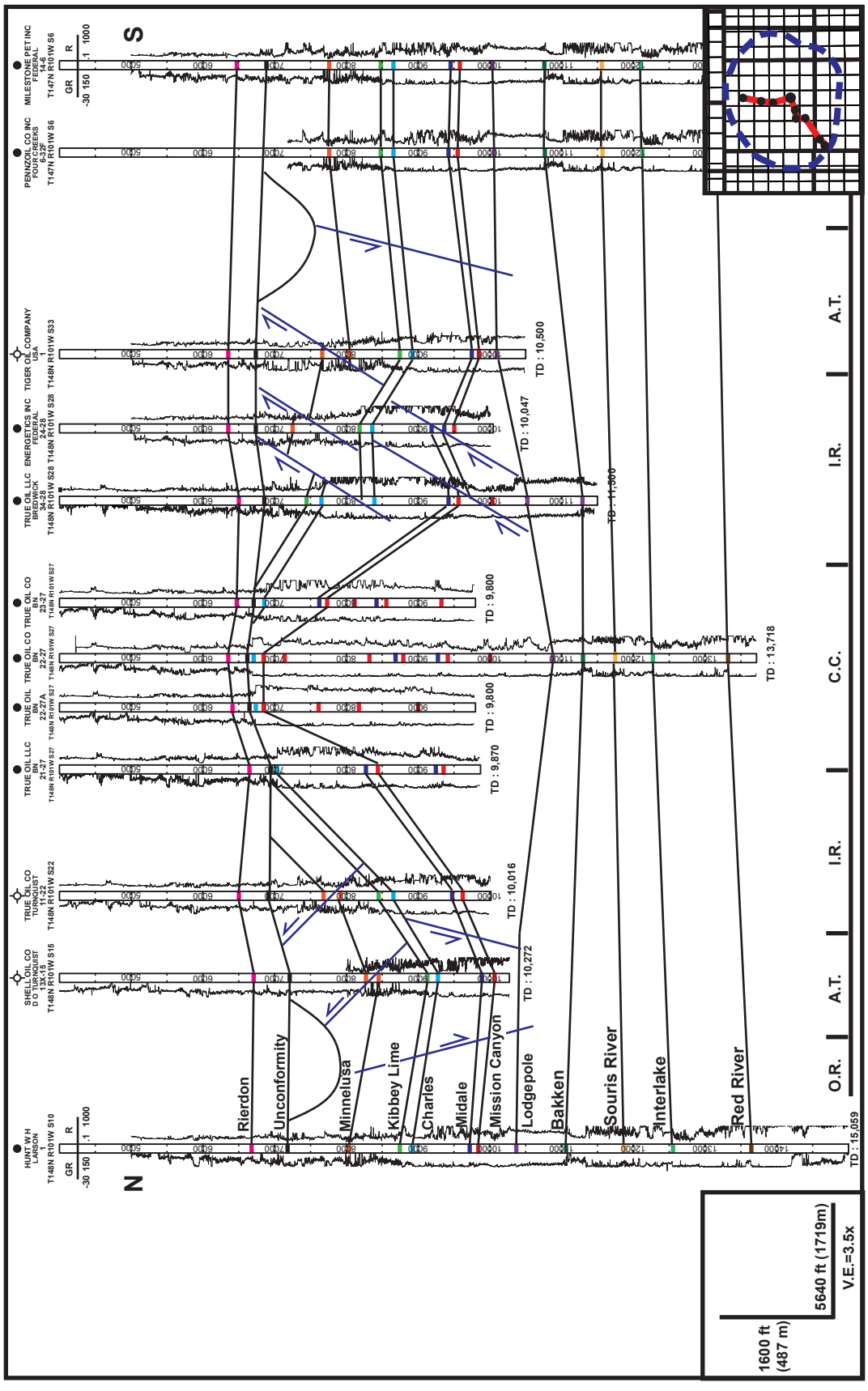

Figure 29. North to south well log cross section across Red Wing Creek. Well data indicates stratigraphic repetition and thrust faulting at the Lodgepole and Charles detachment levels. The central core is composed entirely of the Mississippian Madison group. Due to the quality of the seismic data in this zone, the structural nature of the central uplift can't be determined, but structural studies of other complex craters indicate high angle reverse faulting within this zone. Major structural zones are annotated: outer rim (O.R.), annular trough (A.T.), inner rim (I.R.), and central core (C.C.).

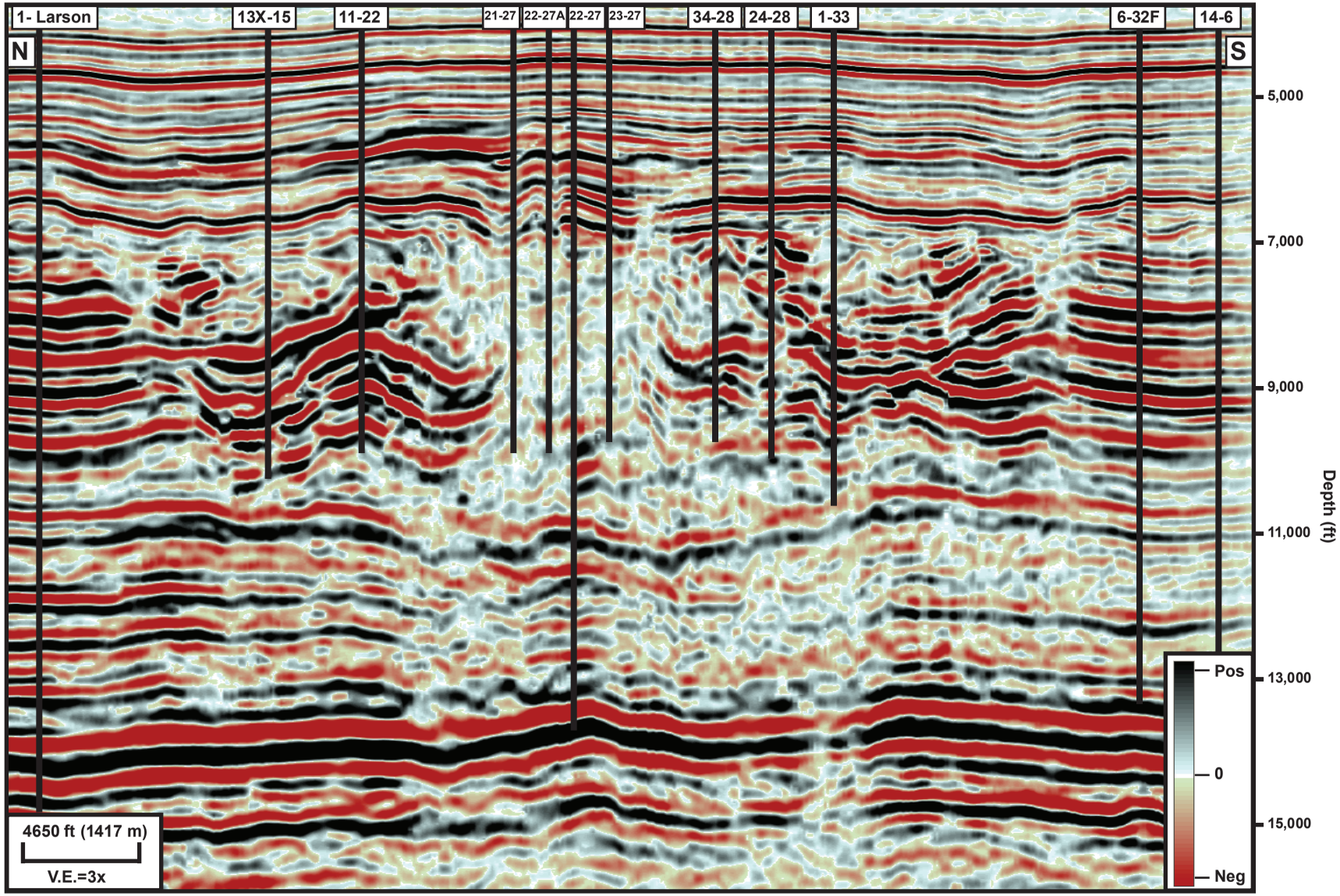

Figure 30a. Uninterpreted seismic profile that corresponds with the seismic profile in Figure 30b. Refer to Figure 29 for location and orientation of seismic profile.

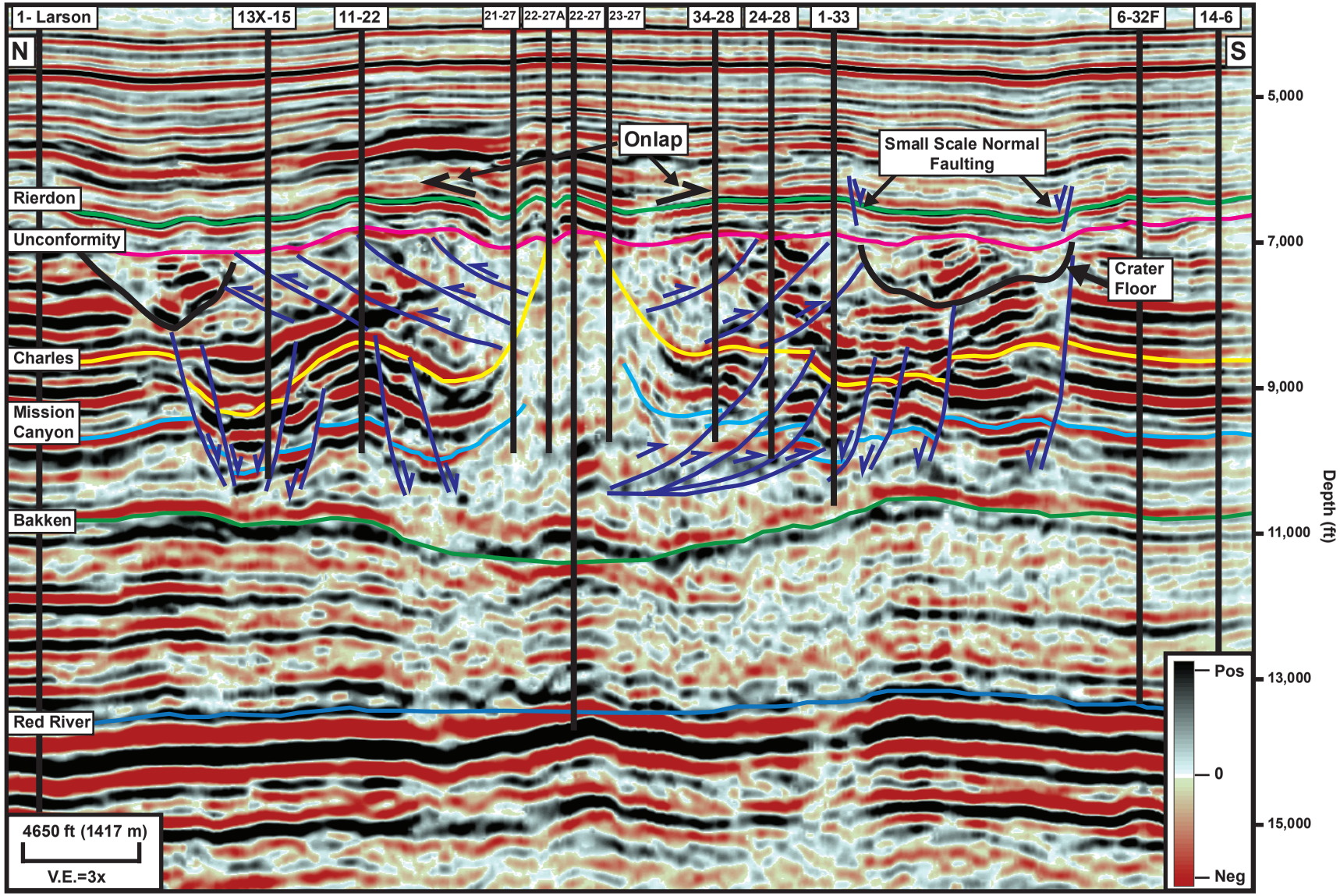

Figure 30b. Seismic profile that corresponds with log cross section in Figure 29. Stratigraphic repition seen in the 13X-15, 11-22, 34-28, and 24-28 corresponds to mapped thrust faults in the 3D seismic volume.The profile location is annotated in Figure 29.

penetrated the Red River Formation within the Red Wing Creek area (**Appendix A, Figures 27-31)**; beneath the central core, the #22-27 is the only well penetrating the Ordovician level (**Figures 3, 23)**. As discussed above, the seismic-to-well mistie at the Red River and Bakken levels in the 22-27 well is approximately 200 feet (61m) and 400 ft (122m) high, respectively, due to seismic migration error (**Figure 23)**.

At the Red River level, the strata shallow gradually from east to west; below the central core, the well data suggest that there are only minor depth variations in this zone (**Figure 32)**. A localized structural high is present in the southwest section of 200 feet (61m) above the regional depth (**H on Figure 32)**. This local high is also present in the overlying Bakken Formation (**H on Figure 33)**, but is less pronounced in the overlying strata. At the Bakken level, this structure is approximately 100 feet higher (31m) than its regional depth. The depth variations and contours beneath the crater have a slightly circular pattern at the Red River and Bakken levels **(Figures 32, 33)**. Possibly, this pattern could be a migration artifact due to the highly variable velocities in the strata in the overlying crater.

Faulting within the Red River to Bakken interval is relatively simple in comparison to the overlying Mississippian section. Significant faults occur in two general areas within the dataset at this level (**Figure 32**). The first area is located within the southwest structural high (**H on Figure 32**). The faults present here have a vertical offset of up to 180 feet (55m) and extend laterally for .85 miles (1.36km). The fault planes dip to the southwest at an angle of up to 70°**.** The faulting present at the Red River Formation is composed solely of high angle reverse faults. The faults extend as deep as 3,000 feet (914m) below the Red River level into the basement and they extend as high as 2,500

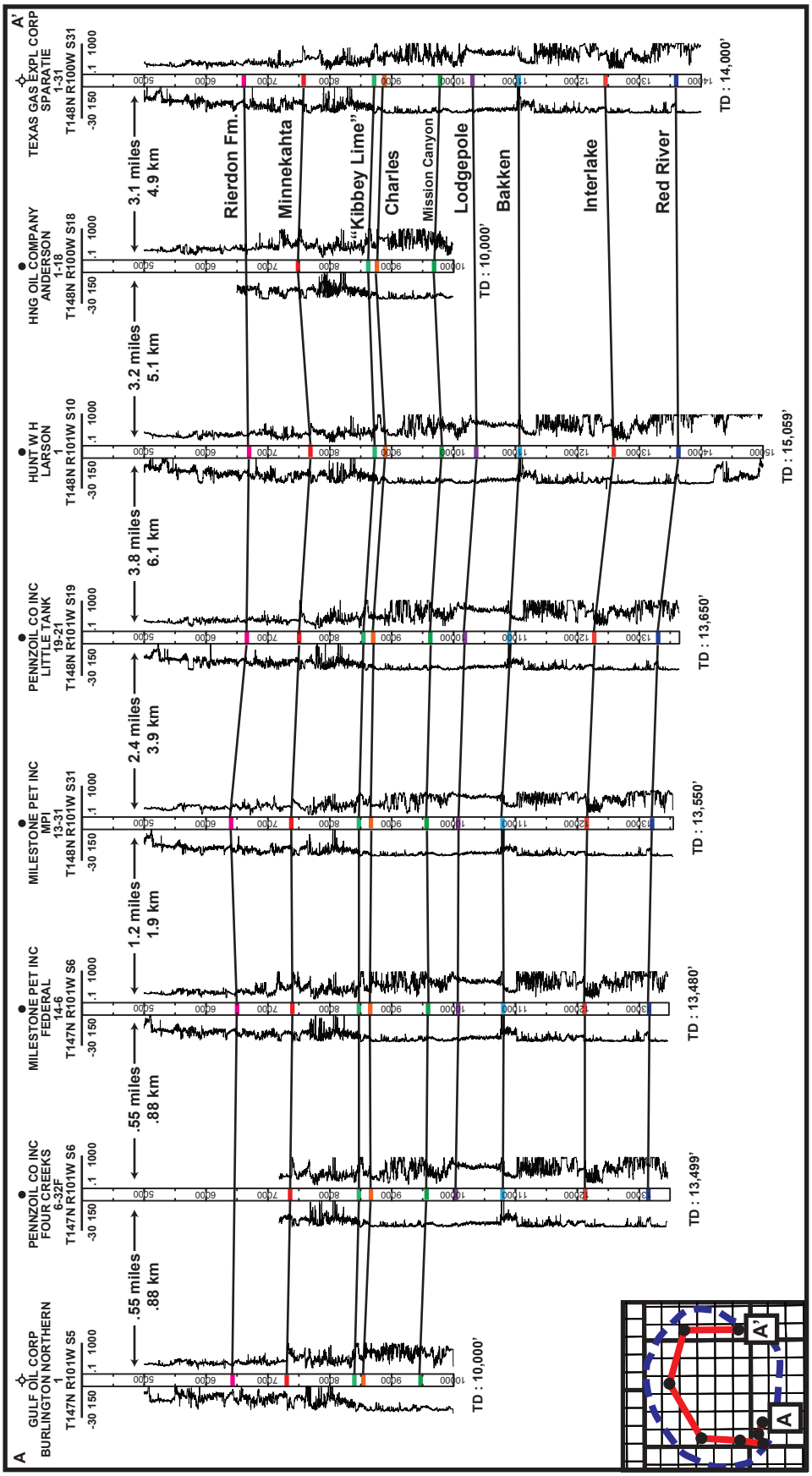

Figure 31. Log cross section of the normal stratigraphic succession seen in the outer rim of the Red Wing Creek structure. In the outer rim, there is minimal structural disruption of the strata, and thicknesses remain relatively constant. Location of cross section is annotated in the index map.

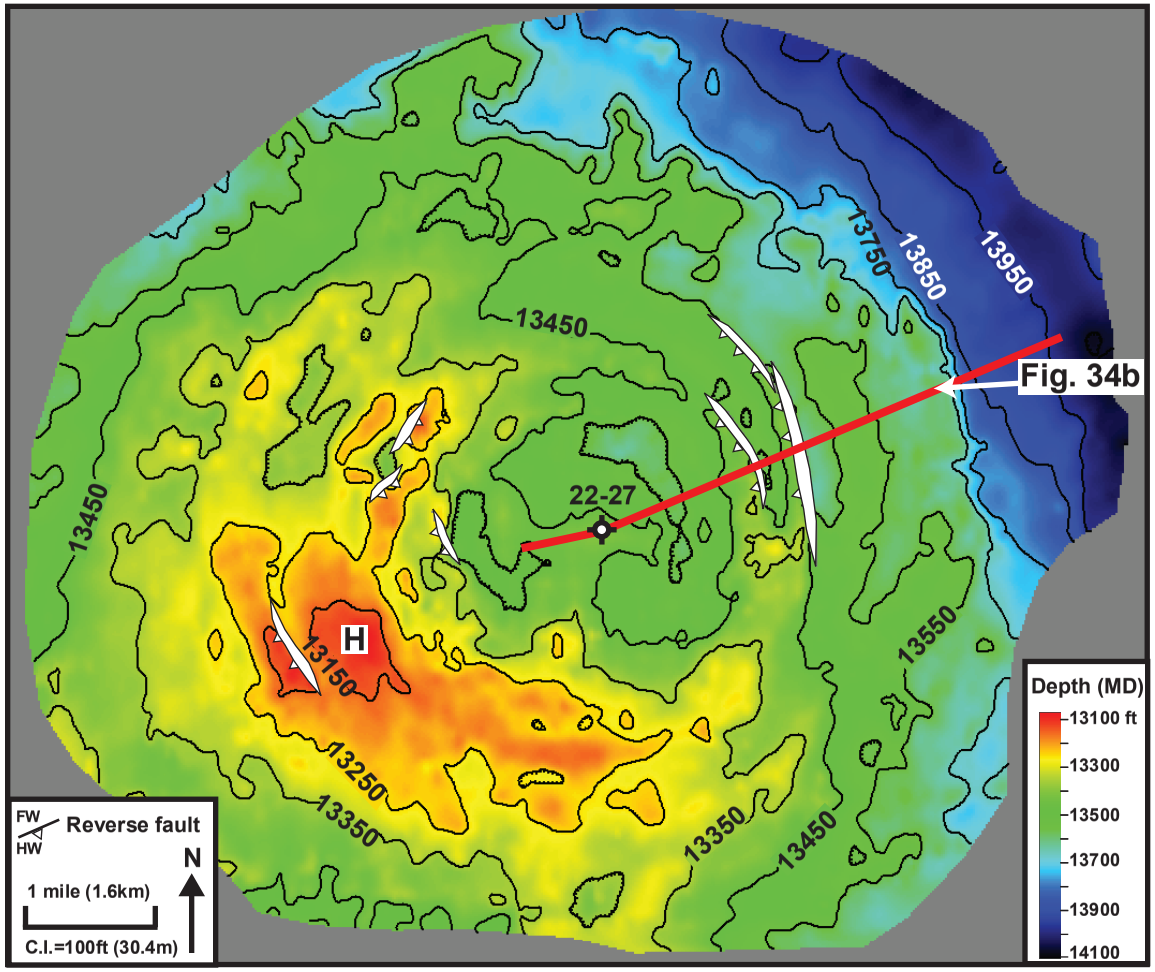

Figure 32. Depth structure map of the Ordovician Red River Formation. Major faults are represented by estimated fault heave polygons. The depth of the Red River formation depths gradually decreases toward the southwest with the exception of the structural high (H) present in the southwest section. The location of Figure 34b is indicated by the red line.

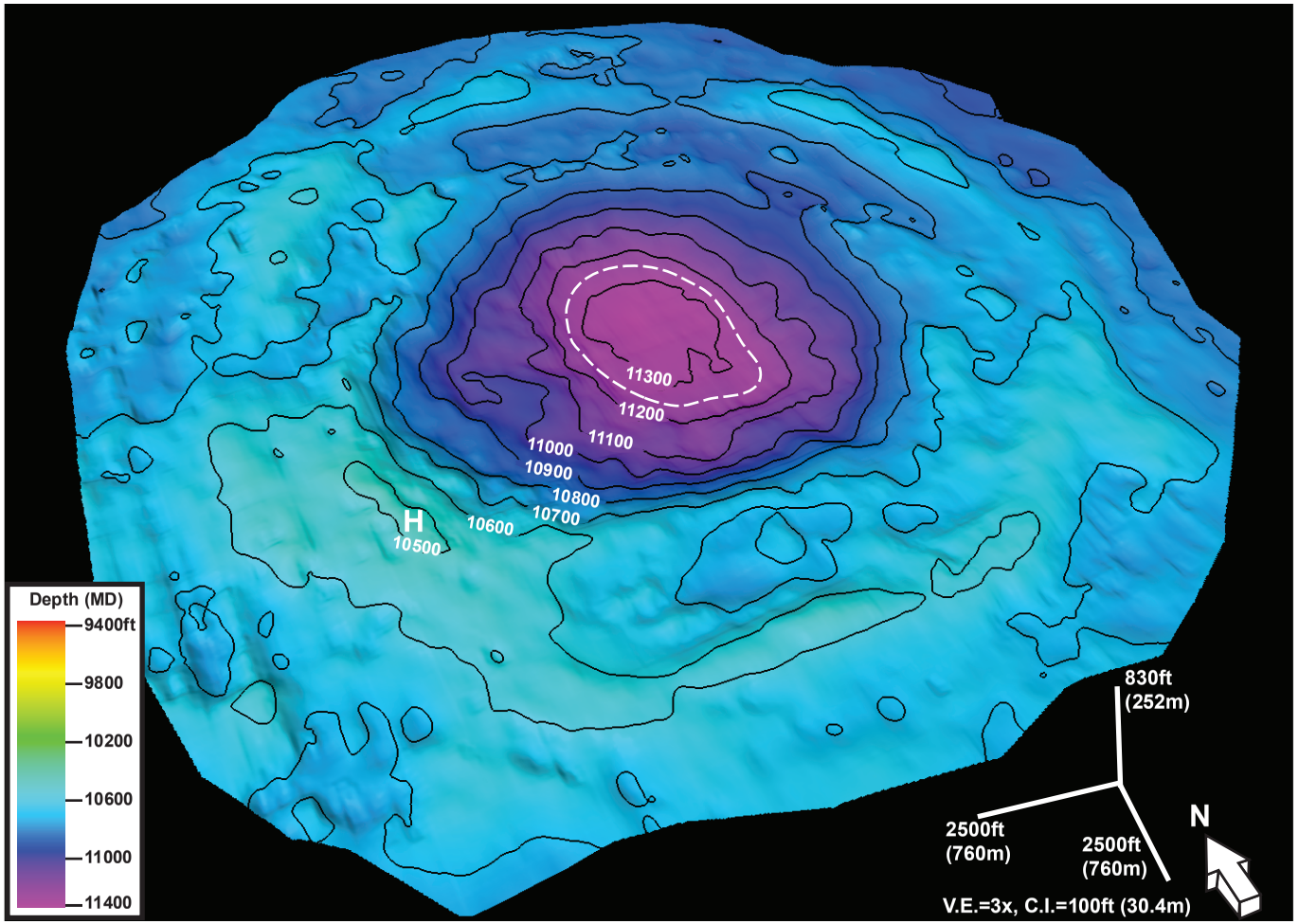

Figure 33. Three-dimensional perspective depth map of the top of the Bakken Formation. Beneath the central uplift, the Bakken is depressed as much as 600 feet (183m) in comparison to the regional Bakken depth (10.700 to 12,300 feet). The dashed white line marks the approximate location of the overlying central core. H represents a structural high, which exists at the Bakken and Red River levels.

feet (762m) above the Red River. None of the faults present at the Red River level appear to intersect the overlying Bakken Formation (**Figure 34)**.

The other faulted zone at the Red River level occurs in the northeast section of the dataset **(Figures 32, 34)**. At the Red River level, in the northeast zone, faults cut the section at two levels. This faulted zone is the most pronounced with 300 feet (91.4 m) of vertical offset. The fault planes dip at 55° to 65° toward the southwest with a thrust direction toward the east-northeast, and extend laterally for as much as 1.7 miles (2.74km). Smaller reverse faults are present at a shallower level with up to 200 feet (61m) of vertical offset and 50° dip angles toward the southwest. These faults appear to be detach at the top of the Red River Formation (**Figure 34)**.

Seismic attributes, utilized to delineate structural patterns, indicate that there are extensive small scale faults that cut the Red River to Bakken interval. The fault pattern seen in the fault enhanced (**Figures 35-36)** and ant tracking seismic attributes suggests the fault pattern is dominantly circular at this level. A circular fault pattern supports the idea that the impact affected the faulting within this interval. The depression of the Bakken Formation, present in the stratigraphic well tops, also suggests that the Red River to Bakken interval has been affected by the impact (**Figures 27, 29)**.

The Bakken Formation, unlike the underlying Red River Formation, shows a significant depression underlying the central portion of the impact structure (**Figure 33)**. In the #22-27 well, the Bakken Formation is depressed by as much as 600 feet (183m) in comparison to its regional depth. The underlying Three Forks, Birdbear, and Duperow Formations (**Figure 8**) are also lower in the #22-27 well in comparison to their regional

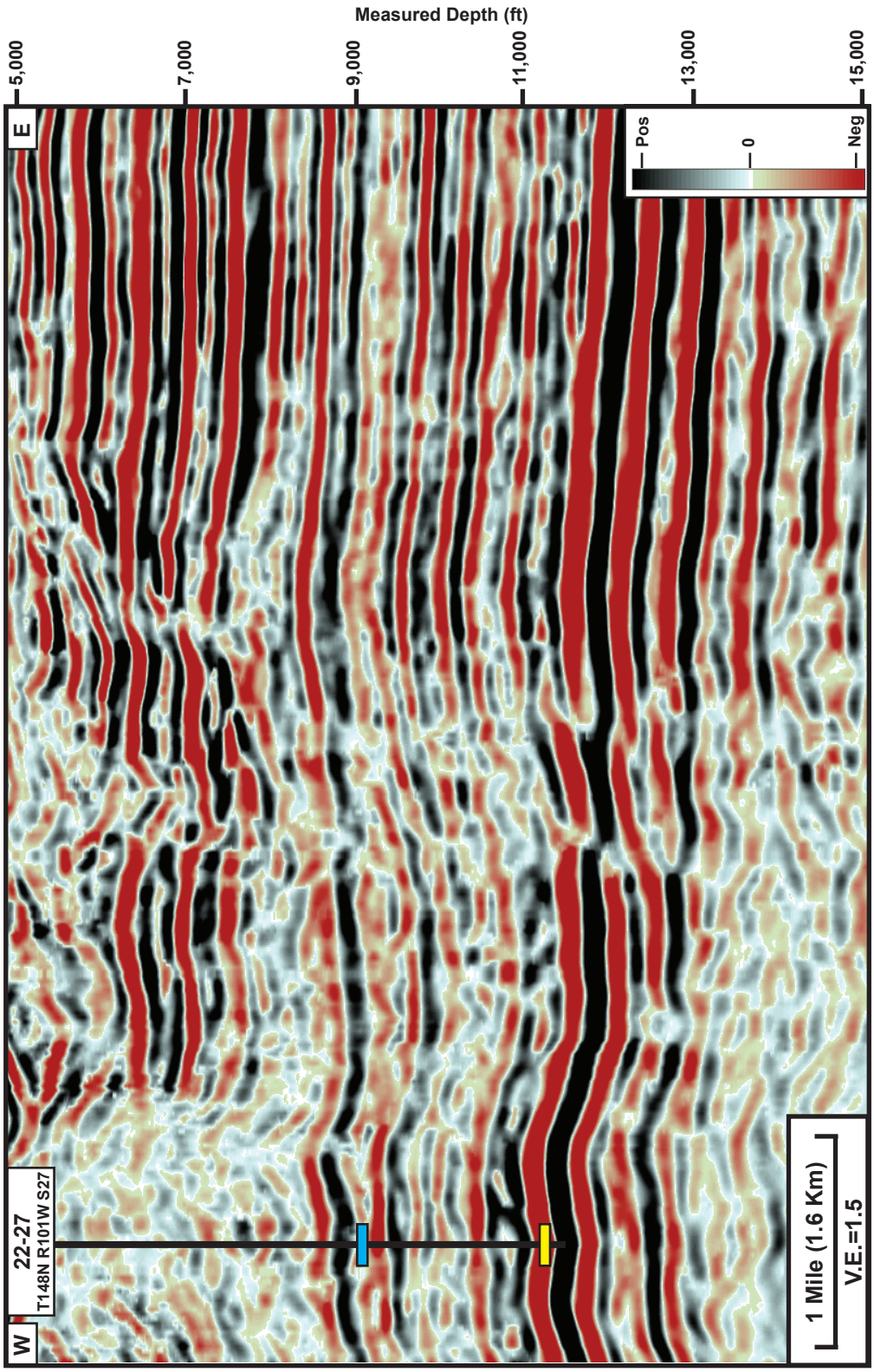

Figure 34a. Uninterpreted seismic profile that corresponds with Figure 34b. See Figure 32 for location of the profile.

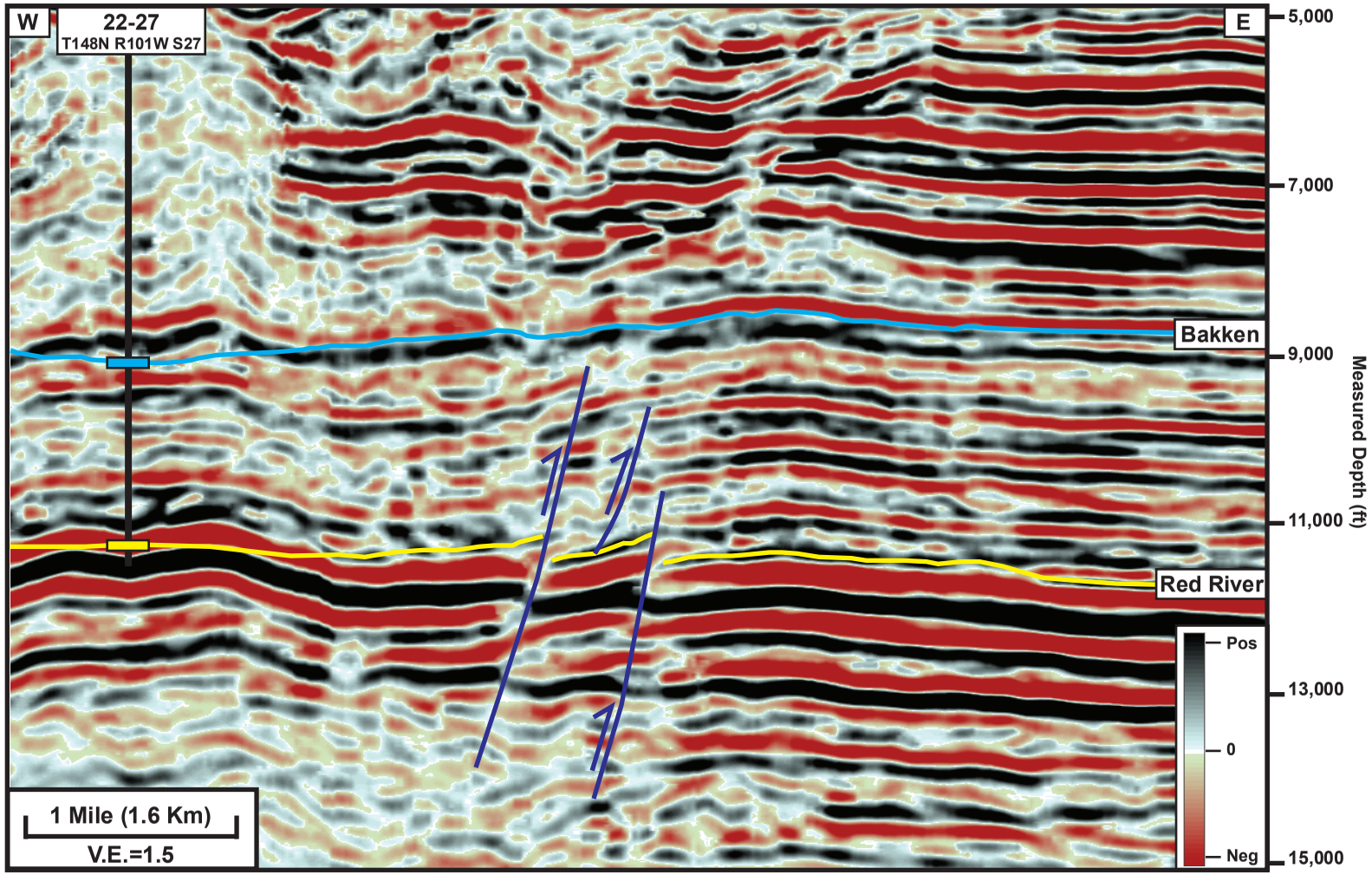

Figure 34b. Seismic profile displaying two levels of high angle reverse faults at the Red River level present in the north-east section of the dataset. The first level is shallow and appears to detach at the top of the Red River. The second group extends much further in depth and intersects the Red River formation. See Figure 32 for location of the profile.

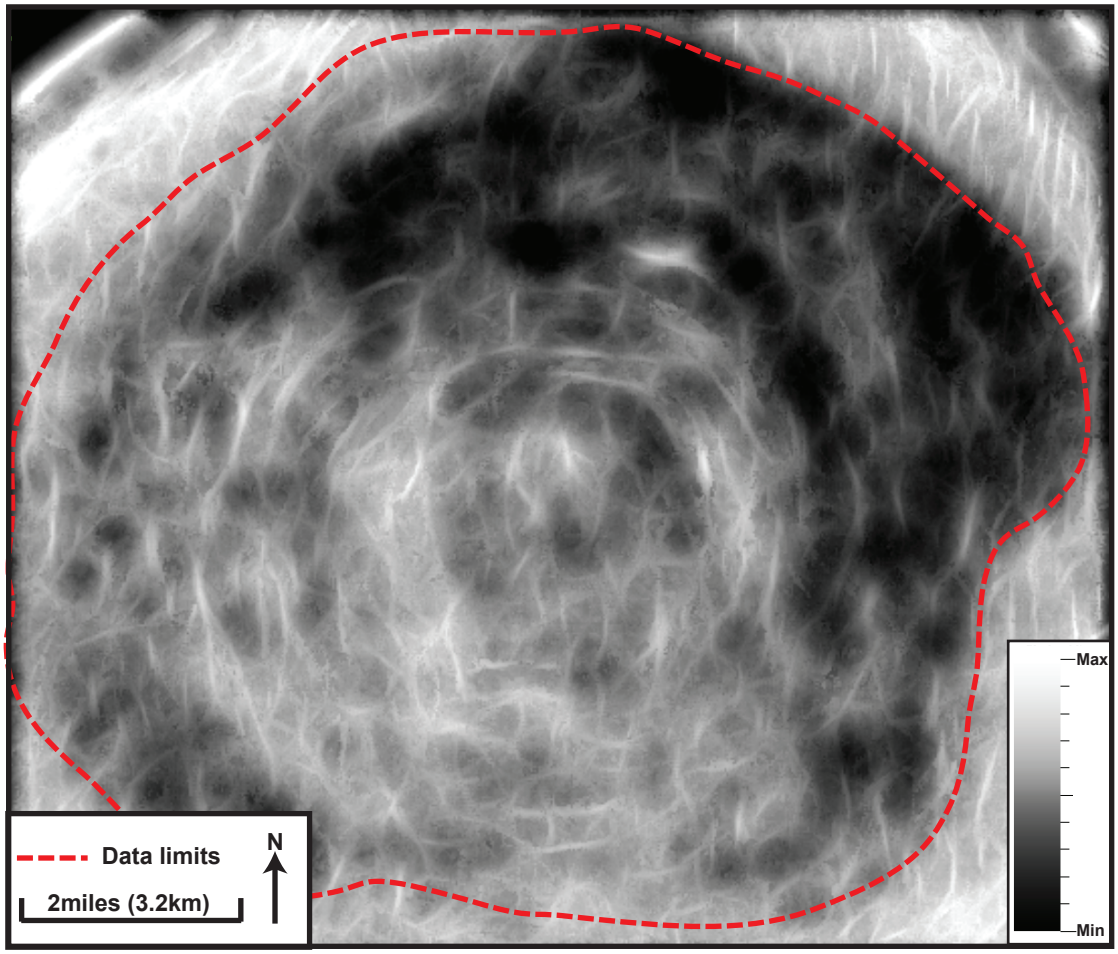

Figure 35. Fault enhanced seismic attribute in plan view below the Devonian Bakken formation (11,400 feet measured depth on Figure 36b). The fault enhanced attribute suggests that minor faulting, within the Red River to Bakken formation interval, are circular in nature. The circular fault pattern indicates the impact has effected the faulting within this interval, but it is possible that this pattern, in the seismic attributes, is a product of velocity variations in the overlying strata.

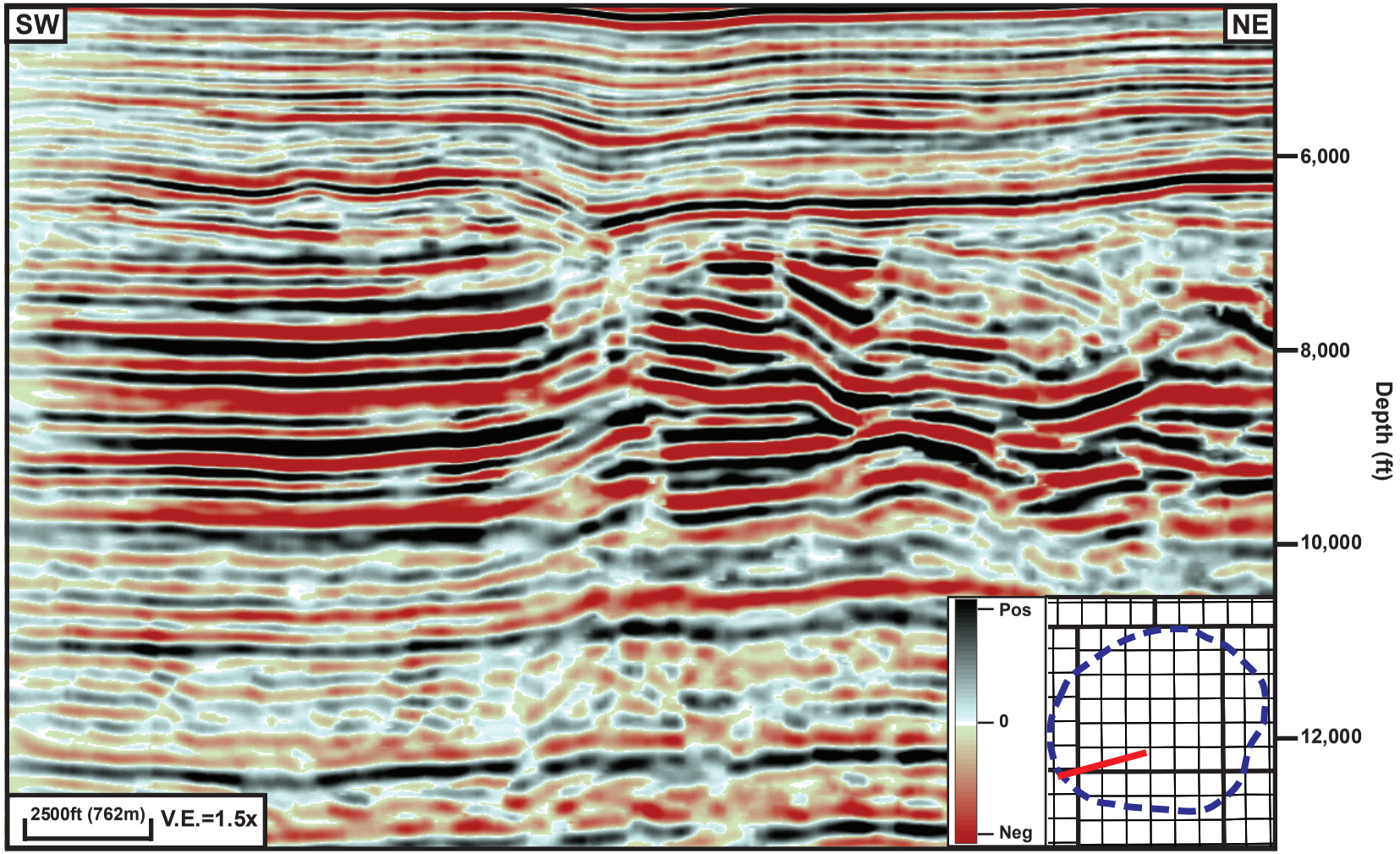

Figure 36a. Uninterpreted seismic profile that corresponds with Figure 36b. Location of the profile is shown in the index map.

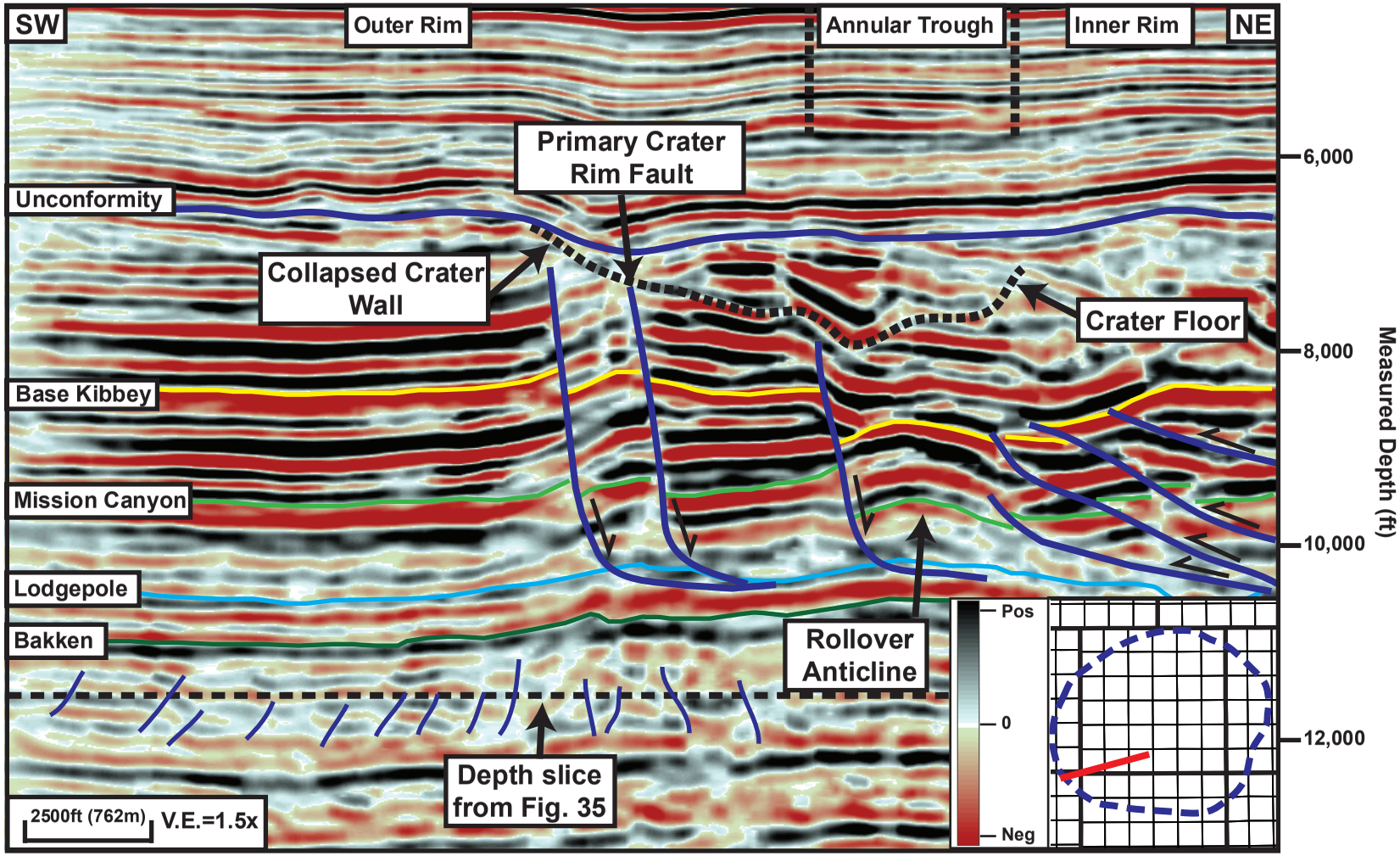

Figure 36b. Seismic profile displaying rim wall terracing at the outer rim to annular trough transition. Note the structural rollover in the hanging wall in the annular trough. The inner limit of the annular trough is bounded by a series of imbricate thrusts faults that detach within the Lodgepole Formation. Small scale faults between the Bakken and Red River formations have been annotated. The dashed black line represents the fault enhanced attribute depth slice in Figure 35. Location of the profile is shown in the index map.

depth. However, at greater depths, the localized depression disappears. By the top of the Souris River Formation, the strata beneath the central area are no longer appreciably deeper that their regional depth (**Figures 27, 29)**.

Primary Impact Structure-Bakken to Spearfish Formation

The main stratal interval modified by the Red Wing Creek impact is the interval from the top of the Bakken Formation to the top of the Permian-Triassic Spearfish Formation. Based on detailed structural interpretation (**Figures 37, 38**) and regional thickness variations (**Figure 39**), four distinct structural zones across the Red Wing Creek structure are recognized within the Bakken to Spearfish interval. Located from the outside toward the central crater the zones are: (1) an outer rim, (2) annular trough, (3) raised inner rim, and (4) central core. The annular trough and inner rim are both situated concentrically around the central core.

The first zone is the outer rim, which surrounds the structure (**Figures 15, 16)**. The strata in the outer rim are relatively undisturbed (**Figure 31)**. Adjacent to the outer rim is the annular trough (**Figures 15, 16)**. The outer rim is separated from the annular trough by high angle listric normal faults, whereas, the annular trough is often bounded externally, toward the crater center, by antithetic normal faults. The third zone is the inner rim (**Figures 15, 16**), which is primarily characterized internally by low angle thrusting away from the central crater as well as high angle thrusts that verge radially away from the central core. The final structural zone is the central core (**Figures 15, 16)**. Traditionally, the centrally uplifted strata, as well as the adjacent inner rim, would be treated as the central uplift. For this study, the central core refers only to the sector

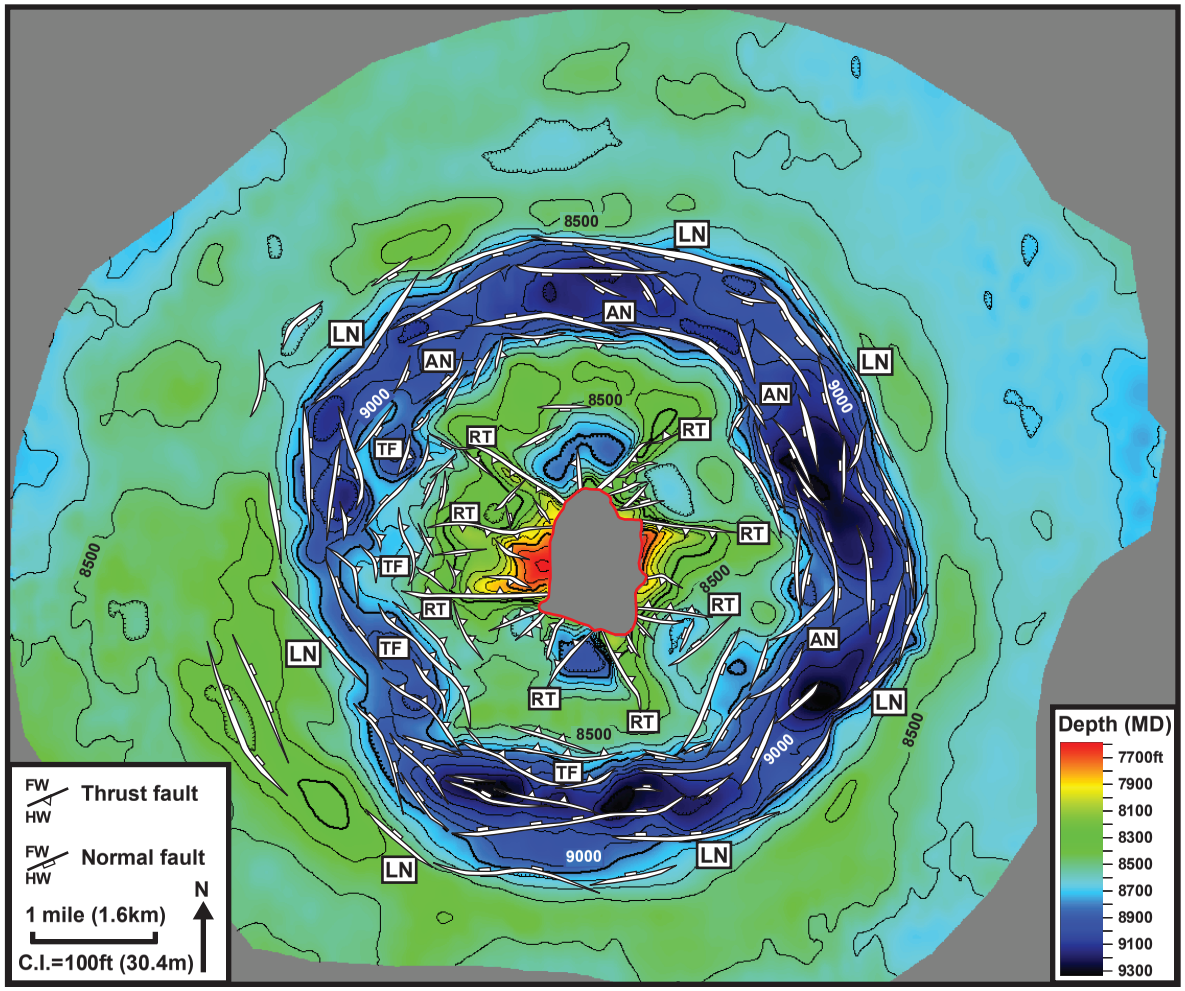

Figure 37. Depth structure map of the base of Kibbey Formation marker. Four major fault styles present at this level: (1) listric normal faults (LN) at the rim edge; (2) antithetic normal faults (AN) at the inner edge of the annular trough; (3) outward verging thrust faults (TF) in the inner rim of the central uplift complex; and, (4) radial thrust faults (RT).

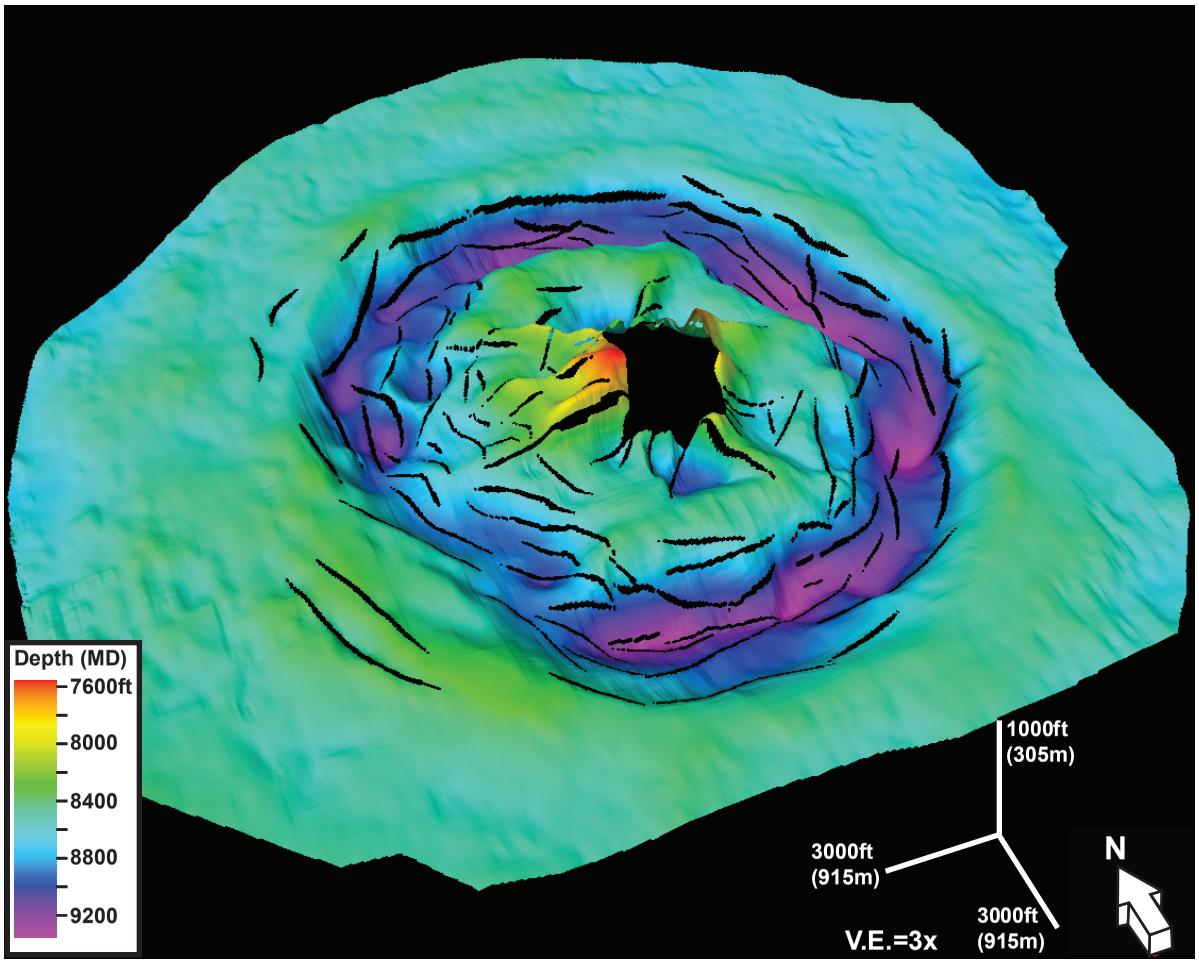

Figure 38. Three dimensional view of the structure map of the Base of Kibbey Formation. The base Kibbey correlates within the same seismic reflection as the Charles Formation, which serves as a major detachment surface for faulting within the upper portion of the crater. Therefore, this horizon marks a distinct change in crater morphology between underlying and overlying stratigraphy. Black lineations represent the locations of intersecting faults.

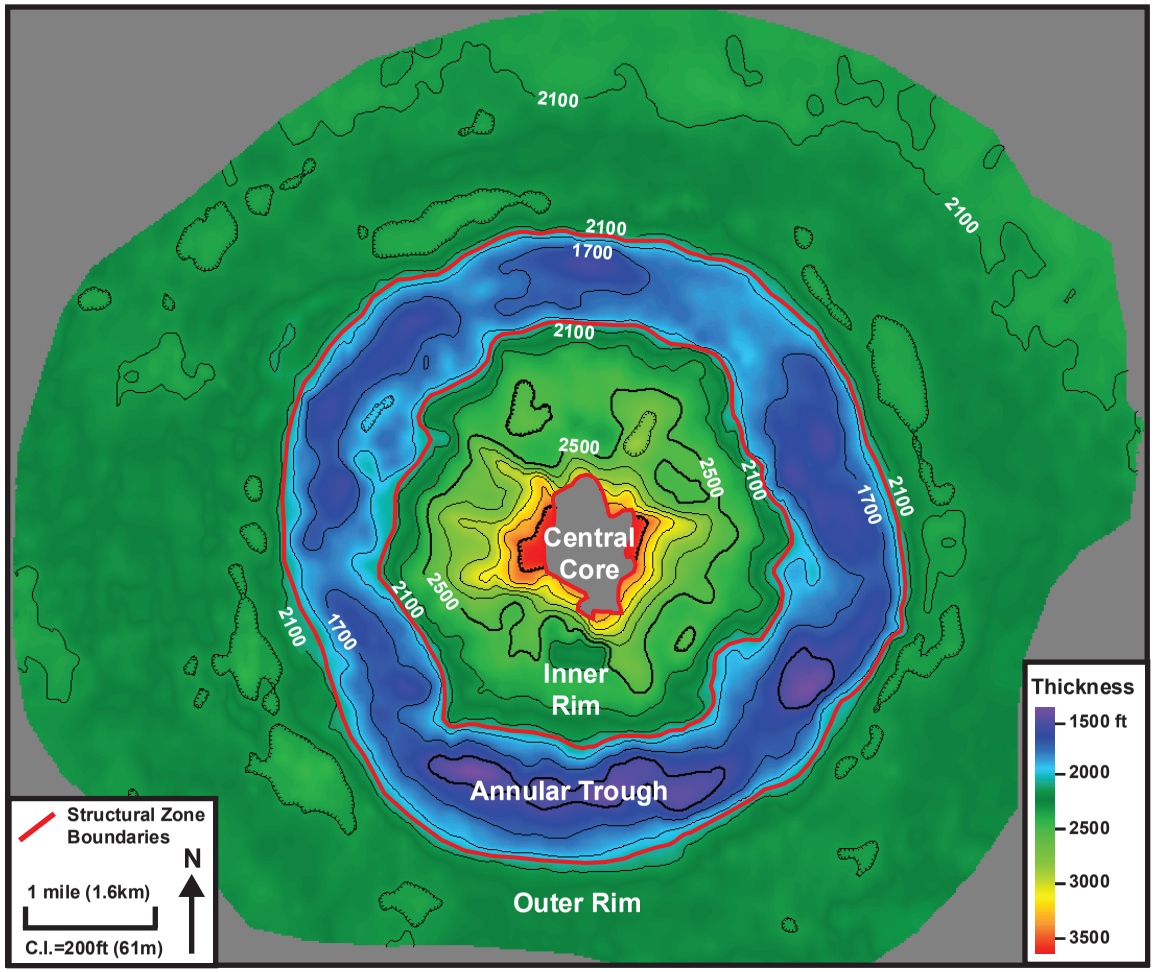

Figure 39. Isopach map of the top of Bakken Formation to the base of the Kibbey Formation. Four discrete structural zones are present within the Red Wing Creek structure: (1) outer rim; (2) annular syncline; and, the “central uplift complex” composed of a (3) raised inner rim, and (4) central core.

that has an anomalous structural uplift and consists of a discontinuous, chaotic seismic facies (**Figure 15).** The central core lacks all Upper Mississippian, Pennsylvanian, and Permian strata above the Charles Formation (**Figures 27-30**). The “inner rim” plus the “central core” make up the “central uplift complex” but they are described separately below, because they have very different seismic characteristics, structural characteristics, and stratigraphic characteristics. Log data suggest that there are extensive thrust faults within this zone, but the seismic data within the region does not adequately image the faulting that is present (**Figures 15, 23)**.

Outer Rim transition to Annular Trough

The outer rim is the first of four unique structural zones at Red Wing Creek. Away from the crater, this zone generally conforms to regional dip, which is less than a degree toward the northeast at the Mission Canyon Formation level (**Figure 16**). Toward the inner edge of the outer rim, which is located at an average distance of 2.4 miles (3.9 km), from the central point of the central core. Close to the edge of the outer rim, the strata are elevated structurally above their regional expression and dips away from the central core (**Figures 16, 38**).

Most of the section present in the outer rim conforms to the regional dip seen within the basin but this begins to change closer to the crater edge (**Figures 16, 28)**. Regionally, the top of the Mission Canyon Formation dips at less than 0.5° toward the northeast (Brenan et al., 1975). At a distance of approximately 0.4 to 0.6 (.64 to .97 km) miles away from the crater edge, the strata begin to dip from 2.5° to 8.5° away from the crater (**Figures 28, 30)**. The exception to this dip pattern is in the southwest sector of

the structure. The crater wall-to-annular trough transition appears symmetrical around the entire crater, except in the southwest section, where the strata begin to dip away from the crater at a distance of 1.2 (1.9 km) miles from the crater wall. The stratigraphic section within the annular trough is considerably thinner than the section present in the outer rim (**Figure 39)**. The top of the Bakken to the Base Kibbey, in the annular trough, is up to 600 feet (183 m) thinner than what is present in outer rim.

At the crater edge, the transition to the downthrown annular trough occurs, which is the second unique structural zone. The transition is marked by a series of linked normal faults that become listric at depth (**Figures 36, 40-41)**. At the crater edge, listric normal faults detach within the shales at the lower Mississippian Lodgepole Formation (**Figure 40**). In map view, the normal faults, which mark the crater edge, have an arcuate geometry and a strike length that ranges from 0.4 to 1.8 miles (0.64 to 2.96 km). These normal faults are overstepped and linked, which is characteristic of fault styles in extensional structural environments (Peacock, 2002).

These normal faults are oriented concentrically around the structure (**Figure 42)**. The faults in the north, east, and southern sections occur at an average distance of 2.4 miles (3.9 km) from the central crater (**Figures 37, 42**), whereas, the faults in the western and especially the southwestern section occur at a distance that is as short as 1.9 miles (3.06 km) from the center. From these measurements, the original diameter of the Red Wing Creek crater is determined to be 4.9 miles (7.89 km). As the crater walls collapsed, the crater widened to a final diameter of 5.7 miles (9.17 km).

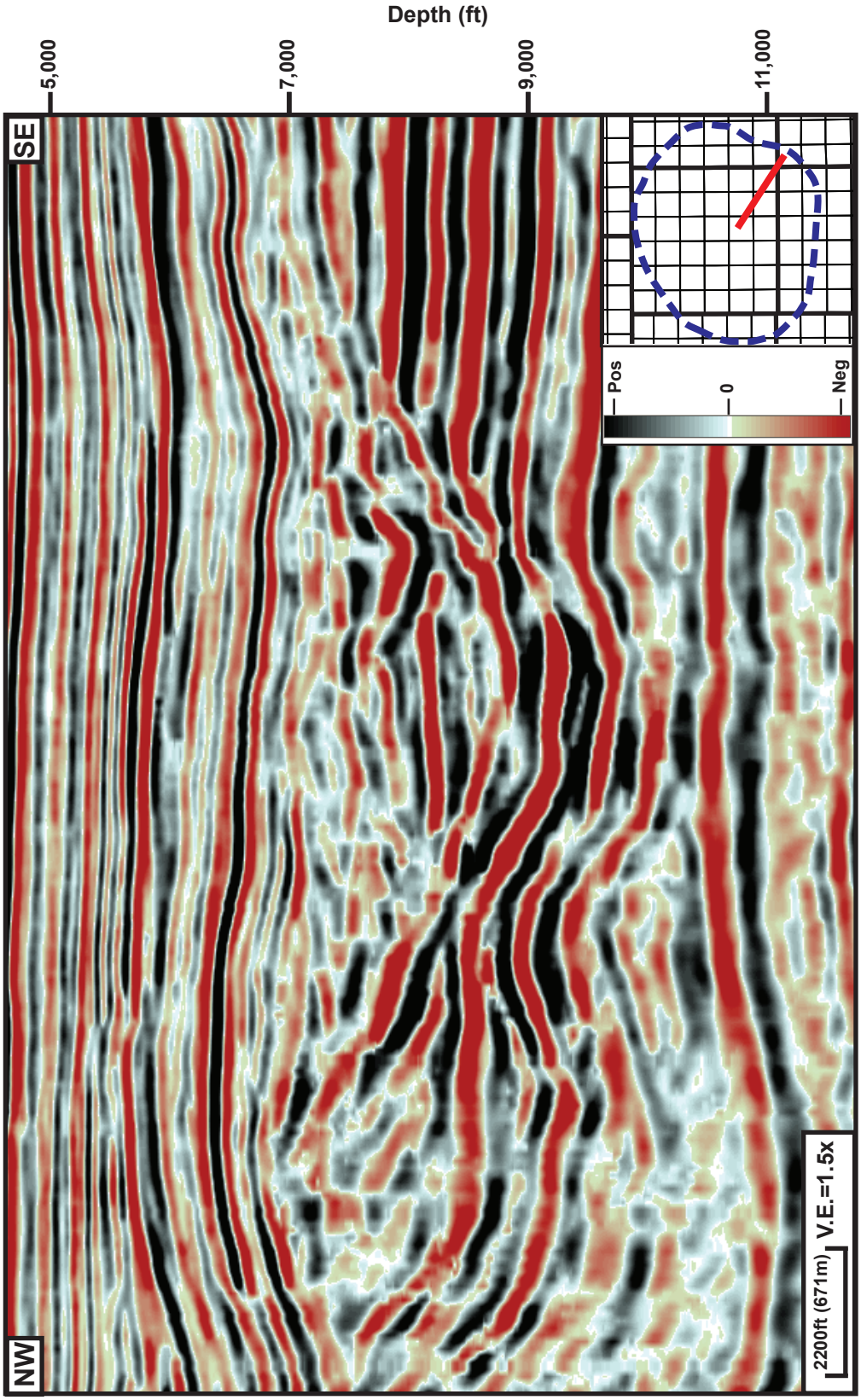

Figure 40a. Uninterpreted seismic profile that corresponds with the interpreted profile in Figure 40b. Location of the profile is shown in the index map.

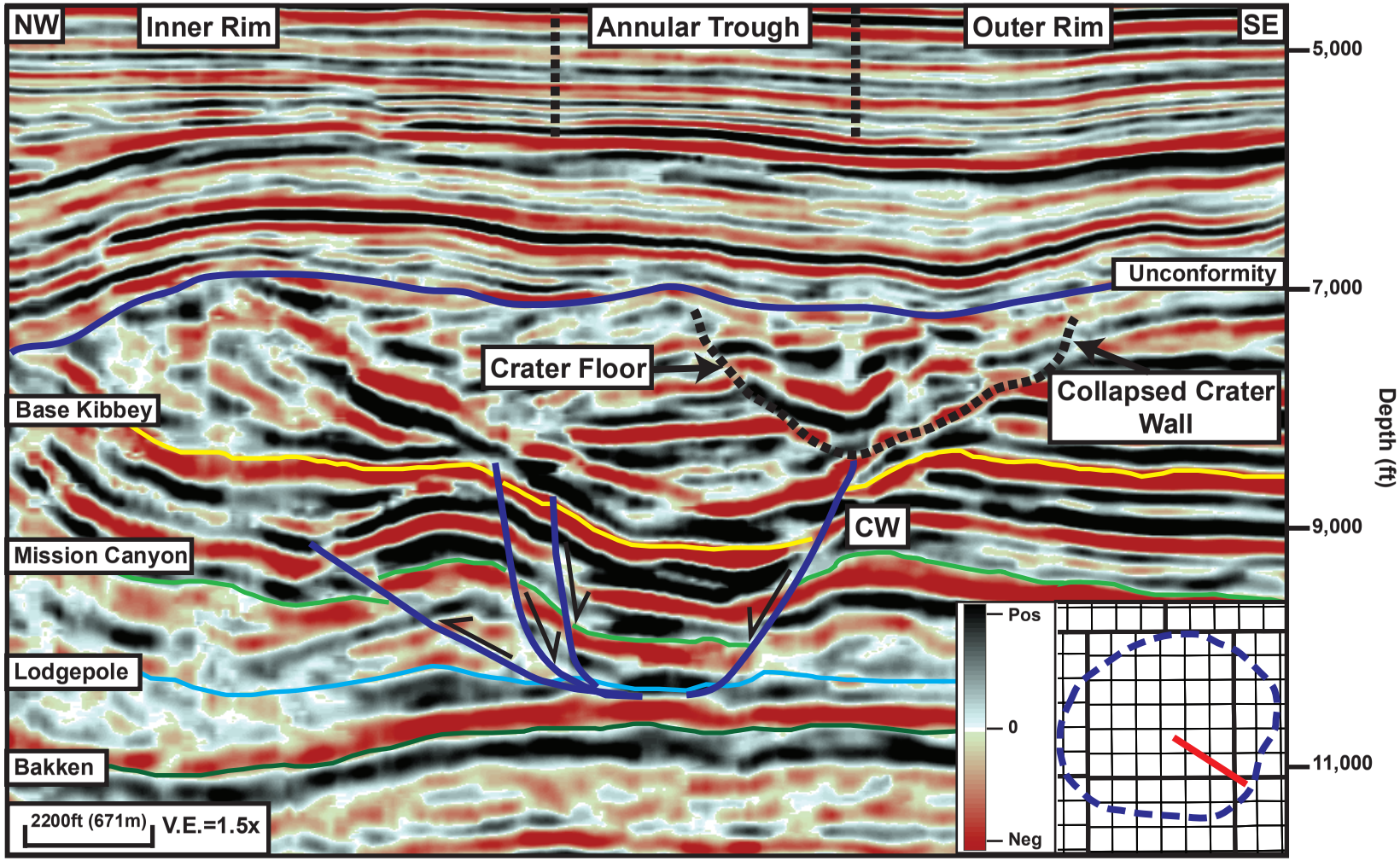

Figure 40b. Seismic profile showing the transition from the outer rim to annular trough to inner rim. The large listric, normal faults of the outer rim dip toward the crater center and mark the edge of the crater wall (CW). These faults terminate within the Lodgepole Formation shales that serve as a detachment surface. The hanging-wall is bounded toward the center by a series of antithetic faults. This is is the only location where there is thrusting toward the central core at Red Wing Creek. The Lodgepole Formation is thin in the annular trough. Location of the profile is shown in the index map.

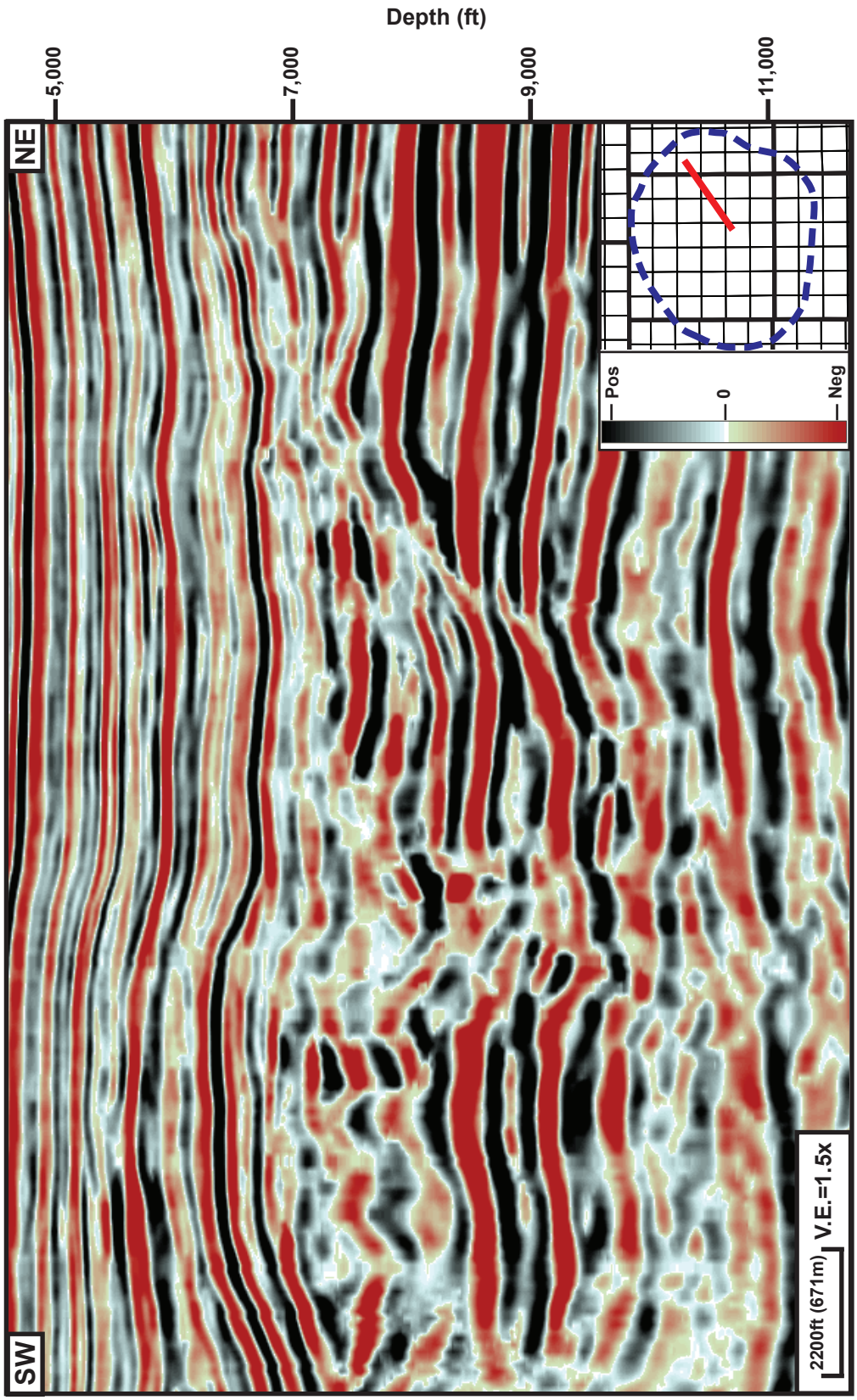

Figure 41a. Uninterpreted seismic profile that corresponds with Figure 41b. Location of the profile is shown in the index map.

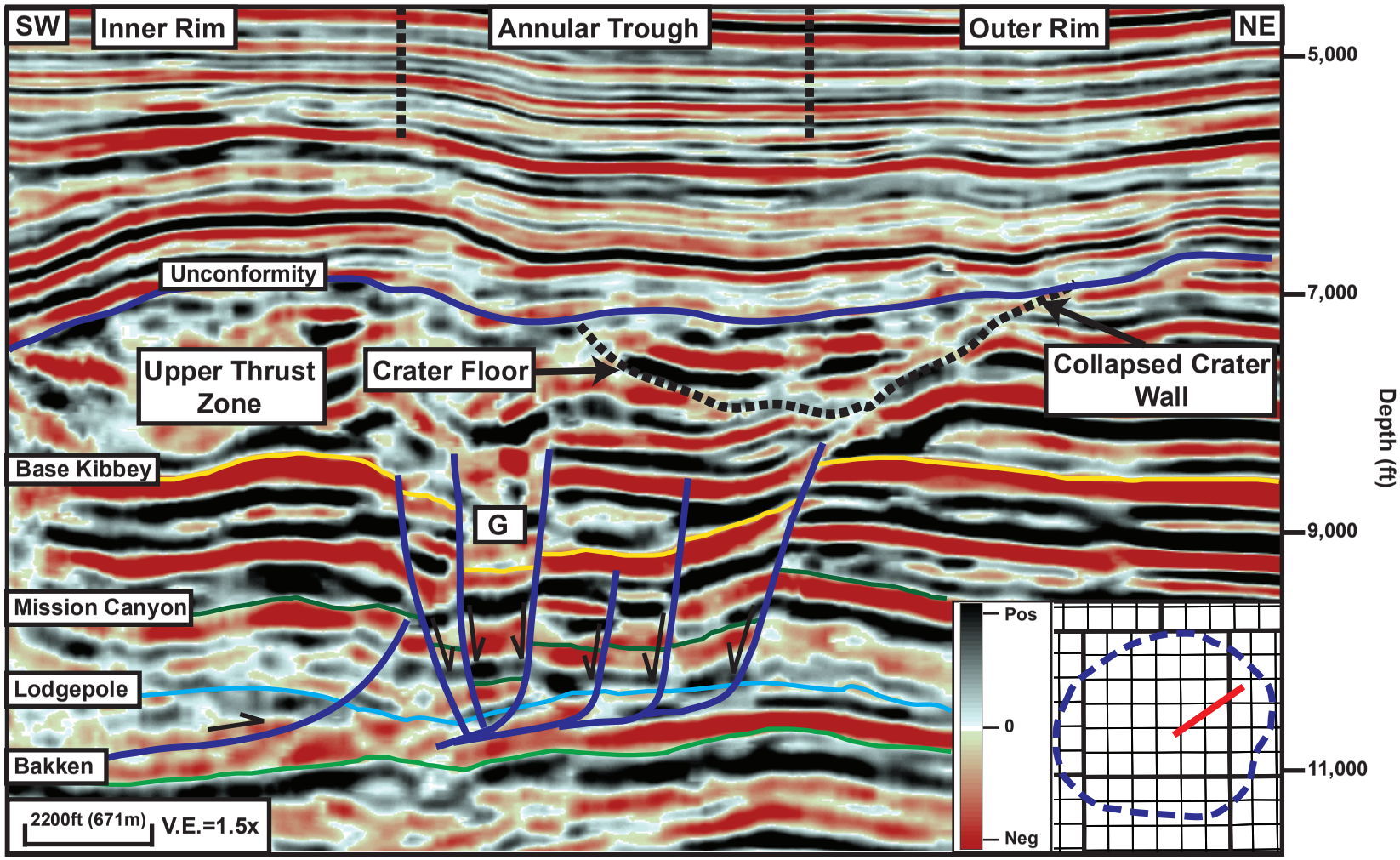

Figure 41b. Seismic profile illustrating the transition from the outer rim to the annular trough to inner rim. In this area, the transition is marked by the primary rim fault followed by a series of listric, normal faults. The inner limit of the annular trough is bounded by antithetic normal faults. At the intersection of the inward and outward dipping faults, a narrow graben has formed at the lowest point of the annular trough. G is the graben formed within the annular trough. Location of the profile is shown in the index map.

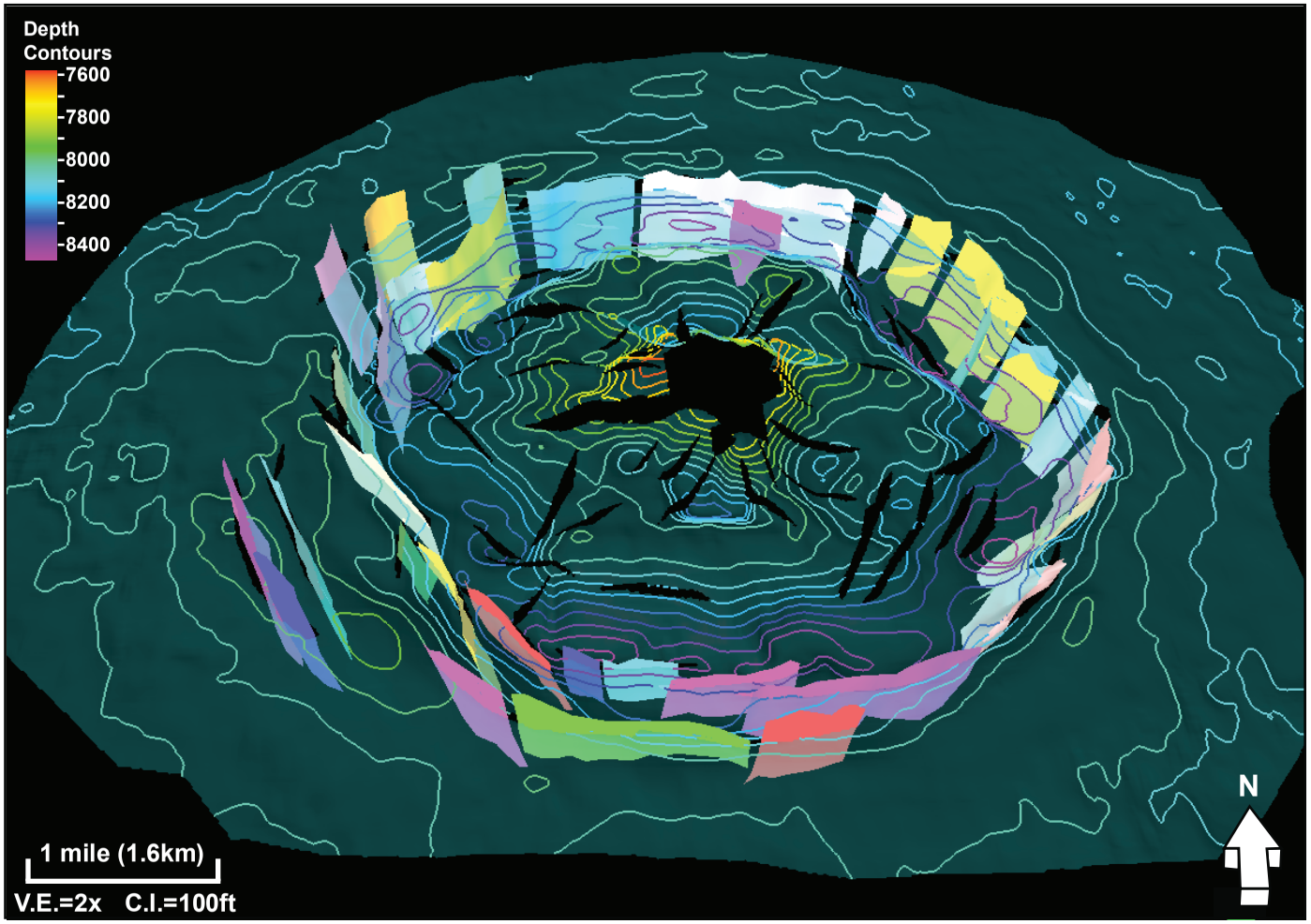

Figure 42. Three dimensional view of the base of the Kibbey Formation horizon cut by the normal faults of the outer rim. These high-angle normal faults have a maximum offset of 600 feet (183 m) and are listric at depth within the Lodgepole Formation. Contour interval is 100 feet (30.4 m). Dark lineations represent locations of intersecting faults that aren't located at the edge of the outer rim.

Along the most areally extensive faults, normal displacement can be up to 600 feet (183 m) at the Mission Canyon level and the dip angle of the major bounding faults ranges from 50° to 70° toward the central crater (**Figures 28, 30**). Their total vertical length ranges from approximately 1,500 to 2,000 feet (457-610m), however their present vertical extent is less than their original length. This is due to the collapse of the original crater walls onto the crater floor (**Figure 43**). Reconstructing the original height of the crater wall above the crater floor isn't possible due to the collapse of the crater wall as well as the Triassic to Jurassic unconformity that caps the Red Wing Creek structure.

Three examples are shown here that illustrate different structural styles in the transition from the outer rim to the annular trough around the Red Wing Creek structure: (a) sharp (**Figure 40**) to (b) gradual (**Figure 41**), to (c) stepped (**Figure 36**) transition to the hanging wall of the normal faults. The structural expression of the hanging wall also varies around the crater.

(a) Sharp: Examples of a sharp transition from the outer rim to the annular trough in the southeast section of the crater are shown in **Figure 40**. The hanging wall is separated from the footwall by a single normal fault that detaches within the Lodgepole Formation. The maximum normal displacement at the Mission Canyon Formation level along this fault is 550 feet (168 m), and the fault dips at an angle of 52° toward the central crater. The hanging wall is bound, toward the crater center, by a series of antithetic normal faults that dip at an angle of 70° to 75° toward the outer rim (**Figures 40**). These antithetic faults are also listric and sole into the Lodgepole detachment; these faults mark the boundary between the annular trough and the inner rim. Within the

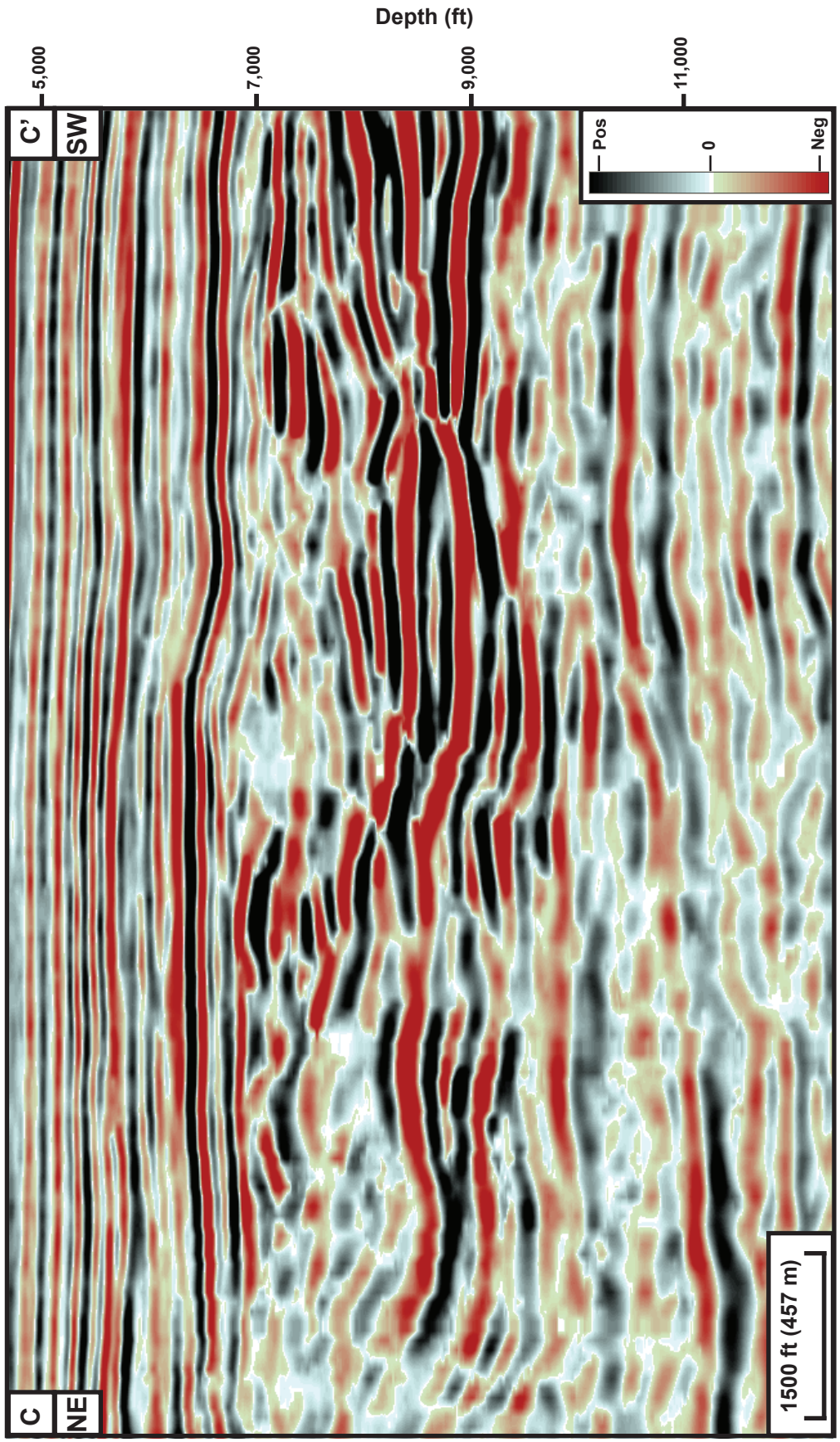

Figure 43a. Uninterpreted seismic profile through sector SW of the inner rim that corresponds to Figure 43b. Refer to Figure 50 for profile location.

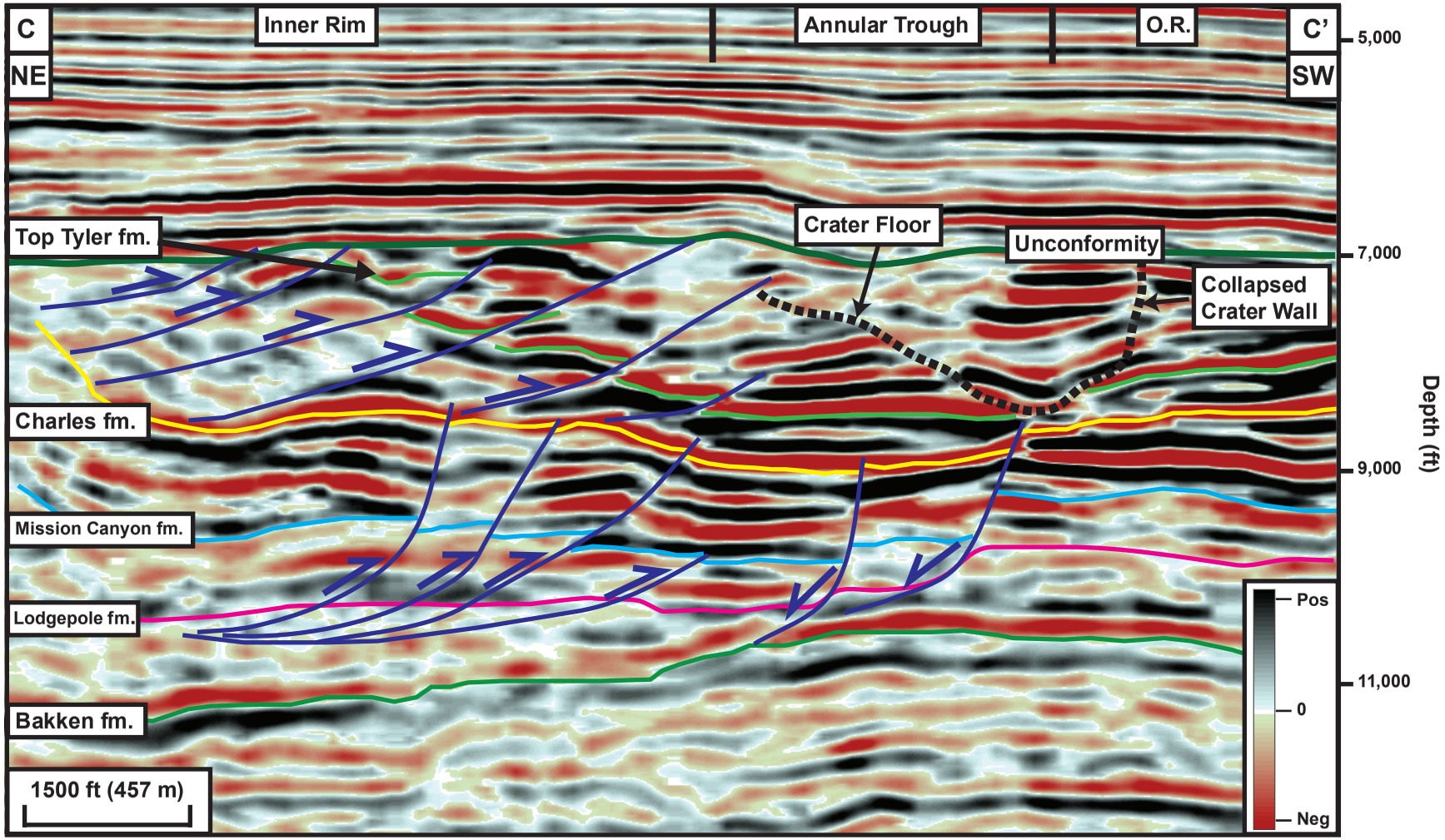

Figure 43b. Seismic profile through sector SW of the inner rim. The lower detachment section is faulted internally by mulitple imbricate thrust faults, where fault planes increase in dip signifciantly upward to 60 degrees at their tip point. The upper thrust section has a maximum thicknes of 1100 feet (335 meters) above the inner limb of the underlying anticline. Major structural zones are annotated: inner rim, annular trough, and outer rim (O.R.). Refer to Figure 50 for profile location.

hanging wall, the Lodgepole to Base Kibbey section is unfaulted but the block is rotated and the section dips at angle of approximately 5° toward the outer rim (**Figure 40**). This type of rotational extension is common when the displacement occurs along a listric, normal fault surface (Wernicke and Burchfiel, 1982).

(b) gradual: The outer rim-to-annular trough transition, located in the northeast section of the crater is shown in **Figure 41**. At this location, the transition is marked by a series of listric, normal faults that dip toward the central crater at a maximum angle of 60° to 70°. The primary offset of 550 feet (168 m) occurs along one fault surface but the hanging wall is cut by three normal faults toward the lowest point of the annular trough (**Figure 41**). Similar to **Figure 40**, the inner limit of the annular trough is bounded by antithetic normal faults that dip at a maximum angle of 70° toward the outer rim. Offset on the antithetic faults can be up to 500 feet (152 m) and they all terminate onto the detachment at the lowest portion of the trough. A narrow graben is present at the intersection of the inner and outward dipping normal faults (**G on Figure 41b**). The hanging wall has rotated along the primary, listric fault but the faulted section dips towards the crater center at an angle of 14°.

(c) Stepped: In the southwestern section of Red Wing Creek, the style of outer rim to annular trough transition is different and is exclusive to this area. The outermost normal faults occur at a distance of approximately 3 miles (4.8 km) from the central crater (**Figures 37, 42**). The vertical offset at these faults is only 250 feet (76 m) at the Base Kibbey level (**Figure 36**). The primary rim fault is 2.1 miles (3.4 km) from the central crater, has a vertical offset of 460 ft (140 m) at the Mission Canyon level, and dips at 70° toward the central crater (**Figure 36)**. This rim fault, in conjunction with the

two adjacent normal faults, form a series of rim terraces that has been rotated along listric faults. The terraced sections dip at 5° and 10° toward the outer rim, and the overall diameter of the rim terraces section is 0.9 miles (1.4 km) at its widest point.

The outer rim of the southwest sector has three unique associations. First, this is the only location at Red Wing Creek where there is a relatively broad rim terrace present before reaching the primary crater rim fault (**Figure 36**). Second, the rollover anticline present in the hanging wall of the rim terrace is a rare feature at Red Wing Creek (**RA on Figure 36b**). Third, the inner boundary of the hanging wall is not bounded by antithetic normal faults (**Figures 40, 41 to Figure 36)**. Instead, the transition to the inner rim is marked by a series of imbricate thrust faults, whose vergence is directed outward from the central crater.

Inner Rim

The zone immediately to the inside of the annular trough is referred to the inner rim in this study (**Figures 16, 39**). The inner rim is considerably more complex structurally than the outer rim and annular trough and is significantly thicker than these two zones (**Figure 39**).

Because the “inner rim” is uplifted stratigraphically, in comparison to the annular trough, it is one of two zones included in the “central uplift complex.” The other is seismically chaotic zone termed the “central core.” Nineteen wells penetrated the inner rim (**Figure 3**) and helped to constrain the structural interpretation. Another unique aspect to this zone is that there are two levels of detachment: an upper detachment level within the Charles Formation evaporites, and the lower detachment level within the

Lodgepole Formation. There is also a series of high angle to sub-vertical thrust faults, referred to as radial transpressional ridges (Kenkmann and Von Dalgwik, 2000), which extend radially outward from the central core. As the Mississippian through Permian section converges toward the central crater, these radial faults divide the inner rim into structurally unique sectors.

Radial thrust faults/radial transpression ridges

Major thrust faults divide the inner rim into to eight sectors or blocks, each of which has a unique internal structural character (**Figure 44**). The dominant structural features extend radially away from the central core (**Figures 44, 45**). Their maximum, areal lengths vary from 0.3 to 1.1 miles (0.48 to 1.77 km), but none extend into the annular trough. The interface between the inner rim and the annular trough marks the distal edge of the strata that is influenced by these radial thrust faults.

This set of thrust faults detaches within the Lodgepole Formation shales (**Figure 44**). Thrust faults cut as high as the Permian-Triassic Spearfish Formation, which is the youngest strata present in the crater, and are overlain by draping Jurassic strata (**Figure 46**). The major thrusts are numbered 1 through 9 and correspond with the fault polygons on the Base of Kibbey depth structure map (**Figures 44, 46).** For the following description, this numbering system will be used when referencing individual faults.

As described above, the length of these faults varies from 0.3 to 1.1 miles (0.48 to 1.77 km) with Thrust 2 being the most areally extensive and Thrust 5 being the least extensive. The following measurements are the distance that the remaining thrusts extend away from the central core: Thrust 1 extends 0.54 miles (.87 km), Thrust 3

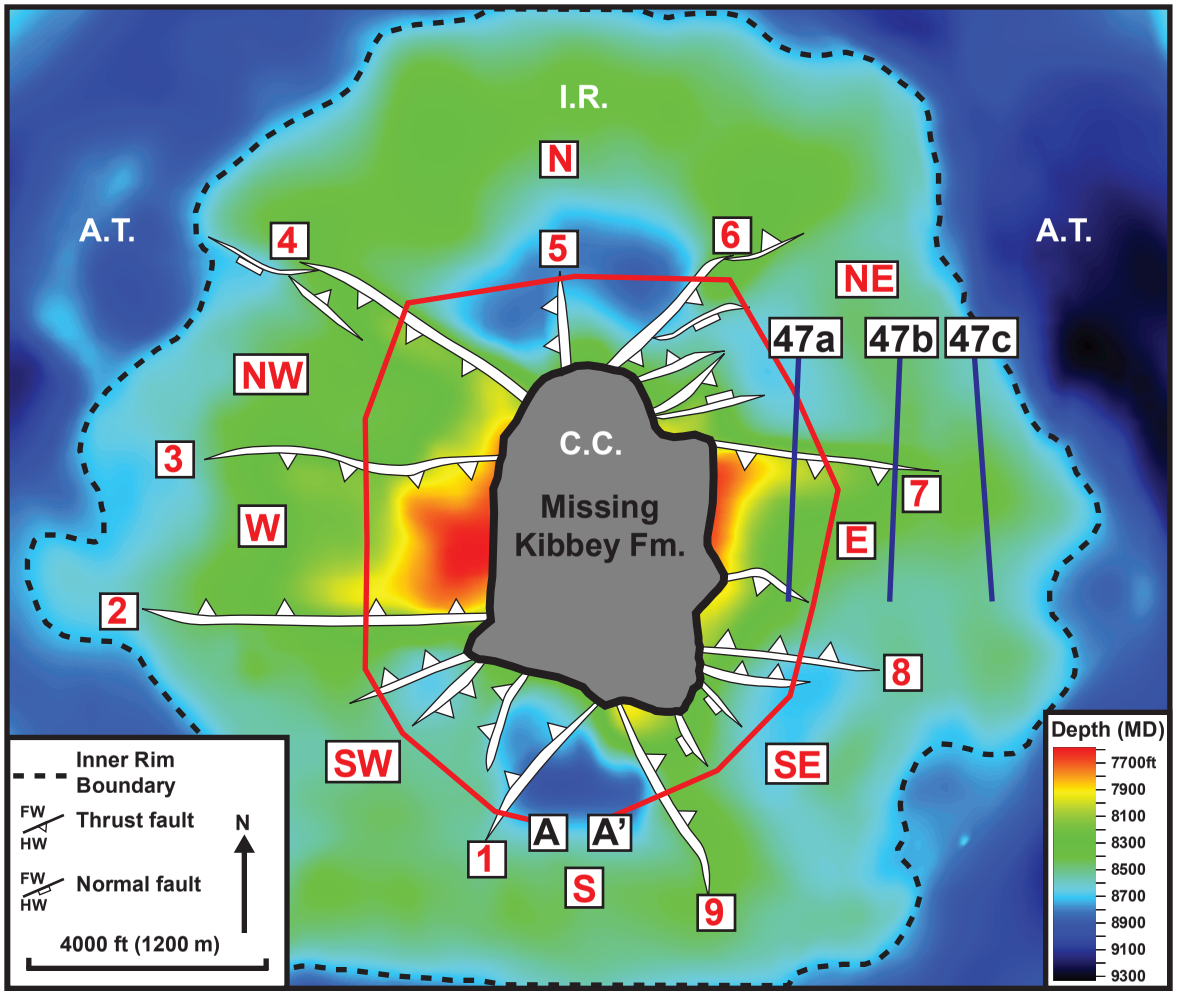

Figure 44. Depth structure map of the base of the Kibbey Formation showing radial thrust faults or “transpressional ridges.” Major thrust faults are numbered (1-9) and seismic lines are annotated and correspond with following figures. These faults divide the thickened section into separate structural zones which are annotated according to their respective locations around the central core (N,NE,E,SE,S,SW,W,NW). Blue lines refer to the seismic profiles in Figure 47 . Major structural zones are annotated: central core (C.C.), inner rim (I.R.), and annular trough (A.T.).

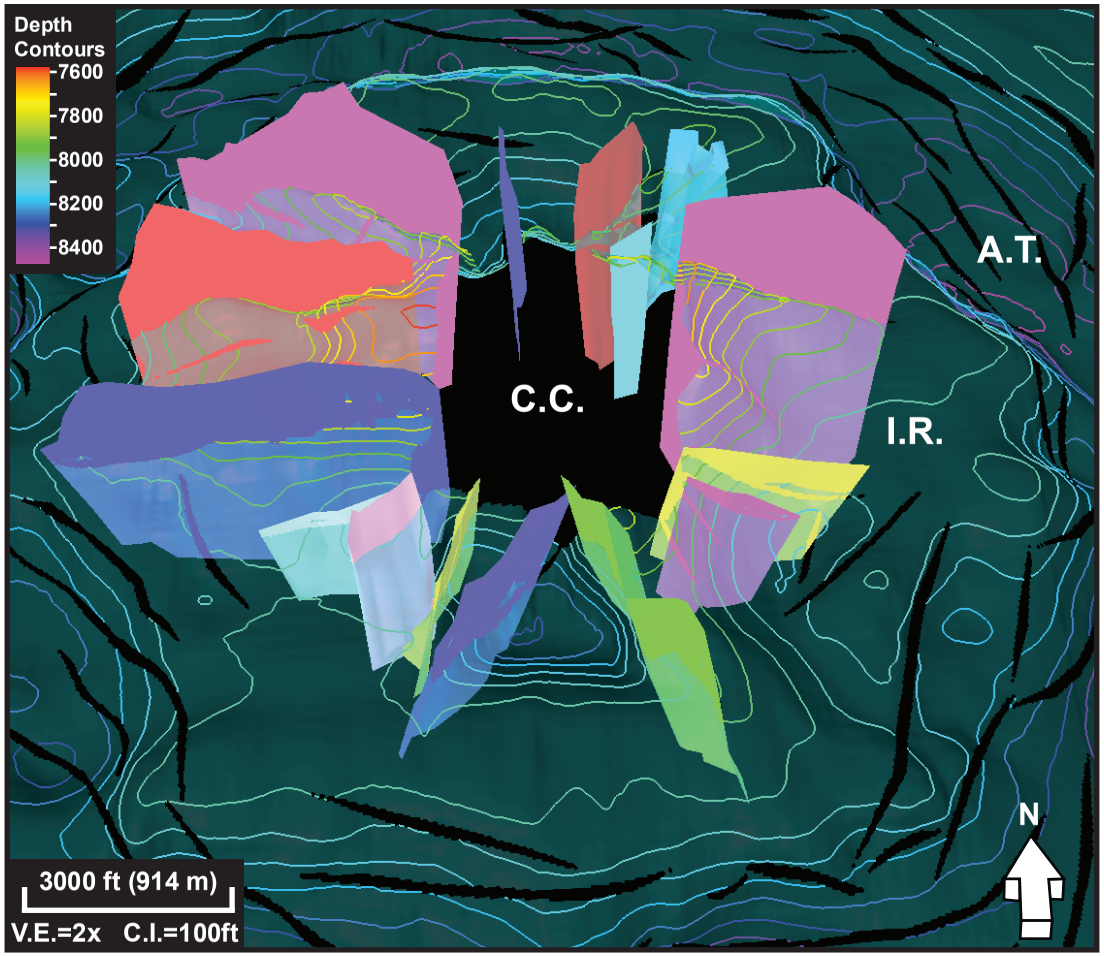

Figure 45. Three dimensional map of the base of Kibbey Formation within the inner rim. The high angle thrust faults extend as far as 1.1 miles (1.77 km) from the central uplift, where the Kibbey Formation is missing, and have up to 1150 feet (351 m) of maximum reverse displacement. They divide the thickened zone into eight structurally unique zones or blocks. The dark lineations represent the locations of fault intersections not related to the radial thrust faults. Major structural zones are annotated: central core (C.C.), inner rim (I.R.), and annular trough (A.T.).

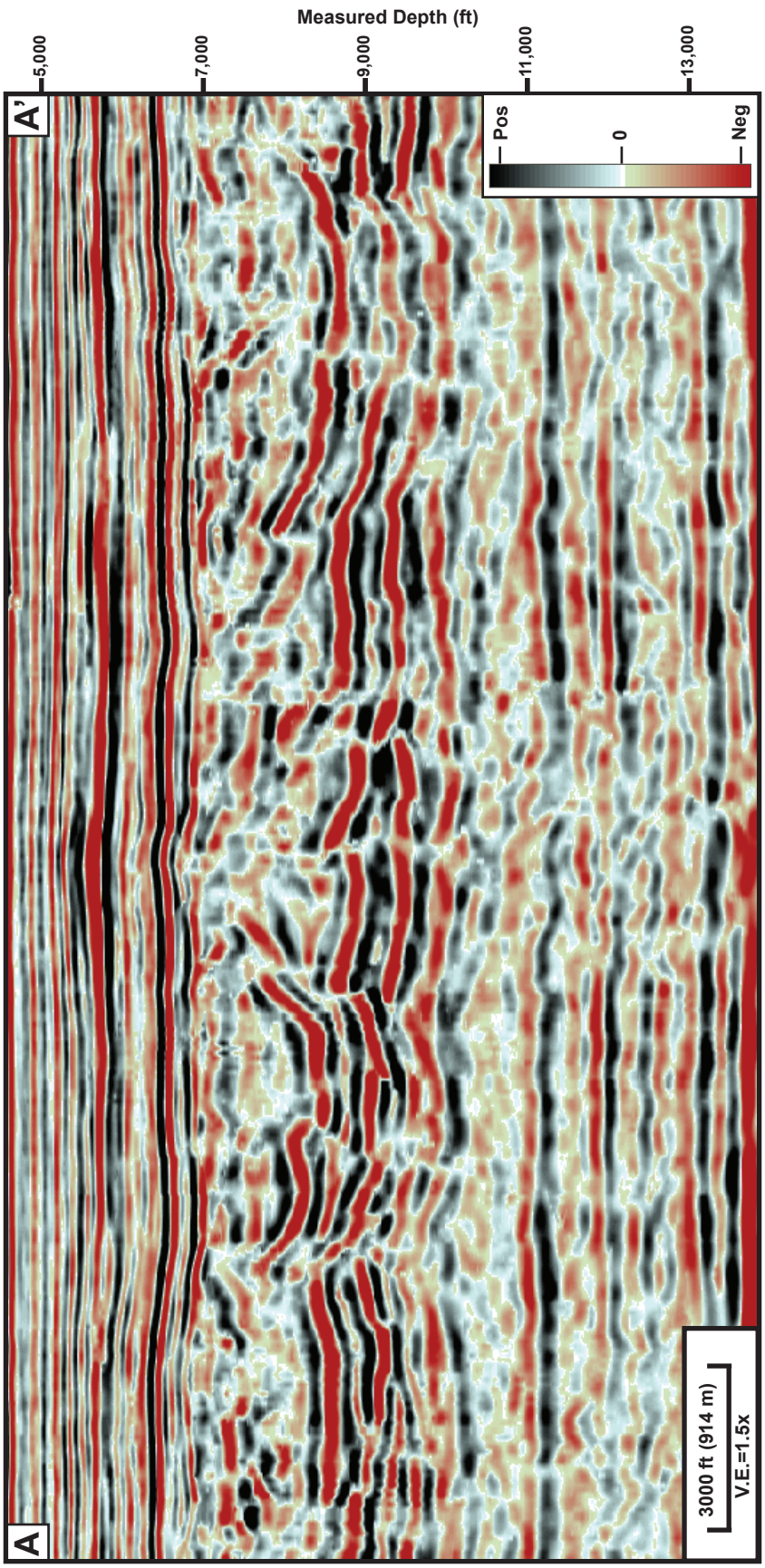

Figure 46a. Uninterpreted arbitrary seismic line that corresponds with Figure 46b. The fault numbers and seismic line annotation correspond with Figure 44.

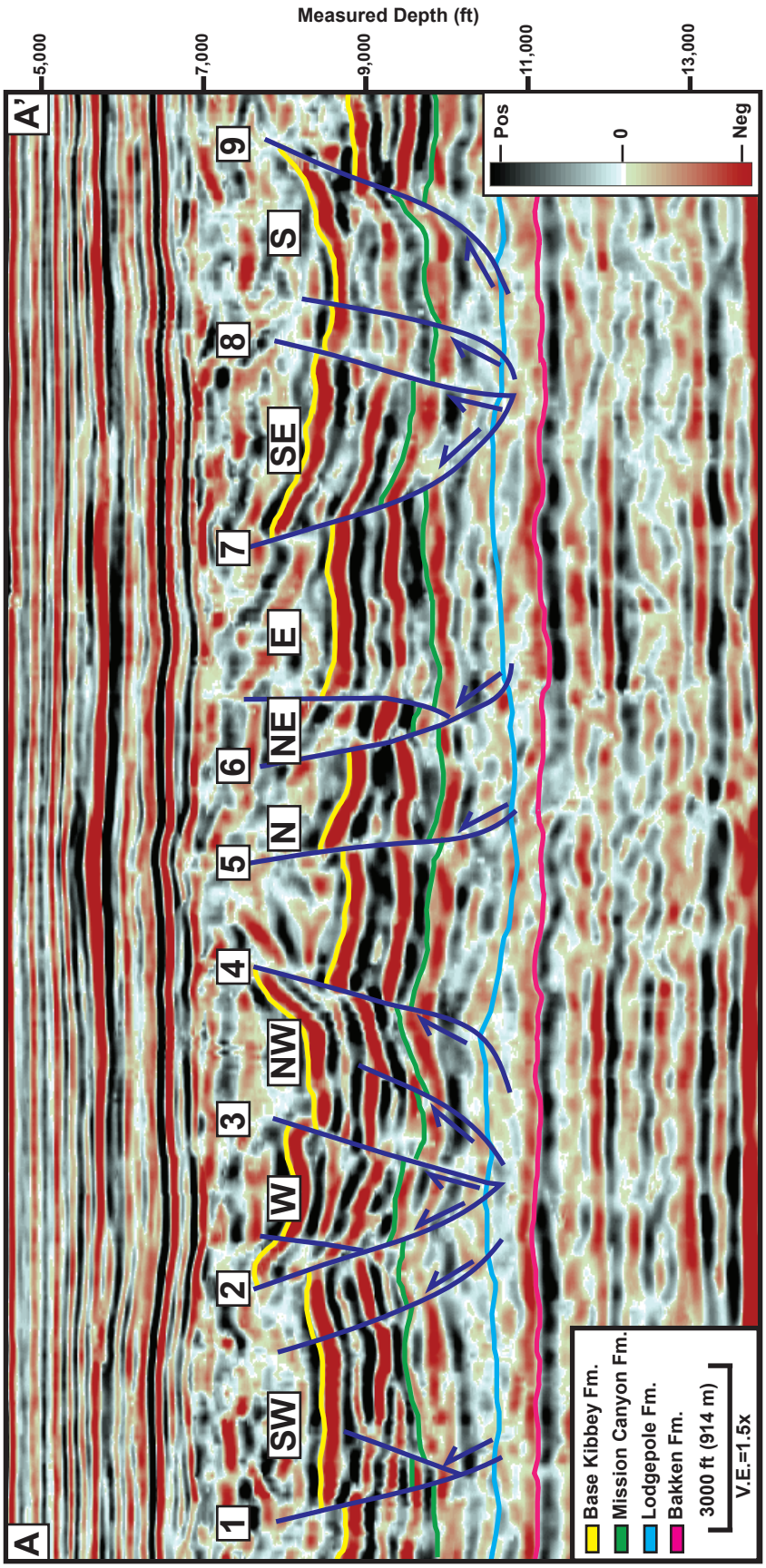

Figure 46b. Arbitrary seismic line through the nine major radial thrust faults or "radial transpression ridges" present at Red Wing Creek. The fault numbers, sectors (letters), and seismic line annotation correspond with Figure 44.

extends 0.97 miles (1.56 km), Thrust 4 extends 0.82 miles (1.32 km), Thrust 6 extends 0.52 miles (.84 km), Thrust 7 extends 0.72 miles (1.16 km), Thrust 8 extends 0.56 miles (.90 km), and Thrust 9 extends 0.65 miles (1.05 km). Thrusts 4 and 6 are unique because at their terminus, they are intersected by other faults that are along the same plane, but the intersecting faults have a different structural styles and orientations. Thrust 4 transitions to a normal fault that dips southwest, whereas Thrust 6, which dips southeast, transitions to another thrust fault that dips northwest.

There is a distinct orientation of the faults according to their location around the central core. The faults that are located to the east and west of the central crater, (Thrusts 2, 3, 7, and 8) strike primarily in an east and west direction. Those located to the north and south of the central core trend toward the NW (Thrust 4), NE (Thrust 6), SW (Thrust 1), and SE (Thrust 9). There is also a dominant trend in thrust vergence according to the fault's location around the central core. Those faults that are located in the northern half of the central uplift complex (Thrusts 3, 4, 6, and 7) verge toward the north, northwest, or northeast, whereas those in the southern half (Thrusts 1, 2, 8, and 9) verge toward the south, southeast, and southwest. Because of this trend, the blocks bounded by Thrusts 2 and 7, as well as 7 and 8 appear as "pop-up" structures that are shallower in the section than the remaining six blocks that surround the central core (**Figure 46)**. Between the major radial thrusts, there are a series of less areally extensive high angle, normal and thrust faults, which radiate away from the central core but do not have a major impact on the inner rim's internal structure (**Figure 44**). Thrust 5 is the most significant of these features and has a maximum vertical offset of 300 feet

(91.4 m) (**Figure 46)**. Some of these smaller thrusts form as back-thrusts to the main fault, such as Thrust 6.

All of the major radial thrust faults extend from the Lodgepole detachment level to the upward to the Spearfish crater floor (**Figure 46)**. The overall vertical length of these faults ranges from 2400 to 3400 feet (731.5 to 1036.3 m). The maximum vertical offset along these faults usually occurs at the shallowest point along the fault plane. For example, the vertical offset at the Mission Canyon Formation level is less than that of the overlying Base of Kibbey Formation marker (**Figure 46)**. Along Thrust 7, the maximum vertical offset at the Mission Canyon level is 710 ft (216.4 m), when at the Base of Kibbey level it is 1150 ft (350.2 m) (**Figures 44**). Maximum vertical offset varies between the faults, with the greatest maximum offset values along Thrusts 2, 4, 6, 7, and 9 (**Figures 44, 46**). Along these faults the maximum vertical offset ranges from 670 to 900 feet (204-274 m) at the Base Kibbey level.

The fault planes dip at similar angles; at the top of the fault, dips range from 60° to 75°, and the dip of the fault plane decreases with depth toward the detachment level (**Figure 46)**. At Thrusts 7 and 9, the dip angle below the Mission Canyon Formation decreases to 40°, in contrast to 60° at the Base of Kibbey level (**Figures 44, 46)**. The dip angle of the strata between the radial thrust faults often varies greatly as well. The dip of the blocks often increases greatly nearer to the thrust faults. This is most significant at Thrusts 3 and 4. The section at the Base of Kibbey level, close to Thrust 3, has an apparent dip of 6° away from thrust 4. Adjacent to Thrust 4, the section, described above, steepens to an apparent dip angle that is as high as 35° away from the fault interface.

The structural expression of these radial thrusts or “radial transpression ridges” varies greatly from the point of maximum vertical offset, adjacent to the central core, to the terminus of the fault at the edge of the inner rim (Kenkmann and Von Dalgwik, 2000). The structural variation along strike of Thrust 7 is illustrated in **Figure 47**. At its shallowest point, adjacent to the central core (**Figure 47a)**, the radial transpression ridge is expressed by a thrust fault with a maximum vertical offset of 780 feet (237.8 m) at the Base of the Kibbey Formation. Away from the central crater, near the Thrust 7 terminus (**Figure 47b**), the radial transpression ridge is expressed as a minor thrust with a maximum vertical offset of 230 feet (70.1 m) at the Base of Kibbey Formation. Beyond the fault terminus, the ridge transitions from a radial thrust fault to a radial fold (**Figure 47c**). The fold is 0.45 miles (0.72 km) across at its widest point in strike view and is 230 feet (70.4 m) higher than the adjacent, unfolded section. The transition from major thrust to minor thrust to radial fold is the typical lateral structural transition of the radial transpression ridges that surround the central core at Red Wing Creek. The exceptions are Thrusts 4 and 6 that transition to a different faulting style before the radial fold develops. In the case of Thrust 4, the faulted zone reaches the edge of the inner rim before a radial fold can develop (**Figure 44)**.

Upper Detachment Zone

Within the inner rim, most of the faulting in the lower interval (base Lodgepole Formation to Top of Charles Formation) detaches within the Lodgepole Formation shale layers, which have an average thickness of 10 feet (3.1 m) in the field. However, directly adjacent to the central core, there is an upper zone of imbricate thrusting between the Charles and the crater floor (**Figure 48)**. The evaporite strata of the Charles Formation

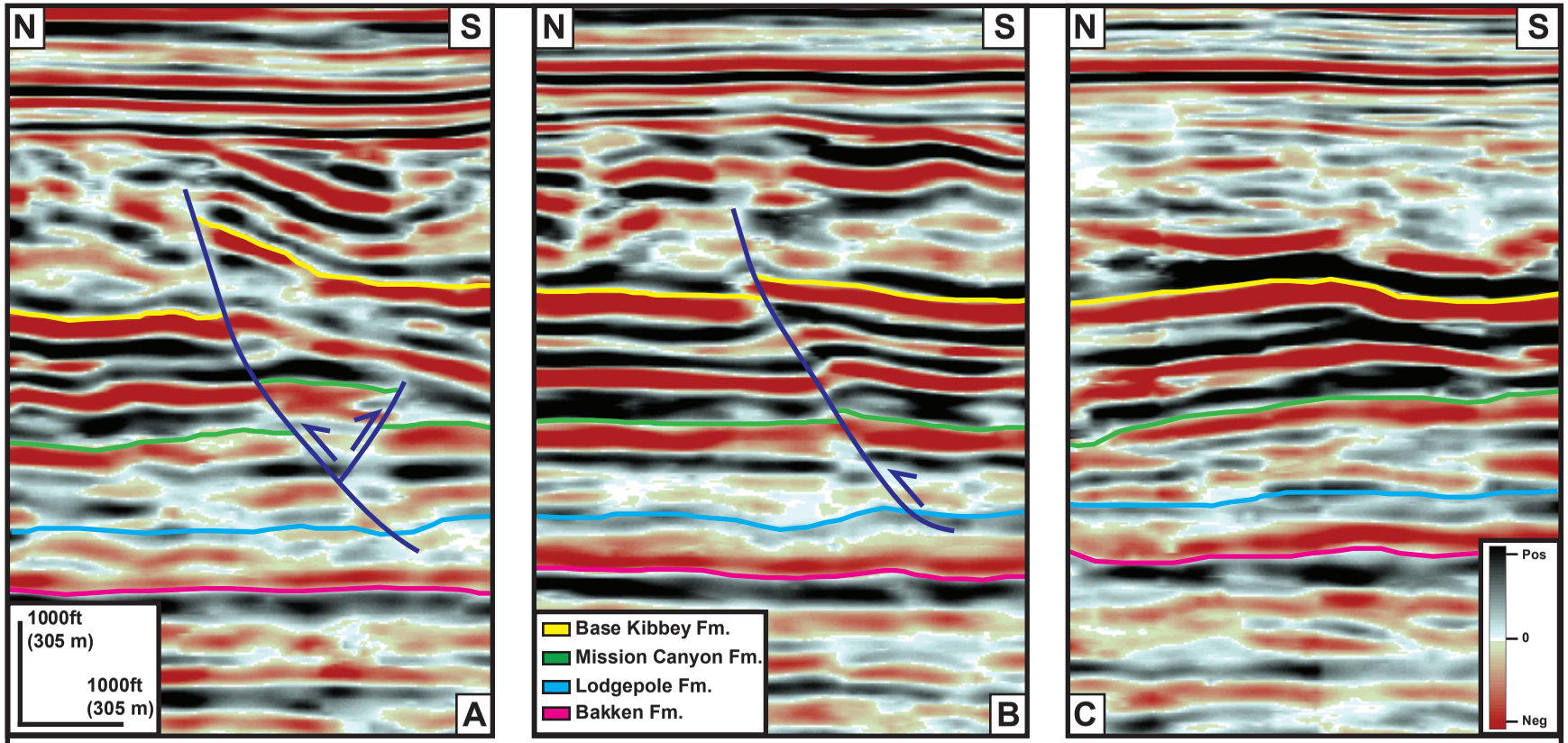

Seismic line through radial thrust fault 7 near the central uplift. Maximum offset is seen in this location.

Seismic line through the end of radial thrust fault 7. There is still reverse offset present but the offset is less pronounced further from he central uplift.

Seismic line through the radial transpression ridge 1000 feet (305m) from the end of fault 7. At this point, the section is no longer faulted but is a radial fold.

Figure 47. Seismic cross sections move along strike of radial thrust fault 7. The radial transpression ridge transitions from a radial thrust fault to a radial fold at its downdip limit, which is adjacent to the edge of the thickened zone to annular trough transition. Refer to Figure 44 for cross section locations.

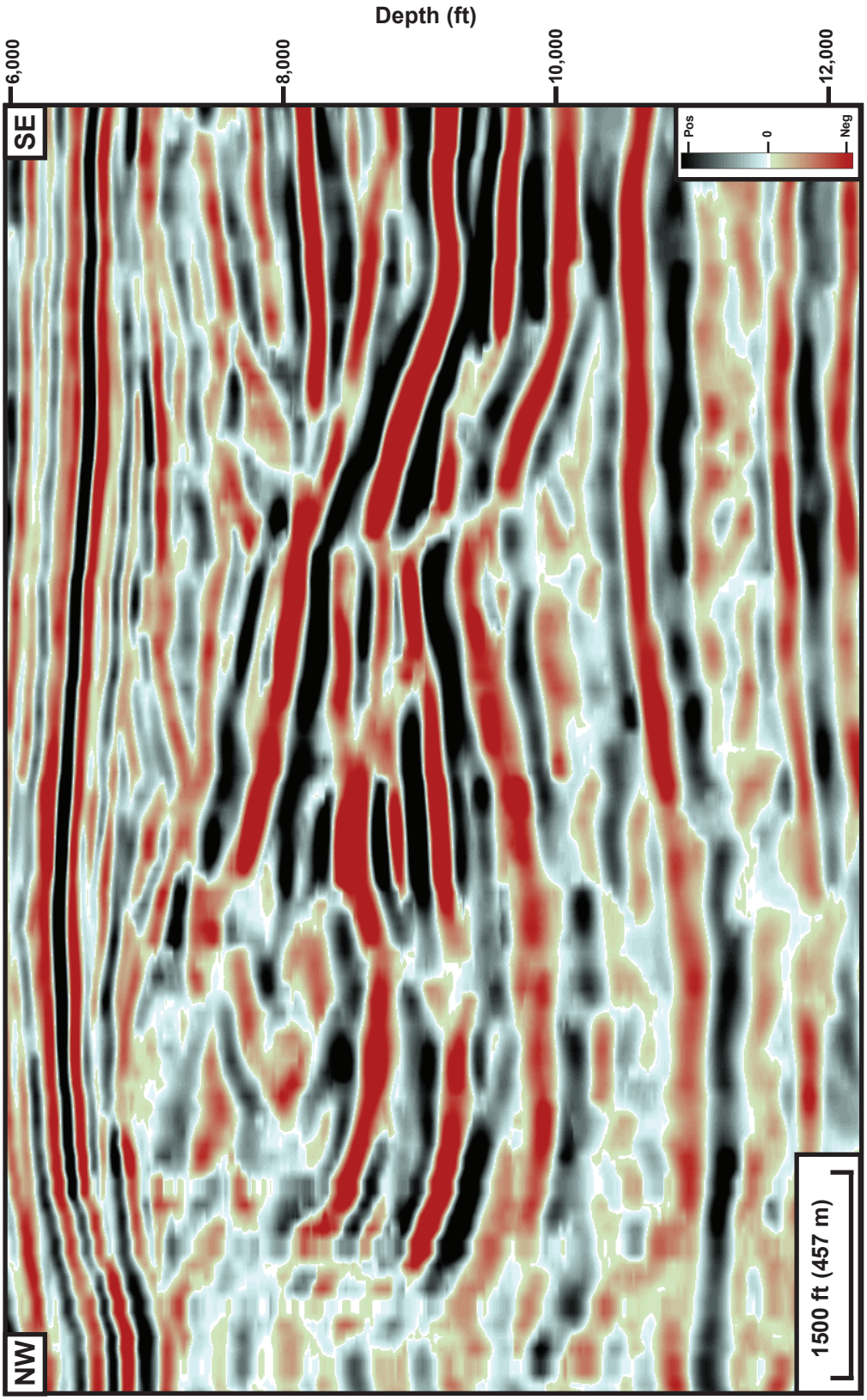

Figure 48a. Uninterpreted seismic profile that corresponds with Figure 48b. Location of profile is shown in Figure 49.

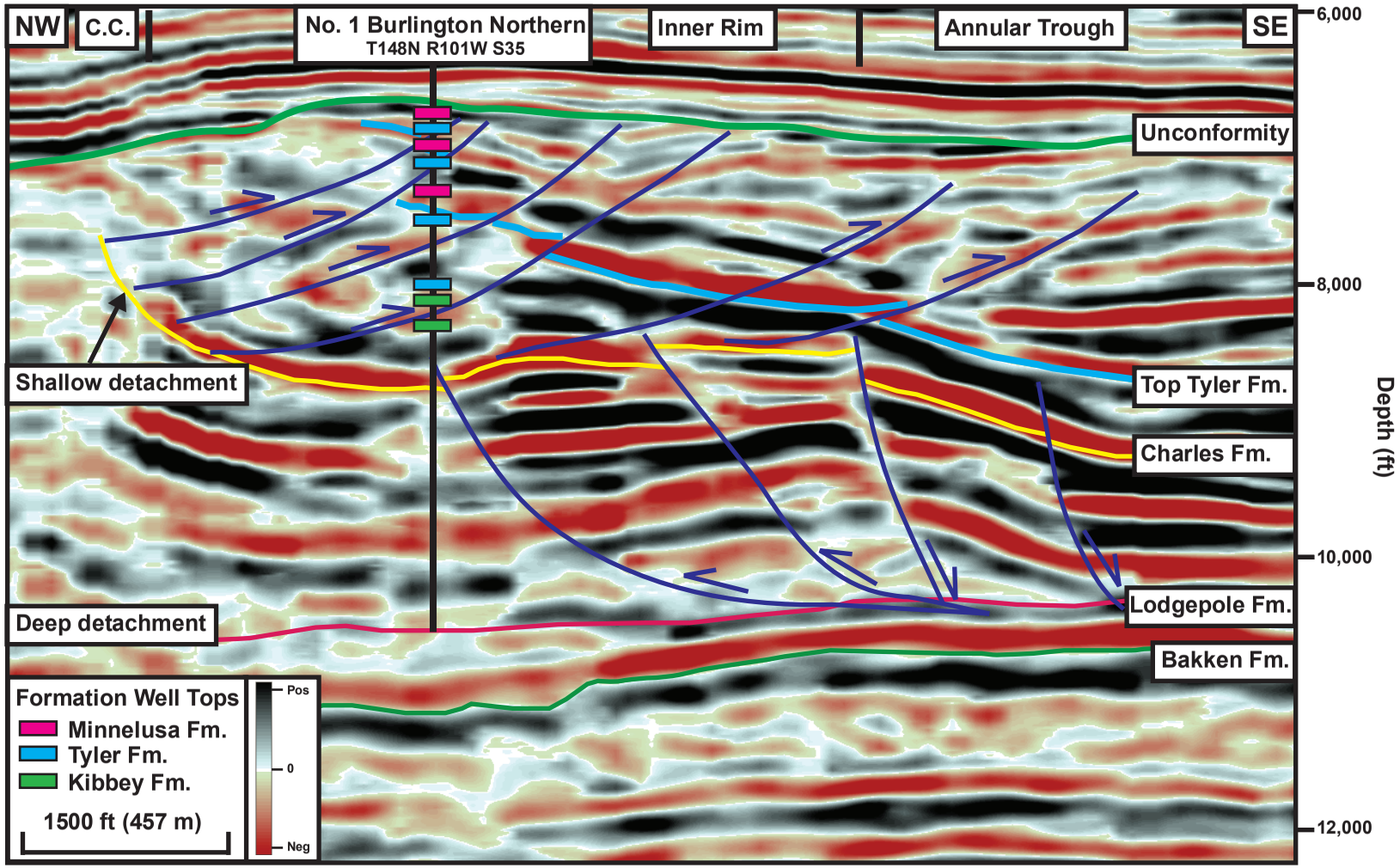

Figure 48b. Seismic profile illustrating the upper thrust zone present above the Charles Formation evaporites, that serve as a detachment surface. The No.1 BN well shows that there are at least five repeated stratigraphic sections in the well bore above the Charles Formation due to imbricate thrusting. This section, that represents the southeastern sector of the thickened section, is unique because it is the only location that has thrusting directed toward the central crater that detaches within the Lodgepole Formation. Signficant structural zones are labeled: central core (CC), inner rim, and annular trough. The location of the profile is annoted on Figure 49.

(primarily anhydrite and halite), serve as the detachment level for the upper imbricate thrust zone. In the field, the Charles formation is highly deformed, but the average thickness of the Charles Formation evaporites is 100 feet (30.5 m) thick. This zone forms a ring of outward thrusted strata around the central crater.

The upper thrusted zone begins 1.1 to 1.3 miles (1.77 to 2.09 km) outside the central point of the crater (**Figure 49)**. The outer limit of this zone appears to be approximately symmetrical around the central core. Like the underlying thrusted strata, the upper thrusted zone is divided into eight individual zones by the radial thrust faults that were described above (**Figure 50)**. The distance from the outer edge of the upper thrusted zone to the outer edge of the inner rim varies around central core. To the north the upper thrust begins 0.47 miles (0.75 km) from the edge; of the inner rim; to the east, it begins 0.41 miles (0.66 km) from the edge, and in the south it begins 0.40 miles (0.64 km) from the edge of the inner rim. The southwest, western, and northwestern zones are structurally unique. In these areas the upper thrusted zones begin from only 0.16 to 0.22 miles (0.26 to 0.35 km) from the inner rim limit. In some locations, the thrusted zone extends to the edge of the inner rim.

The overall thickness of the upper thrusted zone differs greatly from the average thickness of this stratigraphic interval in the field. The drastic increase in thickness between the top of the Charles Formation to the top of the Pennsylvanian Tyler Formation is show in **Figure 49**. In the field, away from the central uplift, the thickness of this interval ranges from 500 to 600 feet (152 to 183 m). Within the upper thrusted zone, this interval thickness can be as high as 1,700 feet (518 m) at its thickest point, due to the multiple imbricate thrust faults present in this zone.

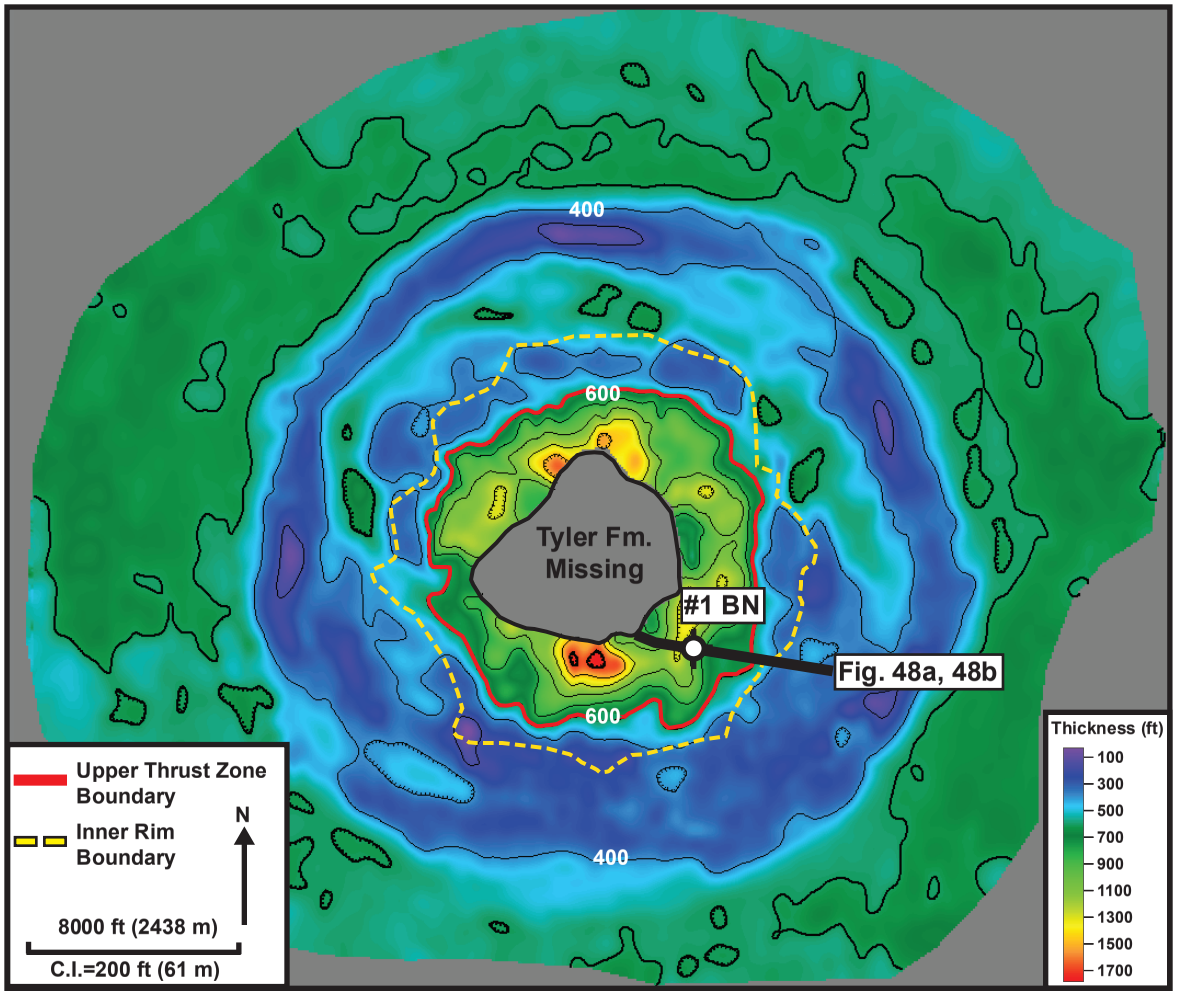

Figure 49. Isopach map from the top of the Charles Formation to the top of the Tyler Formation. The Charles Formation evaporites serve as a major detachment for imbricate thrust faults within the Upper Mississippian through Middle Permian section. Outer limits of the upper thrust zone are shown. Within the inner rim, the upper thrusted zone interval is up to 1,200 feet (366 m) thicker than the Charles to Tyler interval in the outer rim. Locations of structural zones and the location of the seismic profile (Figure 48) with the intersecting #1 BN well are shown.

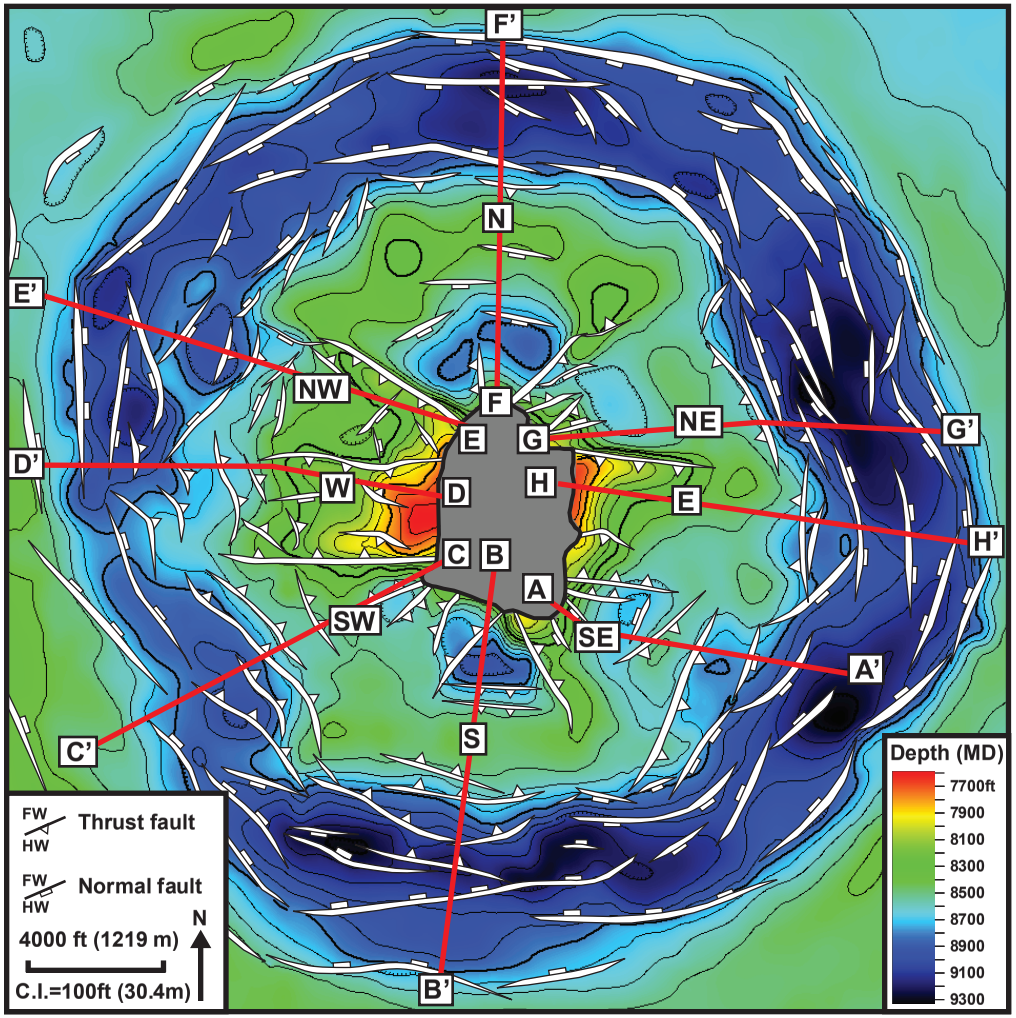

Figure 50. Depth structure map of Base of Kibbey/Top of Charles Formation illustrating the eight structural zones (N,NE,E,SE,S,SW,W,NW) within the inner rim formed by radial thrust faulting. Cross section annotations correspond with following seismic cross sections. For the SE sector seismic cross section, refer to Figure 48.

This zone's structural expression is shown in a dip oriented seismic line that intersects the No. 1 Burlington Northern well in section 35 (**Figures 48)**. In this particular well, there are at least four zones of structurally repeated section (**Figure 48)**. Specifically, the Tyler to Minnelusa Formation interval is repeated three times and the Kibbey Formation shows one zone of repetition. The wireline log data suggest that there is additional structural repetition, but this faulting could be below the resolution of the seismic data set. From the seismic and well data, four imbricate thrust faults can be mapped that detach within the Charles Formation (**Figure 48)**. An additional fault at the top of the thrusted section can be mapped based solely on the seismic. Most of the thrusts faults, in this zone, extend as high as the Spearfish crater floor. These faults dip at an angle of 25° to 35° toward the central crater and all thrust vergence is directed outward. Where the imbricate thrust faults detach, the Charles Formation dips steeply (22°) away from the central core. The dip of the Charles Formation, where it is intersected by the upper thrust faults, varies around the crater according to which radial fault bounded sector it is located in.

The amount of displacement within the upper thrusted zone tends to increase toward the top of the imbricate thrust fans (**Figure 48)**. Thrust fans are a series of thrust faults that diverge upward from a common detachment level (McClay, 1992). The major trailing fault (shallowest fault in the imbricate fan) has a vertical displacement of 450 feet (137 m) at the top of the Tyler Formation, whereas thrust faults deeper in the imbricate, thrust fan have a vertical displacement of 150 feet (46 m) at the top of the Tyler Formation. The fans in this zone, around the central core, are characterized as trailing imbricate fans (offset is greatest in the shallowest thrust fault) with maximum

displacement at the trailing (shallowest) thrust fault (Boyer and Elliott, 1982; McClay, 1992). Importantly, the Triassic to Jurassic unconformity truncates this section. Therefore, the overall thickness of this interval and the vertical extent of the thrust faults can't be determined (**Figure 48**).

Individual Inner Rim Sectors

The inner rim is separated by radial thrust faults into eight structurally unique sectors (**Figure 50, Table 4)**. The internal structure of each sector is variable and has a characteristic structural style (**Figure 51)**, and the dominant structural character of each zone is systematically described below. Also, the discussion of each representative cross section will be divided into the character of the lower detachment zone (Lodgepole Formation detachment) and the upper thrust zone (Charles Formation detachment). Each sector is annotated according to its cardinal direction around the central core.

N Sector

The north sector (N sector) is the largest of the sectors within the inner rim, and it covers 1.6 square miles (4.1 km^2). The external geometry of the lower detachment zone, between the Lodgepole and the Charles Formation, is a non-cylindrical (curved hinge line), anticlinal fold **(Figure 52)**. The fold wavelength is approximately 1.15 miles (1.85 km) at its widest point.

Internally, the fold in the lower zone is underlain by two imbricate thrust faults verging away from the central crater **(Figure 52)**. The fault planes of these two imbricate thrust faults dip toward the central core at a maximum angle of 30° at the

Sector	Maximum number of thrust faults (upper/lower detachment)	Maximum dip of thrusts faults (upper/lower detachment)	Areal Coverage	Other Comments
N	Lower-2 Upper-5	Lower- 30° Upper-15°-20°	1.6 square miles (4.1 km^2)	Characterized by internally thrusted fold
NE	Lower-2 Upper-7	Lower-75° Upper-25°	.73 square miles (1.89 km^2)	
E	Lower-3 Upper-4-5	Lower-60° Upper-35°	.75 square miles (1.94 km^2)	
SE	Lower-2 Upper-6	Lower-60°-70° Upper-30°-40°	.60 square miles (1.55 km^2)	Only sector where thrusting is directed toward central core
S	Lower-5 Upper-6	Lower-50° Upper-30°	.55 square miles (1.42 km^2)	Lower detachment zone is heavily faulted fold
SW	Lower-4 Upper-6-7	Lower-65° Upper-30°	.92 square miles (2.38 km^2)	
W	Lower-6-7 Upper-10	Lower-65° Upper-40°	.64 square miles (1.66 km^2)	
NW	Lower-4 Upper-5-6	Lower-60° Upper-25°	.55 square miles (1.42 km^2)	

Table 4. Summary table of structural sectors within the inner rim.

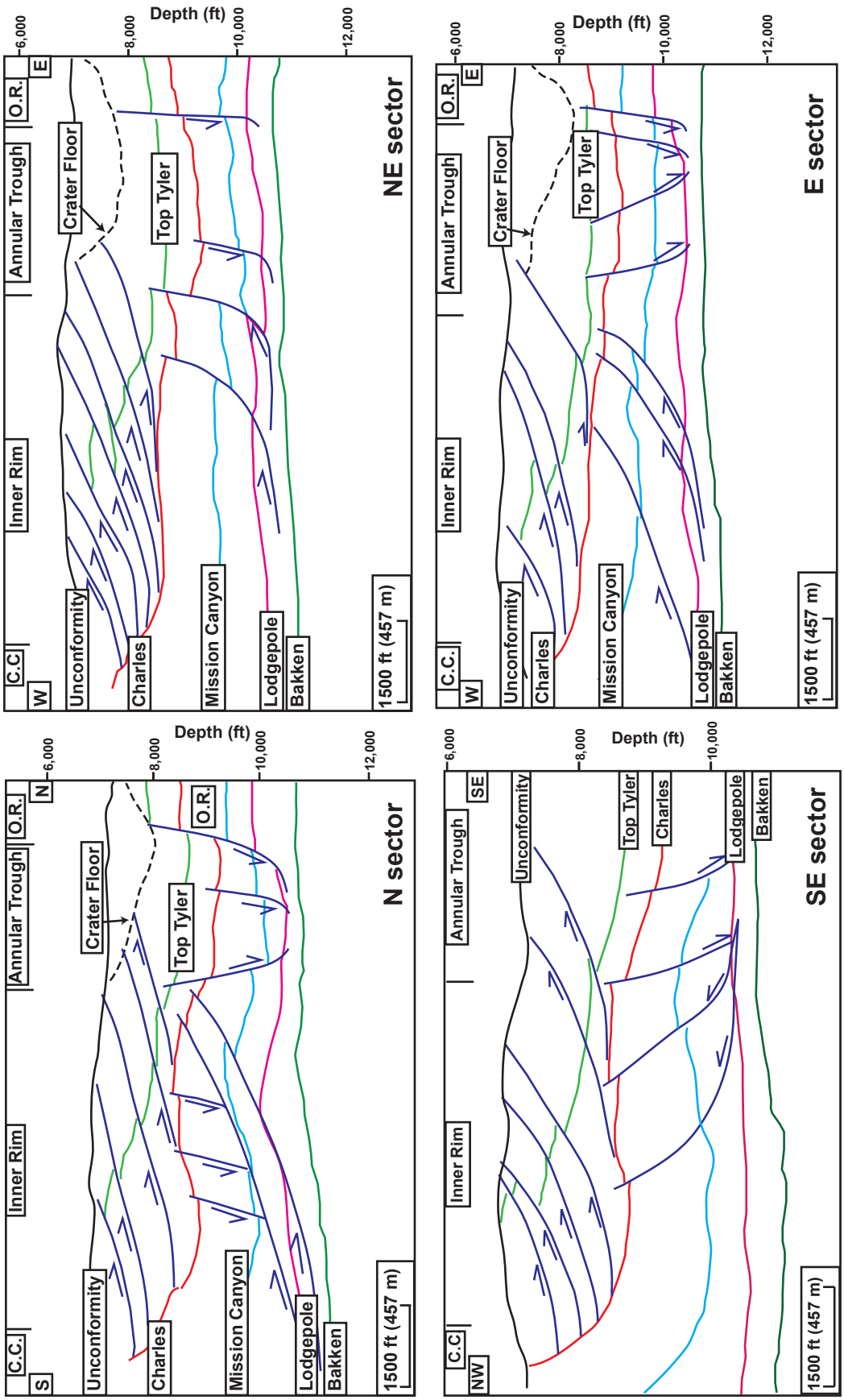

Figure 51a. Line profiles of four, unique structural sectors, which surround the central core. Each sector is separated laterally by radial transpression ridges and each has a unique internal structural style. Clockwise from the top left are sectors: N, NE, E, and SE. Refer to Figure 50 for line locations and figures 48, 52-54 for interpreted seismic profiles corresponding to each line profile.

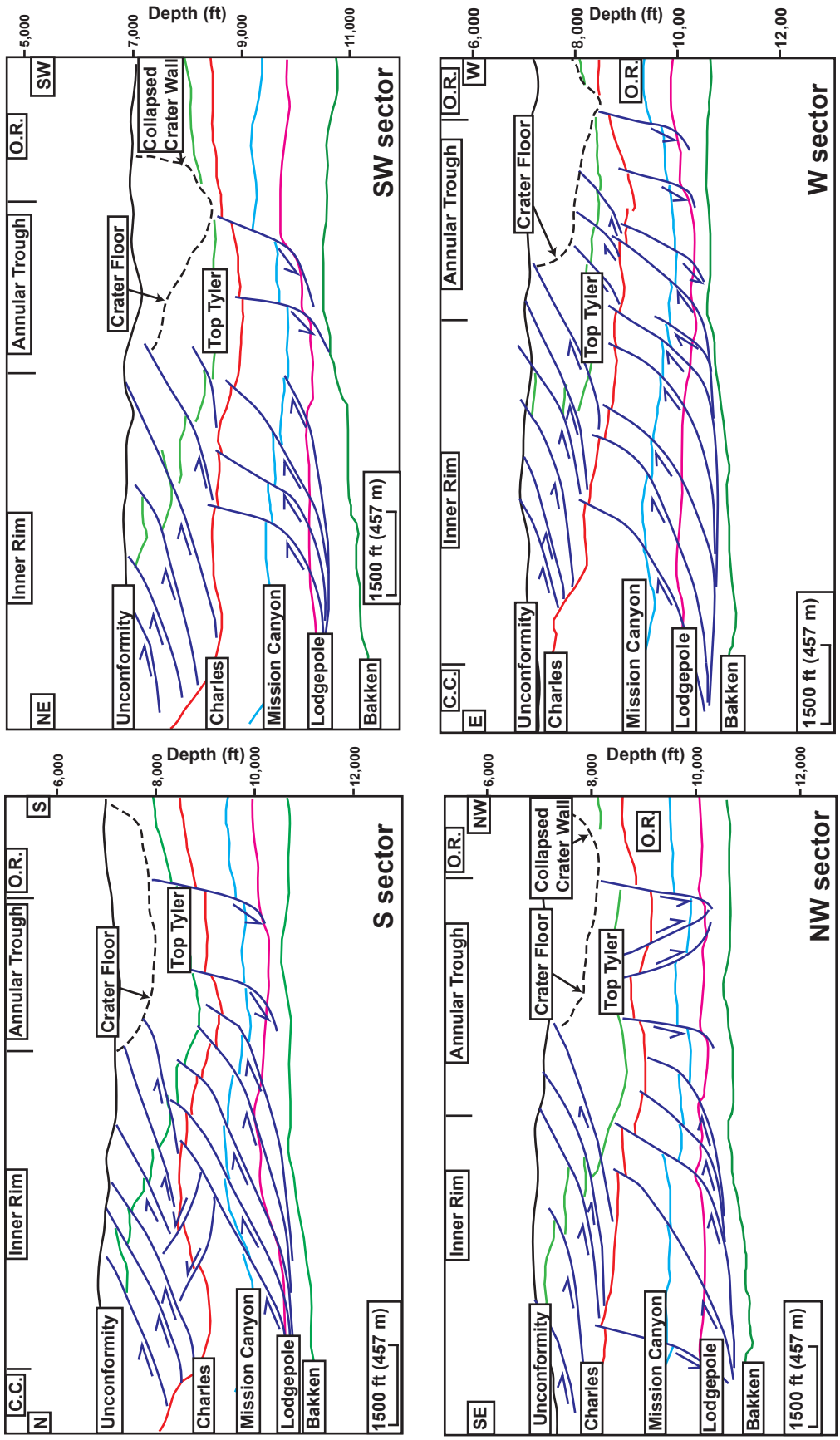

Figure 51b. Line profiles of four, unique structural sectors, which surround the central core. Each sector is separated laterally by radial transpression ridges and each has a unique internal structural style. Clockwise from the top left are sectors: S, SW, W, and NW. Refer to Figure 50 for line locations and figures 43, 55-57 for interpreted seismic profiles corresponding to each line profile.

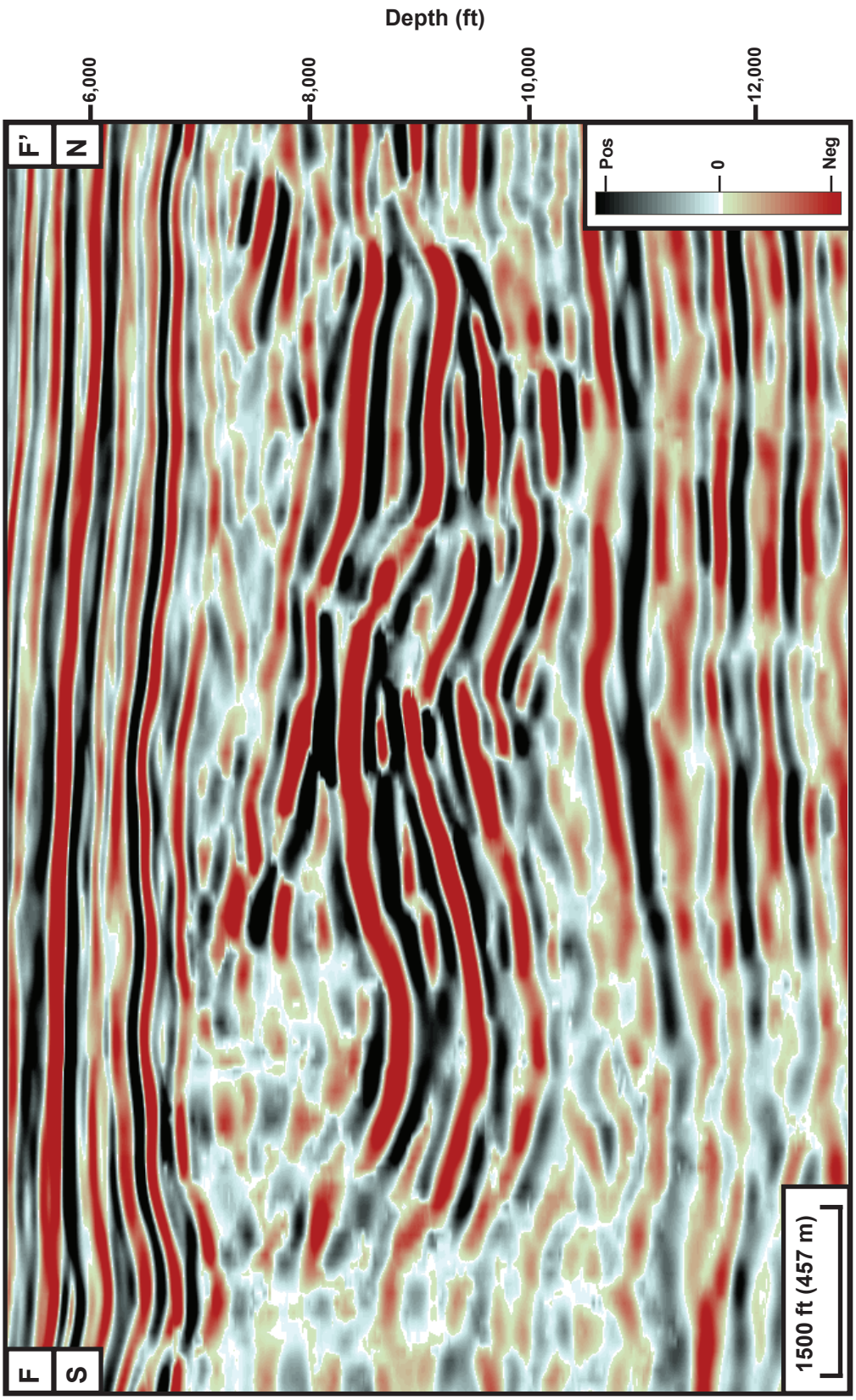

Figure 52a. Uninterpreted seismic profile that corresponds with Figure 52b. See Figure 50 for the location of the profile.

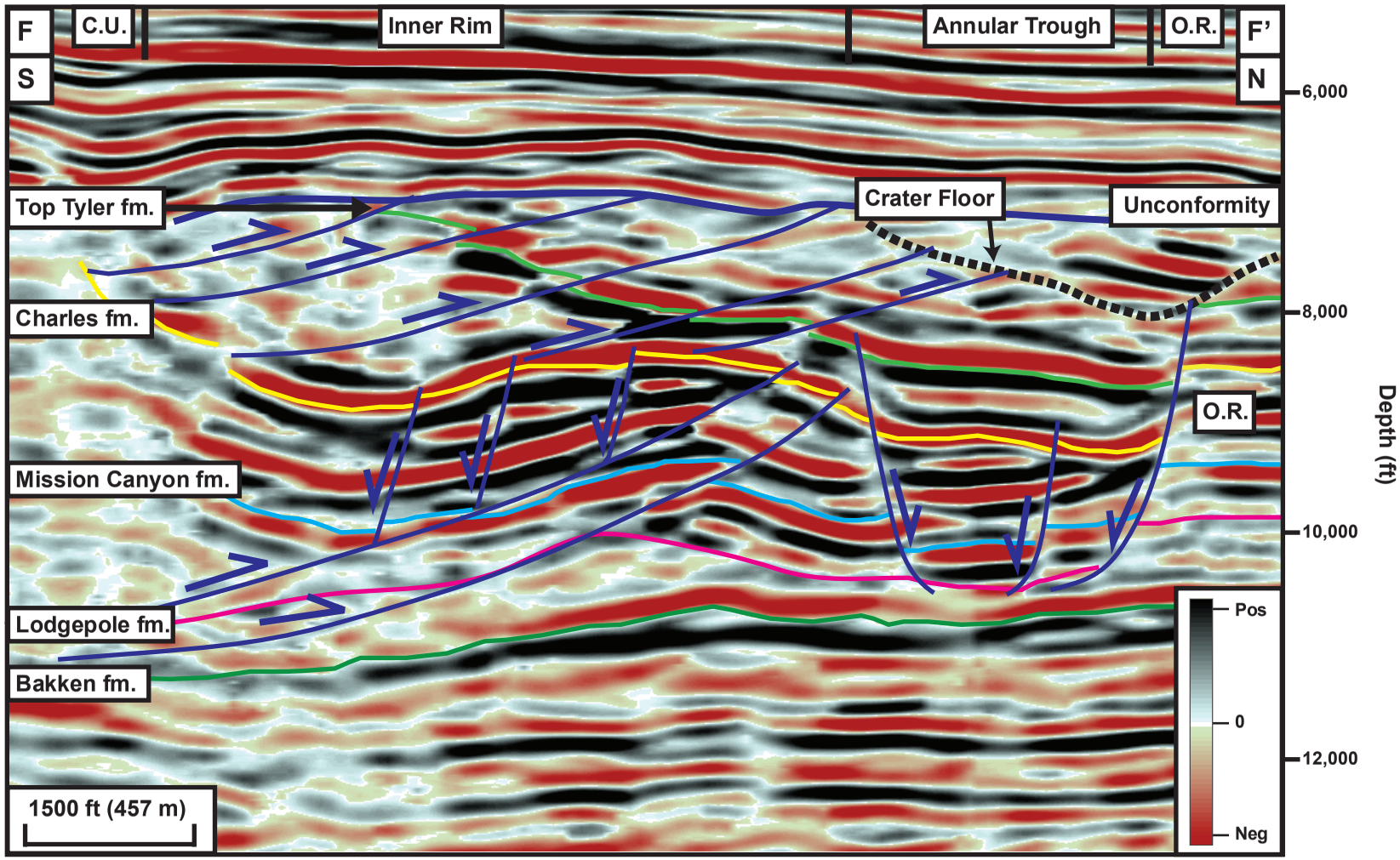

Figure 52b. Seismic profile through sector N of the inner rim. Externally, the lower section is characterized by folding and by imbricate thrusting internally. The upper thrust zone between the Charles and Tyler Formations is 1500 feet thick (457 m) above the inner limb of the underlying fold, and the Tyler is offset up to 180 feet (54.9 m) vertically along the upper thrust faults. Significant structural zones are labeled: central core (C.C.), inner rim, annular trough, and outer rim (O.R.). See Figure 50 for the location of the profile.

upper fault terminus; there is a slight increase in the dip of the fault planes toward the tip point. There is a decrease in the vertical offset of the two toward the top of the faulted section. Specifically at the Mission Canyon level, the maximum vertical offset is 225 feet (68.6 m), whereas at the top Charles to Base Kibbey contact, the vertical offset has decreased to 100 feet (30.5 m). In addition, there is a series of three normal faults along the inner (back) limb of the anticlinal fold, which terminates along the upper thrust plane. These dip at 70° toward the central core and have a maximum displacement at the Charles level of 215 feet (66.5 m). The outer limit of the inner rim and annular trough is marked by a normal fault that dips toward the crater rim.

The upper zone is relatively thick in comparison to other sectors around the central core due to the space created by the inner (back) limb of the underlying anticlinal fold. The upper zone has a maximum thickness, between the Charles and Tyler Formations, of 1,500 feet (457.2 m) where the folding is greatest above the inner fold limb. The thrust faults in this zone verge toward the crater edge and the fault planes have a maximum dip of 15° to 20° toward the central core and detach within the Charles Formation. Vertical offset of the Tyler Formation increases upward in the section from 70 feet along the lower thrust at the base to 180 feet (21.3 to 54.9 m) at the shallowest fault, which makes the trailing thrust (shallowest thrust in the imbricate thrust fan) the fault with greatest displacement.

NE sector

The northeast sector of the inner rim is bounded to the north by radial thrust 6 and to the south by radial Thrust 7 (**Figure 50)**. This sector is approximately 0.73

square miles (1.89 km^2) in area. The lower section, Lodgepole through Charles Formations, is markedly different than the northern sector (**Figure 50).** The strata dip gently at an angle of 2.5 ° toward the central core before experiencing a significant dip change (**Figure 53**). Adjacent to the central core, the dip of the lower detachment section changes abruptly to 20° towards the crater rim. Internally, the lower section has a relatively simple structural style with two outward verging thrust faults that detach at the Lodgepole level (**Figures 53)**. These faults dip toward the central crater and the dip angle along the fault plane increases toward the tip point to a maximum of 78°. Vertical offset is greatest in the lowest portion of the section with a maximum vertical offset of 480 feet (146.3 m) at the Mission Canyon Formation level. The inner rim to annular trough transition is marked by one of these outward verging thrust faults (**Figure 53)**.

The upper interval has a maximum thickness of 800 feet (244 m) between the Charles and top of the Tyler Formations (**Figure 50)**. Internally, this section is marked by seven outward verging imbricate thrust faults that dip at a maximum angle of 25° toward the central crater. They detach at the Charles Formation and cut as high as the Spearfish Formation at the crater floor. Like the northern sector, the vertical offset increases towards the top of the section. The maximum offset at the top Tyler level is 420 feet (128 m); to the west, the Triassic to Jurassic unconformity truncates the upper thrusted section.

E sector

The east sector is bounded by Thrust 7 to the north and by thrust 8 to the south; it covers an area of 0.75 square miles (1.94 km^2) within the inner rim (**Figures 37, 50)**.

Figure 53a. Uninterpreted seismic line that corresponds with Figure 53b. Refer to Figure 50 for the location of the profile.

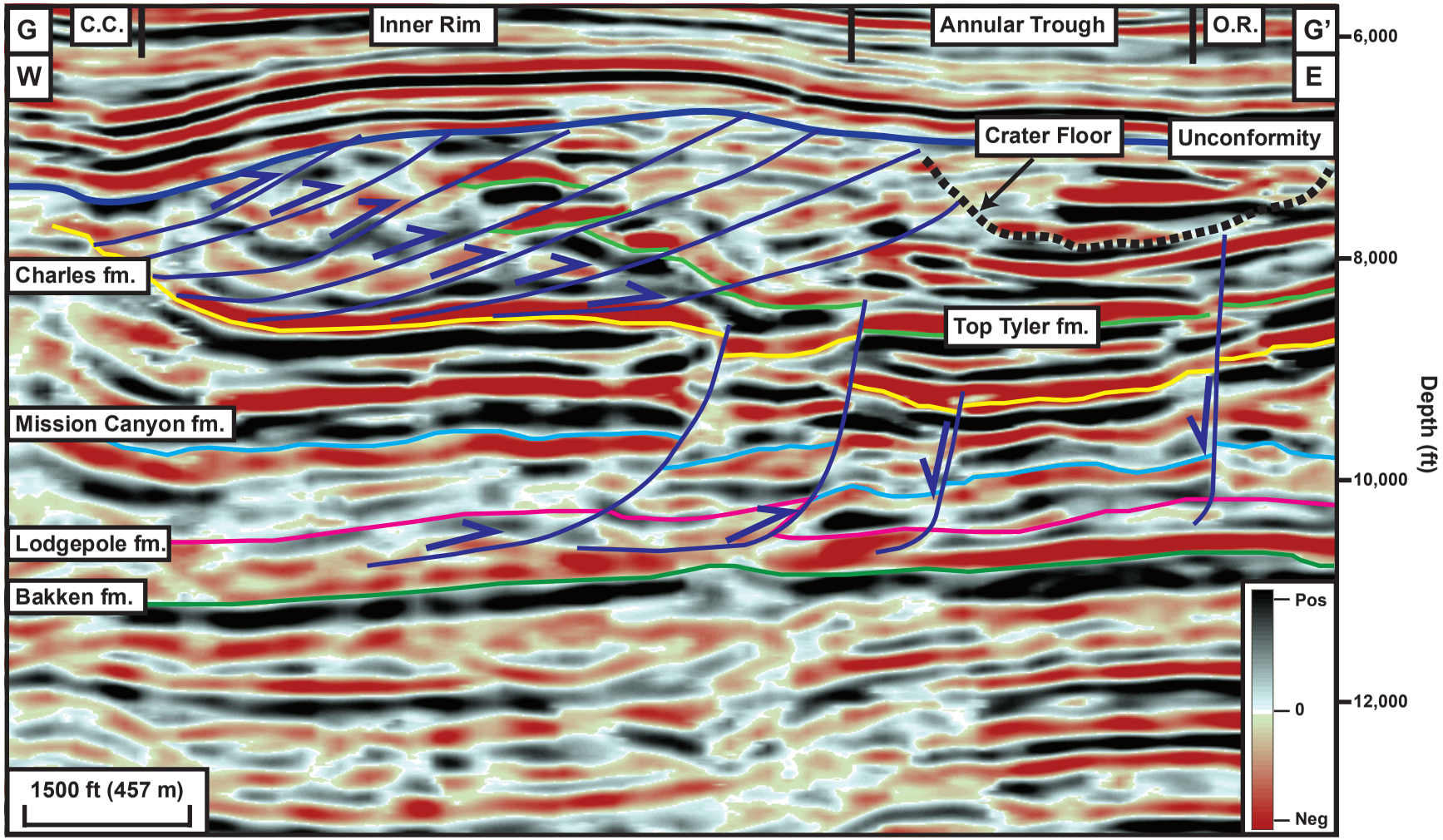

Figure 53b. Seismic profile through sector NE of the inner rim. The lower section is marked internally by a series of steeply dipping thrust faults that detach at the Lodgepole level. The upper thrust section is characterized by multiple imbricate thrust faults that increase the thickness of this interval to 800 feet (244m). Major structural zones are labeled: central core (C.C.), inner rim, annular trough, and outer rim (O.R.). Refer to Figure 50 for the location of the profile.

Most of the lower section dips at an angle of 5° degrees away from the central core; a small anticlinal fold is present at the outer portion of the inner rim, and this sector consists three outward verging thrust faults **(Figures 54)**. The dip of these fault planes increases toward the tip line to a maximum dip of 60° toward the crater center. The maximum offset along these faults is in the middle portion of the section where there is a maximum offset of 270 feet (82.3 m) at the Mission Canyon Formation level. Similar to the outward verging thrust faults in sector NE (**Figure 53)**, the thrust faults detach within the Lodgepole Formation and extend as high as the Charles to Base Kibbey level (but do not extend a significant distance beyond this level). The inner rim to annular trough transition is marked by these outward verging thrust faults (**Figure 54**).

The upper section consists of three outward verging thrust faults that dip toward the central crater at a maximum angle of 35° (**Figure 54**). This section has a maximum thickness of 1,300 feet (396 m) between the top of the Charles Formation and the top of the Tyler Formation (**Figure 49)**. Similar to previous examples, the offset increases along shallower thrust faults to a maximum vertical offset of the Tyler Formation of 415 feet (126.5 m). Most of the faults in this sector cut the crater floor.

SE sector

The structure of this sector is markedly different that the N, NE, and E sectors. The SE sector is bounded to the north by thrust 8 and to the southwest by Thrust 9 (**Figures 37, 50)**. This sector is 0.60 square miles (1.55 km^2) in area. Externally, the sector has an anticlinal fold with a maximum wavelength distance of 0.90 miles (1.45 km). Internally, the sector consists of two inward verging thrust faults (**Figure 48)**. This

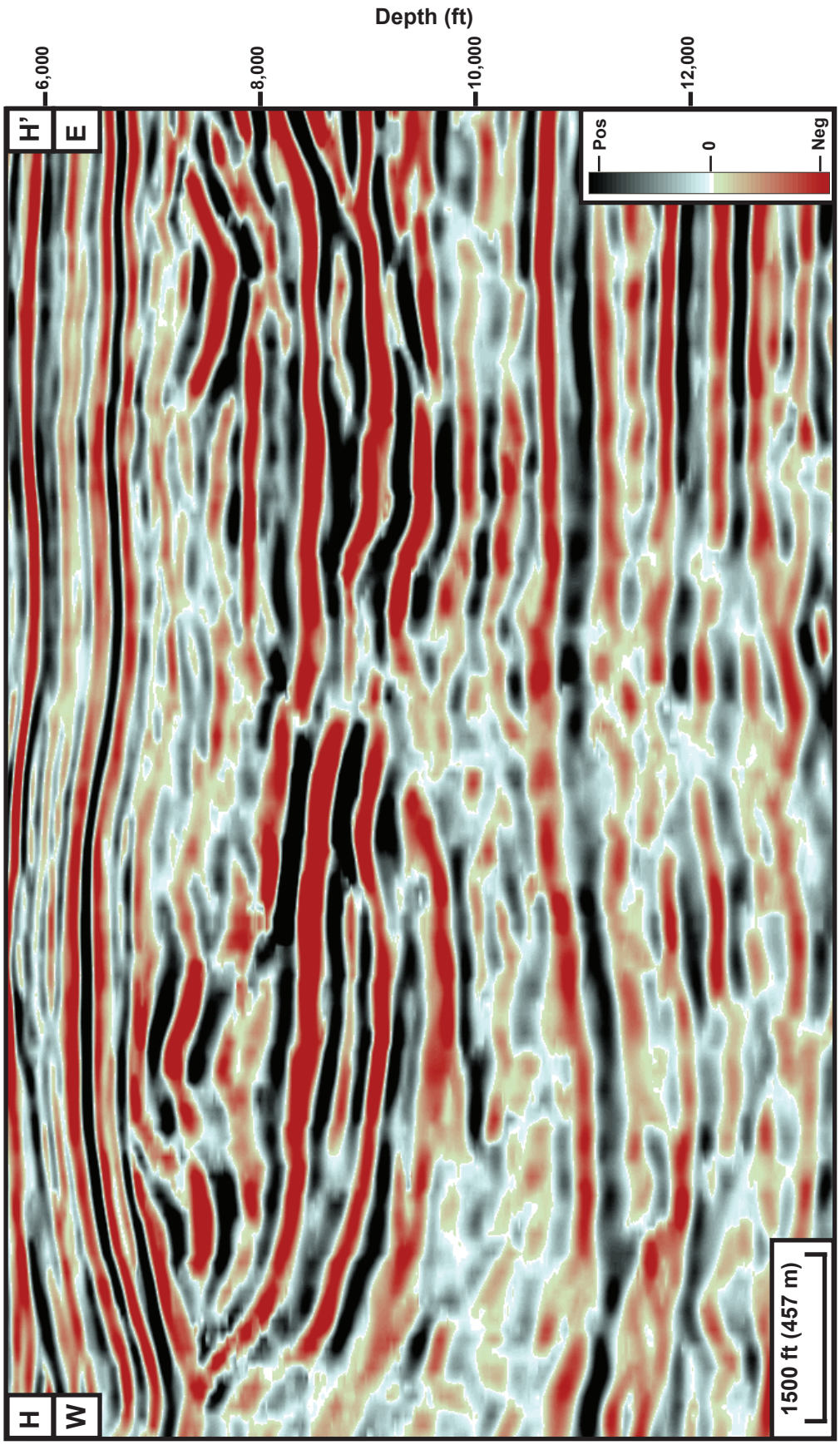

Figure 54a. Uninterpreted seismic profile that corresponds with Figure 54b. Refer to Figure 50 for profile location.

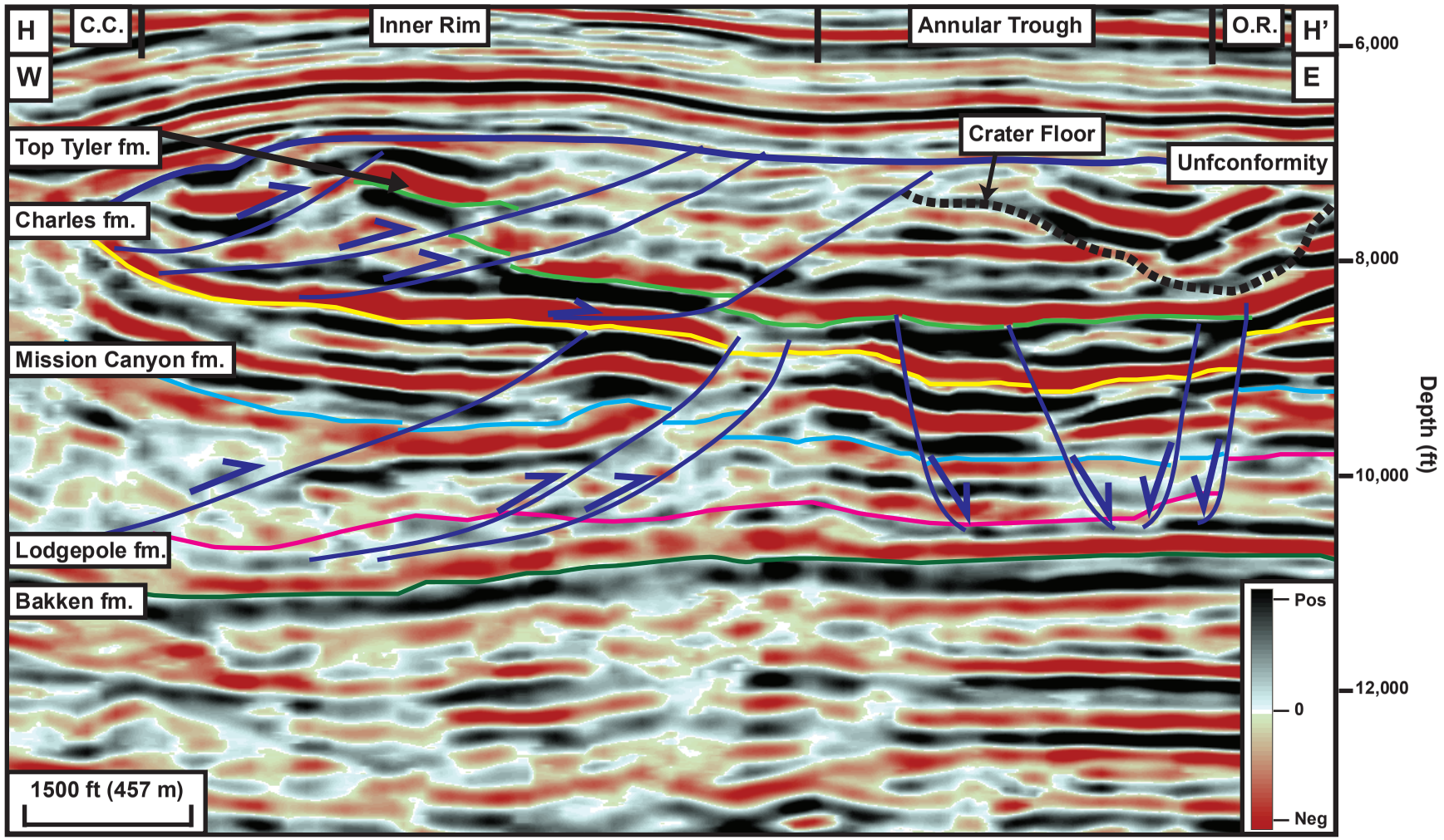

Figure 54b. Seismic profile through sector E of the inner rim. Similar to the northeastern sector, the internal structure of the lower detachment zone is dominated by outward directed thrust faults that steepen significantly toward their tip point at the Charles level. The upper thrust zone has a maximum thickness between the Charles and the top of the Tyler of 1300 feet (396m). Major structural zones are annotated: central core (C.C.), inner rim, annular trough, and outer rim (O.R.). Refer to Figure 50 for profile location.

is the only sector of the inner rim whose structural style is dominated by thrust faults *towards* the central crater. The dip angle of the fault planes increases higher in the section to a maximum angle of 65° toward the crater edge, with a maximum vertical displacement of 140 feet (42.7 m) at the Charles/base of Kibbey level. The transition to the annular trough is marked by antithetic normal faults that dip steeply (75°) toward the crater wall. The upper section for the southeast sector was described above.

S Sector

The southern sector is 0.55 square miles (1.42 km^2) in area and is bound to the east by thrust 9 and to the west by Thrust 1 (**Figures 37, 50)**. Like the northern sector, the external geometry of the lower zone is an anticlinal fold with a maximum wavelength distance of 1.05 miles (1.69 km) **(Figure 55).** Internally, the lower section is heavily faulted by a series of five outward verging, imbricate thrust faults. The dip angle of these faults increases slightly upward to a maximum angle of 50° toward the crater center. The maximum vertical offset at the Mission Canyon level is 225 ft (68.6 m) along the basal imbricate thrust. The amount of offset decreases with shallower thrusts making this a leading thrust fan (shallowest thrust fault has greatest offset) (Boyer and Elliott, 1982). Unlike the thrusts faults in the lower zone in the seven other sectors, these faults extend through the Tyler Formation before terminating. Along the inner, back limb of the anticlinal fold, two back thrust faults terminate on the trailing thrust fault of the under lying fan. These small thrusts verge toward the central crater and have a maximum vertical offset at the Charles Formation level of 200 ft (60.9 m). The boundary between the inner rim and annular trough is unclear due to the extensive faulting present along

Figure 55a. Uninterpreted seismic profile that corresponds with Figure 55b. Refer to Figure 50 for profile location.

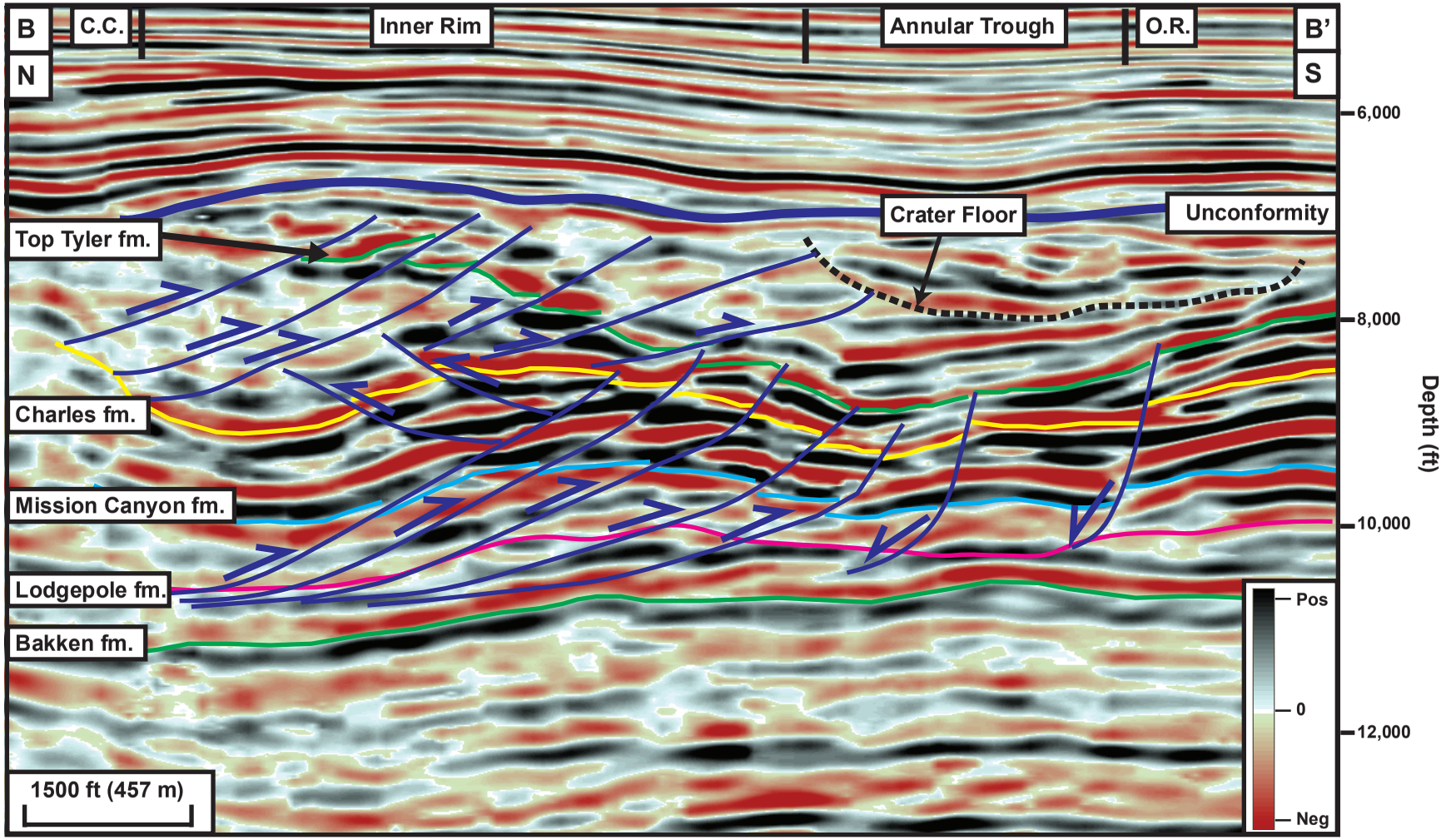

Figure 55b. Seismic profile through sector S of the inner rim that shows two levels of imbricate thrust faults. The external geometry of the lower detachment interval is a broad, faulted anticline that has a maximum wavelength of 5700 feet (1737m). Internally, the folded section is extensively faulted by a series of imbricate thrust faults that extend as high as the crater floor.The upper thrust level is thickest in the southern sector. The interval is 1700 feet (518m) thick between the Charles Formation and the top of the Tyler Formation. Major structural zones are annotated: central core (C.C.), inner rim, annular trough, and outer rim (O.R.). Refer to Figure 50 for profile location.

this boundary. The imbricate thrusts extend a significant distance into the annular trough, which is unique to this sector.

The upper zone in the southern sector is thickest of all sectors with more than 1,700 feet (546m) between the Charles and the top of Tyler Formation (**Figures 49-50)**. The thickest portion of this interval is located over the inner, back limb of the underlying anticlinal fold (**Figure 55)**. The six outward verging thrust faults dip at an angle of 30° toward the central core, and, like other sectors, the vertical offset increases in higher faults to a maximum of 240 feet (73.2 m) at the Tyler Formation level. The imbricate thrust faults clearly cut through and deform the crater floor.

SW Sector

The southwestern sector is bound by Thrust 1 to the southeast and by radial Thrust 2 to the north (**Figures 37, 50).** This sector is 0.92 square miles (2.38 km^2). Externally, the lower zone is characterized as an anticlinal fold with a maximum wavelength distance of 1.04 miles (1.67 km) with the fold axial plane dipping slightly away from the central crater **(Figure 43)**. Internally, four thrust faults cut the anticline bounded by the Lodgepole and Charles/base of Kibbey Formation. The thrust faults are outward verging and dip at a maximum angle of 60° to 70° toward the central crater. Like the imbricate thrusts faults in most sectors, the dip angle of these thrust faults increase significantly toward their tip point at the Charles/base of Kibbey level. The vertical offset decreases upward at the Mission Canyon Formation level to a maximum offset of 150 feet (45.7 m). The inner rim to the annular trough transition is bounded by the leading thrust fault in the lower imbricate fan (**Figure 55)**.

The upper section has a maximum thickness of 1100 feet (335 m) between the Top of the Charles Formation and the top of the Tyler formation above the inner, back limb of the underlying anticline (**Figure 49)**. Six imbricate thrust faults, which detach within the Charles Formation, dip toward the central core at a maximum angle of 20° to 30°. The thrust faults verge outward and the vertical offset along these faults increases upward to a maximum vertical offset at the top of the Tyler Formation of 350 feet (107 m). The imbricate thrust faults cut the crater floor and alter its topography (**Figure 43).**

W Sector

The western sector of the inner rim covers an area of .64 square miles (1.66 km^2). This sector is bound by Thrust 3 to the north and Thrust 2 to the south (**Figures 37, 50)**. Like the eastern sector, the lower interval strata gradually dip away from the central core at an angle of 5° to 8° **(Figure 56)**.

Internally, the western section is quite complex structurally with seven outward verging thrusts that dip toward the central crater (**Figure 56)**. The dip angle of the fault planes increases significantly upward toward the tip point to a maximum of 66°. These faults all detach within the Lodgepole Formation and terminate at the Charles/base of Kibbey Formation level (**Figure 56)**. Maximum vertical offset at the Mission Canyon Formation level occurs with an offset of 200 feet (60.9 m). The inner rim to annular trough transition is bound by these outward verging thrust faults. The thrust faults propagate into the annular trough, which is only seen in the south and west sectors.

The maximum thickness of the upper thrust section in the western sector, which is relatively thin in comparison to the upper sections in other sectors, is 1000 to 1100

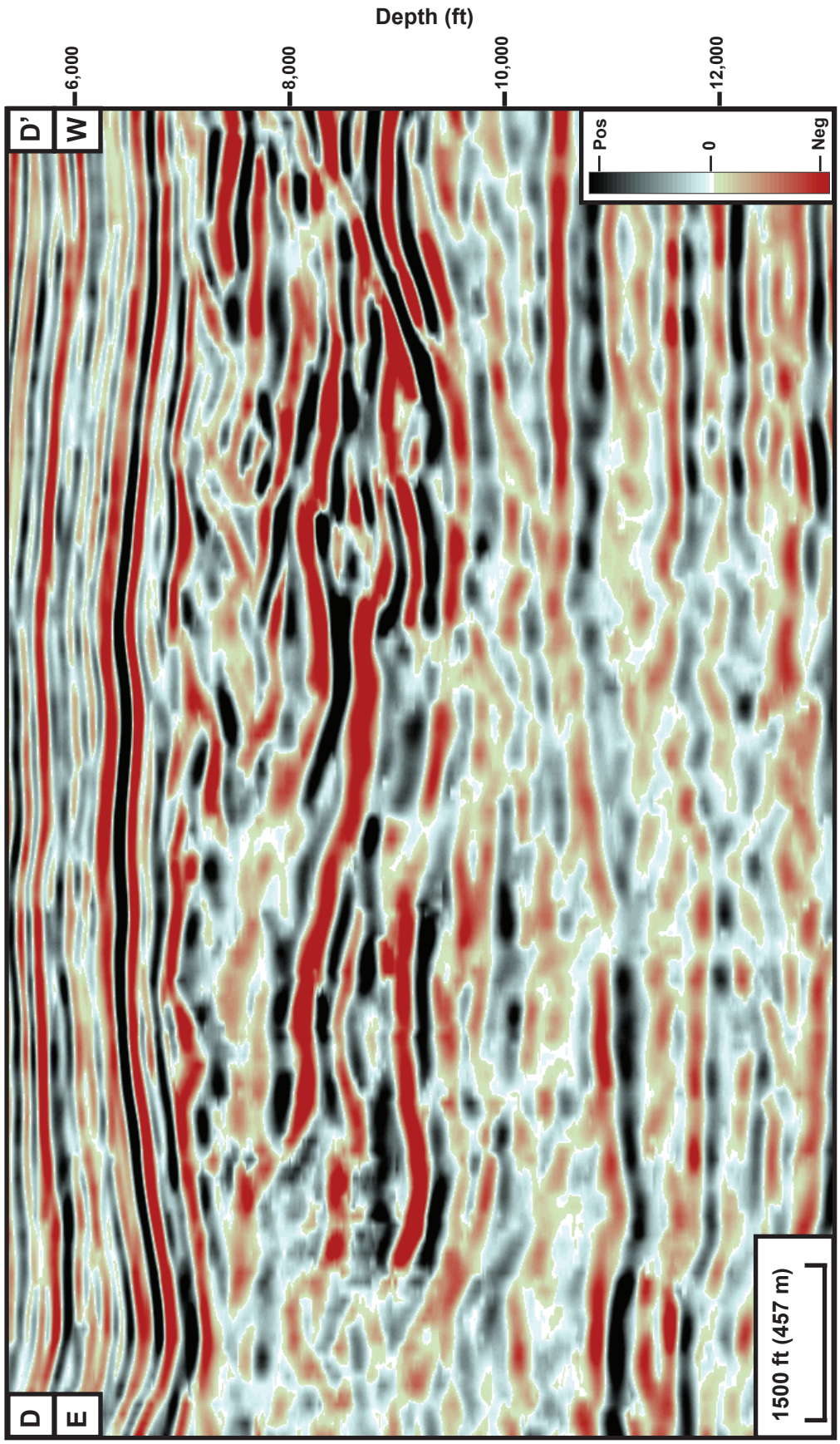

Figure 56a. Uninterpreted seismic profile through sector W of the inner rim that corresponds with Figure 56b. Refer to Figure 50 for profile location.

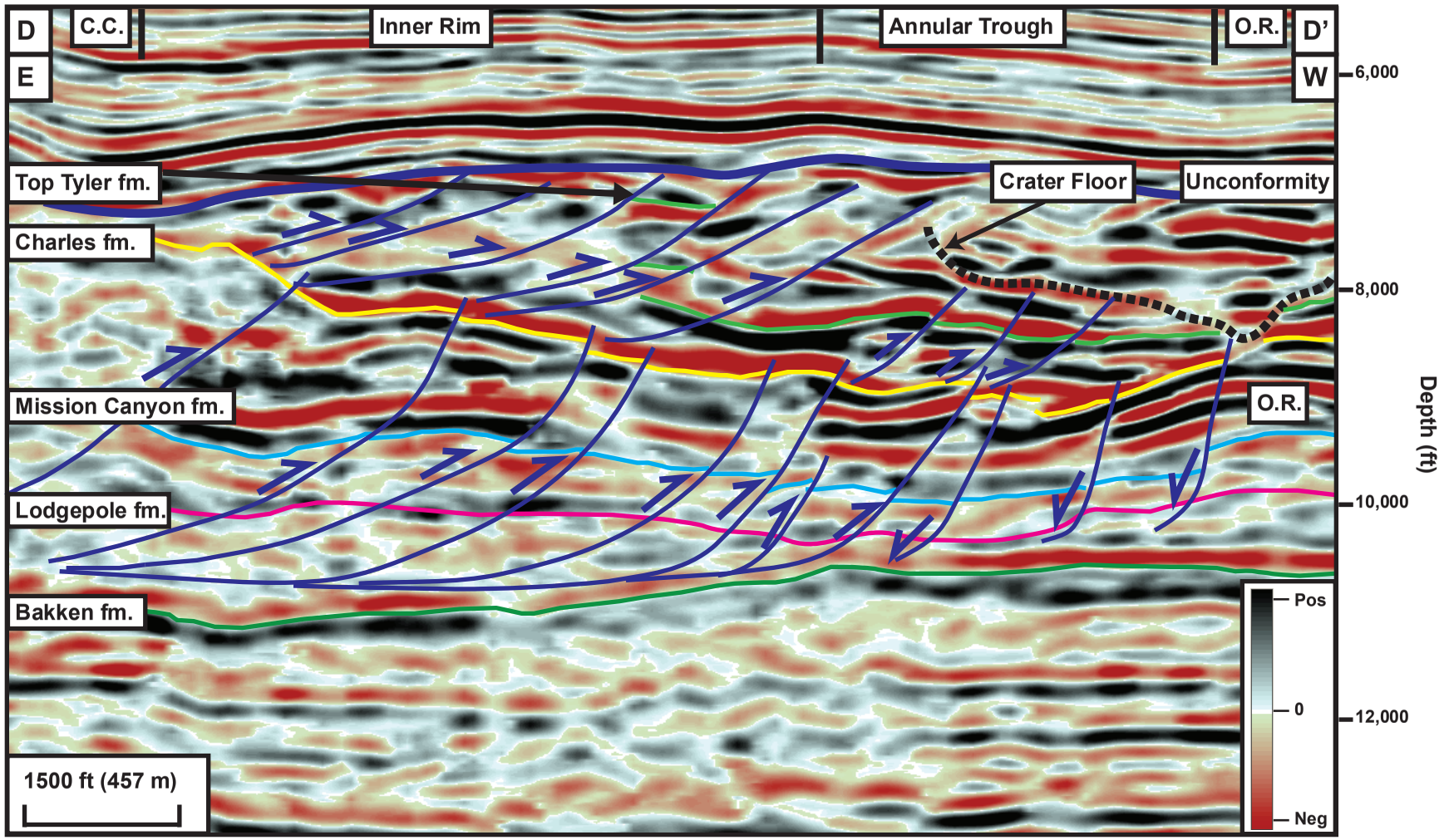

Figure 56b. Seismic profile through sector W of the inner rim. The lower detachment interval, Lodgepole to Charles/base of Kibbey Formations, is internally faulted by relatively high angle, imbricate thrusts. Like the eastern sector, the top of this interval gradually dips away from the central uplift at an angle of 5 to 8 degrees. The upper thrust zone in this sector is thin in comparison to other sectors. Significant structural zones are labeled: central core (C.C.), inner rim, annular trough, and outer rim (O.R.). Refer to Figure 50 for profile location.

feet (305 to 335 m) (**Figure 49**, **50**). The six outward verging thrust faults dip at an angle of 35° to 40° toward the central core (**Figure 56)** and have a maximum vertical offset of the Tyler Formation, along the trailing thrust fault, of 300 feet (91.4 m). Unique to the western sector, minor thrusting of the crater floor forms within the annular trough (**Figure 56)**.

NW sector

The northwest sector is bound to the northeast by Thrust 4 and to the south by Thrust 3 (**Figures 37, 50)**. This sector is 0.55 square miles (1.42 km^2) in area. Like the western and eastern sectors, the strata in the lower interval of the northwestern sector gradually dip away from the central core at an angle of 5° **(Figure 57)**. Internally, this interval is cut by four outward verging imbricate thrust faults that dip toward the central crater at a maximum angle of 60° at their tip point. Maximum fault at the Mission Canyon Formation level is 280 feet (85.3 m). One normal fault dips toward the central crater (away from the thrust faults) (**Figure 57)**. Normal offset has a maximum of 100 feet (30.5 m). Like other sectors around the south and west of the central core, the inner rim to annular trough transition is bounded by these outward verging thrust faults, and the thrust faults propagate into the annular trough.

Like the western and eastern sectors, the upper zone is relatively thin with a maximum thickness of the Charles to top of the Tyler formation of approximately 1000 feet (305 m) (**Figure 49)** due to the lack of folding within the lower detachment interval. Five outward verging thrust faults dip toward the central crater at 25°. The maximum vertical offset at the Tyler formation level is 300 feet (91.4 m). The crater floor is

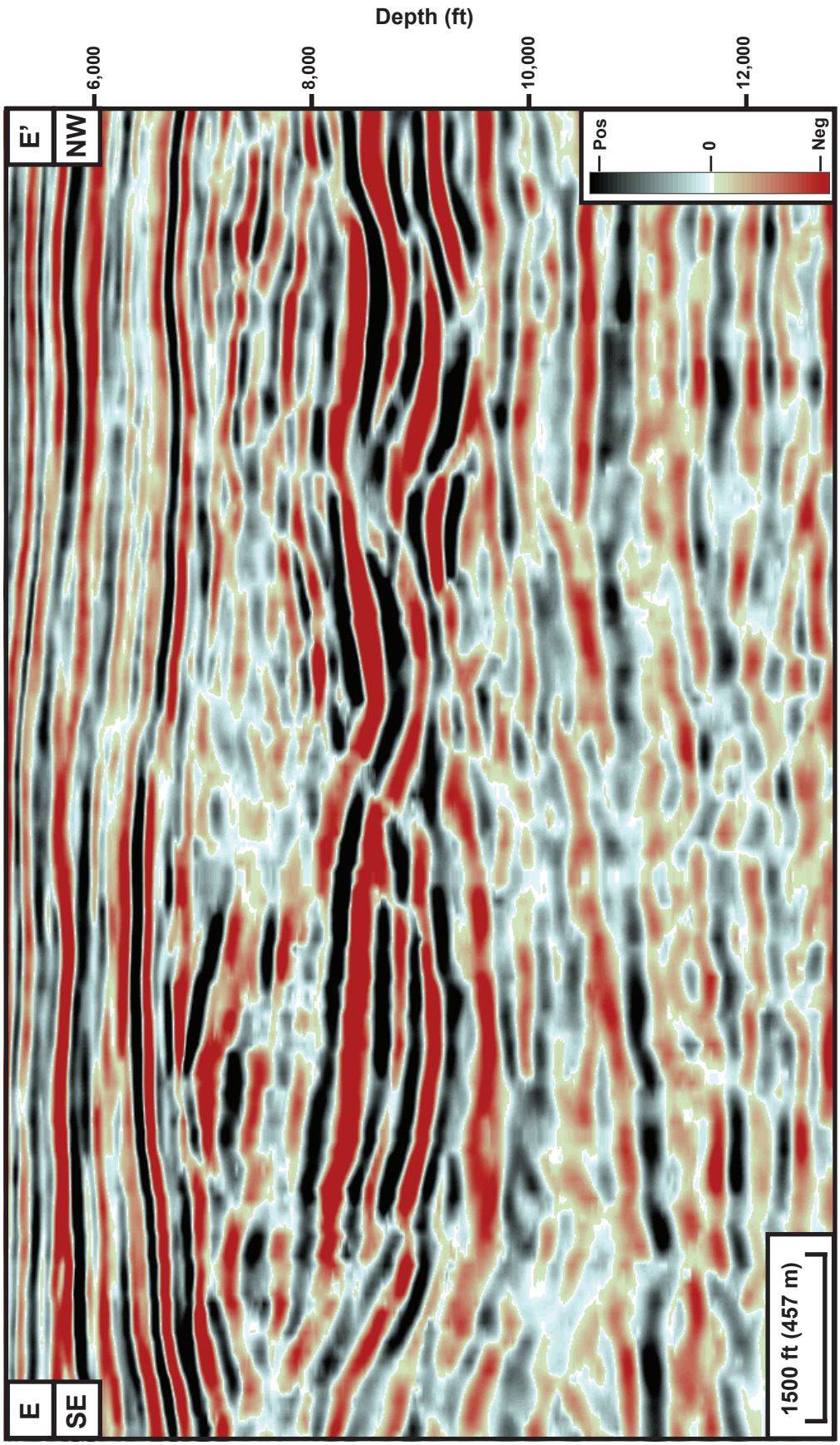

Figure 57a. Uninterpreted seismic profile through sector NW of the inner rim that corresponds with Figure 57b. Refer to Figure 50 for location of the profile.

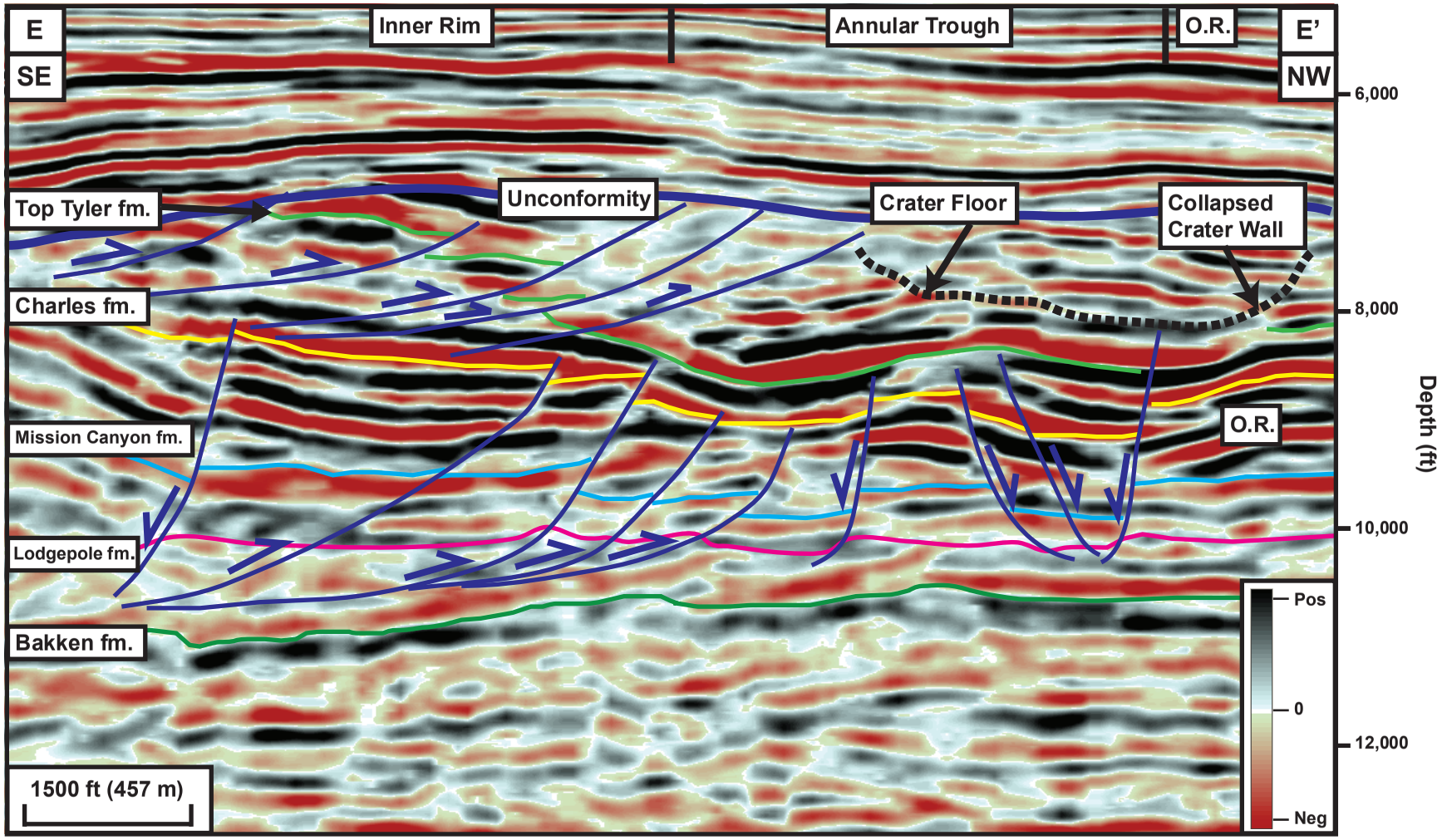

Figure 57b. Seismic profile through sector NW of the inner rim. The top lower detachment interval dips gradually away from the central core and is cut internally by multiple imbricate thrusts. These thrust faults extend into the annular trough before they transition to normal faults that bound the outer rim. Like other sectors that lack folding in the lower detachment interval, the upper thrust zone is relatively thin at 1000 ft (305 m) between the Charles and Tyler Formations. Major structural zones are annotated: inner rim, annular trough, and outer rim (O.R.). Refer to Figure 50 for location of the profile.

deformed by these thrust faults causing the topography of the overlying crater floor to be highly irregular (**Figure 57)**.

Central Core

The dramatic structural uplift along the Mission Canyon level in the central core is shown in **Figure 16.** The surface in the central core represents the first point where the Mission Canyon is encountered in the wells that penetrate this zone. As previously mentioned, there is significant repetition of the Mission Canyon Formation in the wells that penetrate the central core. At its highest point, the Mission Canyon Formation is uplifted more than 3,000 feet (914.4 m) above its depth in the annular trough and 2,000 (609.6) feet above its depth in the outer rim.

Due to the chaotic, discontinuous nature of the seismic reflections within the central uplift, as well as the questionable seismic velocities associated with this zone, a structural interpretation based on the seismic data was not possible (**Figures 15, 17, 20)**. The well data was the only reliable source of information for the central core, and the stratigraphic patterns within the wells suggest that this zone is the most structurally complex sector within Red Wing Creek.

The seismic and well-log expressions, of the central core in cross section view (**Figures 27-30),** illustrate the stratigraphic variation and repetition within this zone. At its widest point, the diameter of the central core is approximately 0.95 miles (1.53 km). As the Mississippian strata adjacent to the central core approaches, their dip angles increase sharply to 20° to 30° degrees away from the central core (**Figures 28, 30)**. When this dip change occurs, the Upper Mississippian through Triassic section, above

the Charles Formation, detaches and is thrust away from the central core, which forms the upper thrust zone (**Figures 48, 52-57)**.

Based on the twenty-seven well penetrations (**Figures 27, 29)**, the central core is composed solely of the Charles, Lodgepole, and the Mission Canyon Formations, which comprise the Madison Group (**Figures 8, 11)**. The Madison Group, in the undisturbed Williston Basin, has an average thickness of 1,000 feet (304.8 m), within the central core, this interval has a maximum thickness of 4,100 (1,249.7 m) feet in the #22-27 well (**Figure 11)**. This anomalous thickness is present in all wells within the central core. Wells that penetrate the central core suggest extensive stratigraphic repetition (**Figures 27, 29**). The BN 22-27 well has at least five repeated intervals within the Mississippian Madison Group (**Figure 27)**. This pattern, as well as those in other central core wells, suggests that the central core is cut by a multitude of high angle reverse faults, which is seen in other terrestrial impacts (Milton et al., 1996; Stone and Therriault, 2003).

In addition to the stratigraphic repetition of the Mission Canyon Formation within the central core, core data indicates the Mission Canyon is highly fractured (**Figure 58).** Two cores within the Mission Canyon Formation were acquired during the drilling of Red Wing Creek at the BN 22-27A well and the BN 24-27. Both cores indicate that the Mission Canyon Formation limestone is intensely fractured. The fractures are discontinuous and their orientations are highly variable, ranging from sub-vertical to sub-horizontal, and the fractures are often filled with anhydrite (**Figure 58)**.

Crater Floor and Crater Fill

Figure 58. Core photograph of the Mission Canyon Formation in the the BN 22-27A well (6862'-6868') in section 27. This core sample represents the Mission Canyon within the central core. It is described as a slightly dolomitic limestone that is heavily fractured throughout the cored section. The fractures are discontinuous and their orientations are highly variable ranging from sub-vertical to sub-horizontal. The fractures tend to be filled with anhydrite.The scale is marked in tenths of a foot.

Most surficial impact craters are initially identified by their crater floor, which is a prominent trough. With sufficient time, this trough will completely fill by multiple depositional processes. Identification of the crater floor at the Red Wing Creek feature is difficult because it is highly deformed by thrust faults (**Figures 52-57)**. Differentiating between the deformed crater floor and crater fill can be difficult, but identification of the crater floor is achieved by observing subtle angular unconformities between the crater floor and the blocks that fill this cavity (**Figures 25, 40)**. Also, it is identified as the location of the tip point for the majority of the thrust faults in the upper section.

Crater floor

Throughout the impact structure, the crater floor is roughly equivalent to the Late Permian to Early Triassic Spearfish Formation (**Figures 25, 59)**. Like the upper zone, the crater floor is also affected by outward verging thrusting. The deformed nature of the crater floor in the northern sector of Red Wing Creek is illustrated in **Figure 25**. As discussed above, there is an unusually thick section of the Spearfish Formation in the Shell 13X-15 well. Koeberl et al., 1996 suggested that this abnormal thickness (768 feet, 234.1 m) could represent a portion of the crater fill at this location. However, the 13X-15 well along with the seismic shows that this section's abnormal thickness is caused by thrust faulting and not because it is crater fill strata. There is a low angle thrust fault that intersects the 13X-15 well bore and this is what is creating the anomalous thickness of the Spearfish Formation (**Figure 48)**. The thrusts faults, which deform the crater floor, detach within the Charles Formation (**Figure 24)**.

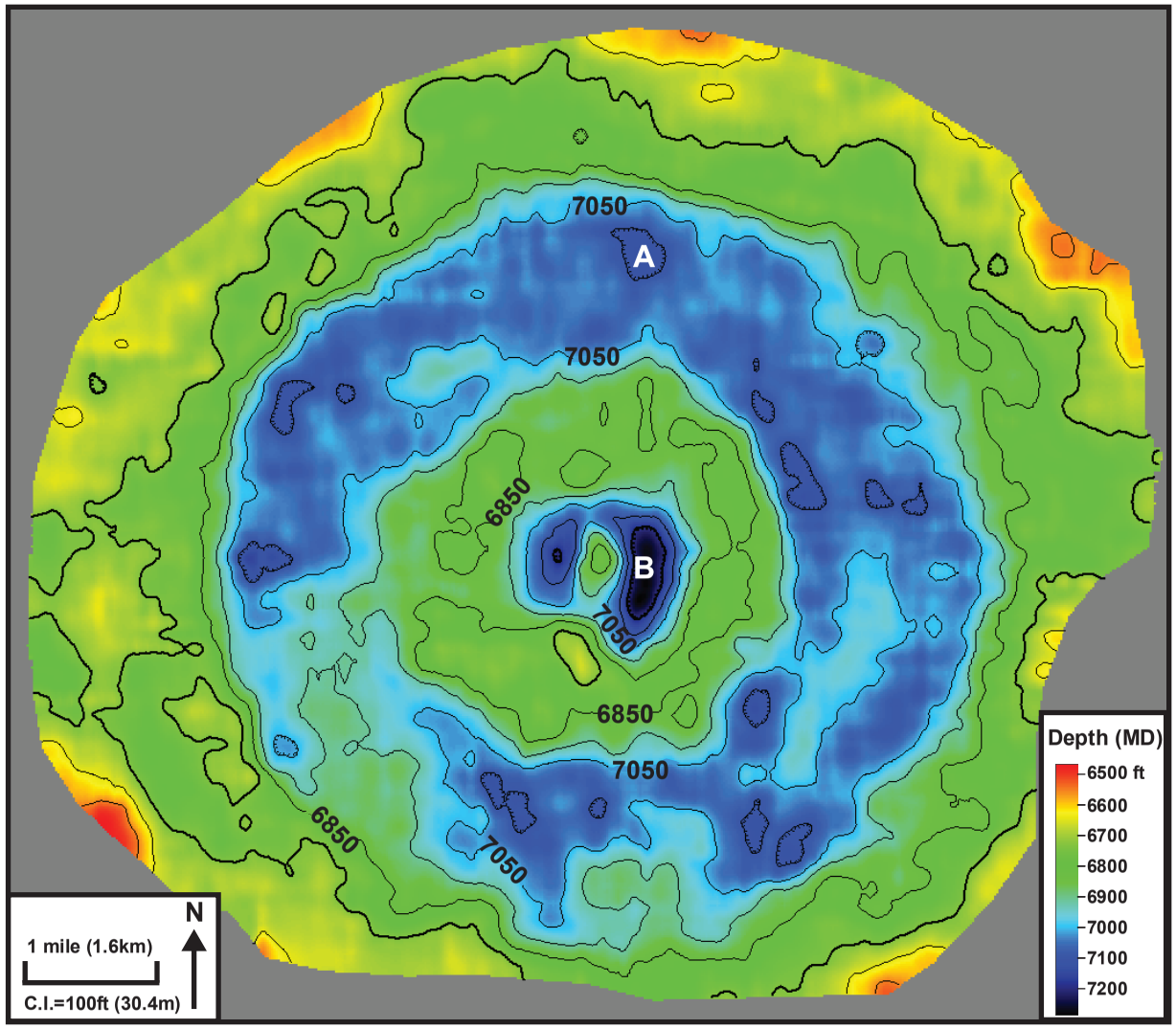

Figure 59. Depth map of the first draping layer over the Triassic to Jurassic unconformity (equivalent to Base Piper Formation). This surface is depressed up to 200 feet (60.9 m) when it overlies the crater fill section (A) and up to 500 feet (152.4 m) when it overlies the Central Core (B).

Although the amount of thrust faults that cut the crater floor and detachment level of these thrust faults varies around the structure, there are certain patterns that remain constant. First, the thrust faults that cut the crater floor begin roughly at the edge of the inner rim to annular trough boundary. Second, the crater floor gradually rises toward the central crater and dips away from the crater edge (**Figures 24, 60)**.

B. Crater fill

The crater-fill strata are categorized primarily as para-autochthonous slide blocks that have collapsed from the original crater wall (French, 1998). No apparent melt layer exists within Red Wing Creek's crater floor. Craters, with diameters less than 12 to 15 miles (19.3-24.1 km), formed from smaller meteorite impacts that lack the energy required to form a melt layer on the crater floor (Dypvik and Jansa, 2003).

On seismic reflection data, the crater-fill strata consist of two seismic facies: (a) areally extensive, coherent, high-amplitude blocks that are derived from the adjacent crater wall, and (b) areas where the reflections are chaotic and discontinuous. The size and distribution of these collapse blocks on the crater floor is show in **Figure 61.** The largest of these blocks is up to 0.6 square miles (1.55 km^2). Thicknesses range from 500 feet to 700 feet (152.4 to 213.4 m). One well penetrates an interpreted collapse block (T10 well in section 15) (**Figure 61)**, and the data suggest that these blocks consist of the Lower to Upper Permian strata present in the outer rim (**Figure 25**). The seismic character of these collapse blocks also indicates that they are derived from the adjacent crater wall (**Figure 25)**.

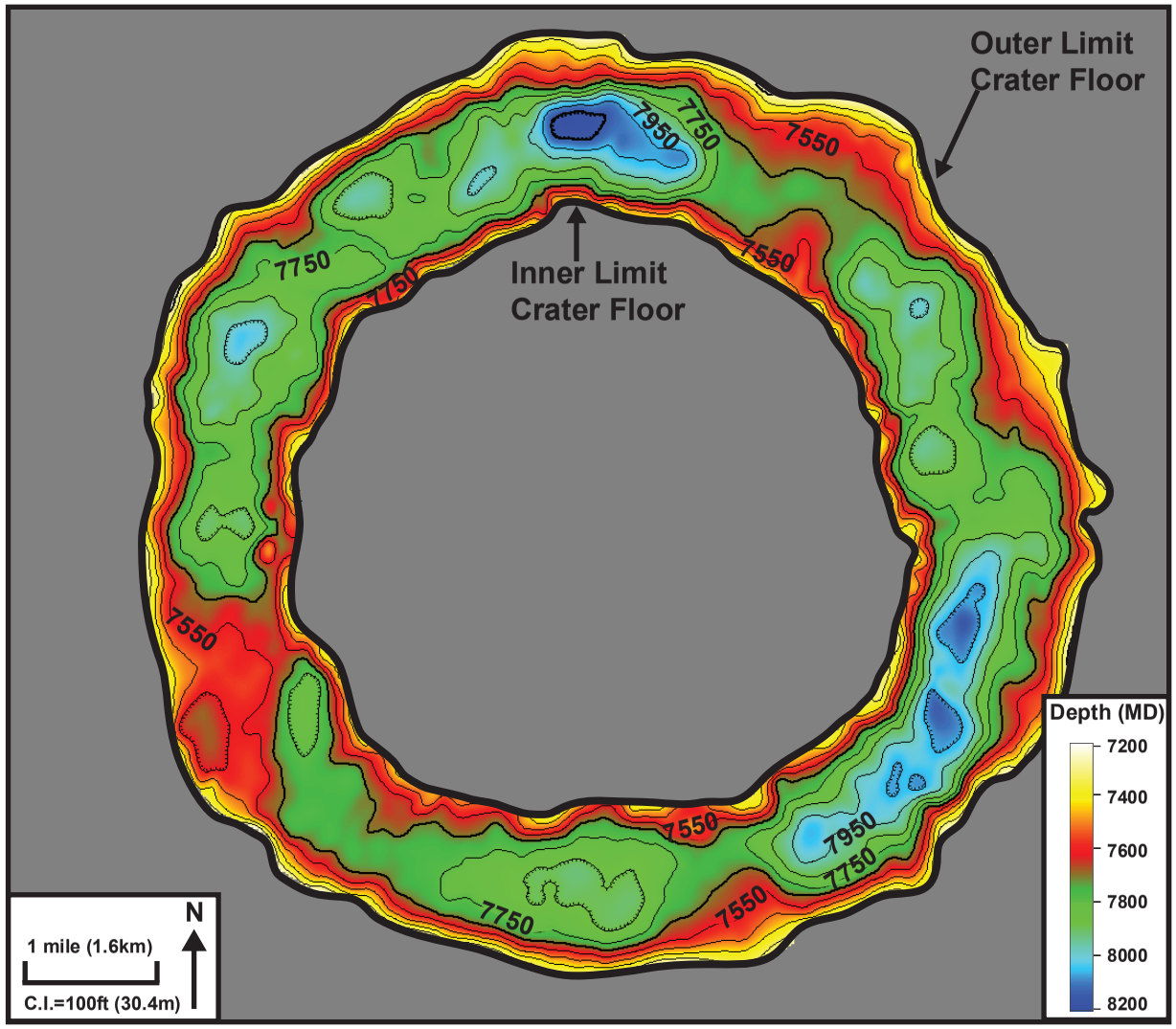

Figure 60. Depth map of the crater floor of Red Wing Creek. The central crater rises steeply toward the central core, which is caused in part by the underlying imbricate thrust faults that detach within the Charles Formation evaporites. The outer limit of the crater floor has been altered and expanded outward due to the collapse of the oversteepened crater rim.

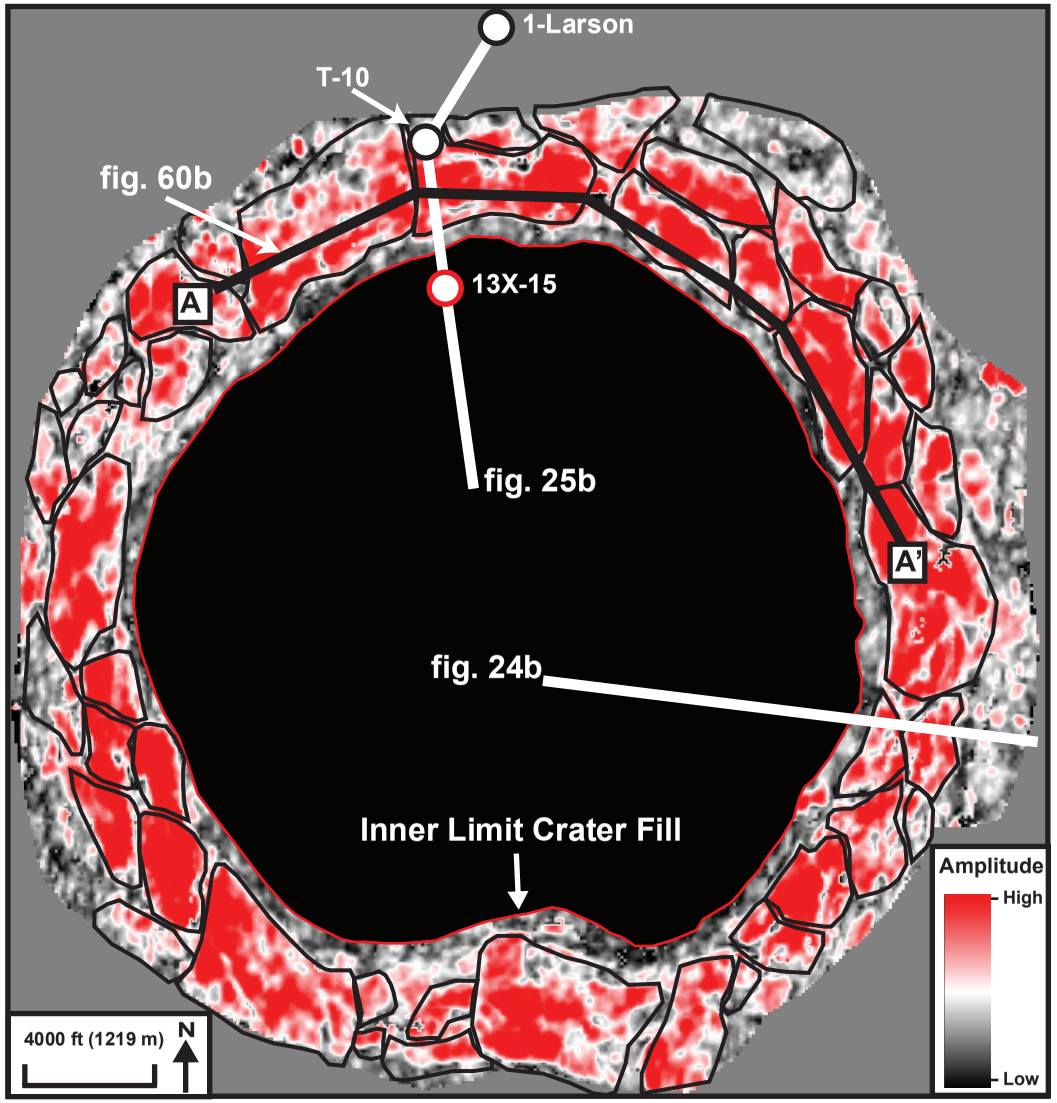

Figure 61. Maximum amplitude extraction map of crater wall collapse blocks between the crater floor and the base of the Piper Formation. The largest of the collapse blocks area is .6 square miles (1.55 square kilometers) and are up to 700 feet (213.4 m) thick. Stratigraphically, the collapse blocks are composed of the Permian strata derived from the outer rim. Locations of seismic profiles and wells in Figures 24b, 25b, and 60b are annotated.

The inner limit of the collapse blocks is controlled by the topography of the crater floor. The crater floor is deformed and compressed directly below the collapse blocks, but because the crater floor rises toward the central crater, the blocks only slide a short distance laterally from their original position before the crater wall collapse (**Figures 24-25)**. The inner limit of the slide blocks is primarily symmetrical around the crater (**Figure 61)**. From the central core, the distance to the northern limit of the blocks is 1.95 miles (3.14 km), to the east is 2.00 miles (3.22 km), to the south is 1.70 miles (2.74 km), and to the west is 2.05 miles (3.30).

Where multiple blocks slid toward the central crater from the collapsed crater wall, they thrust over one another in a dip-oriented direction (**Figure 24)**. In a strike-oriented direction, the boundaries between adjacent blocks suggest lateral thrusting (**Figure 62).** There is evidence of small-scale thrust faults along their edges as they move toward the center of the crater. Besides the coherent collapse blocks, there is evidence of secondary crater fill that is characterized by a less continuous, less reflective seismic expression (**Figure 62)**. At its thickest point, the crater fill is over 1,000 feet thick (**Figure 63**)

The Jurassic Piper Formation overlies the crater fill and the entire Red Wing Creek structure (**Figure 62b**). This layer drapes the structure that has been truncated by the Triassic to Jurassic unconformity (**Figure 59**).

DISCUSSION AND INTERPRETATION

Figure 62a. Uninterpreted arbitrary seismic profile that corresponds with Figure 62b. Profile location is annotated on Figure 61.

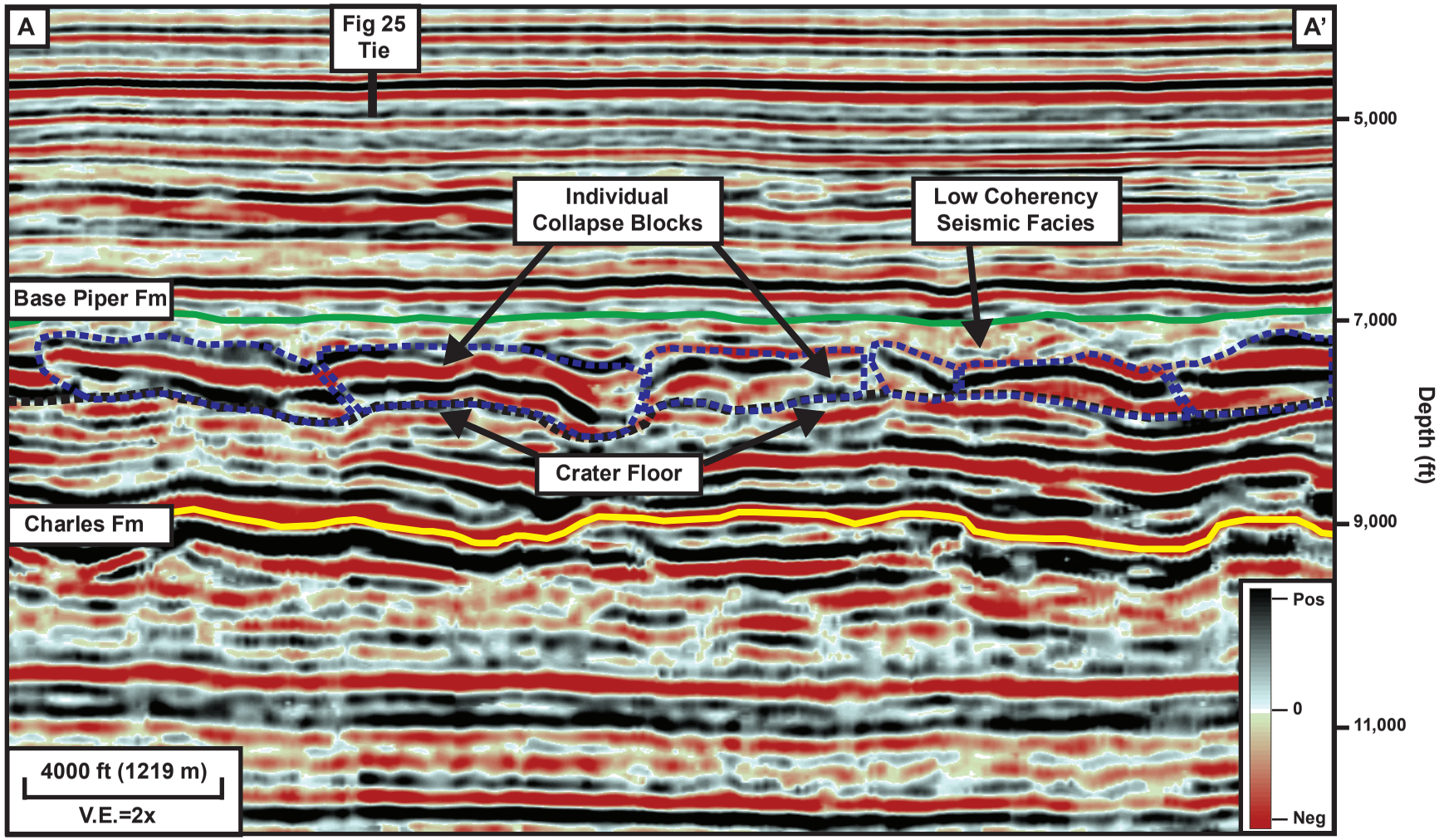

Figure 62b. Arbitrary seismic profile through collapse blocks lying on the crater floor. The collapse blocks are thrusted over one another along their edges. The slide blocks also thrust over one another in dip oriented profiles as their forward motion is limited by the topography of the crater floor. Profile location is located on Figure 61.

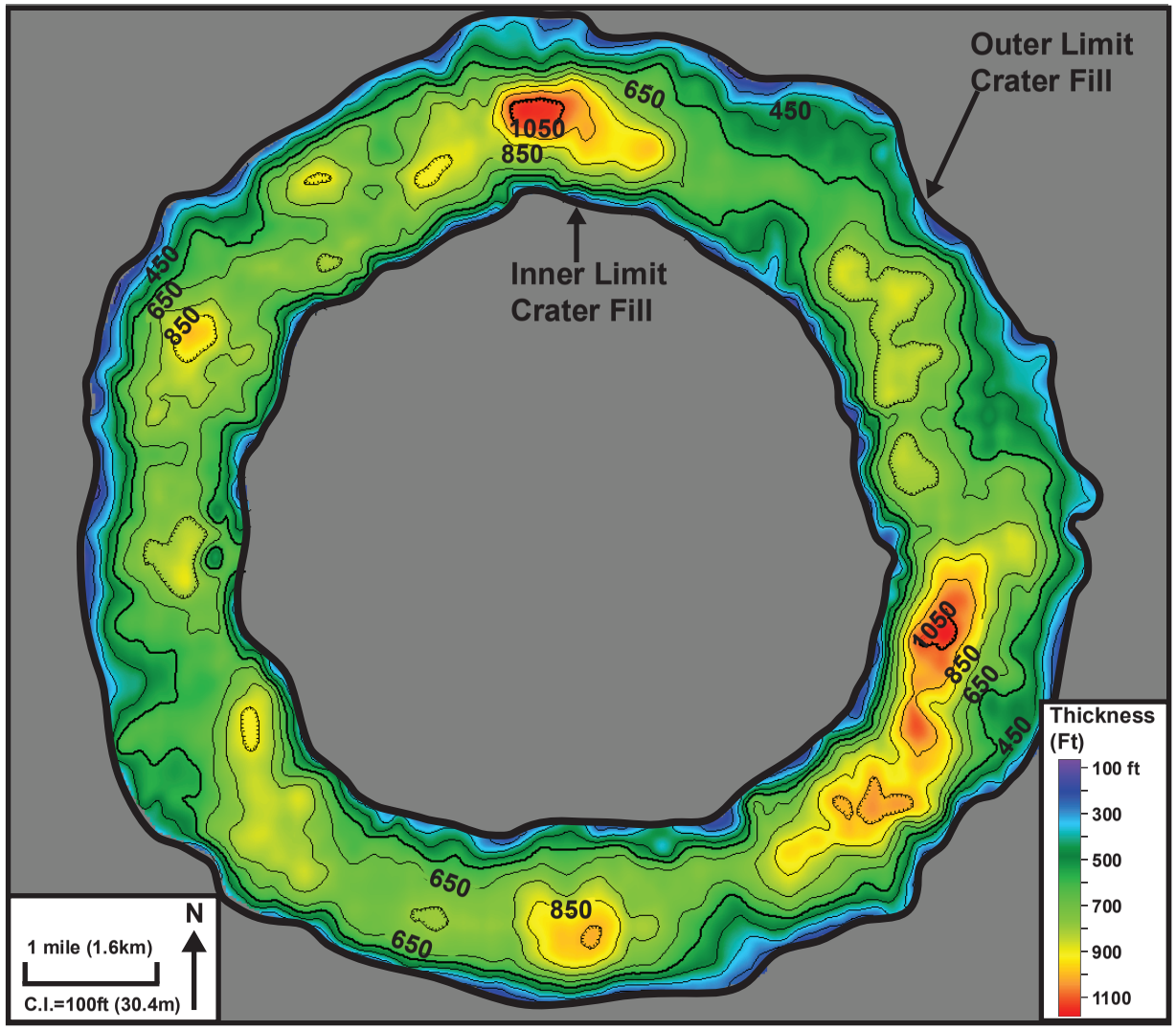

Figure 63. Thickness map of the crater fill between the crater floor and the first draping layer that is equivalent to base of the Jurassic Piper Formation. The thickest portions of the crater fill occur in the north and southeastern portions of the map and correlate to zones where the base of the crater floor (Figure 60) shows maximum depression.

Through field and subsurface observations of terrestrial craters as well as the study of lunar craters, a variety of structural features have been documented and their formation mechanisms have be been interpreted. The Red Wing Creek data set is unique because it provides an almost complete (missing Triassic through Jurassic strata) picture of a complex impact in three dimensions. Studies of other craters have noted most of the dominant features documented at Red Wing Creek: radial transpression ridges (Kenkmann and Von Dalgwik, 2000), normal faulting, folding, and thrust faulting (Osinski and Spray, 2005). Still, the Red Wing Creek data set provides a unique opportunity to fully document these features and their process of formation. For definition of the cratering terminology used below, refer to **Table 5.**

Interpretation of Dominant Structural Styles

Seven unique zones and intervals are present within the Red Wing Creek structure: (1) outer rim, (2) annular trough, (3) lower thrust zone, (4) upper thrust zone, (5) radial transpression ridges, (6) central core, and (7) crater floor and fill (**Figure 64)**. Each of these zones has unique internal and external structural styles (**Figure 64).** In addition, each of the structural styles is interpreted to have formed during a specific stage of the crater's formation. Throughout Red Wing Creek, there are five dominant structural styles: (a) concentric, inward verging normal faulting and outward verging normal faulting, (b) folding, (c) outward verging thrust faulting, and (d) radial thrust faulting.

A. Normal faulting

Term	Definition
Compensation	The crater's structural response to the reduction of space during the inward directed crater collapse.
Excavation flow	The removal of strata outward of the crater during the excavation stage of crater formation.
Particle trajectory	Describes the movement direction of a volume of rock (e.g. The particle trajectory of the collapsing crater walls is inward toward the central core).
Radial transpression ridges	High-angle, radial reverse faults and folds formed due to the lateral convergence of the collapsing crater walls.
Rock volume/mass	Any volume of strata that has a uniform trajectory (e.g. crater walls, central core).
Transient crater	The crater morphology formed by crater wall collapse, which occurs during the modification stage of crater formation.

Table 5. Cratering terminology used in interpretation, discussion, and description of Red Wing Creek.

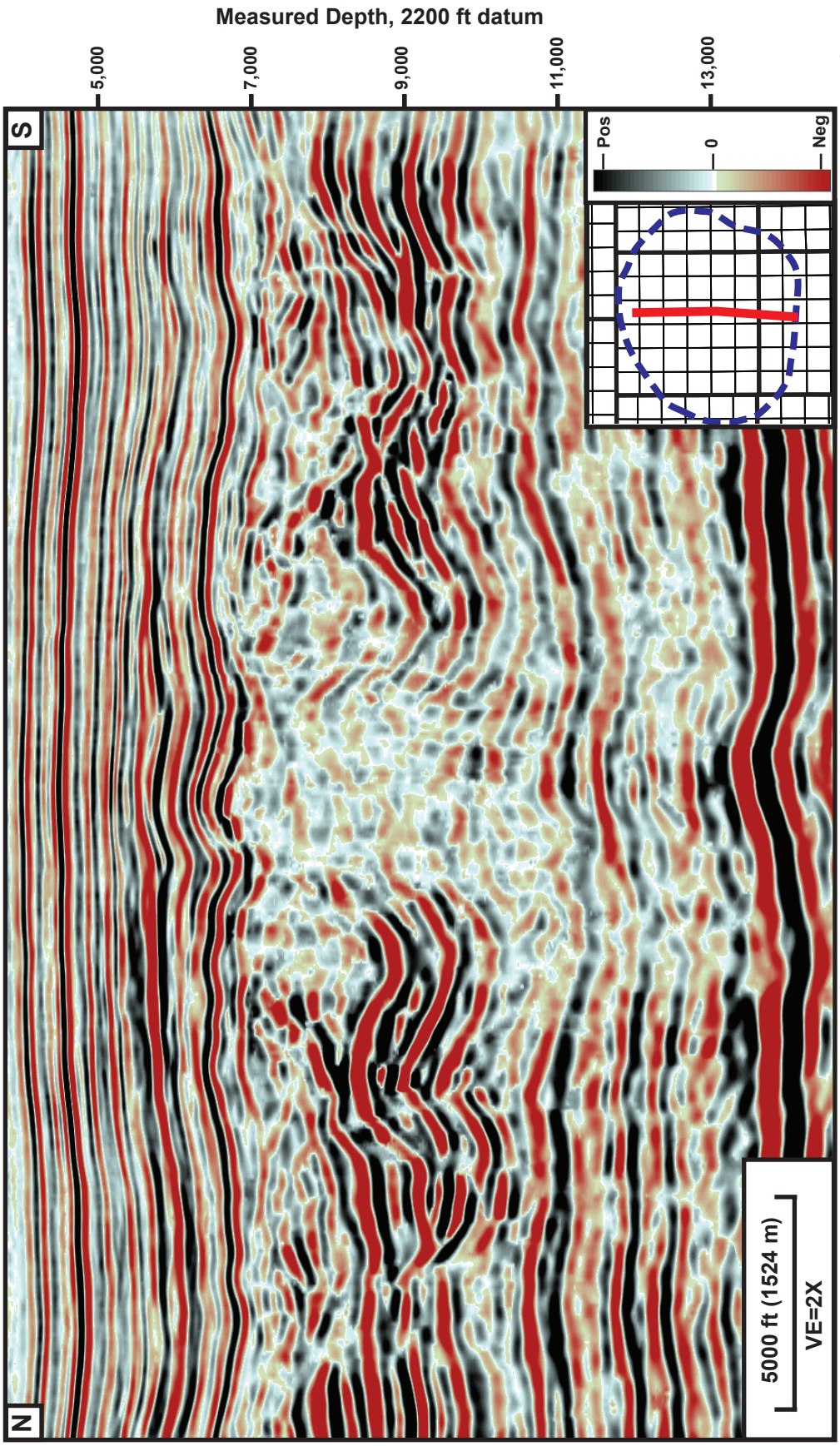

Figure 64a. Uninterpreted seismic profile across Red Wing Creek crater that corresponds with Figure 64b. Location of profile is shown in index map.

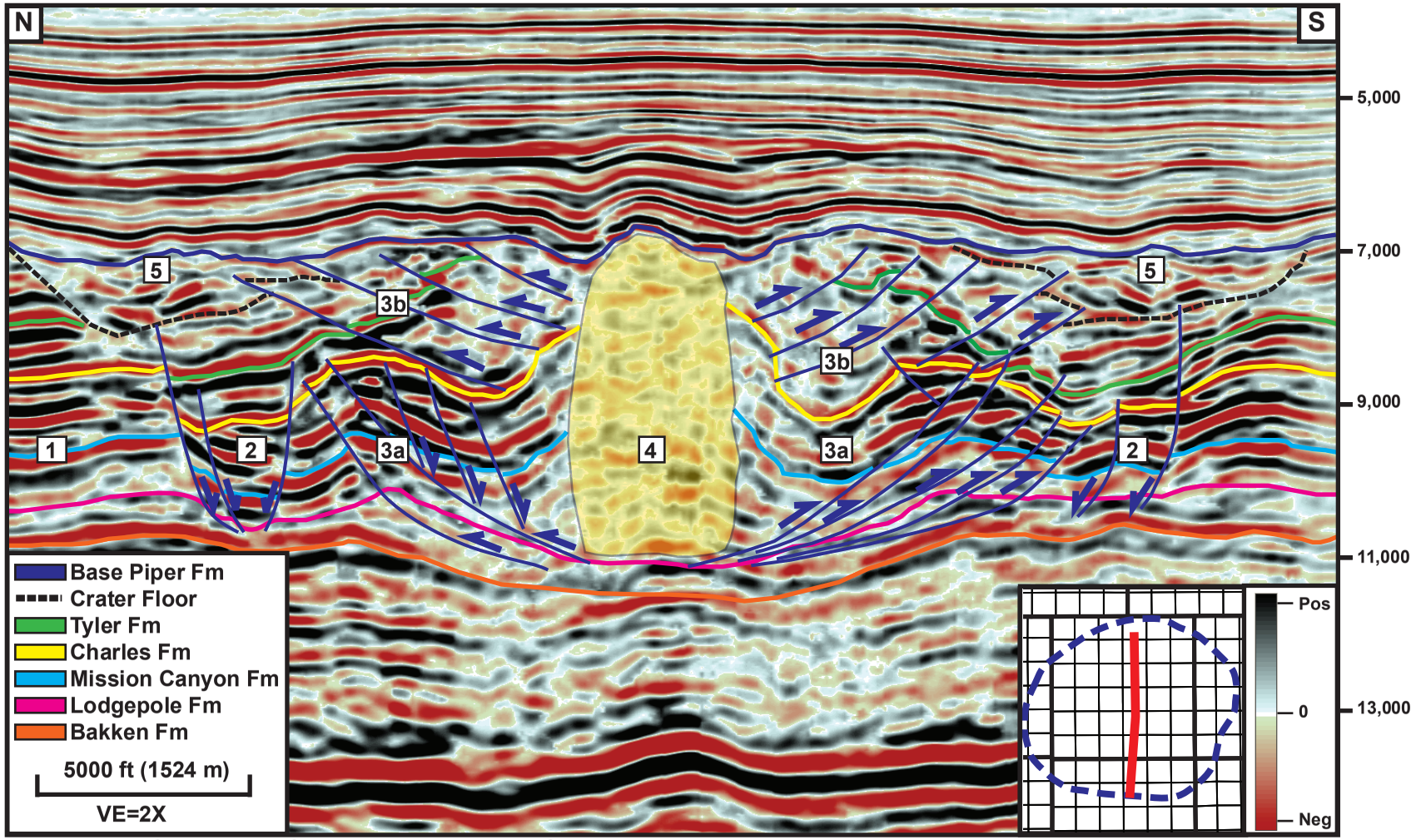

Figure 64b. Seismic profile across Red Wing Creek crater with annotated crater zones: (1) outer rim, (2) annular trough, inner rim: (3a) lower thrust zone, (3b) upper thrust zone, (4) central core (100% Madison Group), (5) crater floor and fill, (6)-radial transpression ridges (not illustrated). Location of profile is shown in index map.

The outer rim to annular trough transition is marked by a series of concentric, linked normal faults that are listric in depth and detach within the Lodgepole shales (**Figures 36, 40-41, 64**). Eventually, these faults merge into sub-horizontal faults toward the center of the crater, similar to studies of other terrestrial craters (Kenkman, et al., 2000). This group of faults marks the original crater wall and gives Red Wing Creek an apparent crater diameter of 4.9 miles (7.89 km). Overall, these faults can have more than 600 feet (183 m) of vertical offset at the Mission Canyon Formation level. Other complex impact craters with similar diameters have concentric normal faults, which have maximum fault offsets greater than 330 feet (100 m) (Wilson and Stearns, 1968; Offeld and Pahn, 1979; Spray, 1997).

These listric normal faults developed in response to the collapse of the oversteepened, transient crater walls, which in turn, form as space is created by the uplift of the crater floor during excavation. As the central crater is uplifted, there is an inward and upward movement of strata, which creates space along the crater rim. Along all of these crater rim faults, extension is directed toward the central core and the walls collapse as large, coherent blocks, which are bounded by normal faults. These gravity driven collapse blocks form the annular trough (**Figures 39, 40-41)**.

The inner limit of the annular trough at Red Wing Creek is commonly bounded by outward verging concentric faults, which dip away from the central crater to form a graben within the annular trough (**Figure 41)**. The outward verging faults, within the annular trough, could have formed in response to the gaps created by the displacement of the inward dipping listric faults (Davis and Reynolds, 1996; Osinksi and Spray, 2005). Some of the outward dipping faults bound the inner rim portion of the central uplift

complex. These faults likely formed due to the collapse of the outer edge of the uplifted, inner rim (Osinski and Spray, 2005).

B. Folding

Between the Lodgepole Formation and the Charles Formation, there is significant folding in two sectors of the inner rim (**Figures 52, 55)**. Maximum folding at Red Wing Creek occurs in the northern and southern sectors and has a maximum fold wavelength of 1.15 miles (1.85 km). Folding occurs in five of the inner rim sectors, except for the E, W, and NW sectors. The Lodgepole to Charles strata are uplifted toward the central crater through the inner rim in these sectors. Folding in the central uplift is a common feature and has been observed in terrestrial complex craters with similar diameters at the Decaturville and Sierra Madera craters (Wilshire, et al., 1972; Offeld and Pahn, 1979).

As the crater wall collapses, there is an inward movement of rock volume toward the crater center. The central core then oversteepens, becomes unstable, and begins to collapse creating an outward particle motion (Kenkmann and Von Dalgwik, 2000; Wieland, et al., 2003). When this occurs, there are conflicting particle trajectories and at Red Wing Creek, the compensation for colliding trajectories occurs within the inner rim of the central uplift crater complex. This compensation comes in the form of folding and thrust faulting within the inner rim (**Figure 52, 55, 64**).

C. Outward directed imbricate thrusting

The Lodgepole through Charles Formation interval is cut internally by outward verging thrust faults (**Figures 52-57)**. The outward verging thrust faults occur in all

sectors of the inner rim (**Figure 50)** and they are present on multiple levels where there is an adequate detachment surface. At Red Wing Creek, the two main structural detachments are the Lodgepole Formation shales and the Charles Formations evaporites, which are both interpreted to be mechanically weak zones. The other major thrust zone is between the Charles and the crater floor, which is approximately equivalent to the Permian-Triassic Spearfish (**Figure 25)**. This group of imbricate thrust faults detach within the Charles Formation evaporites (**Figure 43)**. Maximum thicknesses of the upper thrust interval occur above those areas of maximum folding in the north and south sectors. Because the western as well as the eastern sector rise gradually toward the central core and are not folded, the upper thrust intervals are thin in comparison (**Figure 49)**. The upper thrust zone intersects and heavily deforms the crater floor, which is the main control on how far the collapse blocks slide into the crater (**Figure 24)**.

Similar to folding, the outward verging thrust faults also developed as a form of compensation for converging particle trajectories, which occurs when the transient crater wall collapses and moves downward and inward and the central core collapses and moves downward and outward. Some of this compensation could develop earlier than when the transient crater and central core collapses. When the crater floor is originally uplifted, it creates an inward and upward particle trajectory, which conflicts with the downward and outward particle trajectory created during the excavation of the crater (Osinski and Spray, 2005). Some folding or thrusting could occur at this point but it is more likely that the bulk of the compensation at Red Wing Creek occurred when the central core and transient crater collapsed.

D. Radial thrusting and Folding

Within the Red Wing Creek structure, three main structural mechanisms developed to compensate for converging particle trajectories: folding, outward directed thrusting, and finally radial thrusting and folding. Throughout the inner rim of the central uplift complex, these radial thrust faults are a dominant control on internal structure because they divide the inner rim into eight structurally independent zones (**Figures 44-46)**.

When the transient crater collapses, the crater walls are converging toward the crater center and laterally to form “radial transpression ridges” at the edges of these collapse blocks (Kenkmann and Von Dalgwik, 2000). Because the rock mass is colliding laterally, the strata are uplifted and thrusted forming radial thrust faults. These faults extend away from the central core to a maximum distance of 1.1 miles (1.77 km) (**Figure 44, 46**). The height of these radial transpression ridges decreases away from the central crater. The point of maximum vertical offset along these thrust faults is immediately adjacent to the central core and maximum offset can be up to 300 feet (91.4 m) (**Figure 47a)**. At the terminus of the radial thrust faults, the ridge transitions to a radial fold (**Figure 47c)**. All of the major radial thrust faults detach within the Lodgepole Formation and do not extend into the annular trough (**Figure 44, 46)**.

Radial thrust ridges have been observed and described in craters with similar diameters (less than 10 miles (16 km)) (Kriens, et al., 1999, Abels, 2005); and in larger craters, these radial transpression ridges are expressed as brecciated ridges and

positive flower structures instead of high angle thrusts and folds (Kenkmann and Von Dalgwik, 2000).

Structural Symmetry of Red Wing Creek and General Impact Angle

Because 50% of asteroids or comets impact the earth at an angle that is less than 45° and that the likelihood of a vertical impact is extremely low (Kenkmann and Poelchau, 2008), the probability that Red Wing Creek is the product of an oblique impact is relatively high. The major uncertainty is whether the likely oblique impact is greater or less than 45°. By observing patterns of certain structural features, as well as the angle of impact, the relative direction of impact can be determined. Studies at impact sites of Upheaval Dome, USA and Spider Crater, Australia, which are both comparable in size to Red Wing Creek, have shown distinct, oblique impact directions from their structural characteristics (Kriens et al., 1999). These craters both have radial thrust faults that dip in one general direction (Scherler et al., 2006). This asymmetry indicates a single maximum shortening direction and an impact angle.

Unlike these two craters, whose structural asymmetries indicate a low angle, oblique impact, the Red Wing Creek crater is much more symmetric. The radial thrusts in the northern half of the structure all thrust to the north or a general northern direction. The radial thrusts in the southern half of the structure are thrusting solely toward the south or a general southern direction (**Figures 44, 46)**. Maximum folding is also present in the northern and southern sectors of the inner rim (**Figures 50, 52, 55)**, within the central uplift complex. These two structural trends of vergence suggest that the maximum shortening direction is on a general north-south trend and that the crater is

primarily axial symmetric along an E-W axis. This indicates that Red Wing Creek is not the product of an oblique, low angle impact; likely, it is the result of an impact angle greater than 45°. Maximum shortening in a north-south trend could also indicate impact direction. Due to this trend, it is possible that the impactor struck from the north or from the south at an angle that is greater than 45°.

Generally, Red Wing Creek is structurally symmetrical, with the exception of the major asymmetry present in the southwestern section of the outer rim to annular trough transition. The edge of transient crater collapse is 1.9 miles (3.05 km) from the central crater, while the average distance of the transient crater wall from the central crater in other zones is 2.4 miles (3.86 km). This could also be indicative of impact direction but further work is needed to determine whether this is a factor.

Differential Compaction of Pre and Post-unconformity Strata

An unconformity, spanning the Late Triassic to Early Jurassic, overlies the entire Red Wing Creek structure (**Figures 28, 30**). In wells, this unconformity is usually recognized where the base of the Lower Jurassic Piper Formation is penetrated. The age of the strata below the unconformity vary across the structure. In the central core, the Lower Jurassic Piper Formation overlies the Mississippian Charles Formation and in the outer rim, the Piper Formation overlies the Triassic Spearfish Formation.

Differential compaction of strata directly above and below the unconformity is evident (**Figure 30**). Areas which were structurally high after the impact, tended to compact less than areas that were structurally lower. Specifically, the central core and the inner rim compacted less than the crater fill (**Figure 59**). The first stratum that

covers the entire impact structure is the Jurassic Piper Formation. Where the Piper overlies the crater fill section, it is up to 250 feet (76.2 m) deeper than its regional depth (**Figure 59**). In the area rimming the central core, the base of the Piper Formation is as much as 500 feet (152.4 m) deeper than its regional expression (**Figure 59**).

To understand the origin of the differential compaction of the underlying strata, the relative induration of the strata deformed in the crater and their degree of compactibility must be understood. If the meteorite impacted during the Late Permian-Early Triassic, then the thickness of the stratigraphic section (undecompacted) that was deformed was about 3500 feet (1067 m) (top Lodgepole; to Spearfish: **Figure 25**). The deeper strata that were deformed (i.e. Mission Canyon) were shallow marine carbonates that likely were cemented and indurated fairly early in their burial. These strata form the central core of the impact feature, and are the structurally shallowest deformed portion and they are the least likely to compact (**Figures 27, 29**). The inner rim consists of two sets of imbricate thrust faults (**Figure 51**). The shallower set of thrust faults deforms Pennsylvanian to Permian strata. The inner rim strata are less compacted than those in the central core, but remain structurally higher than the topographic low created by the crater in the annular trough (**Figures 28, 30**). In contrast, the space above the crater was differentially filled with thicker strata of the Triassic and Jurassic (**Figure 63**).

In the local depression rimming the central core (**Figure 59**), the compaction of the overlying strata may also have been caused by the dissolution of the Charles Formation evaporite strata within the central core (Brenan et al., 1975). Differential compaction began to develop as early as deposition of the Middle to Upper Jurassic

Rierdon Formation. Stratal onlap has been mapped directly above the top Rierdon Formation in the seismic data set (**Figure 30b**). This onlap surface indicates that the Jurassic strata began to infill the depressions caused by compaction of the crater fill section and dissolution of Charles Formation anhydrites as early as the Middle Jurassic.

In addition to some strata being deeper than their regional depths due to differential compaction, there is evidence of small scale normal faulting cutting the portions of the overlying Triassic to Jurassic strata (**Figure 30b**). The strata overlying the crater fill section are often bounded by small-scale normal faults on its inner and outer edge that have vertical offsets that are less than 150 feet (45.7 m) (**Figure 30b**). Much of the small scale faulting, caused by the compaction of the underlying section, is likely below seismic resolution.

KINEMATIC MODEL FOR RED WING CREEK CRATER

Red Wing Creek shows structural and stratigraphic features that correlate with the three stages of complex crater formation described for other craters (Haughton Impact Crater, Canadian Arctic (Osinski and Spray, 2005). Crater formation has been divided into three stages: (1) contact and compression (compression propagates to the Middle Devonian strata), (2) excavation (the strata have been excavated as deep as the Mississippian Charles Formation in the central core), and (3) modification (production of inward dipping normal faults, radial thrust faults, folds, and outward verging imbricate thrusts), which includes most of the structural processes (collapsing of the crater rim) that contribute to the final morphology of the crater (Osinski and Spray, 2005). Although

the cratering process has been divided into separate stages, some of the processes that form the crater likely overlap these boundaries (Osinski, 2006). Therefore, these stages are used only to describe the dominant processes that occur during a given time during crater formation (Melosh and Ivanov, 1999).

Contact/Compression Stage

Theoretical Process

The first stage of a high velocity impact involves the contact of the projectile, an asteroid or comet, with the target lithology. Once the projectile strikes, it displaces the target rock downward (**Figure 65)**. The projectile velocity abruptly decreases due to the resistance of the target rock, and the sudden decrease in projectile velocity is compensated by the creation of shock waves at the interface of the compressed and uncompressed target material (Melosh, 1989). The shock wave then propagates through the target and the projectile, and such high pressures are encountered that the projectile and portions of the target are either melted or completely vaporized. When the projectile has transferred all of its kinetic energy and the high pressures have been released, the contact/compression stage comes to an end (Melosh, 1989). Overall, this is the shortest stage of the three stages associated with crater formation. For a 1.0 km (0.62 miles) diameter projectile that travels at 15 km/s (9.3 mi/s) at a 45° angle, this stage is calculated to last 0.1 seconds (Melosh and Ivanov, 1999).

Contact/Compression Stage at Red Wing Creek

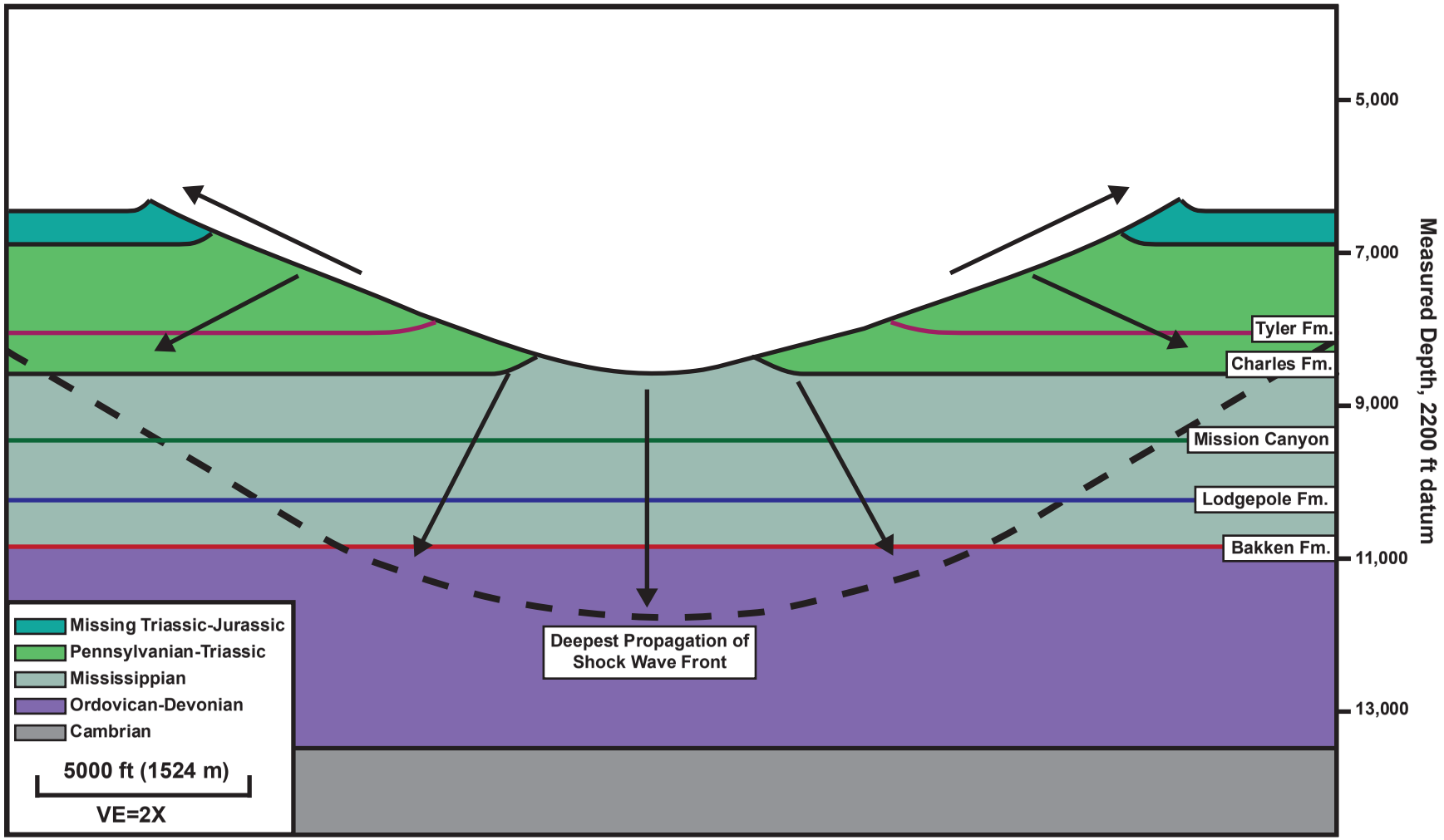

Figure 65. Schematic cross section of the compact/compression to excavation stage of crater formation at Red Wing Creek. The dominant deformational processes during this stage are the downward and outward displacement of material due to the shock wave and the upward and outward excavation of material forming the crater floor. The Charles Formation was the deepest point of excavation.

Because of the short duration of the compression, there is no obvious structural evidence of it besides the depressed and fractured strata at the base of the structure. The depressed section below the crater is due to the shock wave that is generated during contact and compression. The ground surface, during the contact and compression stage, is missing due to the Triassic to Jurassic unconformity that drapes the final structure at Red Wing Creek. Therefore, the surface stratigraphy is assumed as either Triassic or Early Jurassic during contact. This gives the crater an estimated age of formation of 220 to 200 Ma (Koeberl, et al., 1996).

Excavation Stage

Theoretical Process

The following stage is a continuation of the compression and contact stage, but the dominant mechanism transitions to excavation of the target lithology. The shock wave, which developed upon contact, continues to propagate and compress the material it encounters, but the target material is set in motion in an outward radial trajectory from the initial point of impact (**Figures 65, 66)** (Melosh and Ivanov, 1999). As shockwaves rebound and moved upward toward the surface, they produce downward directed rarefaction waves (Melosh, 1989), and the combination of the rarefaction and shock waves causes the excavation flow that produces the transient crater (Osinski, 2006). The excavation flow results in equal amounts of target material to be ejected or to be displaced farther downward into the target, and most of the ejected material is deposited adjacent to the transient crater as an ejecta blanket. Late in the excavation stage, the material that was transported downward and radially outward changes to an

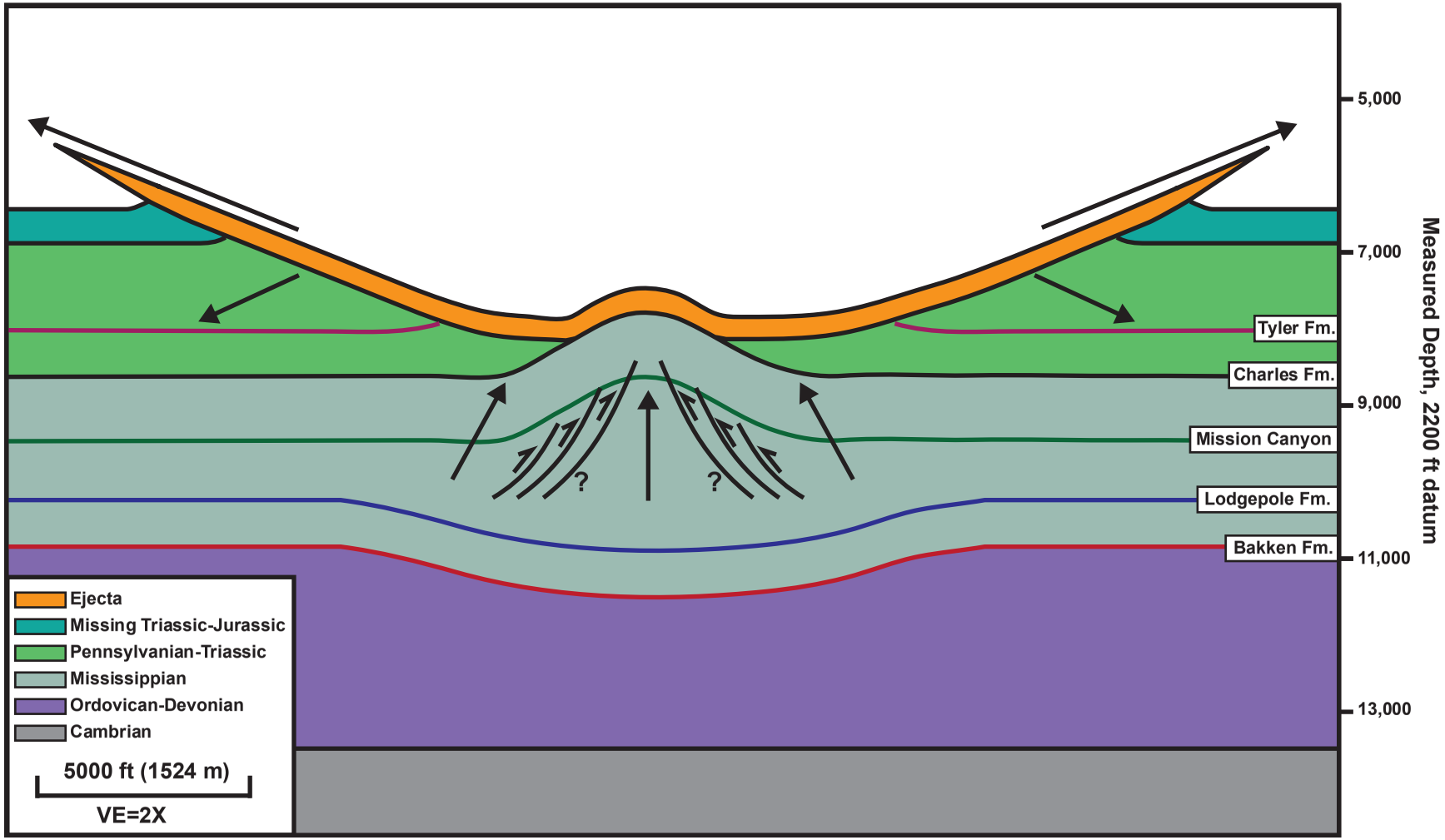

Figure 66. Schematic cross section of the late excavation stage of crater development at the Red Wing Creek crater. During late excavation, the underlying material is no longer displaced downard by the shock wave. Uplift commences during this period in the central crater. The top of the centrally uplifted strata is marked by the top of the Charles Formation. The Bakken Formation has been depressed a maximum of 600 feet (182.8 m) by the previous shock wave.

inward and upward particle trajectory, which begins to form a central uplift within the transient crater (**Figure 66)** (Osinski and Spray, 2005).

Compared to the initial contact and compression stage, the total time required for completion of the excavation stage is significantly longer, which is thought to last seconds to minutes depending on the final size of the transient crater (Melosh, 1989). The final dimensions of transient crater are dependent upon properties of the target lithology such as density, strength, and gravity acceleration, but the depth to diameter ratio appears to be independent of target properties (Melosh and Ivanov, 1999).

Excavation Stage at Red Wing Creek

The excavation stage of crater formation at Red Wing Creek can be divided into two distinct sub-stages (early and late excavation) based upon the dominant deformational processes that occur within each stage (**Figure 67**). Two dominant processes characterize early excavation. The first is the continued progression of the shock wave that was generated during the contact and compression stage. At Red Wing Creek, evidence of the shock wave is manifested in the strata underlying the primary structure (**Figures 27, 29, 33)**. As described above, well data show that the Bakken Formation is depressed up to 600 feet (183m) from its regional depth in the field (**Figure 33)**. In addition, sidewall cores collected from the Bakken Formation consist of indurated shale with brecciated sandstone clasts and secondary concretions. These samples are markedly different in lithology than the Bakken shale in the surrounding area, which are more fissile, darker shales. Wells outside of the depression (1-Larson, Turnquist 10-1) have significant gas shows in the Bakken Formation. However, none of

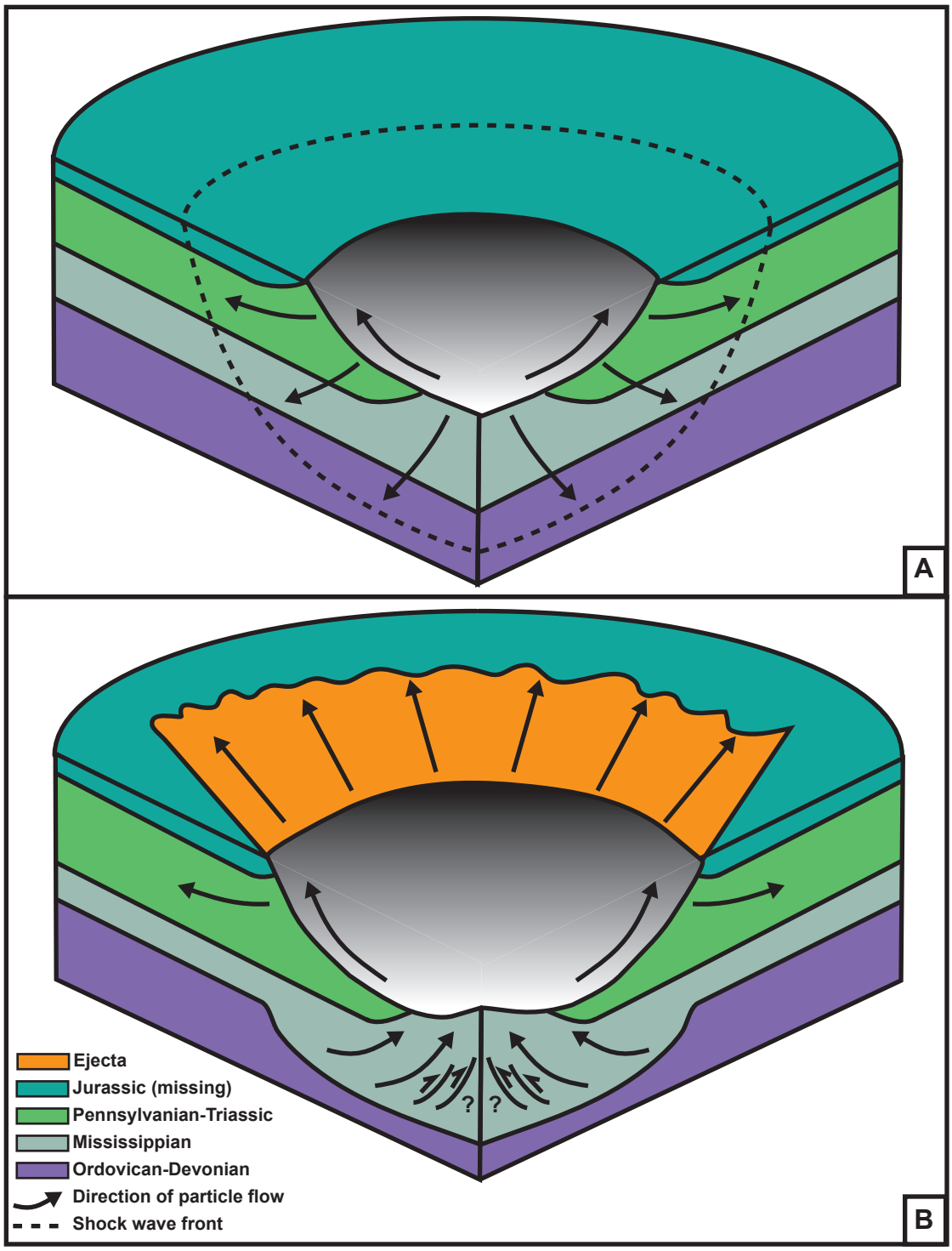

Figure 67. Simplified, schematic block diagram of the (A) contact/compression to excavation stage and (B) primary excavation stage of the formation of Red Wing Creek Crater. (A) The shock wave reaches a maximum depth at the Souris River Formation and the strata above the Mississippian strata are excavated. (B) Excavation continues and the crater expands, but underlying strata are no longer compressed downward but begins to uplift in the central-most portions of the crater.

the wells located within the depression (22-27, 34-28), have gas shows at the Bakken Formation level (R. Barton, personal communication, 2010). The side-wall cores and lack of gas shows in these wells indicate that the Bakken source rock is overmature within the depression due to the shockwave. Below the Bakken at the top of the mid-Devonian Souris River Formation, the strata are no longer structurally depressed in comparison to the strata in the outlying areas of the crater. Therefore, the Middle Devonian strata, underlying the central crater, are interpreted to be the deepest point that the shock wave had reached (**Figure 27, 29)**.

Besides the downward particle trajectory generated by the shock wave, there is also an outward and upward particle trajectory, which created an excavation flow within the overlying strata. Overlying the central crater, the entire Upper Mississippian through Triassic/Jurassic section is missing (**Figures 27-30)**. Excavation propagated deepest within the central crater, and the depth of excavation decreases toward the edges of the crater forming an initial bowl shaped crater geometry (**Figure 65**). There is no obvious expression of the ejecta blanket in the well and seismic data in the outer rim strata; the ejecta blanket was likely removed during the erosion that occurred at the Triassic-Jurassic unconformity, and/or the ejecta blanket is below seismic resolution (<100 ft, 30.5 m). Well log data are also inadequate for detection and core data or image logs are required to detect an ejecta blanket .

The late excavation stage is a direct continuation of the early excavation stage, but there is a major change in processes that occur during the transition. Late in the excavation stage, the downward particle trajectory ceases and the inward and upward trajectory commences in the central crater (**Figure 66**). This is the first stage of central

uplift formation. Because the previous excavation removed the overlying section, the top of the central uplift complex at Red Wing Creek is marked by the Mississippian Charles Formation.

Fourteen geological and geophysical studies of terrestrial complex craters have yielded the following relationship of structural uplift to final crater diameter:

$$SU=0.1D$$

,where SU is the maximum vertical displacement within the central uplift complex in kilometers and D is the final crater diameter (Grieve et al., 1981; Melosh, 1999). At Red Wing Creek, the Mission Canyon Formation is uplifted a total of 3,275 feet (998.2 m) above the annular trough and the maximum final crater diameter is 5.7 miles (9.17 km). According to this relationship, the theoretical structural uplift within the central uplift complex should be approximately 0.57 miles (0.91 km). Thus, the actual value of 0.62 miles (0.99 km) correlates fairly well with what has been observed at other terrestrial, complex craters

C. Modification Stage

Theoretical Processes

The final stage of crater formation overlaps with the late portions of the crater excavation period. Uplift of the central portion of the crater begins during the late excavation stage and continues through modification. As discussed above, crater diameters that reach 4 km (2.4 miles) usually transition to a complex crater. Craters, which have diameters less than this threshold, will not change appreciably during the

modification stage; the only active process during this stage will be debris slides from the crater walls into the adjacent bowl shaped crater floor, and the final morphology of the crater will be similar to what is present at the end of its excavation.

The morphology of complex craters, on the other hand, is modified significantly during the modification stage. As the central crater continues to be uplifted, the crater walls begin to collapse to form large debris flows or slide blocks, and, in some cases, stepped terraces (Melosh, 1989). Once the uplift of the transient crater floor ceases, the shape of the central uplift will have formed but the diameter of the crater may continue to increase as the crater walls continue to collapse. The continual increase of crater diameter suggests that there is no definitive end to the modification stage as erosion and collapse may continue indefinitely (Osinski, 2006), but numerical modeling estimates the total gravity collapse time of 10 to 100 km (6.2-62 miles) diameter craters are in the range of 10-30 seconds (Melosh and Ivanov, 1999).

Modification Stage at Red Wing Creek

The modification stage of the Red Wing Creek crater is divided into two sub-intervals based upon significant dominant morphological processes (**Figure 68**). During the modification stage, most of the previously discussed structural conditions developed (**Figures 64, 68)**.

During the early modification stage, the central crater continues to uplift and the crater reacts to the instability by wall collapse along listric normal faults (**Figure 69**). At this point of formation, the crater walls extended from the Lodgepole Formation to the missing Triassic/Jurassic section (**Figures 68a, 69**), and once collapsing commenced, a

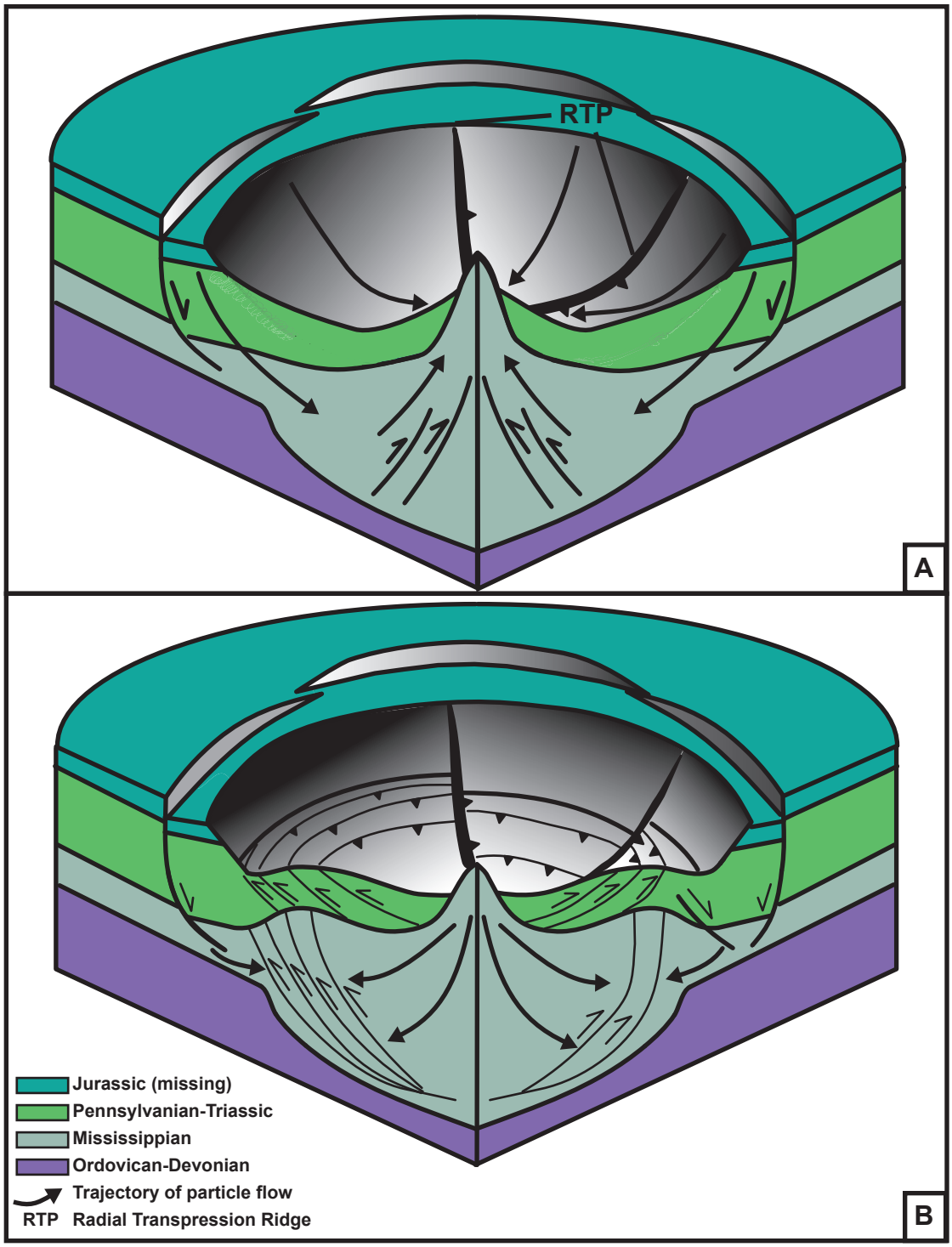

Figure 68. Simplified schematic block diagram of the (A) early modification and (B) late modification stages of deformation. (A) In the early modification stage, the crater begins to collapse inward along listric normal faults as the central crater continues to be uplifted. (B) The late stage of modification is marked by the collapse of the over-steepened central uplift causing a convergence of particle trajectories and the development of folding and outward thrusting.

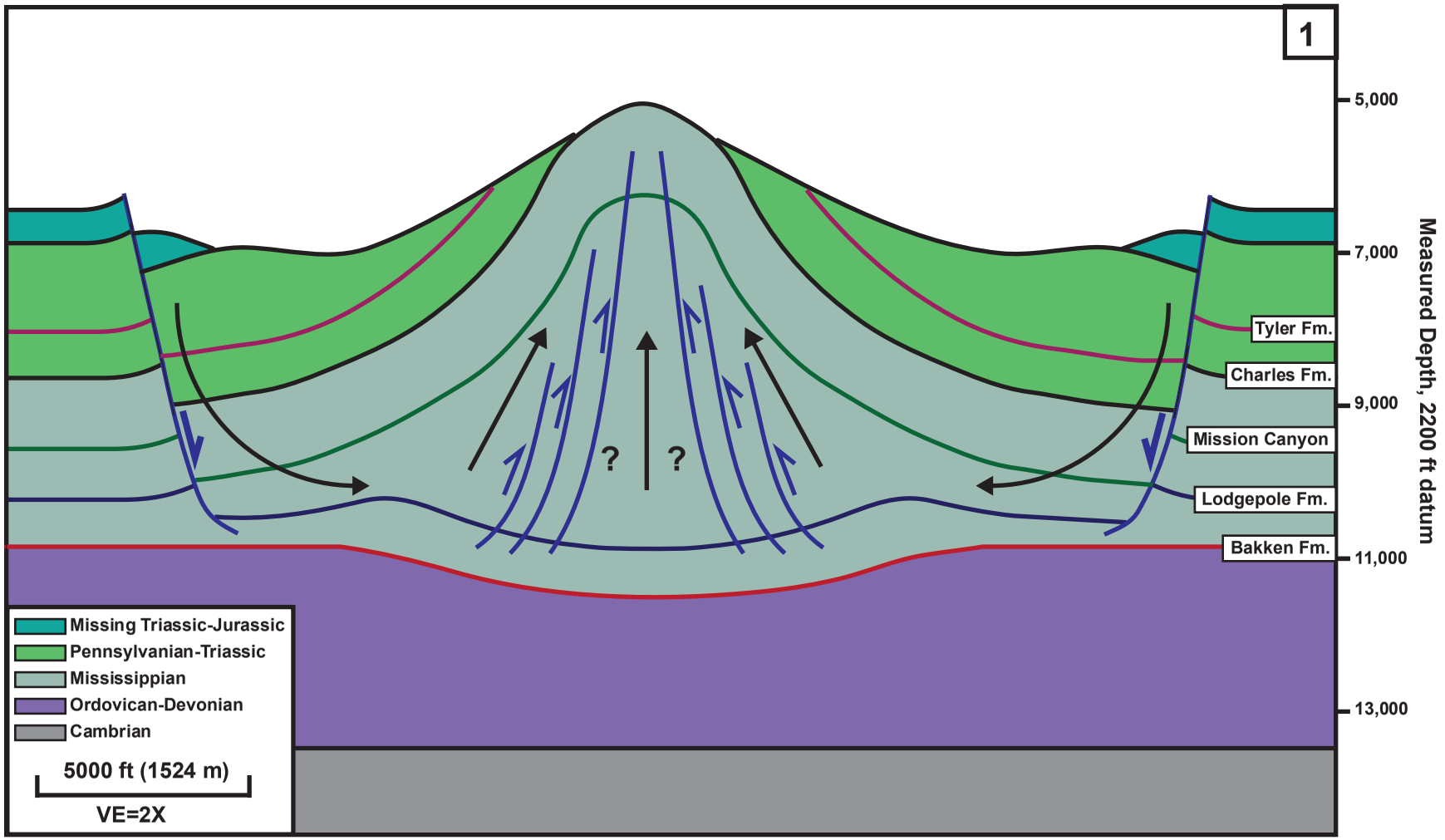

Figure 69. Schematic cross section of the early modification stage of crater development at Red Wing Creek. This interval is characterized by the inward collapse of the crater along listric normal faults due to the space created by the uplift of the central portion of the crater. Field studies of complex craters indicate that the central core is likely cut by converging high angle reverse faults.

downward and inward particle flow was generated. The downthrown blocks, composed of Mississippian through Permian (and possibly missing Triassic strata, although this is not indicated by well log data), were rotated and displaced inward along listric fault planes, which began the formation of the annular trough. The radial transpression ridges began to form during this interval. As the crater was collapsing downward and inward, this section was being thrusted laterally at its edges along high angle, thrust faults.

Most of the structural complexity within the final Red Wing Creek crater was generated during the latter stages of crater modification, due to cessation of uplift within the central crater. The central core reached a point of instability and over steepened causing the collapse of the central core (Osinski and Spray, 2005), and the generation of an outward and downward particle trajectory from the central crater. The convergence of the inward collapsing crater and the outward collapsing central uplift complex generated the extensive folding and thrusting present within the Lodgepole to Spearfish Formation interval (**Figure 70**). Finally, the top of the over-steepened crater edge collapsed and filled the crater floor with large slide blocks composed of the Permian to Triassic section present in the outer rim. As the blocks slide toward the central crater, they were thrust over each other laterally to compensate for the space lost during the downward and inward movement (**Figure 71)**. Secondary slides and erosion of material likely filled the remainder of the space within the crater floor cavity completing the formation of the Red Wing Creek crater.

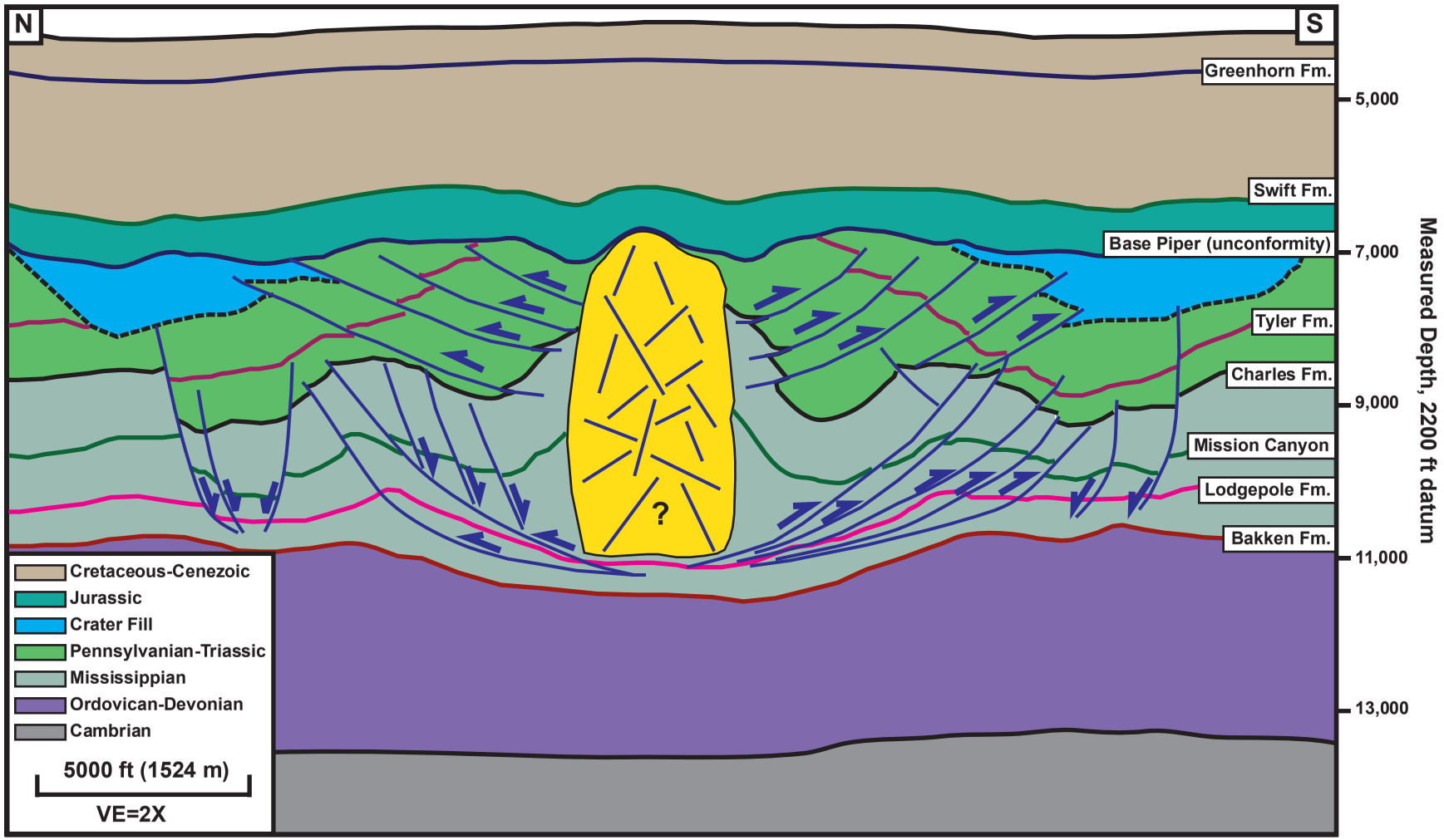

Figure 70. Structural cross section through the Red Wing Creek structure showing the final morphology of the crater. Central core is shown as undifferentiated but is likely cut by high angle reverse faults that detach within the Lodgepole Formation. The Mississippian through Triassic interval is dominated by structural features caused by the outward collapse of the central uplift and the inward collapse of the crater walls.The final morphology of the crater is truncated by the Triassic-Jurassic unconformity.

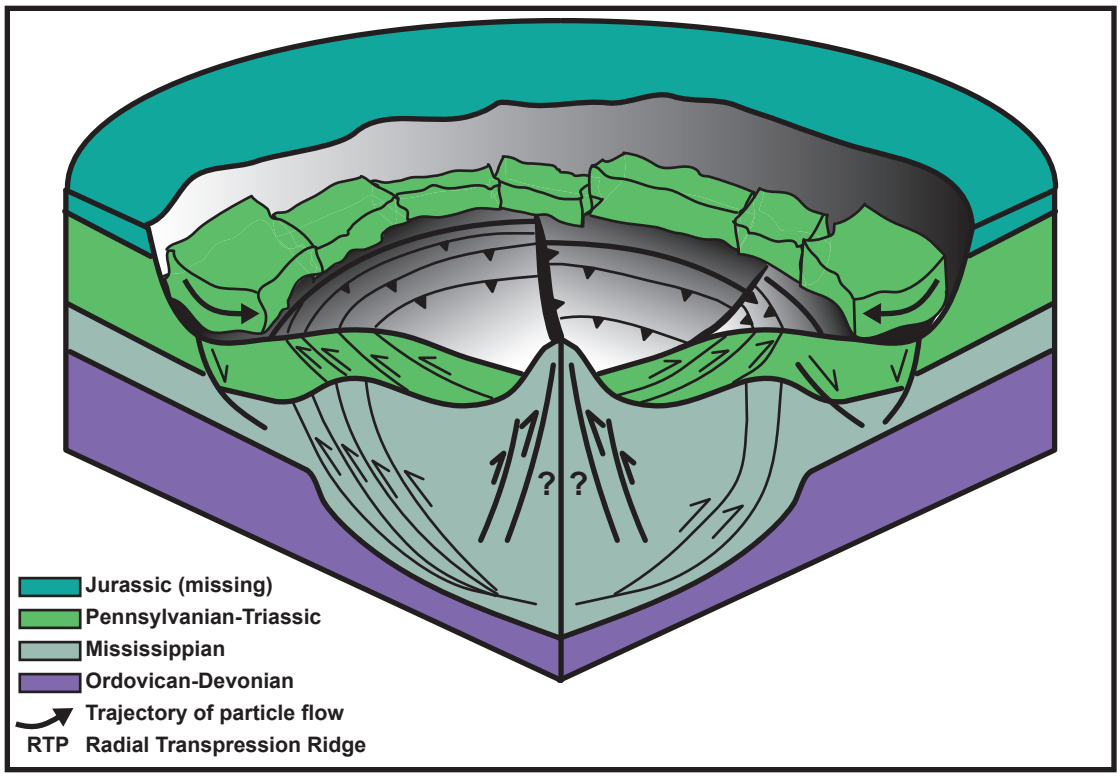

Figure 71. Simplified schematic block diagram of Red Wing Creek after primary modification has ceased. The final event of crater collapse commences, which is the collapse of the oversteepened crater rim blocks onto the crater floor. The final structural character of Red Wing Creek crater is illustrated. It is likely that the crater fill contains portions of the missing Jurassic strata but there is no well data to support their presence.

Conclusions

1. The Red Wing Creek structure is a complex impact crater located in McKenzie County, Western North Dakota in the Williston Basin. It is also a producing oil field that to date has produced 17 MMBO from Mississippian carbonates and its estimated total reserves are 60 MMBO. The original (apparent) diameter of the Red Wing Creek crater was 4.9 miles (7.89 km). After collapse of the over-steepened crater walls, the crater diameter increased to a final length of 5.7 miles (9.17 km). Because the upper-most strata has been removed by an unconformity, an exact date of impact cannot easily be determined, but best estimates from the youngest strata within the impact structure suggest that the impact occurred during the Upper Triassic or Lower Jurassic (220-200 Ma).

2. The Red Wing Creek crater is composed of three discrete structural zones that are differentiated by their internal and external characteristics. The first is the outer rim. Internally, the outer rim is relatively simple but it is bound toward the crater center by large normal faults. This marks the second zone, which is the annular trough. It is often rotated and there are zones where there is rollover related to the listric faulting. They are usually bound toward the crater center by antithetic normal faults or thrust faults. The third and final zone is the “central uplift complex” composed of the “inner rim” and the “central core.” Internally, the “inner rim” displays multiple structural styles that compensate for loss of space. The “central uplift” can only be characterized from the well data, and multiple stratigraphic repetitions suggest intense thrusting in this zone. .

3. The loss of space, due to convergence of the collapsing central uplift complex and the inward collapsing crater walls, is compensated for by three dominant structural styles: folding, outward directed thrusting, and radial thrusting. These three structural styles are seen within the “inner rim” of the “central uplift complex.” The inner rim is divided into an upper and lower level according to two regional detachment surfaces. The lower level is composed of the Lodgepole through Charles Formations and is characterized internally by folding and intense imbricate thrusting that detaches within the Lodgepole Formation shales. The upper thrust zone, composed of the Kibbey through Pine Salt Formations, is characterized internally by outward directed thrusting, which detaches within the Charles Formation evaporites. Both the upper and lower intervals of the “inner rim” are bound laterally by radial thrust faults or transpressional ridges. These radial thrust faults form as the crater collapses inward and converges laterally.

4. The crater floor topography is highly irregular due to the intense thrust faulting present between it and the Charles Formation detachment zone, and the crater fill is composed primarily of separate collapse blocks derived from the over-steepened Permian through Triassic section of the crater rim. Internally, the blocks are thrust over each other laterally as space is lost inward and they are thrust over one another in a dip direction, where the crater floor rises dramatically toward the central core. Secondary crater fill was likely produced by additional collapsing, traditional depositional processes, and fall back of material expelled during excavation.

5. Red Wing Creek is not the product of an oblique, low angle impact; likely, it is the result of an impact angle greater than 45°. Unlike craters whose structural asymmetries

indicate a low angle, oblique impact, the Red Wing Creek crater is much more symmetric. The radial thrusts in the northern half of the structure all thrust to the north or a general northern direction. The radial thrusts in the southern half of the structure are thrusting solely toward the south or a general southern direction. Maximum folding is also present in the northern and southern sectors of the inner rim, within the central uplift complex. These two structural trends of vergence suggest that the maximum shortening direction is on a general north-south trend and that the crater is primarily axial symmetric along an E-W axis.

6. An unconformity overlies the entire Red Wing Creek structure, which spans the Late Triassic to Early Jurassic. The unconformity is recognized in the wells where the base of the Early Jurassic Piper Formation is encountered. The age of the strata underlying the unconformity varies across the structure. In addition, there is substantial differential compaction of the Triassic-Jurassic strata that overlie the impact feature. Generally, the compaction is greater where the younger strata overlie areas that were structurally low (the area that overlies the crater fill).

7. The formation of the Red Wing Creek crater can be divided into three separate stages: contact/compression, excavation, and modification. The contact and compression stage produced a shockwave that reached as deep as the Devonian Souris River formation. The Bakken Formation was depressed significantly by the shockwave produced during this stage. The excavation stage removed the Upper Mississippian through Triassic/Jurassic section in the central portion of the crater. Away from the central crater, the excavation was shallower and the Pennsylvanian through Triassic section is present toward the edges of the crater. The modification stage

produced most of the structural features present in crater's final morphology. In this stage the crater walls collapsed inward and the central crater was uplifted. Toward the end of the modification stage the central core over-steepened, which caused a convergence with the inward collapsing crater walls. The majority of thrusting, folding, and radial faulting is a product of this event.

References

Abels, A., 2005, Spider impact structure, Kimberley Plateau, Western Australia: interpretations of formation mechanism and age based on integrated map-scale data: Australian Journal of Earth Sciences, v. 52 , p. 653-664.

Anna, L.O., R.M. Pollastro, S.B. Gaswirth, M.D. Lewan, P.G. Lillis, L.N.R. Roberts, C.J. Schenk, R.R. Charpentier, T.A. Cook, and T.R. Klett, 2008, Assessment of undiscovered oil and gas resources of the Williston Basin Province of North Dakota, Montana, and South Dakota, 2008: U.S. Geological Survey Fact Sheet 2008–3092, 2 p.

Barringer, D.M., 1905, Coon Mt. and its crater:. Proceedings of the National Academy of Sciences, v. 55, p. 861-886.

Bluemle, J. P., S. B. Anderson, and C. G. Larence, 1981, Williston Basin stratigraphic nomenclature chart: Miscellaneous Series North Dakota Geological Survey, no 61.

Boyer, S.E., and D. Eliot, 1982, Thrust systems: AAPG Bulletin, v. 66, no. 9, p. 1196-1230.

Brenan, R.L., B.L. Peterson, and H.J. Smith, 1975, The Origin of the Red Wing Creek Structure: McKenzie County, North Dakota: The Wyoming Geological Association Earth Science Bulletin, v. 8, no 3, p 1-41.

Bridges, L. W. D., 1978, Red Wing Creek field, North Dakota; a concentricline of structural origin, *in* D.Rehrig, ed, The economic geology of the Williston basin: Williston Basin Symposium, Montana Geol. Soc., p. 315-326.

Bridges, L. W. D., 1987, Red Wing Creek Field, North Dakota: a growth faulted or meteorite impact structure? *in* M. W. Longman, ed., Williston basin anatomy of a cratonic oil province: Rocky Mountain Association of Geologists, p. 433-440.

Chopra, S., and K. J. Marfurt, 2007, Seismic attributes for prospect identification and reservoir characterization,1st ed.: Tulsa, Oklahoma, Society of Exploration Geophysicists. 464 p.

Davis, G.H., and S.J. Reynolds, 1996, Structural Geology of Rocks and Regions, 2nd ed.: New York, John Wiley and Sons. 776 p.

Donofrio, R. R., 1997, Survey of hydrocarbon-producing impact structures in North America: Exploration results to date and potential for discovery in Precambrian basement rock. *in* K. S. Johnson and J. A. Campbell, eds., Ames structure in northwest Oklahoma and similar features: origin and petroleum production: Oklahoma Geological Survey Circular 100, p. 17-29.

Dorn, G.A., H.E. James, and L. Evins, 2005, Automatic fault extraction in 3D seismic data: CSEG National Convention, p. 247-250.

Dypvik, H., and L.F. Jansa, 2003, Sedimentary signatures and processes during marine bolide impacts: a review: Sedimentary Geology, v. 161, no. 3-4, p. 309–337.

Earth Impact Database, 2009: http://www.unb.ca/passc/ImpactDatabase/ (accessed April 9, 2010)

French, B.M., 1998. Traces of catastrophe: a handbook of shock-metamorphic effects in terrestrial meteorite impact structures: LPI Contrib., v. 954. Lunar and Planetary Institute, Houston, 120 p.

Gerhard, L. C., S. B. Anderson, and J. A. LeFever, 1991, Petroleum geology of the Williston basin, *in* H. W. Leighton, ed., Interior cratonic basins: AAPG Memoir 34, p. 507-559.

Grajales-Nishimura, J.M., P.E. Cedillo, C. Rosales-Dominguez, D.J. Moran-Zenteno, W. Alvarez, P. Claeys, J. Ruiz-Morales, J. Garcia-Hernandez, P. Padilla-Avila, A. Sanchez-Rios, 2000, Chicxulub impact; the origin of reservoir and seal facies in the southeastern Mexico oil fields: Geology, v. 28/4, p. 307-310.

Grieve, R. A. F., 1997, Terrestrial impact structures: basic characteristics and economic significance, with emphasis on hydrocarbon production, *in* K. S. Johnson and J. A. Campbell, eds., Ames structure in northwest Oklahoma and similar features: origin and petroleum production: Oklahoma Geological Survey Circular 100, p. 3-16.

Grieve, R.A.F., 2005. Economic natural resource deposits at terrestrial impact structures. *in* I, McDonald, A.J. Boyce, I.B. Butler, R.J. Herrington, and D.A. Polya, eds., Mineral deposits and Earth evolution. Geological Society, London, Special publications, 248,1-29.

Grieve, R.A.F., W.U. Reimold, J.V. Morgan, U. Riller, and M. Pilkington, 2008, Observations and interpretations at Vredefort, Sudbury, and Chicxulub; towards an empirical model of terrestrial impact basin formation: Meteoritics & Planetary Science, v. 43, p. 855-882.

Grieve, R.A.F., and V.L. Masaitis, 1994, The economic potential of terrestrial impact craters: International Geology Review, v. 36, p. 105-151.

Grieve, R.A.F., P.B. Robertson, and M.R. Dence, 1981, Constraints on the formation of ring impact structures, based on terrestrial data, *in* R.B. Merrill and P.H. Schultz, eds., Multi-Ring Basins, Proc. Lunar Planet. Sci. Conf., v. 12A, p 37-57.

Grieve, R.A.F., M.R. Dence, and P.B. Robertson, 1977, Cratering processes: as interpreted from the occurrence of impact melts, *in* D.J. Roddy, R.O. Pepin, R.B. Merrill, eds., Impact and explosion cratering, Pergamom Press, p. 791-814.

Gutschick, R. C., and C. A. Sandberg, 1983, Mississippian continental margins of the conterminous United States, *in* D. J. Stanley and G. T. Moore, eds., The shelfbreak: Critical interface on continental margins: SEPM Special Publication 33, p. 79– 96.

Hodge, P., 1994, Meteorite craters and impact structures of the Earth: Cambridge University Press, Cambridge, 124 p.

Kenkmann, T. and M.H. Poelchau, 2008, The structural inventory of oblique impact craters: large meteorite impacts and planetary evolution IV, LPI Contribution, no. 1423, paper id. 3057.

Kenkmann, T., and I. Von Dalgwik, 2000, Radial transpression ridges: a new structural feature of complex impact craters: Meteoritics and Planetary Science, v. 35 p. 1189-1201.

Kenkmann, T., B. A. Ivanov, and D. StØffler, 2000, Identification of ancient impact structures: Low-angle faults and related geological features of crater basements, *in* I.Gilmour and C. Koeberl, eds., Impacts and the early Earth: Springer-Verlag, Berlin, p. 279–307.

Koeberl, C., W.U. Reimold, and D. Brandt, 1996, Red Wing Creek structure, North Dakota; petrographical and geochemical studies, and confirmation of impact origin: Meteoritics, v. 31, no. 3, p. 335-342.

Kriens, B.J., E.M. Shoemaker, and K.E. Herkenhoff, 1999, Geology of the Upheaval Dome impact structure, southeast Utah: J. Geophys. Res., v. 104 no. E8 p. 18867–18887.

Lindsay, R.F., 1988, Mission Canyon Formation reservoir characteristics in North Dakota. *in* S.M. Goolsby and M. W. Longman, eds., Occurrence and petrophysical properties of carbonate reservoirs in the Rocky Mountain region: Rocky Mountain Association of Geologists, p. 317-346.

McClay, K.R., 1992, Thrust tectonics: Chapman and Hall, London, 447p.

Melosh, H. J., 1989, Impact cratering: a geologic process: Oxford University Press, New York, N.Y., 245 p.

Melosh, H.J., and B.A. Ivanov, 1999, Impact crater collapse: Annual Review of Earth and Planetary Science, v. 27, p. 385-415.

Milton D. J., A. Y. Glikson , and R. Brett, 1996. Gosses Bluff: a latest Jurassic impact structure central Australia. Part 1: Geological structure, stratigraphy, and origin:

Australian Geological Survey Organization Journal of Australian Geology and Geophysics. v. 16, p. 453-486.

Morgan J., et al. 1997. Size and morphology of the Chicxulub impact crater: Nature, v. 390, p. 472–476.

North Dakota Industrial Commission, Oil and Gas Division, 2009, North Dakota Cumulative Oil Production By Formation Through December 2009: https://www.dmr.nd.gov/oilgas/stats/2009CumulativeFormation.pdf (accessed April 1st, 2010).

Offield, T. W., and H. A. Pohn, 1979, Geology of the Decaturville impact structure, Missouri: U.S. Geological Survey Professional Paper 1042, 48 p.

Osinski, G.R., 2006. The geological record of meteorite impacts. Proceedings of the 1st International Conference on Impact Cratering in the Solar System: European Space Agency Special Publication SP-612 (CD-ROM).

Osinski, G.R., and J.G. Spray, 2005, Tectonics of complex crater formation as revealed by the Haughton impact structure, Devon Island, Canadian High Arctic: Meteoritics and Planetary Science, v. 40, p. 1813-1834.

Peacock, D.C.P. 2002, Propagation, interaction and linkage in normal fault systems: Earth Science Reviews, v. 58, p. 121-142.

Peterson, J. A., and L. M. MacCary, 1987, Regional stratigraphy and general petroleum geology of the U.S. portion of the Williston basin and adjacent areas, *in* J. A. Peterson, D. M. Kent, S. B. Anderson, R. H. Pilatzke, and M. W. Longman, eds., Williston basin: anatomy of a cratonic oil province: Denver, Rocky Mountain Association of Geologists, p. 9-43.

Peterson, J., 1995, Williston Basin Province, in U.S. Geological Survey 1995 Assessment of United States Oil and Gas Resources, Digital Data Series DDS-30, Release 2, CD-ROM.

Scherler D. T., Kenkmann, and A. Jahn, 2006, Structural record of an oblique impact: Earth Planet. Sci. Lett., v. 248, p. 43–53.

Sloss, L.L., 1963, Sequences in the cratonic interior of North America: Geological Society of America Bulletin, v. 74, p 93-114.

Sonnenberg, S.A. and A. Pramudito, 2009, Petroleum geology of the giant Elm Coulee Field, Williston Basin: AAPG Bulletin, v. 93, p. 1127-1153.

Sonnenfeld, M. D., 1996, Sequence evolution and hierarchy within the lower Mississippian Madison Limestone of Wyoming, *in* M. W. Longman and M. D.

Sonnenfeld, eds., Paleozoic systems of the Rocky Mountain region: SEPM Rocky Mountain Section, p. 165– 192.

Spray, J.G., 1997, Superfaults: Geology, v. 25, p. 579-582.

Stone, D.S. 2005, On illogical interpretation of geological structures in the Rocky Mountain foreland province: The Mountain Geologist, v. 42, p. 159-185.

Stone D. S., and A. M Therriault. 2003, Cloud Creek structure, central Wyoming, USA: Impact origin confirmed: Meteoritics & Planetary Science v. 38. p. 445-456.

Wernicke B., and Burchfiel, B.C. 1982, Modes of extensional tectonics: Journal of Structural Geology v. 4, no. 2. p.105-115.

Wieland F., R. L.Gibson , W. U. Reimold, and C. Lana, 2003, Structural evolution of the central uplift of the Vredefort impact structure, South Africa: Meteoritics & Planetary Science v. 38 no. A21. (abstract)

Wilshire H. G., Offield T. W., K. A. Howard, D. Cummings, 1972, Geology of the Sierra Madera Cryptoexplosion Structure, Pecos County, Texas: USGS Professional Paper #599-H. 42 p.

Wilson, C. W., and R. G. Stearns, 1968, Geology of the Wells Creek structure, Tennessee: State of Tennessee Department of Conservation, Division of Geology Bulletin 68, 236 p.

WELLNAME	WELL #	WELL KB	KIBBEY LIME	CHARLES	SALT B	RATCLIFF	MIDALE	NESSON	MISSION CANYON	LODGEPOLE	CHARLES 2	CHARLES 3	BASE LAST SALT	MISSION CANYON 2	MISSION CANYON 3	MISSION CANYON 4
BURLINGTON RESOURCE	11-1	2289		8879	9380	9387	9535	9610	9623							
Burlington Resources	11-1H															
BURLINGTON NORTHERN	1															
FOUR CREEKS	6-32F	2233	8488	8628	9280	9298	9413	9472	9525	10067						
FEDERAL	14-6	2263	8500	8639	9300	9316	9430	9498	9510	10067						
FEDERAL	14-6															
BN	21-7	2182	8437	8575	9236	9251	9370	9430	9464	10005						
BN	21-7															
DEPCO-FEDERAL	10-41	2244			9220	9235	9361	9425	9462	10056						
NORTH BRANCH	2-32F	2257	8476	8620	9288	9305	9419	9478	9513	10058						
NORTH BRANCH	2-22	2257	8480	8615	9284	9300	9418	9423	9516	10053						
NORTH BRANCH										10053						
NORTH BRANCH	41-3	2254	8470	8612	9278	9294	9412	9468	9500	10053						
NORTH BRANCH																
NORTH BRANCH	11-11	2290	8510	8650	9313	9330	9433	9500	9553	10086						
SNOWCOVER	12-24F	2336	8530	8670	9330	9348	9455	9517	9563	10110						
FEDERAL	13-2	2273														
ANDERSON AA	1-5	2242	8610	8750	9408	9423	9552	9630		10219						
ANDERSON	1-5	2242														
TRAVIS LEE	1	2272	8640	8773	9445	9458	9581	9648	9688	10238						
STATE-NELSON	1-6	2216	8568	8706	9382	9398	9527	9598	9629	10178						
NELSON	1	2216														
BUFFALO WALLOW	21-7	2202														
JOHNSON AI	2	2246	8625	8766	9410	9428	9566	9627	9620	10228						
JOHNSEN	2-7	2246														
NELSON STATE 7	2	2240														
NELSON 7	2	2240														
NELSON	1-7X	2236														
NELSON	1-7X	2236														
STEVENS	3-7	2241														
NELSON	1-7	2233	8585	8732	9379	9393	9528	9589	9627	10183						
SCHULTZ	3-8	2287		8788	9437	9453	9584	9646	9687	10244						
CENYAR ET AL	2-8	2312	8676	8819	9465	9500	9614	9674	9696	10278						
SCHULTZ	1-8	2283	8650	8795	9450	9464	9592	9653	9692	10248						
NEAL JOHN NELSON	1															
NO STOCK BUTTE FED	1	2406	8810	8950	9598	9612	9742	9805	9840	10418						
STATE ROGNESS	1-43-16	2357	8740	8876	9518	9530	9663	9728	9757	10332						
GUDMUNSEN-FEDERAL	1-17	2313								10290						
GUDMUNSEN FEDERAL	1-17	2313														
GUDMUNSEN-FEDERAL	1-17	2313														
ANDERSON	1-18	2250														
FEDERAL	1-13-21	2397	8777	8912	9556	9593	9702	9765	9795	10373						
BULLY FEDERAL-A	4	2415														
SPARATIE	1-31	2402	8720	8863	9510	9545	9651	9730	9757	10310						
TURNQUIST 10	1	2248	8485	8632	9280	9296	9426	9492	9529	10156						
LARSON	1	2444	8773	8913	9570	9586	9714	9775	9795	10362						
D O TURNQUIST	13X-15	2246	9149	9293	9831	9836	9901	9968	9996							
LITTLE TANK	19-21	2302	8575	8710	9367	9402	9512	9568	9605	10162						
TURNQUIST	44-21	2190	7717	7813	8687	8706	9580	9652	9682		8758		9430			
TURNQUIST	11-22	2245	8456	8652	9322	9343	9480	9550	9564							
WRIGHT	24-22A	2177	8150	8255	9384	9400	9504	9580	9600							
WRIGHT	24-22	2182		8032	9260	9280	9410	9441	9465					9571		
WRIGHT	33-22	2187	8492	8671	9452	9472	9594	9660	9690							
EVANSON	21-24	2193		8665	9280	9295	9423	9495	9507							
HAGEN	22-25	2253	9233	9380	9763	9778	9871	9988	9913.75	10120.12						
WRIGHT	13-26	2165	8130	8299	9060	9078	9210	9290	9310				27X-31BN	9406		
HAGAN	33-26	2190	8520	8654	9253	9265	9378	9453	9485							
PERRY J WRIGHT	11-26	2161	8326	8495	9230	9264	9438	9528	9574							
BN	44-27	2179	8091	8302	9278	9298	9810	9892	9913							
BURLINGTON NORTHERN	31-27	2158		7874	9024			9074	9178					9376	9644	
BURLINGTON NORTHERN	43-27	2166	8076	8248	8844	8863	9016	9110	9130							
BURLINGTON NORTHERN	12-27	2171		7412	8538	8567	8622	8854	8872		9212			9374	9412	

BURLINGTON NORTHERN	21-27	2190		7105			8218	8360	8382			9070		9296		
BURLINGTON NORTHERN	13-27A	2167		7048	8442				7688		8254			8730	8985	9130
BN	23-27	2158		6888				7706	7716		7883	8151		8084	8518	9296
BN UNIT	32-27	2162		7036			7900	7954	7980							
BURLINGTON NORTHERN	24-27	2138	7600	8010	8713	8736	9090	9198	9249							
BURLINGTON NORTHERN	22-27	2165		6690					6830.98	10886.92						
BURLINGTON NORTHERN	11-27	2177	7728	7988	8630	8659	8898	9036	9058		9242		9463	9705		
BURLINGTON NORTHERN	33-27			7060			8255	8310	8348					9140	9413	
BURLINGTON NORTHERN	22-27A	2188		6734				6904	6810							
BURLINGTON NORTHERN	13-27	2175		7002				7616	7670		7780			8258	8946	
BN	42-27	2162	7800	7964	8578	8595	8748	8829	8844					8886	8917	
BURLINGTON NORTHERN	31-27A	2160		7202	9706				9830							
BREDWICK	43-28	2169	7750	8072	9022	9044	9230	9319	9332							
BREDWICK	33-28	2182	8005	8150	9000	9032	9266	9427	9445							
BREDWICK	43-28	2169	7750	8072	9022	9044	9230	9319	9332							
GOVT	22X-28-1	2214	7965	8150	9107	9122	9241	9293	9316	10210				9568		
GOVT	22X-28-1	2214														
BREDWICK	31-28	2184	8220	8402	9220	9237	9394	9478	9510							
FEDERAL	24-28	2211	8204	8350	9145	9192	9340	9418	9475							
BREDWICK	44-28	2170	8444	8650	9261	9610	9747	9810	9840		9272		9556			
BREDWICK	42-28	2169	7950	8139	9004	9022	9170		9644		9260		9386	9644		
Bredwick	34-28	2236		7688	9190		9410	9493	9506	10528						
BREDWICK	34-28			8100	9190	9208	9407	9497	9528	10526						
BN	1-29	2245	8764	8908	9550	9553	9623	9692	9730							
MPI	13-31	2245	8482	8627	9296	9332	9428	9500	9525	10068						
MPI	13-31	2245														
USA	1	2190	8782	8944	9676	9694	9766	9798	9813							
BN-FEDERAL	33-34	2178	8480	8638	9410	9446	9556	9645	9668							
BURLINGTON NORTHERN	32-35	2237	8840	9009		9359	9494	9600	9633							
BURLINGTON NORTHERN	1	2222	8440	8596	9315	9341	9482	9620	9647							
BURLINGTON NORTHERN	14-35	2218		8780	9351	9387	9498	9550	9572	10124						
BN	13-35	2202	NDE						NDE							
SORENSEN	2-41	2295	8584	8727	9400	9418	9545	9605	9640	10180						
SHEEP FEDERAL	1-A	2389	8604	8748	9382	9408	9530	9593	9616	10183						
SHEEP FEDERAL	1	2385														
SHEEP FEDERAL	1-A	2389														
FEDERAL	12-15	2369	8591	8730	9382	9401	9523	9585	9628	10165						
FEDERAL	12-15	2389														
USA-A	1	2386														
FEDERAL-CABOOSE	1-22	2288	8530	8665	9320	9339	9462	9516	9550	10110						
FEDERAL-CABOOSE	1-22	2288														
FEDERAL-22	1	2422	8652	8789	9435	9450	9542	9630	9668	10230						
SPRING CREEK	27-31BN	2290	8512	8654	9299	9335	9442	9500	9528	10090						
BN SPRING CREEK	27X-31	2277														
SPRING CREEK		2277														
BOXCAR BUTTE BN	27-33	2296	8528	8670	9328	9345	9468	9526	9561	10108						
BOXCAR BUTTE BN	27-33	2296														
BOXCAR BUTTE	27-33BN	2296														
MTS FEDERAL	34-1	2268	8490	8615	9298	9315	9428	9485	9510	10064						
F NORTH BRANCH	34-42	2345	8565	8708	9380	9399	9515	9576	9612	10107						
BOWLING CREEK	35-24BN	2263														
BOWLINE CREEK BN	35-24	2263														
BN-NORTH BRANCH	35-24	2295	8473	8612	9287	9306	9419	9475	9513	10053						
BRANCH NORTH	35-24															
DEPCO-BOWLINE CREEK	35-24BN	2263														
NORTH BRANCH	7-35	2223	8436	8577	9247	9264	9376	9438	9465	10012						
NORTH BRANCH	7-35	2223														
NORTH BRANCH	22-35	2250								10052						
NORTH BRANCH	22X-35		8475	8617	9268	9282	9400	9460	9499	10055						
NORTH BRANCH	22X-35															
BN NORTH BRANCH	35X-34	2227	8430	8561	9242	9260	9375	9432	9458	10012						
BOWLINE CREEK	35-34BN	2245														
NORTH BRANCH	22-35	2249														

Appendix A. Well tops used for horizon interpretation within the reservoir zone at Red Wing Creek field.